Protein and Viral Partitioning in Two-Phase Aqueous Micellar Systems

by

Daniel Takashi Kamei

Submitted to the Department of Chemical Engineering
in partial fulfillment of the requirements for the degree of

Doctor of Philosophy

at the

MASSACHUSETTS INSTITUTE OF TECHNOLOGY

June 2001

Author .....
Department of Chemical Engineering
May 9, 2001

Certified by .....
Daniel Blankschtein
Professor of Chemical Engineering
Thesis Supervisor

Certified by .....
Daniel I.C. Wang
Institute Professor
Professor of Chemical Engineering
Thesis Supervisor

Accepted by .....
Robert E. Cohen
St. Laurent Professor of Chemical Engineering
Chairman, Committee for Graduate Students

Protein and Viral Partitioning in Two-Phase Aqueous Micellar Systems

by

Daniel Takashi Kamei

Submitted to the Department of Chemical Engineering
on May 9, 2001, in partial fulfillment of the
requirements for the degree of
Doctor of Philosophy

Abstract

Several biotechnological applications require the separation of proteins from viruses. These include large-scale industrial applications, such as viral clearance and production of gene delivery viral vectors, as well as small-scale academic applications, such as preparative biochemistry. A readily scalable unit operation that is capable of separating proteins from viruses is therefore desirable. One unit operation that has been proven to be scalable in the chemical industry is liquid-liquid extraction. However, conventional oil-water solvents cannot be used because nonpolar solvents tend to denature biomolecules. This thesis therefore focused on using two-phase aqueous micellar systems for the liquid-liquid extraction, since both the micelle-rich and micelle-poor phases are predominantly composed of water. The objective of this thesis was to develop a fundamental understanding of protein and viral partitioning in two-phase aqueous micellar systems.

This thesis was comprised of two directions, *Directions A* and *B*, that were investigated simultaneously. In *Direction A*, studies were conducted to identify the mechanisms responsible for the observed discrepancy between the experimentally measured viral partition coefficients in the two-phase aqueous nonionic $C_{10}E_4$ micellar system and those that were predicted based on the excluded-volume theory developed previously by our group. By identifying any additional mechanisms influencing viral partitioning, it may be possible to eliminate these mechanisms in the future to yield the extreme viral partition coefficients predicted by the excluded-volume theory. This, in turn, will enhance the separation of protein from virus.

Competitive inhibition and partitioning studies were conducted to investigate possible attractive interactions between the $C_{10}E_4$ micelles and the tailspikes/capsids of bacteriophage P22 (model virus). These possible attractive interactions were investigated because they could counter the effect of the excluded-volume interactions. However, the attractive interactions between the bacteriophage P22 particles and the $C_{10}E_4$ micelles were found to be negligible.

An experimental study was also performed to examine whether *all* the micelle-rich and micelle-poor domains that are formed at the onset of phase separation are in their corresponding macroscopic phases prior to quantifying the viral concentrations in the two phases. In this study, the entrainment of micelle-poor domains in the top, micelle-rich phase was

found to be the key factor influencing the partitioning behavior of viruses. In addition, a new theoretical description of partitioning was developed that combines the excluded-volume theory with this entrainment effect. Good agreement between the measured and the predicted viral partition coefficients was attained. It was therefore concluded that the primary mechanisms governing viral partitioning are the entrainment of micelle-poor domains in the top, micelle-rich phase and the excluded-volume interactions between the viruses and the micelles.

Direction B centered around the less optimistic point-of-view that the viral partition coefficients could not decrease and approach the extreme viral partition coefficients predicted by the excluded-volume theory. However, even with the viral and protein partition coefficients that had already been achieved in the two-phase aqueous $C_{10}E_4$ micellar system, the virus was excluded more strongly than the protein into the bottom, micelle-poor phase. Accordingly, the volume ratio was varied in order to attain a 75% yield of lysozyme (model protein) in the top phase and a 97% yield of bacteriophage P22 in the bottom phase.

To further increase the yield of protein in the top phase, another mode of interaction was introduced to attract the protein into the top, micelle-rich phase. Specifically, a two-phase aqueous mixed (nonionic/ionic) micellar system was formed by the addition of the anionic surfactant SDS to $C_{10}E_4$. An experimental study was conducted to demonstrate proof-of-principle that two-phase aqueous mixed (nonionic/ionic) micellar systems could indeed be used to modulate both electrostatic and excluded-volume interactions between the proteins and the micelles. A theory was also developed and found to provide reasonable quantitative predictions of protein partition coefficients in these mixed micellar systems.

An important benefit of this theory is to provide guidelines for optimizing the protein partition coefficient without any required experimentation. As an example, the effects of three experimentally controllable variables (the solution pH, the ionic strength, and the distance from the end of the hydrocarbon tail to the charge of the ionic surfactant) on the protein partition coefficient were examined in a 2^3 factorial design, and a response surface for the protein partition coefficient was generated. The theory was also extended to include: (i) ionic surfactants having charges located beyond the hydrophilic heads of the nonionic surfactants, and (ii) zwitterionic surfactants in place of the nonionic surfactants.

Different two-phase aqueous mixed ("noncharged"/ionic) micellar systems were investigated experimentally regarding their ability to separate protein from virus using $C_{10}E_4$ and the zwitterionic C_8-lecithin surfactant as "noncharged" surfactants, and SDS and SDE_6S as ionic surfactants. The addition of an ionic surfactant into the "noncharged" micellar system improved the separation of lysozyme from bacteriophage P22 in all cases. In particular, it was possible to increase the yield of lysozyme in the top phase from 75% to 95%, while maintaining the same yield of bacteriophage P22 in the bottom phase.

Thesis Supervisor: Daniel Blankschtein
Title: Professor of Chemical Engineering

Thesis Supervisor: Daniel I.C. Wang
Title: Institute Professor
Professor of Chemical Engineering

This is for

Obaachan,

my grandmother.

Acknowledgments

To quote Paul McCartney, it has been a "long and winding road." No one completes a thesis alone, and I would like to thank the many people who have made this possible.

I would first like to thank Professor Daniel Blankschtein, one of my advisors, for his mentoring and friendship. He has been an integral part of my life at MIT, and I appreciate all the time, effort, and energy he has directed toward my overall education. In addition to teaching me material in his courses, he has taught me approaches to attacking problems and has emphasized fundamentals in my research. We have also shared a good number of discussions, whether it be on research, course material, philosophy, or life.

I would next like to thank Professor Daniel I.C. Wang, also my advisor, for his support during my thesis. He provided an essential practical perspective and taught me about different aspects of biochemical engineering through his courses. He also shared stories with his students to illustrate particular points. For example, his "coin in the dark" story taught us that the "coin may not be in the light" and that sometimes we need to search for the answer where we would least expect it.

I am grateful for the help and guidance provided by all of my thesis committee members. None of the bacteriophage P22 experiments could have been performed without the help of Professor Jonathan King. He made me feel at home in his laboratory, and that meant a lot to me. I was also able to benefit from his protein folding course as well as from his knowledge about viruses. I have always appreciated Professor Douglas Lauffenburger's genuine interest in this thesis. His comments during the committee meetings were very helpful, and he kept me updated on biotechnology by informing me about BPEC and BEH seminars. I learned a lot from his bioengineering course and am especially thankful to him for allowing me to continue to learn from him as a post-doc. Dr. Jill Myers taught me a great deal about the applications of viral clearance and gene therapy in industry. I would like to thank her for references to pertinent government documents and for explaining the details about the FDA guidelines and the way they are followed in industry. Her perspective as an insider in the biotechnology industry has been invaluable.

I would also like to thank Dr. Chia-li Liu of the Blankschtein group for getting me started on this project. She was the graduate student who worked on two-phase aqueous micellar systems before I came to MIT. When I joined the group, she was a post-doc, and she patiently taught me the experimental techniques that were involved. She also helped me perform my first two experimental studies (competitive inhibition test and partitioning capsids only). I especially enjoyed our conversations when we worked in the lab together.

I am grateful for the assistance of my UROP students: Phil Huang, Soojin Son, Luwam Semere, and Nicole Botcheos. Phil, Luwam, and Nicole helped map out phase diagrams for different surfactant systems. Soojin investigated an enzymatic assay for lysozyme in the presence of surfactants.

I appreciate all the guidance Cammie Haase-Pettingell gave me regarding bacteriophage P22. She always took time out of her busy schedule to help me in the King lab and was my source for all the bacteriophage P22 stock solutions. I would also like to thank Dr. Scott Betts from the King lab for providing the purified tailspike solution in the experimental study involving the partitioning of capsids only.

I am grateful for the opportunity to have worked with Professor Adalberto Pessoa Jr. from the University of São Paulo in Brazil. Professor Pessoa Jr. performed the experiments with glucose-6-phosphate dehydrogenase (G6PD) and taught me about Brazil.

I was also fortunate enough to be able to collaborate with Biogen. In particular, I performed two experimental studies that allowed me to further test the capabilities of two-phase aqueous micellar systems. Dr. Jim Barsoum helped me perform baculovirus stability experiments in the presence of two surfactants. His group member, Pam Moy, helped me partition recombinant adenovirus in the two-phase aqueous $C_{10}E_4$ micellar system. I also benefited from discussions with Dr. Cyrus Karkaria.

During my thesis, I was able to spend six weeks at the University of Lund in Sweden to learn about different two-phase aqueous complex fluid systems and their associated experimental methods. I would like to thank Professor Folke Tjerneld for being a fantastic host during my stay in Sweden. I am also thankful for the friendship of the Tjerneld group members, especially Dr. Ulf Sivars, Dr. Hiroshi Umakoshi, and Dr. Josefine Persson. In addition, I was able to have good discussions with Professor Per-Åke Albertsson and Professor Göte Johansson.

I will definitely miss the members of the Blankschtein group. I could not have worked with a nicer group of people who made it easy to call Da Lab my home. They helped create a fun working environment, and all are good friends. Dr. Nancy Zoeller Diggs always had a smile to brighten up the lab. I enjoyed talking to Dr. Anat Shiloach, my lab neighbor for the first half of my thesis. Peter Moore always kept me up to date with current events and Canadian commercials. Mike Mulqueen was the ever knowledgeable source regarding baseball and NASCAR. Hua Tang, my lab neighbor for the latter half of my thesis, was always very energetic and happy. Betty Yu, a fellow Berkeley Golden Bear, provided a different, but funny sense of humor. Dr. Isaac Reif has always been a very giving individual

and a constant source of wisdom. Vibha Srinivasan taught me about Hinduism and India. Dave Cochran kept me updated on good movies and barbecue ribs. Arthur Goldsipe began the trend of having lunch with the members in the group, and I had many good times at these lunches. I am passing the two-phase aqueous micellar torch to Henry Lam who I am sure will continue to push this technology further. Although Joe Kushner and I have only overlapped for about 4 months, he has been a good addition to Da Group.

I would also like to thank the members, past and present, of the Wang and King groups for making me feel at home in their labs and offices. I would especially like to thank Inn Yuk, Dr. Patricia Clark, and Dr. Ajay Pande.

I am grateful for the friends I made in the first-year class of 1995, especially Pat Walton, Dr. Venkat Ganesan, and Dr. Jenny Fujii. In addition, I am thankful to have gone to Practice School with Chuck Cheung, Fouad Saad, Shinya Fukuda, and Mike Derden. During my thesis, I also enjoyed working with the 10.40 class of 1999 as their T.A. I would also like to thank the secretaries who have made my stay here enjoyable: Arline Benford, Janet Fischer, Elaine Aufiero, Barbara Driscoll, Carol Phillips, and Patsy Sampson.

I would like to thank all my friends back in Cali for their support. I know I can't mention all of them, but I especially would like to thank my three best friends for always being there: Felix Lau, Seiji Morioka, and Bryan Yoshida. They have been true friends for the longest time, and they have made sure that I stay in touch with music. I wish them luck in their jobs as well as in the band they have started. I am also grateful for the friendship of Chris Hwang, my roommate during my Berkeley years. If there was a best roommate award, he would certainly win it. I would also like to thank my friends Norman Lau, Carri Matsumoto, and Sunny Choi for checking up on me.

As for my family, I would like to begin by thanking Obaachan, my grandmother. She passed away last October, and this thesis is dedicated to her. She was generous, loving, giving, unselfish, intelligent, humble, and dignified. Even under the most unbearable circumstances, she never complained and was courageous. She, as well as my mom, taught me the importance of character. She was going to come to Boston for the first time in her life to see me graduate, but now I know she has already seen the city and is with me everyday.

I am also grateful for my big brother, Richard, who has always looked after me. He has always been concerned about my well-being, and I have learned a lot from his actions and words. I would also like to thank my sister-in-law, Staci, for caring about my family ever since she and my brother started dating over 11 years ago.

My parents have been extremely supportive of me, and that has always given me strength.

My father, Pops, emphasized not being afraid to fail and has always been encouraging. I learned my work ethic from the examples he set when I was a child. He also taught me to appreciate basketball and baseball, and he has given me sports updates whenever I call home. He also helped me pick teams for the ChemE March Madness pool, and we even won one year. My mother, Mom, is and has been the heart of the Kamei family. Her unconditional love has made it easy for me to talk to her throughout my life. She is always willing to lend an ear and listens to the good news as well as the bad news. She has sacrificed so much for all of us, and I am forever grateful.

I don't know what I would do without my fiancée, Dr. Ginger Tse. She has given me so much love and support and is always willing to listen to my problems. I can talk to her about anything and am able to share my thoughts, stories, and jokes with her. She has helped me in so many ways and is the backbone of our relationship. She is extremely giving and unselfish. She is my happiness and means the world to me. In the words of Peter Gabriel, "In your eyes, the light, the heat. In your eyes, I am complete." I have enjoyed everyday we have been together and look forward to sharing the rest of my life with her.

Finally, I am grateful for the award of a Department of Defense National Defense Science and Engineering Graduate Fellowship, and the financial support provided by the NIH Interdepartmental Biotechnology Program Grant no. 5 T32 GM08334.

Contents

PART I: MOTIVATION AND BACKGROUND 25

1 Introduction 27

1.1 Applications Involving the Separation of Proteins from Viruses 27

1.1.1 Viral Clearance 27

1.1.2 Gene Therapy 31

1.1.3 Preparative Biochemistry 32

1.2 Motivation 33

1.3 Two-Phase Aqueous Micellar Systems 34

1.3.1 Surfactants and Micellization 34

1.3.2 Phase Separation in Aqueous Micellar Solutions 36

1.4 Previous Applications Involving Two-Phase Aqueous Nonionic Micellar Systems 38

1.4.1 Extracting Metal Chelates and Organic Compounds Based on Hydrophobicity 40

1.4.2 Separating Proteins Based on Hydrophobicity 41

1.4.3 Separating Hydrophilic, Water-Soluble Biomolecules Based on Size Differences 41

1.5 Thesis Overview 52

PART II: UNDERSTANDING VIRAL PARTITIONING IN THE TWO-PHASE AQUEOUS $C_{10}E_4$ MICELLAR SYSTEM 57

2 Competitive Inhibition Study to Investigate Possible Attractive Interactions between the Tailspikes of Bacteriophage P22 and the $C_{10}E_4$ Micelles 59

2.1 Introduction 59

2.2 Materials and Methods 62
2.2.1 Materials 62
2.2.2 Stability of DB7136 Cells in $C_{10}E_4$ Solutions 63
2.2.3 Competitive Inhibition Test 63
2.2.4 Plaque Assay 66
2.3 Results and Discussion 67
2.3.1 Stability of DB7136 Cells in $C_{10}E_4$ Solutions 67
2.3.2 Competitive Inhibition Test 67
2.4 Conclusions 69

3 Partitioning the Capsids of Bacteriophage P22 without the Tailspikes 73
3.1 Introduction 73
3.2 Materials and Methods 74
3.2.1 Materials 74
3.2.2 Synthesis of the Capsids of Bacteriophage P22 without the Tailspikes 74
3.2.3 Partitioning the Capsids of Bacteriophage P22 75
3.2.4 The Thermo-Regulated Device 76
3.3 Theory 77
3.4 Results and Discussion 78
3.5 Conclusions 80

4 Investigating the Possible Existence of a Heterogeneous Population of Bacteriophage P22 Particles 81
4.1 Introduction 81
4.2 Materials and Methods 82
4.2.1 Materials 82
4.2.2 Mapping the Coexistence Curve of the Two-Phase Aqueous $C_{10}E_4$ Micellar System 83
4.2.3 Double-Stage Partitioning of the Bacteriophage P22 Particles 84
4.3 Theory 85
4.4 Results and Discussion 87
4.4.1 Mapping the Coexistence Curve of the Two-Phase Aqueous $C_{10}E_4$ Micellar System 87
4.4.2 Double-Stage Partitioning of the Bacteriophage P22 Particles 88
4.5 Conclusions 91

5 Investigating the Effect on the Viral Partition Coefficient of Micelle-Poor Domains Being Entrained in the Macroscopic, Top, Micelle-Rich Phase **93**

5.1 Introduction 93

5.2 Materials and Methods 99

5.2.1 Materials 99

5.2.2 Photographing the Two-Phase Aqueous $C_{10}E_4$ Micellar System with Different Volume Ratios 99

5.2.3 Partitioning Bacteriophage P22 and Cytochrome *c* with Different Volume Ratios 100

5.2.4 Experimentally Evaluating the Partition Coefficient of Cytochrome *c* 102

5.2.5 Measuring the Viscosities of Buffered $C_{10}E_4$ Solutions 105

5.3 Theory 106

5.3.1 Estimation of the Effect of Micelle-Poor (Virus-Rich) Domains Being Entrained in the Macroscopic, Top, Micelle-Rich Phase 106

5.3.2 Estimation of the Effect of Micelle-Rich (Virus-Poor) Domains Being Entrained in the Macroscopic, Bottom, Micelle-Poor Phase 109

5.3.3 The Settling Velocity of a Micelle-Poor Domain Entrained in the Macroscopic, Top, Micelle-Rich Phase 111

5.4 Results and Discussion 113

5.4.1 Photographing the Two-Phase Aqueous $C_{10}E_4$ Micellar System with Different Volume Ratios 113

5.4.2 Partitioning Bacteriophage P22 and Cytochrome *c* with Different Volume Ratios 114

5.4.3 Measuring the Viscosities of Buffered $C_{10}E_4$ Solutions 118

5.4.4 Comparison between the Experimentally Measured and Theoretically Predicted Partition Coefficients 119

5.5 Conclusions 128

PART III: MANIPULATING THE VOLUME RATIO AND EXPLOITING ELECTROSTATIC INTERACTIONS BETWEEN MIXED MICELLES AND PROTEINS **131**

6 Manipulating the Volume Ratio in the $C_{10}E_4$-Buffer Two-Phase System to Achieve Good Separation of Protein from Virus **133**

6.1 Introduction 133

6.2 Materials and Methods 134
6.2.1 Materials 134
6.2.2 Separating Lysozyme from Bacteriophage P22 in the $C_{10}E_4$-Buffer System 134
6.3 Theory 135
6.3.1 Protein and Viral Partition Coefficients 135
6.3.2 Protein and Viral Yields 136
6.3.3 Viral Concentration Factor 137
6.3.4 Analysis of the Protein and Viral Yields and the Viral Concentration Factor 137
6.4 Results and Discussion 138
6.5 Conclusions 140

7 A Fundamental Investigation of Protein Partitioning in the $C_{10}E_4$-SDS-Buffer Two-Phase System 141

7.1 Introduction 141
7.2 Materials and Methods 144
7.2.1 Materials 144
7.2.2 Mapping the Three-Dimensional Phase Diagram of the $C_{10}E_4$-SDS-Buffer System between 19.8°C and 23.1°C 145
7.2.3 Mapping the Coexistence Curve of the $C_{10}E_4$-SDS-Buffer System at a Temperature of 25.2°C 146
7.2.4 Partitioning Proteins in the $C_{10}E_4$-Buffer and the $C_{10}E_4$-SDS-Buffer Systems 146
7.3 Theory 147
7.3.1 Review of Expressions for the Volume Ratio in Two-Phase Aqueous Micellar Systems 147
7.3.2 Brief Review of the Excluded-Volume Theory 148
7.3.3 Development of a Theory Incorporating Electrostatic Interactions . . . 149
7.3.4 Estimation of the Net Charges of the Proteins 158
7.4 Results and Discussion 160
7.4.1 Mapping the Three-Dimensional Phase Diagram of the $C_{10}E_4$-SDS-Buffer System between 19.8°C and 23.1°C 160
7.4.2 Mapping the Coexistence Curve of the $C_{10}E_4$-SDS-Buffer System at a Temperature of 25.2°C 163

7.4.3 Partitioning Proteins in the $C_{10}E_4$-Buffer and the $C_{10}E_4$-SDS-Buffer Systems 164
7.4.4 Theoretically Predicting Protein Partition Coefficients in the $C_{10}E_4$-SDS-Buffer System 167
7.5 Conclusions 171

8 Theoretical Analyses of Protein Partitioning in Two-Phase Aqueous Mixed Micellar Systems 173
8.1 Introduction 173
8.2 Analyzing the Relative Effects of Various Experimentally Controllable Variables on the Protein Partition Coefficient 174
8.3 Conducting a Theoretical 2^3 Factorial Design and Generating a Response Surface 183
8.4 Examining the Effect of Using an Anionic Surfactant Having its Negative Charge Located Beyond the Hydrophilic Head of the Nonionic Surfactant . . 191
8.4.1 Investigating Two-Phase Aqueous Zwitterionic Micellar Systems 194
8.5 Conclusions 203

9 Separating Lysozyme from Bacteriophage P22 in Two-Phase Aqueous Mixed Micellar Systems 205
9.1 Introduction 205
9.2 Materials and Methods 206
9.2.1 Materials 206
9.2.2 Separating Lysozyme from Bacteriophage P22 in the $C_{10}E_4$-SDS-Buffer and the $C_{10}E_4$-SDE_6S-Buffer Two-Phase Systems 206
9.2.3 Separating Lysozyme from Bacteriophage P22 in the C_8-lecithin-Buffer and the C_8-lecithin-SDS-Buffer Two-Phase Systems 207
9.3 Theory 208
9.4 Results and Discussion 211
9.4.1 Separating Lysozyme from Bacteriophage P22 in the $C_{10}E_4$-SDS-Buffer and the $C_{10}E_4$-SDE_6S-Buffer Two-Phase Systems 211
9.4.2 Separating Lysozyme from Bacteriophage P22 in the C_8-lecithin-Buffer and the C_8-lecithin-SDS-Buffer Two-Phase Systems 214
9.5 Conclusions 217

PART IV: CONCLUDING REMARKS 219

10 Conclusions and Future Research Directions 221
10.1 Thesis Summary 221
10.2 Future Research Directions 226
10.2.1 Experimentally Attaining Even Lower Viral Partition Coefficients . . . 226
10.2.2 Exploiting Electrostatic Interactions between the Mixed Micelles and the Proteins 226
10.2.3 Varying the Solution pH and the Salt Governing Electroneutrality . . 230
10.2.4 Partitioning in Two-Phase Aqueous Polymer/Surfactant Systems . . . 230
10.3 Concluding Remarks 231

APPENDICES 233

A Recipes for the Solutions Used in the Plaque Assay 235

B Estimating the Densities of the Micelle-Poor Phase and the Micelle-Rich Phase 237

C Pseudo-Binary and Pseudo-Ternary Systems 239
C.1 The Pseudo-Binary $C_{10}E_4$-Buffer System 239
C.2 The Pseudo-Ternary $C_{10}E_4$-SDS-Buffer System 242

D Derivation of an Expression for the Protein Chemical Potential Using the Number Density as the Unit of Concentration 243

E A Preliminary Investigation of the Possible Existence of an Electrostatic Potential Difference Between the Two Coexisting Macroscopic $C_{10}E_4$ Micellar Phases 251
E.1 Introduction 251
E.2 Theory 252
E.2.1 Incorporation of the Electrostatic Potential Difference in the Derivation of the Protein Partition Coefficient 252
E.2.2 Derivation of Expressions for the Electrostatic Potential Difference in Terms of Interaction Parameters 268
E.3 Materials and Methods 272
E.3.1 Materials 272

E.3.2 Partitioning BSA in the $C_{10}E_4$-Buffer Two-Phase System at Different pH Conditions . . . 273
E.3.3 Partitioning Lysozyme in the $C_{10}E_4$-Buffer Two-Phase System at pH=7.2 in the Absence and in the Presence of Added $NaClO_4$ . . . 274
E.4 Results and Discussion . . . 275
E.4.1 Partitioning BSA in the $C_{10}E_4$-Buffer Two-Phase System at Different pH Conditions . . . 275
E.4.2 Partitioning Lysozyme in the $C_{10}E_4$-Buffer Two-Phase System at pH=7.2 in the Absence and in the Presence of Added $NaClO_4$ . . . 276
E.5 Conclusions . . . 277

F A Preliminary Investigation of Glucose-6-Phosphate Dehydrogenase Partitioning in the $C_{10}E_4$-Buffer Two-Phase System **279**
F.1 Introduction . . . 279
F.2 Materials and Methods . . . 279
F.2.1 Materials . . . 279
F.2.2 Assaying G6PD in Aqueous $C_{10}E_4$ Solutions . . . 280
F.2.3 Mapping the Coexistence Curve of the Two-Phase Aqueous $C_{10}E_4$ Micellar System . . . 282
F.2.4 Partitioning G6PD in the $C_{10}E_4$-Buffer Two-Phase System . . . 282
F.3 Theory . . . 283
F.4 Results and Discussion . . . 286
F.4.1 Assaying G6PD in Aqueous $C_{10}E_4$ Solutions . . . 286
F.4.2 Mapping the Coexistence Curve of the Two-Phase Aqueous $C_{10}E_4$ Micellar System . . . 288
F.4.3 Partitioning G6PD in the $C_{10}E_4$-Buffer Two-Phase System . . . 288
F.5 Conclusions . . . 291

G Contributions of V_t^{ex} and V_b^{ex} to $(\mu_{p,t}^{ex} - \mu_{p,b}^{ex})$ **293**

H Evaluation of the Surface Charge Density of Every Micelle in Phase α **297**

I Derivation of the Boundary Conditions for the Three Concentric Charged Cylinders **299**

BIBLIOGRAPHY **305**

List of Figures

1-1 Examples of ionic and nonionic surfactants. 35
1-2 An example of a zwitterionic surfactant. 35
1-3 Schematic representation of the coexistence curve of the two-phase aqueous $C_{10}E_4$ micellar system. 38
1-4 Schematic representation of the two-phase aqueous $C_{10}E_4$ micellar system. . . . 39
1-5 Schematic representation of an operating tie line on the coexistence curve of the two-phase aqueous $C_{10}E_4$ micellar system. 43
1-6 Comparison between the theoretically predicted and experimentally measured partition coefficients of cytochrome *c*. 44
1-7 Comparison between the theoretically predicted and experimentally measured partition coefficients of ovalbumin. 45
1-8 Comparison between the theoretically predicted and experimentally measured partition coefficients of catalase. 46
1-9 The protein partition coefficient, K_p, as a function of the ratio, R_p/R_0, in the two-phase aqueous $C_{10}E_4$ micellar system. 47
1-10 Comparison between the theoretically predicted and experimentally measured partition coefficients of bacteriophage ϕX174. 49
1-11 Comparison between the theoretically predicted and experimentally measured partition coefficients of bacteriophage P22. 50
1-12 Comparison between the theoretically predicted and experimentally measured partition coefficients of bacteriophage T4. 51

2-1 Schematic representation of bacteriophage P22. 61
2-2 Experimental results corresponding to the stability study conducted on *Salmonella typhimurium* strain DB7136 cells in $C_{10}E_4$ solutions. 68
2-3 Experimental results corresponding to the first competitive inhibition test. . . . 69
2-4 Experimental results corresponding to the second competitive inhibition test. . 70

3-1 Schematic representation of the thermo-regulated device used in the partitioning experiments. 77
3-2 Experimentally measured capsid and intact bacteriophage P22 partition coefficients at 21.0°C in the two-phase aqueous $C_{10}E_4$ micellar system. 79

4-1 The coexistence curves of the two-phase aqueous $C_{10}E_4$ micellar system for $C_{10}E_4$ from two different lots. 88
4-2 The partition coefficients of bacteriophage P22 from the double-stage partitioning experiments conducted in the two-phase aqueous $C_{10}E_4$ micellar system. . . 90
4-3 The partition coefficients of three bacteriophages as a function of temperature. 91

5-1 Schematic representation of: (a) the entrainment of micelle-poor (virus-rich) domains in the macroscopic, top, micelle-rich phase, and (b) the entrainment of micelle-rich (virus-poor) domains in the macroscopic, bottom, micelle-poor phase. 95
5-2 Schematic representation of the onset of the phase separation process when employing a volume ratio that is: (a) much less than one, and (b) much greater than one. 97
5-3 The two-phase aqueous $C_{10}E_4$ micellar system three to four hours after initiating phase separation for a volume ratio: (a) much less than 1, and (b) much greater than 1. 115
5-4 Experimentally measured partition coefficients of bacteriophage P22 as a function of temperature for different volume ratios. 117
5-5 Experimentally measured partition coefficients of cytochrome *c* as a function of temperature for different volume ratios. 118
5-6 Comparison between the theoretically predicted and experimentally measured partition coefficients of cytochrome *c*. 122
5-7 Comparison between the theoretically predicted and experimentally measured partition coefficients of bacteriophage P22. 123
5-8 Comparison between the theoretically predicted and experimentally measured partition coefficients of bacteriophage P22 for a volume ratio of 1. 125
5-9 Comparison between the theoretically predicted and experimentally measured partition coefficients of bacteriophage ϕX174 for a volume ratio of 1. 126
5-10 Comparison between the theoretically predicted and experimentally measured partition coefficients of bacteriophage T4 for a volume ratio of 1. 127

6-1 The results of separating lysozyme from bacteriophage P22 in the $C_{10}E_4$-buffer system. 139

7-1 Schematic representation of the two-phase aqueous mixed ($C_{10}E_4$/SDS) micellar system. 142
7-2 The three-dimensional phase diagram of the $C_{10}E_4$-SDS-buffer system between 19.8°C and 23.1°C. 162
7-3 The coexistence curve of the $C_{10}E_4$-SDS-buffer system at 25.2°C. 163
7-4 The coexistence curve of the $C_{10}E_4$-SDS-buffer system at 25.2°C with the located tie line. 165
7-5 The coexistence curve of the $C_{10}E_4$-buffer system with the tie line at 19.3°C. . 166
7-6 The experimentally measured protein partition coefficients in the $C_{10}E_4$-buffer and the $C_{10}E_4$-SDS-buffer systems. 168
7-7 Comparison between the experimentally measured (shown by the white bars) and theoretically predicted (shown by the gray bars) protein partition coefficients in the $C_{10}E_4$-SDS-buffer system. 170

8-1 The predicted partition coefficient of lysozyme as a function of the solution pH. 178
8-2 The predicted partition coefficient of lysozyme as a function of the ionic strength of the solution. 179
8-3 The predicted partition coefficient of lysozyme as a function of d_{ch}, the distance from the end of the hydrocarbon tail to the negative charge of the anionic surfactant. 181
8-4 Schematic representation of a portion of a cylindrical mixed micelle where a nonionic surfactant is mixed with an anionic surfactant that has: (a) a smaller d_{ch}, and (b) a larger d_{ch}. 183
8-5 The effect on K_p of the two-factor interaction between pH and IS at the low d_{ch} condition. 188
8-6 The effect on K_p of the two-factor interaction between pH and IS at the high d_{ch} condition. 188
8-7 The theoretical response surface for the predicted partition coefficient of lysozyme as a function of the solution pH and ionic strength. 190
8-8 The chemical formulas of sodium dodecyl hexa(ethylene oxide) sulfate (SDE_6S) and sodium dodecyl sulfate (SDS). 191
8-9 The chemical formula of dioctanoyl phosphatidylcholine (C_8-lecithin). 194

8-10 Previously measured coexistence curve of the two-phase aqueous C_8-lecithin micellar system. 195

8-11 In (a), a portion of the cylindrical mixed (C_8-lecithin/anionic) micelle is schematically represented, where the micelle is comprised primarily of the zwitterionic C_8-lecithin surfactant. In (b), the three concentric charged cylinders used to model the mixed micelle are shown. 197

8-12 In (a), the negative charge of the anionic surfactant (for example, SDS) is positioned before the negative charge of the C_8-lecithin molecule. In (b), the negative charge of the anionic surfactant (for example, SDE_6S) is positioned after the positive charge of the C_8-lecithin molecule. 203

10-1 Schematic representation of using liquid-liquid extractions in series. 229

E-1 Schematic representation of: (a) the orientation of positive and negative ions in the two macroscopic phases and the three-dimensional interfacial region, and (b) the net charges that may be present across the two-dimensional model for the liquid-liquid interface. 252

E-2 The variation of $e(\psi_t - \psi_b)$ with temperature when the electrostatic potential difference was fitted to the partitioning data of ovalbumin. 261

E-3 Comparison between the theoretically predicted and experimentally measured partition coefficients of ovalbumin. 262

E-4 Comparison between the theoretically predicted and experimentally measured partition coefficients of cytochrome *c*. 263

E-5 Comparison between the theoretically predicted and experimentally measured partition coefficients of catalase. 264

E-6 Experimentally measured partition coefficients of BSA in the presence of 0.50 M NaCl at different pH conditions. 276

E-7 Experimentally measured partition coefficients of lysozyme at pH=7.2 in the absence and in the presence of 0.50 M $NaClO_4$. 277

F-1 Enzymatic activity measurements of G6PD solutions in the absence and in the presence of $C_{10}E_4$. 287

F-2 The coexistence curves of the two-phase aqueous $C_{10}E_4$ micellar system for $C_{10}E_4$ from three different lots. 289

F-3 Comparison between the theoretically predicted and experimentally measured partition coefficients of G6PD. 290

List of Tables

1-1 The $\log_{10}$ of viral removal achieved for different viruses with two membranes manufactured by Millipore. 30

2-1 The conditions of the first competitive inhibition test. 65
2-2 The conditions of the second competitive inhibition test. 66

4-1 The initial, overall concentrations of bacteriophage P22 in the different partitioning experiments. 84

5-1 The conditions of the six bacteriophage P22 and the six cytochrome *c* partitioning experiments in the two-phase aqueous $C_{10}E_4$ micellar system. 101
5-2 Experimentally measured viscosities of buffered $C_{10}E_4$ solutions. 119

7-1 Proteins partitioned in the $C_{10}E_4$-buffer and $C_{10}E_4$-SDS-buffer systems. 144
7-2 Typical pKa's of amino acids and terminal groups. 161

8-1 The values of the variables used to predict the partition coefficient of lysozyme in Chapter 7. The corresponding predicted values of K_p^{EV}, K_p^{elec}, and K_p from Chapter 7 have also been included for completeness. 176
8-2 Low (-) and high (+) conditions for the three variables examined in the 2^3 factorial design of the protein partition coefficient, K_p. 184
8-3 Theoretically predicted protein partition coefficients for lysozyme under the conditions that were specified in a 2^3 factorial design. 185
8-4 Example calculation of the main effect of pH on K_p. 185
8-5 Example calculation of the effect on K_p for the two-factor interaction between pH and IS. 186
8-6 Estimates of the individual main effects and the interactive effects between the three variables, pH, IS, and d_{ch}, for the 2^3 factorial design on the protein partition coefficient, K_p. 187

9-1 Separating lysozyme from bacteriophage P22 in different $C_{10}E_4$ micellar systems. 212
9-2 Separating lysozyme from bacteriophage P22 in different C_8-lecithin micellar systems 215
9-3 Experimentally measured viscosities of buffered C_8-lecithin and $C_{10}E_4$ solutions. 216

D-1 Ion concentrations in phase α. 248

E-1 Estimates of $z_i C_{i,\alpha}$ for the partitioning solutions. 257

F-1 The conditions of the G6PD partitioning experiments in the two-phase aqueous $C_{10}E_4$ micellar system. 283

PART I

MOTIVATION AND BACKGROUND

Chapter 1

Introduction

1.1 Applications Involving the Separation of Proteins from Viruses

Several biotechnological applications require the separation of proteins from viruses. With regard to viral clearance, an industrial downstream process must be validated for its ability to inactivate and/or remove viruses from a desired therapeutic protein. In the case of gene therapy, a recombinant virus capable of delivering nucleic acids into cells must be produced industrially and separated from proteins in a fermentation broth. With regard to preparative biochemistry, a gentle preparative method for isolating biologically active viruses from a solution containing proteins can aid in characterizing the viruses, which may otherwise be rendered inactive by standard academic laboratory techniques. Sections 1.1.1, 1.1.2, and 1.1.3 provide more details regarding these applications.

1.1.1 Viral Clearance

Inactivation and/or removal, that is, clearance,[1] of mammalian viruses from therapeutic proteins represents a major challenge in the biotechnology industry. A cell culture solution containing a therapeutic protein may contain endogenous retroviruses (that is, retroviruses that originate from within the cells) and/or adventitious viruses (that is, viruses accidentally entering from the environment).[1–3] Adventitious viruses could be present in the cell culture solution if the media is contaminated during formulation and handling. The media might also be contaminated if it contains serum from an infected animal.[3–5]

Each downstream purification scheme must therefore be validated in its ability to clear viruses. This is a portion of the overall viral safety package, which also includes testing of the unprocessed bulk and control of the sources of raw materials. Viral validation studies serve the purpose of: (i) proving that the downstream purification scheme can achieve a

certain reduction in retroviruses that are determined to be in the cell culture solution, and (ii) demonstrating that the same process is robust enough to clear a range of viruses that are not suspected to be in the solution.[4] In the validation studies, a scaled-down version of the significant viral clearance steps in the actual purification scheme is set-up in a laboratory at a special test facility. Into this model of the purification process, certain viruses are introduced and assayed at different steps to determine the amount of viral clearance achieved in each step.[1,4] Viral clearance or reduction is usually reported in $\log_{10}$ of viruses cleared. The $\log_{10}$ of viral clearance for a downstream purification process is generally evaluated by summing the $\log_{10}$ of viral clearance (LVC) for each significant step tested in the validation studies, which is given by the following relation:[1,4,5]

$$LVC = \log \frac{(V_0 \times C_{v,0})}{(V_f \times C_{v,f})} \tag{1.1}$$

where V_0 and V_f are the volumes of the solution before and after a particular step, respectively, and $C_{v,0}$ and $C_{v,f}$ are the viral concentrations before and after a particular step, respectively. With regard to the retroviruses, the $\log_{10}$ viral safety margin is evaluated as follows. Retroviral assays are first performed on the unprocessed bulk, which corresponds to "one or more pooled harvests of cells and culture media"[1] that will become one lot of product.[6] Sometimes, only the unpurified supernatant, or conditioned medium without cells, is treated as the unprocessed bulk.[7] The amount of retrovirus that could theoretically be present in one dose of product is evaluated based on the results of the retroviral assays and an estimation of the volume of unprocessed bulk that will eventually become one dose of product. To ensure maximum safety, this amount of retrovirus must be inactivated and/or removed in addition to an added safety margin of 3 to 6 $\log_{10}$ as recommended by the FDA.[1,8] If no retroviral particles are detected, the FDA recommends assuming that 1×10^6 retroviral particles/mL are in the unprocessed bulk.[9] If any adventitious viruses are detected, the unprocessed bulk is automatically discarded.[7] However, model adventitious viruses must still be tested in the validation studies representing a range of potential viruses in terms of nucleic acid, size, and envelope. No standard currently applies to all biotherapeutic proteins regarding the required $\log_{10}$ of viral clearance that must be attained with the model adventitious viruses examined in the validation studies. The FDA treats each license application on a case-by-case basis, looking for an appropriate risk profile.[8]

At least one viral clearance step should be included in the train of downstream steps.[2,6,9,10] However, it is recommended that the validation studies investigate more than one downstream step in the ability to clear viruses.[3] Generally, since both enveloped and non-

enveloped viruses might survive in a cell culture solution, at least one inactivation step is used, which typically inactivates the enveloped viruses (primarily retroviruses). The non-enveloped viruses, on the other hand, are eliminated with other physical removal steps.[7]

Viral inactivation methods include pasteurization, solvent-detergent treatment, pH treatment, β-propiolactone (a mutagen) treatment, and UV treatment.[3,5,10–13] A clearance step does not necessarily have to be an independent step dedicated solely to viral inactivation and/or removal. For example, a pH treatment step can actually be the low pH elution of a therapeutic protein product from a column in chromatography.[3,10] Pasteurization, pH treatment, and solvent-detergent treatment have been found to achieve good viral inactivation. Specifically, these methods have been found to inactivate 3 to 5 $\log_{10}$ of retroviruses and to perform consistently at different pH and ionic strength conditions. These methods are also scalable, which is an important factor, since the production-scale units must perform similarly to the laboratory-scale units used in the validation studies.[10]

Column chromatography has also been investigated with respect to its viral removal capability, which is a natural consequence of its traditional use in purifying therapeutic proteins from other biomolecules in a cell culture solution. However, column chromatography is generally not used as a step dedicated solely for viral removal, since it is expensive and not as robust in terms of viral clearance (that is, it does not always achieve greater than 3 $\log_{10}$ of viral clearance).[7,10] In addition, regulatory agencies in Europe tend to be skeptical of chromatography as a robust method for viral removal.[8] The behavior of viruses on columns can be affected by many factors, such as the shape of the virus, size of the virus, exterior of the virus, type of resin, buffer, and flow rate. For example, an enveloped virus, due to it being surrounded by a phospholipid bilayer membrane, can have greater hydrophobic attractions with certain resins than a non-enveloped virus.[13] When performing chromatography, the reusability of resins must also be examined to ensure the same performance during each run and at the end of the column lifetime. The inactivation of all viruses bound to the resin during the column regeneration step must also be verified.[10,13]

Membranes, however, are attaining widespread use for removing viruses from a therapeutic protein in a cell culture solution.[10,11,14,15] This separation method is attractive because viruses with sizes greater than the membrane cut-off size are removed significantly from the protein. Filtration achieves good viral clearance, is readily scalable, is easy to use, is predictable with regard to protein recovery and viral removal, and has been found to perform consistently at different pH and ionic strength conditions.[9–11,14] Pall Filtron Corporation, Millipore, and Asahi are major producers of viral removal membranes. 0.015–0.04 μm mem-

branes have been found to remove 4 to 8 $\log_{10}$ of retroviruses.[9] A 0.04 μm rated Nylon 66 (grade ND) filter from Pall was found experimentally to remove 4.7 and 3.8 $\log_{10}$ of ecotropic murine leukemia virus (MuLV) and xenotropic MuLV, respectively, in one pass. Titer reduction for reovirus (having a diameter between 700 and 750 Å) with the 0.04 μm rated filters was 3.7 $\log_{10}$ after one filter and more than 7.3 $\log_{10}$ after two filters in series.[11] Pall now has a line of viral reduction membranes known as OMEGA®VR membranes. The membranes are rated at 500, 300, 200, 150, and 100 kilodaltons (K). The 300K and 100K membranes have been found experimentally to remove about 5–6 $\log_{10}$ of murine leukemia virus (>800 Å) and porcine parvovirus (>200 Å), respectively.[16] Millipore, on the other hand, markets two types of viral removal membranes, Viresolve/70®and Viresolve/180®. Viresolve/70®and Viresolve/180®membranes pass biomolecules that are less than 70 and 180 kilodaltons, respectively, and their viral clearance values are listed in Table 1-1 below.[17]

Table 1-1: The $\log_{10}$ of viral removal achieved for different viruses with two membranes manufactured by Millipore.[17]

Virus	$\log_{10}$ of Viral Removal	
	Viresolve/70®	Viresolve/180®
Poliovirus	3	2
Hepatitis A	not tested	4
Simian Virus-40	5	not tested
Sindbis	5.5	4.5
Reovirus	6.5	5.5
Murine Leukemia Virus	6.6	6.0
Human Immunodeficiency Virus	8.5	not tested

Membranes, however, also have disadvantages. Typically, membranes cannot be reused. For Asahi's membranes, expensive monodisperse gold particles must also be purchased from Asahi to validate the integrity of the membranes with respect to pore size after filtration of the cell culture solution.[7,15] Millipore, similarly, sells CorrTest®integrity kits which are designed to test the integrity of membranes before and after use.[17] These factors act to increase the cost of the filtration process. Membranes with smaller pores, for example, 0.015 μm membranes, are also very expensive, and tend to foul easily. These membranes with smaller pores, however, are valuable because: (i) the regulatory agencies recommend that a range of virus types are tested, and (ii) the regulatory agencies strongly encourage

the testing of the 20 nm minute virus of mice (MMV), since occurrences of infection by this virus have been reported in industry.[8,18] MMV is also particularly robust with regard to standard viral inactivation methods and can sometimes be difficult to clear. Due to these disadvantages regarding membranes, biotechnology companies are looking for other methods to physically remove viruses.[7] Consequently, it is desirable to find another unit operation capable of separating biomolecules primarily based on size. Size appears to be an excellent characteristic on which to base viral removal from a therapeutic protein since: (i) high recovery of the therapeutic protein can be achieved due to its size being much smaller than that of viruses (for example, in the case of membranes, 92% protein recovery has been reported in a two-stage operation using Viresolve/70®membranes[14]), (ii) the viruses with sizes greater than the membrane cut-off size should be removed effectively from the smaller, desired protein, and (iii) no other common characteristic can be exploited for separation purposes because viruses are diverse in many aspects, including their exterior and shape. For example, enveloped viruses differ from protein-coated or naked viruses, and there are also exterior differences within these two classified groups as well.

1.1.2 Gene Therapy

In the future, gene therapy may be exploited to treat diseases. The major disease categories are single-gene inherited disorders, multifactorial diseases, cancer, and infectious diseases. Single-gene inherited disorders include hemophilia, sickle cell anemia, adenosine deaminase deficiency, hypercholesterolemia, and cystic fibrosis. Since single-gene inherited disorders result from one gene being mutated, several of these may be remedied by the delivery of the non-mutated gene. There is also much potential in utilizing gene transfer to correct multifactorial diseases, which include coronary heart disease and diabetes. Many possible gene therapy strategies are being investigated for the treatment of cancer. One method involves delivering tumor suppresor genes, such as p53 and Rb, to cancerous cells. Infectious diseases, such as hepatitis, herpes, and AIDS, may become treated in the future by the delivery of a gene that prevents the virus in the cell from replicating.[19]

One of the challenges in gene therapy is the delivery of the genes into the cells. Since viruses are natural vectors or gene-delivery vehicles, they have potential for being utilized in this application. Viral vectors that have been studied for gene therapy include retrovirus, adenovirus, adeno-associated virus, herpes virus, poxvirus, and baculovirus.[19–22] Efficiently concentrating and purifying viruses from a fermentation broth containing many proteins will become increasingly important when gene therapy treatments are approved by the FDA.

Column chromatography is generally used as a purification unit in many industrial biotechnology processes. However, since gene therapy is still a new therapeutic strategy, it is not clear if column chromatography will be the best candidate for viral vectors. Even though column chromatography has been shown to have strong potential for purifying a particular type 5 recombinant adenovirus[23] and a particular adenoassociated adenovirus,[24] there are many variants among these recombinant viruses. For adenoviruses, the variants include particles which are dodecahedral and lack hexons (the key immunogenic targets),[25] and particles which can only replicate in tumor cells.[26] Wild type (that is, natural or non-mutant) adenovirus serotypes also have differences in the lengths and antigenic properties of their penton fibers.[27] In addition, it is not obvious that column chromatography will be the best purification unit for a particular vector because many issues, such as viral aggregation, must be considered.

Accordingly, other separation methods may be more effective in the large scale purification of viruses. However, these separation methods must be scalable, since production-scale units will be built based on the basic research that is conducted with the laboratory-scale units. They must also be cost effective. A gentle separation method is also desirable, since such a process may prevent loss of infectivity and/or aggregation of the viral vectors. In addition, a separation method capable of concentrating and purifying viruses according to the universal property of size is also useful, since a single method may be applied to a wide variety of viral vectors. Such a unit operation is desirable because it is predicted that more than one viral vector will be necessary for treating the many different diseases.[19] Therefore, if one biotechnology company is producing more than one viral vector, the ability of a single concentration scheme to accomodate all the different viral vectors can give rise to several desirable features, such as ease in automation, simplicity, and commonality of materials that remove any need for viral-specific compounds such as biospecific affinity ligands, metals, and ionic molecules.

1.1.3 Preparative Biochemistry

In academia, one of the main goals of preparative biochemistry has been to develop separation methods that can aid in studying biochemical systems.[28] With regard to viruses, preserving their infectivity during their purification is necessary for conducting biochemical, immunological, and virological research.[28,29] In general, viruses must be purifed and concentrated from a fermentation broth that contains a wide variety of proteins.[30] Several methods were developed for purifying viruses prior to 1970,[31] and many of these methods, with and

without variations, are still in use today. However, these methods may be preventing the characterization of some viruses by damaging the viral parts required for their infectivity or by causing aggregation of the viral particles. Some viruses that have been known to be sensitive to the purfication process include murine leukemia viruses (MuLV), the human immunodeficiency virus (HIV), and the endogenous baboon type-C virus.[29,32] Loss of biological activity during the purification process can result from physical forces, certain chemicals used in the separation process, and high temperatures.[32] Consequently, a gentle preparative method for purifying viruses from proteins and other cellular material is desirable.

In preparative biochemistry, the purification processes are generally conducted on a laboratory scale. Centrifugation and ultracentrifugation, with and without density gradients, have achieved widespread use as a preparative method for viruses.[30,33–37] However, due to the large centrifugal forces involved, these techniques may damage some sensitive viruses. Filtration and ultrafiltration,[29,32,38–40] along with column chromatography,[30,36,40,41] are also used for purifying viruses. These methods, however, may also damage sensitive viruses due to the shear stresses involved. Accordingly, a purification technique involving low centrifugal forces and shear stresses would be useful.

1.2 Motivation

As discussed in Section 1.1, there is room for improvement in the separation processes currently used in the three above-mentioned applications. Any alternative separation process that is considered should be readily scalable, since production scales typically increase during development and after licensure of biotherapeutics.[8] In addition, viral clearance validation studies, as well as basic research, are conducted on a laboratory scale. A scalable process is also useful because it can be applied to preparative biochemistry (which is a small-scale operation), as well as to viral clearance and the production of gene delivery viral vectors (which can be large-scale operations). One unit operation that has been proven to be scalable and very effective in the chemical industry is liquid-liquid extraction. However, conventional oil-water solvents cannot typically be used in the liquid-liquid extraction process of biological materials because nonpolar solvents tend to denature biomolecules. Therefore, in order to capitalize on the benefits of liquid-liquid extraction, novel aqueous complex-fluid solvents must be used in the liquid-liquid extraction process because both phases contain predominantly water, and therefore, provide a mild environment for the biomolecules. Consequently, this thesis investigates the partitioning behavior of proteins and viruses in two-phase aqueous micellar systems (see Section 1.5).

Two-phase aqueous micellar systems also have the capability of separating biomolecules based on size (see the discussion in Section 1.4.3), which is a very desirable feature for both viral clearance and the production of gene therapy viruses. Liquid-liquid extraction is also attractive for preparative biochemistry because it can be performed without the large centrifugal forces encountered in centrifugation and ultracentrifugation. It may also involve less shear on the biomolecules when compared to filtration, ultrafiltration, and column chromatography because flows through small pores are not required. Accordingly, two-phase aqueous micellar systems have the potential of being used in the applications discussed in Section 1.1.

1.3 Two-Phase Aqueous Micellar Systems

This section provides useful background information regarding two-phase aqueous micellar systems. In Section 1.3.1, surfactants and the process of micellization are described. Section 1.3.2 provides details regarding phase separation in aqueous nonionic micellar solutions.

1.3.1 Surfactants and Micellization

Surfactant molecules, hereafter referred to as surfactants, are amphiphilic molecules composed of a hydrophilic or polar "head" and a hydrophobic or nonpolar "tail". Surfactants can be classified into three broad classes: (i) ionic (having either a positively-charged or negatively-charged head), (ii) nonionic (having a head that can hydrogen bond with water molecules), and (iii) zwitterionic (dipolar or having a head that has both positive and negative charges, therefore giving rise to a dipole moment). Sodium dodecyl sulfate (SDS), cetyltrimethylammonium bromide (CTAB), *n*-decyl tetra(ethylene oxide) ($C_{10}E_4$), and dioctanoyl phosphatidylcholine (C_8-lecithin) illustrate typical anionic (negatively-charged), cationic (positively-charged), nonionic, and zwitterionic surfactants, respectively,[42–44] and their chemical formulas are shown in Figures 1-1 and 1-2.

Surfactants in aqueous solution exhibit different types of behavior depending on their overall concentration. At surfactant concentrations below the critical micelle concentration (CMC), which varies with the surfactant, surfactants adsorb at the air-water interface and extend their hydrophobic tails into the air phase to minimize their contact with water. As a result, surfactants are surface active (hence the name surfactant). However, most surfactants also exhibit minimal solubility in the bulk aqueous phase, which is dependent

SDS: CH_3–$(CH_2)_{11}$–OSO_3^- Na^+

CTAB: CH_3–$(CH_2)_{15}$–$N(CH_3)_3^+$ Br^-

$C_{10}E_4$: CH_3–$(CH_2)_9$–$(OCH_2CH_2)_4$–OH

Figure 1-1: Examples of ionic and nonionic surfactants. Sodium dodecyl sulfate (SDS) and cetyltrimethylammonium bromide (CTAB) are examples of anionic and cationic surfactants, respectively, while *n*-decyl tetra(ethylene oxide) ($C_{10}E_4$) is an example of a nonionic surfactant.

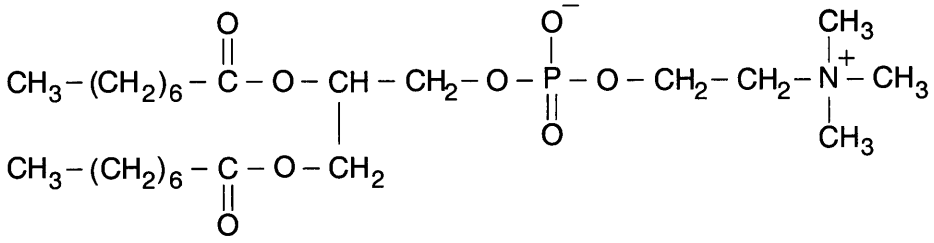

Figure 1-2: An example of a zwitterionic surfactant. For dioctanoyl phosphatidylcholine (C_8-lecithin), the negative charge is on the phosphate group, while the positive charge is on the amino group.

on the hydrophobic character of the surfactant tail. At surfactant concentrations above the CMC, surfactants form aggregates known as micelles, which can also be viewed as microscopic oily phases inside the macroscopic aqueous phase. In these micelles, the hydrophobic tails flock to the interior to minimize their contact with water and maximize their contact with other hydrophobic tails. The hydrophilic heads, on the other hand, remain on the periphery of the micelles to maximize their contact with water.[42]

Micellization in water results from a balance of intermolecular forces, including steric, electrostatic, hydrophobic, hydrogen bonding, and van der Waals interactions.[45,46] The main attractive force results from the hydrophobic effect associated with the hydrophobic tails (see the discussion below). The opposing repulsive force results from the steric (between hydrated nonionic heads) and electrostatic (between like-charged heads) interactions associated with the hydrophilic heads. Micellization occurs when the attractive force balances the repulsive force.

The hydrophobic effect is governed by the gain in entropy when contact between the hydrophobic tails and the water molecules is minimized. Although there is a loss in the translational entropy of the surfactant molecules when they form micelles, there is a significant increase in the translational entropy of the water molecules surrounding the hydrophobic tails. This increase in the translational entropy of the water molecules has the greater effect

because of the vastly greater number of water molecules. This gain in entropy is associated with the decrease in the number of structured clathrate "cages" that the water molecules form around the hydrophobic tails. It is this ability of water molecules to form these structured clathrate "cages" and maximize the number of hydrogen bonds in the presence of hydrophobic molecules which allows the hydrophobic molecules to be partially soluble. However, this ordering of water molecules near hydrophobic molecules decreases the number of configurations that the water molecules can have, and therefore, decreases their entropy.[45,46] When the contact between the hydrophobic tails and the water molecules is minimized by the process of micellization, the water molecules near the hydrophobic tails are liberated from these structured clathrate "cages", and there is an overall net gain in translational entropy. Although this gain in entropy is the dominant contribution to the hydrophobic effect, there is also an enthalpic contribution based on the enthalpic difference between water-water and water-tail interactions. Indeed, the attraction between water molecules is greater than that between water molecules and hydrophobic tails, because water molecules interact with each other through both hydrogen bonding and van der Waals attractions, while water molecules can only interact with the hydrophobic tails via van der Waals attractions.

Micelles can be spherical (or globular), cylindrical (or rodlike), or disc-like in the form of bilayers. Depending on the surfactant type and concentration, as well as on the solution conditions (such as temperature, ionic strength, pH), micelles can grow one-dimensionally as cylinders or two-dimensionally as bilayers or discs. Micellar growth is governed by the surfactant heads, because growth requires bringing the heads into close contact. Accordingly, ionic surfactants in the absence of salt generally exhibit minimal growth, and form spherical micelles as a result of the strong repulsive interactions between the equally charged surfactant heads. On the other hand, nonionic surfactants can exhibit significant growth, because the heads repel each other only through weaker steric, and not coulombic, interactions. For example, the nonionic surfactant $C_{10}E_4$, which will be used in this thesis to generate the two aqueous phases, forms cylinders and exhibits one-dimensional growth. Note that the micelles which can exhibit significant growth will also display a greater degree of polydisperisty than those which exhibit minimal growth.[47,48]

1.3.2 Phase Separation in Aqueous Micellar Solutions

For some micellar solutions, an isotropic, homogeneous micellar solution can phase separate into a micelle-rich phase coexisting with a micelle-poor phase. Since the surfactant concentration in both phases is greater than the CMC, there are micelles in both phases.

The average micelle size and the polydispersity of the micelles are different in the two phases because the concentration of surfactant in each phase is different, and as discussed in the previous section, surfactant concentration can influence micellar size. Knowledge of the coexistence or binodal curve of phase-separated micellar solutions is essential when working with these systems. The coexistence curve delineates the two-phase region from the one-phase region in a temperature-surfactant concentration phase diagram at constant pressure. The coexistence curve can either be concave upward or downward depending on whether phase separation is induced by increasing or decreasing the temperature, respectively. The minimum (maximum) in the coexistence curve is known as the lower (upper) consolute or critical point. The surfactant mole fraction and temperature corresponding to the critical point are known as the critical surfactant concentration, X_c, and the critical temperature, T_c.[43,44,47,49]

For some nonionic surfactants, such as those of the C_iE_j or alkyl poly(ethylene oxide) family, phase separation can be induced by increasing the temperature. Consequently, the coexistence curve is concave upward and the system exhibits a lower consolute point as shown schematically for $C_{10}E_4$ in Figure 1-3.[47,49–52] At a first glance, this seems counterintuitive, because one phase is generally favored (entropy dominates) as the temperature is increased, since:

$$G = H - TS \tag{1.2}$$

where G is the solution Gibbs free energy, H is the solution enthalpy, T is the absolute temperature, and S is the solution entropy. However, for micelles comprised of C_iE_j surfactants, the attractive interactions between the micelles increase as the temperature is increased.[43,44,47] This can be rationalized by recognizing that the hydrophilic ethylene oxide (E) units of the C_iE_j surfactants experience significant hydrogen bonding with water molecules. Accordingly, the ethylene oxide units are heavily hydrated. As the temperature is increased, the molecules in solution experience more thermal motion, and the strength of the hydrogen bonds is weakened due to the decrease in the directionality of the bonds. Since water molecules are "melted" away from the micelles, the micelles can establish closer contacts with each other and therefore experience greater attractive interactions. These attractive interactions allow the formation of a micelle-rich phase.[43,44]

For the case of $C_{10}E_4$, the top phase is micelle-rich, while the bottom phase is micelle-poor, as shown schematically in Figure 1-4. The $C_{10}E_4$ micelles, as discussed in Section 1.3.1, are cylindrical. Theoretically, a cylindrical micelle is modeled by our group as a spherocylinder, or a cylindrical body capped by two hemispheres.[53–55] The micelles in the top, micelle-

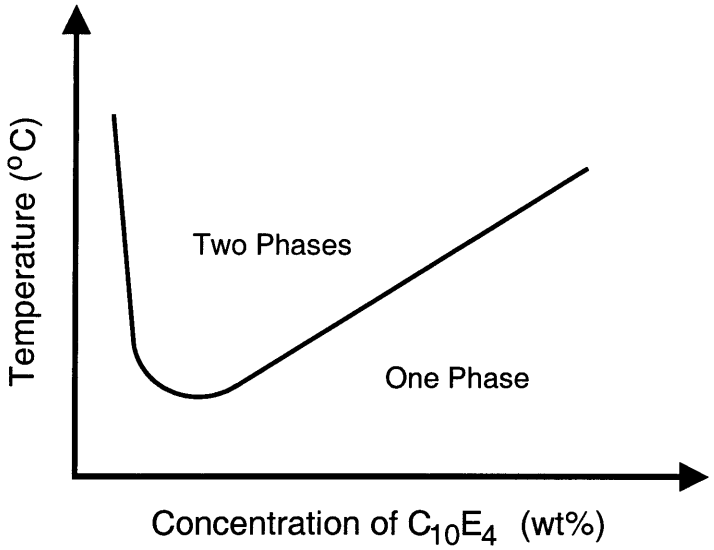

Figure 1-3: Schematic representation of the coexistence curve of the two-phase aqueous $C_{10}E_4$ micellar system.

rich phase are longer and more abundant than those in the bottom, micelle-poor phase. Note that Figure 1-4 is only a schematic representation, and that the water content in both phases is very high. The top, micelle-rich phase has at least 80 wt% water, while the bottom, micelle-poor phase has at least 98 wt% water.

1.4 Previous Applications Involving Two-Phase Aqueous Nonionic Micellar Systems

This section provides a brief review of past applications of two phase aqueous *nonionic* micellar systems. In Section 1.4.1, the use of two-phase aqueous nonionic micellar systems in extracting organic compounds and metal ions (after complexing them into sparingly water-soluble chelates) is discussed. Section 1.4.2 describes previous work regarding the separation of proteins based on hydrophobicity in two-phase aqueous nonionic micellar systems. In Section 1.4.3, the research performed previously by our group to extend the applications of two-phase aqueous nonionic micellar systems to include separating hydrophilic biomolecules based on size differences is discussed.

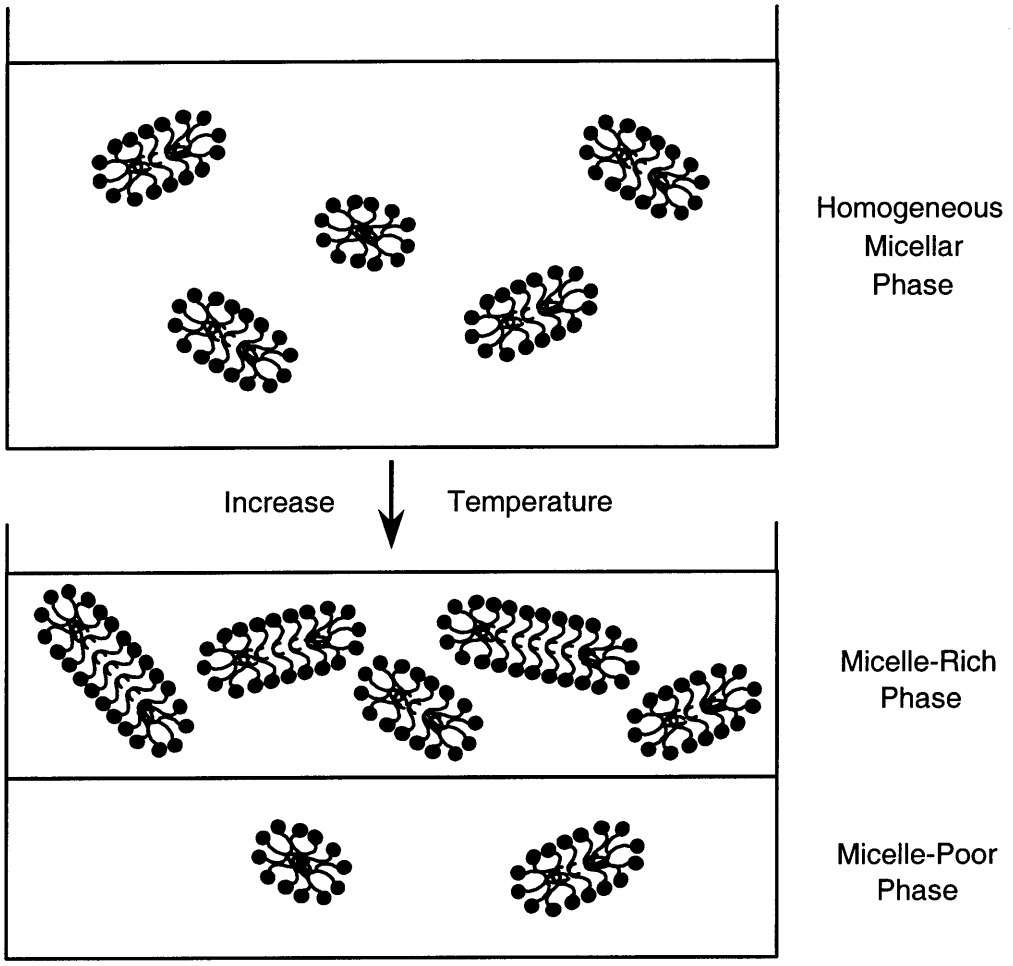

Figure 1-4: Schematic representation of the two-phase aqueous $C_{10}E_4$ micellar system. This system will also be referred to as the $C_{10}E_4$-buffer system. The black circle represents the surfactant hydrophilic head, while the black curved line represents the surfactant hydrophobic tail. This system exhibits a single phase at low temperatures, and phase separates at high temperatures into a micelle-rich phase coexisting with a micelle-poor phase.

1.4.1 Extracting Metal Chelates and Organic Compounds Based on Hydrophobicity

Metal chelates and organic compounds have limited water solubility. Therefore, they prefer to maximize their contact with the hydrophobic cores of the micelles and minimize their contact with water. Since the two phases in these micellar systems are micelle-rich and micelle-poor, these compounds are favorably extracted into the micelle-rich phase.[56–61] Accordingly, it is no surprise that the first application of two-phase aqueous nonionic micellar systems was the extraction of metal chelates. The concentration of metal chelates into the micelle-rich phase can act in conjuction with spectrophotometric or flow injection analysis to quantify the amount of trace metals in water and soil. For example, surfactant and a chelating agent (ligand) can be added to a water sample, which is suspected to have metals. The metal ions and ligands will first form metal chelates. These metal chelates will then be concentrated into the micelle-rich phase after the temperature is adjusted to form the two phases. Concentrating these metal chelates facilitates their quantification in a subsequent analytical step.[56] This method of complexing metal ions and then extracting them into the micelle-rich phase has been carried out experimentally utilizing nonionic surfactants such as Triton X-100 and PONPE-7.5. The metal chelates of Ni(II) ions with the ligands TAN (1-(2-thiazolylazo)-2-naphthol), PAN (1-(2-pyridylazo)-2-naphthol), and TAC (2-(2-thiazoylazo)-4-methylphenol) have been extracted into the micelle-rich phase of two-phase aqueous Triton X-100 micellar systems.[56,61] The metal complexes of Zn(II) ions with the ligands PAN, QADI (2-(8-quinolylazo)-4,5-diphenylbenzimidazole), PAMP (2-(2-pyridylazo)-5-methyphenol), and thiocyanate have been similarly extracted in two-phase aqueous PONPE-7.5 micellar systems.[56,59,60]

Organic compounds, due to their hydrophobic character, are also solubilized in the hydrophobic cores of the micelles. By the addition of surfactant to contaminated water and the subsequent adjustment of temperature, two-phase aqueous nonionic micellar systems can be generated, in which the organic compounds are concentrated in the micelle-rich phase. Such a procedure can aid in the detection of organic compounds and in the clean-up of contaminated water.[56–58] Some of the organic compounds which give rise to environmental problems include phenols, pesticides, and polycyclic aromatic hydrocarbons. The two-phase aqueous C_8E_3 micellar system has been used to extract 4-Chlorophenol, 2,4-dichlorophenol, 2,4,5-trichlorophenol, pentachlorophenol, benzene, toluene, *p*-xylene, and *o*-xylene into its micelle-rich phase. Fluoranthene has been similarly extracted in two-phase aqueous Triton X-100 micellar systems.[56]

1.4.2 Separating Proteins Based on Hydrophobicity

Since the two coexisting micellar phases contain at least 80 wt% water, two-phase aqueous nonionic micellar systems provide a mild and nondenaturing environment for proteins. The majority of the protein separation work in these systems has exploited differences in hydrophobicity.[56,62–68] Bordier was the first to separate proteins using two-phase aqueous nonionic micellar systems. Utilizing the Triton X-114 system, Bordier showed that hydrophilic, water-soluble proteins (serum albumin, catalase, ovalbumin, concanavalin A, myoglobin, and cytochrome *c*) preferentially partition into the micelle-poor phase, while hydrophobic or integral membrane proteins (acetylcholinesterase, bacteriorhodopsin, and cytochrome *c* oxidase) preferentially partition into the micelle-rich phase.[63] In practice, surfactant was first added to the buffer containing the proteins to generate the micelles. While still in the one-phase region, these micelles incorporated the hydrophobic, and not the hydrophilic, proteins. The temperature was then adjusted to form the two phases and to concentrate the hydrophobic proteins into the micelle-rich phase. Two-phase aqueous nonionic micellar systems have also been used in many other applications involving protein separations.[56] For example, large-scale purification of pyruvate oxidase from other enzymes, with 95% recovery into the micelle-rich phase, has been demonstrated using the Triton X-114 system.[56,62] Two-phase aqueous nonionic micellar systems may also be used to purify platelet compounds, since platelet glycoproteins have been found to partition favorably into the micelle-rich phase, while fibrinogen, albumin, and actin have been observed to partition favorably into the micelle-poor phase.[56,69]

1.4.3 Separating Hydrophilic, Water-Soluble Biomolecules Based on Size Differences

The potential for separating hydrophilic, water-soluble biomolecules based on size differences was first recognized by our group when the partitioning behavior of hydrophilic, water-soluble proteins (cytochrome *c*, ovalbumin, catalase, soybean trypsin inhibitor, and bovine serum albumin) was investigated in the two-phase aqueous micellar system composed of the nonionic surfactant $C_{10}E_4$.[70–74] The protein partition coefficient, K_p, defined as the ratio of the protein concentration in the top, micelle-rich phase, $C_{p,t}$, to that in the bottom, micelle-poor phase, $C_{p,b}$, that is,[75]

$$K_p \equiv \frac{C_{p,t}}{C_{p,b}} \tag{1.3}$$

was evaluated as a quantitative measure of the protein partitioning behavior. The hydrophilic, water-soluble proteins were found experimentally to partition preferentially into the bottom, micelle-poor phase, with partition coefficients, K_p, ranging between 0.1 and 1. The partition coefficients were also found experimentally to deviate further from 1, that is, approach 0.1, as the protein became larger or as the difference in the micellar concentrations of the two coexisting micellar phases became more pronounced. These experimental findings suggested that the observed protein partitioning behavior is driven by repulsive, steric, excluded-volume interactions between the proteins and the micelles. Specifically, hydrophilic, water-soluble proteins will partition preferentially into the bottom, micelle-poor phase where they experience fewer excluded-volume interactions with the micelles.[74] In addition, the protein partitioning behavior can also be understood from a purely entropic point-of-view, since the hydrophilic, water-soluble proteins partition preferentially into the bottom, micelle-poor phase where they can sample a greater number of configurations due to the larger available volume.[71] Based on this excluded-volume hypothesis, statistical thermodynamics was used to derive the following expression for the protein partition coefficient, K_p, in the two-phase aqueous micellar system composed of cylindrical $C_{10}E_4$ micelles:[70,71,74]

$$K_p = \exp\left[-(\phi_t - \phi_b)\left(1 + \frac{R_p}{R_0}\right)^2\right] \tag{1.4}$$

where ϕ_t and ϕ_b are the surfactant volume fractions in the top and bottom phases, respectively, R_p is the hydrodynamic radius of the protein, and R_0 is the cross-sectional radius of each cylindrical micelle (modeled as a spherocylindrical entity). The hydrodynamic radii of different proteins are available in the literature, while the cross-sectional radius of the cylindrical $C_{10}E_4$ micelle can be estimated from its molecular structure. The (ϕ_t - ϕ_b) values, on the other hand, can be obtained from the coexistence curve as follows. By selecting the partitioning temperature, an operating tie line can be drawn on the coexistence curve of the two-phase aqueous $C_{10}E_4$ micellar system as shown schematically in Figure 1-5. Accordingly, for this temperature, a solution having a $C_{10}E_4$ concentration corresponding to any position on the operating tie line will phase separate into two phases having $C_{10}E_4$ concentrations corresponding to the intersections of the horizontal operating tie line with the coexistence curve. In Figure 1-5, the weight percent concentrations of $C_{10}E_4$ in the top and bottom phases have been denoted ζ_t and ζ_b, respectively. Since both phases have densities of approximately 1 g/mL, weight percent concentrations are approximately equal to volume percent concentrations, and the value of (ϕ_t - ϕ_b) corresponds to the tie line length in Fig-

ure 1-5 divided by 100, that is, $(\zeta_t - \zeta_b)/100$. The division by 100 is necessary to convert between percents and fractions.[70–74]

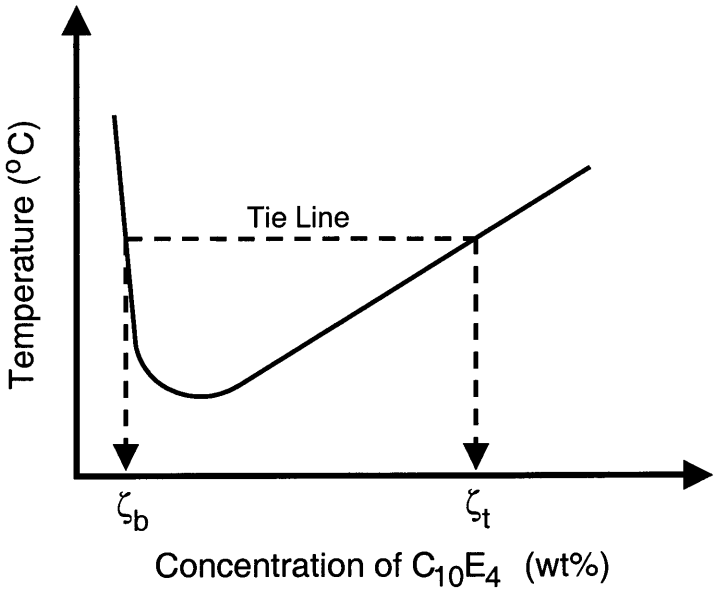

Figure 1-5: Schematic representation of an operating tie line on the coexistence curve of the two-phase aqueous $C_{10}E_4$ micellar system. The top, micelle-rich and bottom, micelle-poor phases connected by the operating tie line contain $C_{10}E_4$ at ζ_t wt% and ζ_b wt%, respectively.

The predictions from the excluded-volume theory (Eq. (1.4)) were compared to the experimentally measured protein partition coefficients.[70–73] As shown in Figures 1-6, 1-7, and 1-8, reasonable agreement was achieved between the theoretically predicted and experimentally measured partition coefficients of cytochrome *c*, ovalbumin, and catalase. Good agreement between the theoretically predicted and experimentally measured protein partition coefficients can also be seen by plotting the protein partition coefficient, K_p, as a function of R_p/R_0 for a fixed temperature,[70] as shown in Figure 1-9. Accordingly, it was concluded that the partitioning behavior of hydrophilic, water-soluble proteins in the two-phase aqueous $C_{10}E_4$ micellar system is primarily driven by steric, excluded-volume interactions between the proteins and the micelles.

Figure 1-9 suggests that hydrophilic, water-soluble biomolecules having a relatively large size, with radii exceeding 100 Å, should distribute extremely unevenly between the two coexisting micellar phases and partition strongly into the micelle-poor phase.[70–74] To test this hypothesis, the partitioning of viruses, which have radii on the order of 100 Å, was

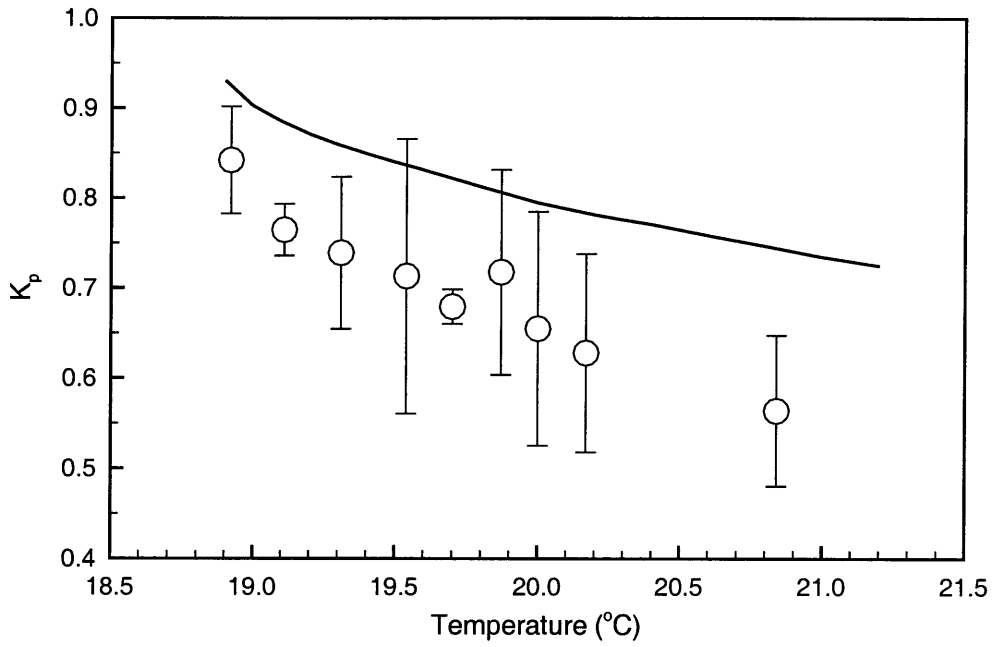

Figure 1-6: Comparison between the theoretically predicted and experimentally measured partition coefficients of cytochrome *c*. The solid line corresponds to the partition coefficients that were predicted based on the excluded-volume theory. The white circle symbols correspond to the partition coefficients of cytochrome *c* that were measured previously.[70,73] The error bars represent 95% confidence limits for the measurements.

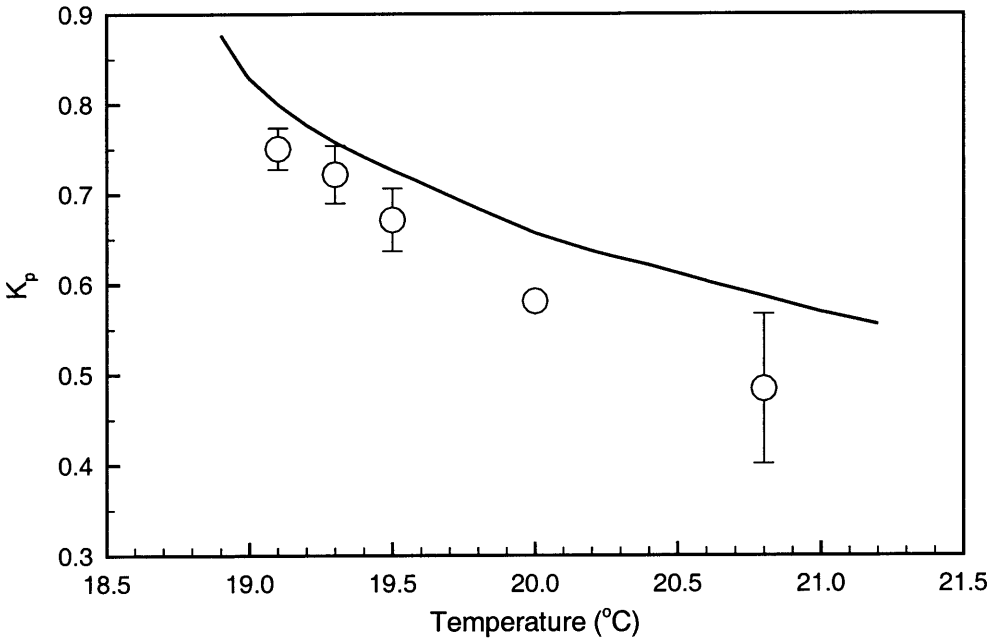

Figure 1-7: Comparison between the theoretically predicted and experimentally measured partition coefficients of ovalbumin. The solid line corresponds to the partition coefficients that were predicted based on the excluded-volume theory. The white circle symbols correspond to the partition coefficients of ovalbumin that were measured previously.[70,73] The error bars represent 95% confidence limits for the measurements.

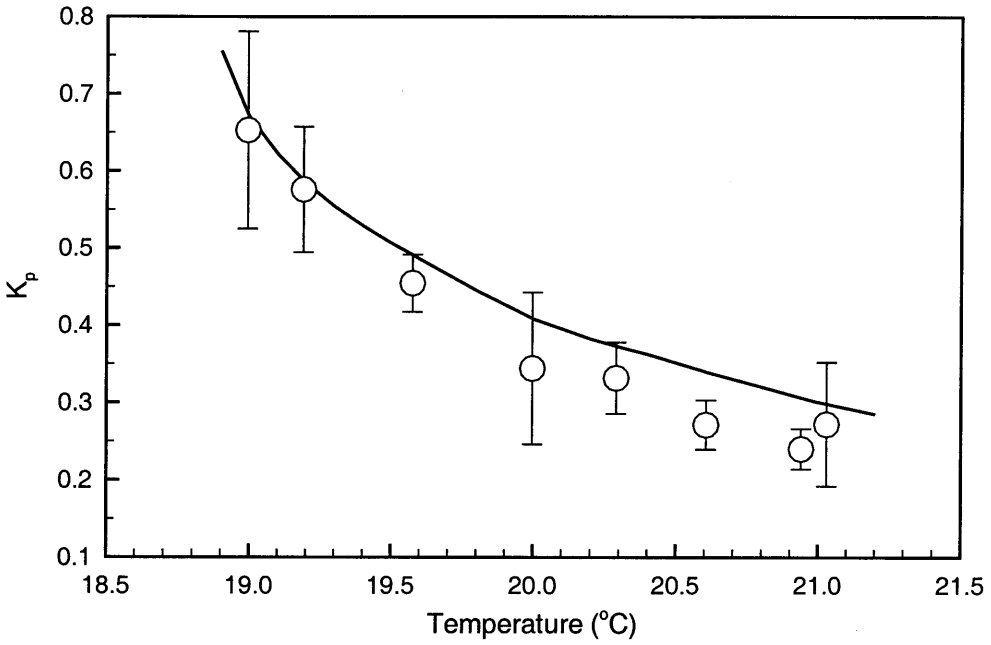

Figure 1-8: Comparison between the theoretically predicted and experimentally measured partition coefficients of catalase. The solid line corresponds to the partition coefficients that were predicted based on the excluded-volume theory. The white circle symbols correspond to the partition coefficients of catalase that were measured previously.[70,73] The error bars represent 95% confidence limits for the measurements.

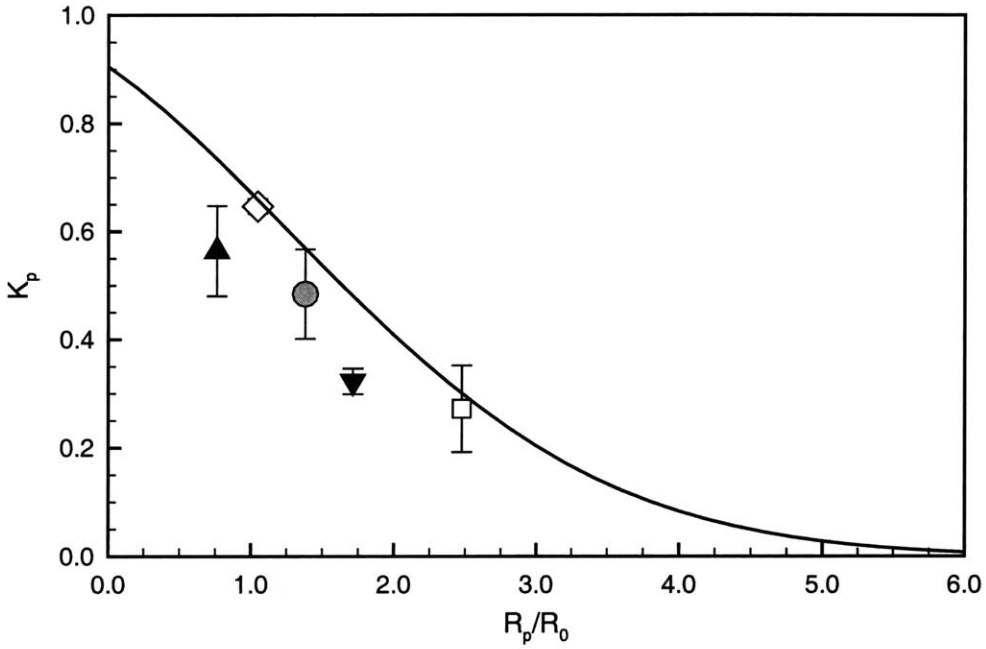

Figure 1-9: The protein partition coefficient, K_p, as a function of the ratio, R_p/R_0, in the two-phase aqueous $C_{10}E_4$ micellar system. R_p is the protein hydrodynamic radius obtained from various sources in the literature.[76,77] R_0 is the cross-sectional radius of a $C_{10}E_4$ cylindrical micelle, which has been estimated to be 21 Å.[70,71] The $(\phi_t - \phi_b)$ value at the partitioning temperature of 21°C is 0.10. The solid line corresponds to the partition coefficients that were predicted based on the excluded-volume theory. The various symbols correspond to the partition coefficients that were measured previously[70,73] for the following proteins: cytochrome *c* (R_p=16 Å, black triangle), soybean trypsin inhibitor (R_p=22 Å, white diamond), ovalbumin (R_p=29 Å, gray circle), bovine serum albumin (R_p=36 Å, black inverted triangle), and catalase (R_p=52 Å, white square). The error bars represent 95% confidence limits for the measurements.

examined, where the viral partition coefficient, K_v, is defined as follows:[75]

$$K_v \equiv \frac{C_{v,t}}{C_{v,b}} \tag{1.5}$$

where $C_{v,t}$ and $C_{v,b}$ denote the viral concentrations in the top and bottom phases, respectively.

The viruses that were partitioned were bacteriophages ϕX174, P22, and T4.[70,78] All three bacteriophages are protein-coated and non-enveloped, that is, their exterior is comprised of proteins and not of a phospholipid bilayer. Bacteriophage ϕX174 has an icosahedral capsid, spikes located at each of its twelve vertices, a radius of 180 Å, and single-stranded DNA.[79–81] Bacteriophage P22 has an icosahedral capsid, a short neck with attached tailspikes, a radius of 300 Å, and double-stranded DNA.[81–87] Bacteriophage T4, which also has double-stranded DNA, is more complicated in shape. It has a width of about 850 Å, a capsid length of 1150 Å, an average, uncontracted tail sheath length of 950 Å, and six long tail fibers (1400 Å $\times$ 25 Å) which come out of the tail sheath.[79,81,88] The effective hydrodynamic radius of bacteriophage T4 has been determined to be 750 Å.[80]

The experimentally measured partition coefficients for the three bacteriophages are shown in Figures 1-10, 1-11, and 1-12. As expected *qualitatively*, all three bacteriophages partitioned much more strongly into the bottom, micelle-poor phase than any of the water-soluble proteins studied, which indicates that the two-phase aqueous $C_{10}E_4$ micellar system is capable of separating hydrophilic biomolecules based on size. However, as shown in Figures 1-11 and 1-12, the theoretically predicted and experimentally measured partition coefficients differ by orders of magnitude for bacteriophages P22 and T4. Even for bacteriophage ϕX174 (see Figure 1-10), there is a discrepancy between the theoretically predicted and experimentally measured partition coefficients, especially as the difference in the micellar concentrations of the two coexisting micellar phases increases, that is, as the temperature increases. Specifically, all the viral partition coefficients plateau at about 10^{-3} to 10^{-2}. Accordingly, the partitioning of viruses in the two-phase aqueous $C_{10}E_4$ micellar system is not yet understood. However, if the mechanisms that are preventing the viruses from partitioning according to the excluded-volume theory can be identified, they may be eliminated in the future to attain viral partition coefficients that are close to the extreme partition coeffiicents predicted by the excluded-volume theory. This, in turn, can enhance the separation of proteins from viruses. Accordingly, one part of this thesis, as discussed in Section 1.5 below, focused on challenging the underlying assumptions of the excluded-volume theory to fundamentally understand viral partitioning in the two-phase aqueous $C_{10}E_4$ micellar system.

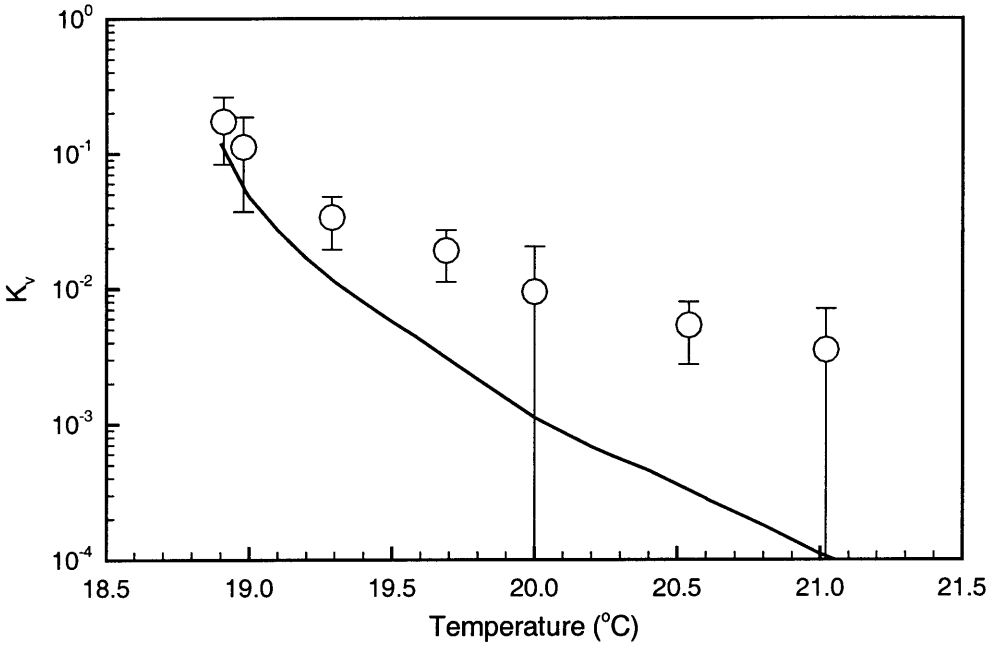

Figure 1-10: Comparison between the theoretically predicted and experimentally measured partition coefficients of bacteriophage ϕX174. The solid line corresponds to the partition coefficients predicted based on the excluded-volume theory. The white circle symbols represent the partition coefficients of bacteriophage ϕX174 that were measured previously.[70] The error bars, which correspond to 95% confidence limits for the measurements, appear asymmetric due to the use of a semi-logarithmic plot.

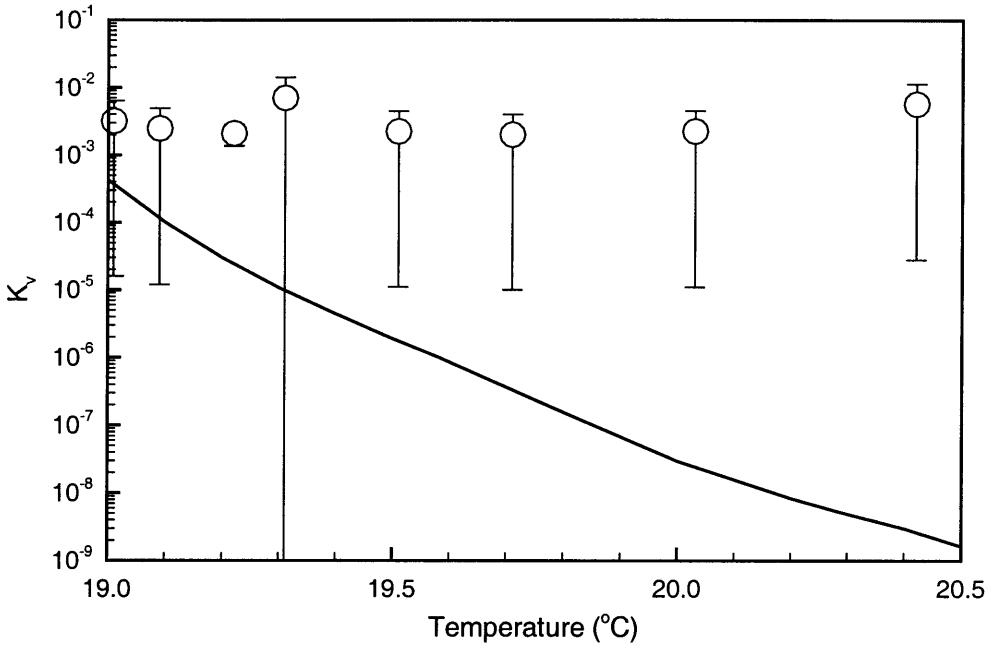

Figure 1-11: Comparison between the theoretically predicted and experimentally measured partition coefficients of bacteriophage P22. The solid line corresponds to the partition coefficients predicted based on the excluded-volume theory. The white circle symbols represent the partition coefficients of bacteriophage P22 that were measured previously.[70] The error bars, which correspond to 95% confidence limits for the measurements, appear asymmetric due to the use of a semi-logarithmic plot.

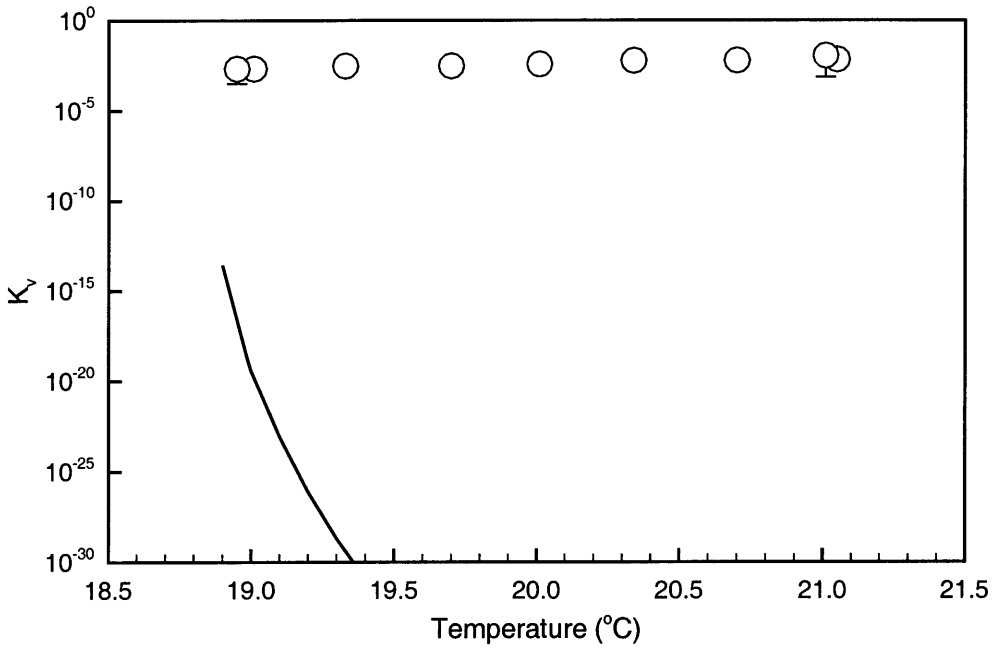

Figure 1-12: Comparison between the theoretically predicted and experimentally measured partition coefficients of bacteriophage T4. The solid line corresponds to the partition coefficients predicted based on the excluded-volume theory. The white circle symbols represent the partition coefficients of bacteriophage T4 that were measured previously.[70] The error bars, which correspond to 95% confidence limits for the measurements, appear asymmetric due to the use of a semi-logarithmic plot.

1.5 Thesis Overview

In an effort to achieve good separation of protein from virus using two-phase aqueous micellar systems, this thesis investigated two directions that were pursued simultaneously. Although *Directions A* and *B* will be discussed in more detail below, the overall objective of this thesis was to develop a fundamental understanding of protein and viral partitioning in two-phase aqueous micellar systems. It should also be noted that, to the best of our knowledge, no other research group has investigated the utilization of two-phase aqueous micellar systems for the removal and/or concentration of viruses from proteins.

Model surfactants, water-soluble proteins, and protein-coated viruses were selected to focus the studies that were conducted in this thesis. However, many of the results and conclusions presented in this thesis can be generalized to other surfactants, water-soluble proteins, and protein-coated viruses. For example, the results obtained with the nonionic surfactant $C_{10}E_4$ should also be applicable to other nonionic surfactants that form cylindrical micelles and phase separate in aqueous solutions. Although more experiments are required to fully demonstrate this generalization, they are beyond the scope of this thesis.

As discussed in Section 1.4.3, the viral partition coefficients predicted theoretically using the excluded-volume theory are orders of magnitude lower than the experimentally measured values. Accordingly, viral partitioning in the two-phase aqueous $C_{10}E_4$ micellar system is not yet fully understood. The central objective of *Direction A* of this thesis was to determine other possible mechanisms that are governing viral partitioning in the two-phase aqueous $C_{10}E_4$ micellar system. By identifying these mechanisms, they may, if possible, be eliminated in the future to yield the extreme viral partition coefficients predicted by the excluded-volume theory. If these extreme viral partition coefficients can be attained experimentally, the separation of protein from virus can be enhanced. Since the excluded-volume theory is capable of predicting reasonably well the partition coefficients of water-soluble proteins, our approach to determining other possible mechanisms was based on challenging the assumptions underlying the excluded-volume theory in order to identify the assumptions that are valid for water-soluble proteins but not for viruses. In other words, the search for other possible mechanisms was similar to the search for the culprits in a murder mystery, where the biggest "clue" was that the "suspect" mechanisms significantly influence viral partitioning, while having little or no impact on protein partitioning.

The research conducted in *Direction A* is described in Part II of this thesis, that is, Chapters 2, 3, 4, and 5. Specifically, Chapters 2 and 3 describe the experimental studies that were performed to investigate the possible existence of attractive interactions between the

tailspikes of bacteriophage P22 and the $C_{10}E_4$ micelles. Bacteriophage P22 was selected as the model virus, since: (i) it is readily available in high purity from Professor Jonathan King's laboratory, (ii) it is safer to employ than mammalian viruses, and (iii) its concentration can be measured with good accuracy using the plaque assay. These possible attractive interactions involving the tailspikes of bacteriophage P22 were investigated because: (i) the excluded-volume theory assumes that only repulsive, excluded-volume interactions operate between the micelles and the partitioning solute, and (ii) the previously studied water-soluble proteins were not expected to have similar attractive interactions for reasons discussed in Chapter 2. Possible attractive interactions could counter the excluded-volume interactions, and allow more of the viral particles to remain in the top, micelle-rich phase. This, in turn, would result in the measured viral partition coefficients being larger than those predicted based on the excluded-volume theory, which was observed experimentally. Chapter 2 presents the competitive inhibition study that was performed to compete *Salmonella typhimurium* cells and the $C_{10}E_4$ micelles for the tailspikes of bacteriophage P22. In Chapter 3, a "cleaner," follow-up experimental study is described. In this study, the capsids of bacteriophage P22 without the tailspikes were synthesized and partitioned. The partitioning behavior of the capsids was then compared to that of intact bacteriophage P22 particles with tailspikes.

Chapter 4 describes the double-stage partitioning study that was conducted to investigate possible attractive interactions between the capsids of bacteriophage P22 and the $C_{10}E_4$ micelles. These possible attractive interactions were examined because the capsid of bacteriophage P22 is comprised of approximately 420 proteins. Accordingly, these capsids have a greater tendency of exhibiting heterogeneous surface properties than the previously studied water-soluble proteins, and certain groups of capsids may exist which have strong attractive interactions with the $C_{10}E_4$ micelles.

In Chapter 5, an investigation of another underlying assumption of the excluded-volume theory is presented. Specifically, the excluded-volume theory assumes that macroscopic phase separation equilibrium is attained in the two-phase aqueous $C_{10}E_4$ micellar system. Macroscopic phase separation equilibrium refers to the condition in which *all* the micelle-rich and micelle-poor domains, which are formed at the onset of phase separation, are in their corresponding macroscopic phases prior to withdrawing the top and bottom phases. However, this may not be true experimentally, since there could be micelle-poor domains entrained in the macroscopic, top, micelle-rich phase, as well as micelle-rich domains entrained in the macroscopic, bottom, micelle-poor phase. Consequently, the concentration of viral particles measured in each phase could be affected by the presence of these entrained domains. In

accordance with the biggest "clue" concept, the concentration of protein in each phase, on the other hand, was expected to be negligibly affected by these entrained domains (see the discussion in Chapter 5). This chapter describes protein and viral partitioning experiments that were conducted at different experimental conditions, where the degree of entrainment was varied. A new theoretical description of partitioning was also developed in this chapter, and the theoretical predictions were compared to the experimentally measured protein and viral partition coefficients.

While the mechanisms governing viral partitioning were being investigated in the context of *Direction A*, *Direction B* of this thesis was being pursued simultaneously. *Direction B*, which corresponds to Part III of this thesis (Chapters 6, 7, 8, and 9), centered around the less optimistic point-of-view that the viral partition coefficients would not decrease below the observed values of 10^{-3} to 10^{-2} in the two-phase aqueous $C_{10}E_4$ micellar system. However, even with these viral partition coefficients, the virus is generally excluded more strongly than the protein into the bottom, micelle-poor phase. Accordingly, Chapter 6 describes our investigation of manipulating the volume ratio, which is a key operating parameter in liquid-liquid extraction, to attain good separation of lysozyme (model protein) from bacteriophage P22 (model virus). Specifically, lysozyme was recovered in the top, micelle-rich phase, while bacteriophage P22 was recovered in the bottom, micelle-poor phase.

Since only steric, excluded-volume interactions between the proteins and the micelles have been exploited until now, introducing another mode of interaction to attract or "fish" the proteins into the top, micelle-rich phase may further improve the separation of protein from virus. Electrostatic interactions were introduced in Chapter 7 by the addition of the anionic surfactant SDS to the aqueous $C_{10}E_4$ solution. An experimental study was conducted to demonstrate proof-of-principle that two-phase aqueous mixed (nonionic/ionic) micellar systems can indeed be used to modulate both electrostatic and excluded-volume interactions between the proteins and the micelles. A theory was also developed, which incorporated the dominant interactions, namely, the excluded-volume and electrostatic interactions, between the proteins and the mixed micelles. To test the ability of the theory to capture the underlying physics involved in protein partitioning, the theoretically predicted protein partition coefficients were compared to the experimentally measured ones.

Chapter 8 presents some examples of using the theory developed in Chapter 7 to develop useful design strategies to optimize the protein partition coefficient without conducting any experiments. Since an analytical expression is available for the protein partition coefficient, the theory can be used to quickly ascertain the relative importance of various experimentally

controllable variables that can affect the protein partition coefficient. Possible coupled effects between three of the variables were also investigated using the theory in a 2^3 factorial design. A theoretical response surface was also generated for the protein partition coefficient as a function of two of the variables that were found to have a strong coupled effect from the theoretical design. The theory was also extended in this chapter to include: (i) ionic surfactants with charges located beyond the hydrophilic heads of the nonionic surfactants, and (ii) zwitterionic surfactants in place of nonionic surfactants.

In Chapter 9, the experimental study involving the separation of lysozyme from bacteriophage P22 in different two-phase aqueous mixed ("noncharged"/ionic) micellar systems is presented. The "noncharged" surfactants that were investigated include $C_{10}E_4$ and C_8-lecithin, while the ionic surfactants that were examined include SDS and SDE_6S (sodium dodecyl hexa(ethylene oxide) sulfate). The yields of lysozyme and bacteriophage P22 in the top and bottom phases, respectively, were measured to determine the effect of introducing an ionic surfactant on the separation efficiency.

Finally, Part IV (Chapter 10) provides a summary of the thesis. In addition, possible directions for future research and concluding remarks are presented.

PART II

UNDERSTANDING VIRAL PARTITIONING IN THE TWO-PHASE AQUEOUS $C_{10}E_4$ MICELLAR SYSTEM

Chapter 2

Competitive Inhibition Study to Investigate Possible Attractive Interactions between the Tailspikes of Bacteriophage P22 and the $C_{10}E_4$ Micelles

2.1 Introduction

As discussed in Chapter 1, the partitioning behavior of viruses cannot be fully explained by considering solely the excluded-volume interactions that operate between the $C_{10}E_4$ micelles and the viruses. *Direction A* of this thesis was therefore aimed at determining other possible mechanisms, in addition to the excluded-volume interactions, that govern viral partitioning in the two-phase aqueous $C_{10}E_4$ micellar system. Since the excluded-volume theory is capable of predicting reasonably well the partition coefficients of water-soluble proteins, our approach to determining other possible mechanisms was based on challenging the assumptions underlying the excluded-volume theory in order to identify the assumptions that are valid for water-soluble proteins but not for viruses. In other words, the search for other possible mechanisms was similar to the search for the culprits in a murder mystery, where the biggest "clue" was that the "suspect" mechanisms significantly influence viral partitioning, while having little or no impact on protein partitioning.

One of the major assumptions of the excluded-volume theory (as discussed in Chapter 1) is that only repulsive, excluded-volume interactions operate between the micelles and the partitioning solute. However, possible attractive interactions that operate between the micelles and the viruses, but not between the micelles and the previously studied water-soluble proteins, may be present. These possible attractive interactions may counter the excluded-volume interactions, and allow more of the viruses to remain in the top, micelle-rich phase.

This, in turn, would result in the measured viral partition coefficients being larger than those predicted based on the excluded-volume theory, which is what is observed experimentally. In this study, one such possible attractive interaction was experimentally investigated.

Bacteriophage P22 was selected as our model virus because: (i) its experimentally measured partition coefficients differ significantly from its predicted ones (see Figure 1-11), (ii) it is readily available in high purity from Professor Jonathan King's laboratory, (iii) it is safer to use than mammalian viruses, and (iv) its concentration can be measured with reasonable accuracy using the plaque assay described in Section 2.2.4. Bacteriophage P22 is a protein-coated virus, with proteins comprising its icosahedral capsid, short neck, and tailspikes.[82–86] The capsid contains double-stranded DNA,[81,85,87] and a schematic representation of bacteriophage P22 is shown in Figure 2-1. In order to find its host bacterium, *Salmonella typhimurium*, the tailspikes of bacteriophage P22 seek and recognize lipopolysaccharide receptors on the outer membrane of the bacterium.[82,83,89–93] Although the tailspikes are known to have a biospecific affinity towards the polysaccharide portion of the receptors,[82,83,89–93] they still may exhibit attractive interactions with the lipid portion of the lipopolysaccharide. Accordingly, it is possible that attractive interactions may also exist between the tailspikes of bacteriophage P22 and the hydrophobic lipid-like moieties of the $C_{10}E_4$ surfactant molecules. In addition, the tailspikes of bacteriophage P22 may have attractive interactions with the outer membrane of the bacterium as well, since the bacteriophage P22 particle physically resides on the membrane during infection. Therefore, similar attractive interactions may also exist between the tailspikes and the $C_{10}E_4$ micelles, since the structure of the micelles resembles that of membranes, which are phospholipid bilayers. The water-soluble proteins discussed in Chapter 1, however, do not have such an affinity for lipopolysaccharide receptors, and they also do not physically reside on the cell membrane. Consequently, these possible attractive interactions between the tailspikes of bacteriophage P22 and the $C_{10}E_4$ micelles should not operate between the previously studied water-soluble proteins and the $C_{10}E_4$ micelles. Indeed, this is one possible mechanism that can significantly influence the partitioning behavior of bacteriophage P22, while negligibly affecting the partitioning behavior of the water-soluble proteins.

In this experimental study, the kinetics associated with bacteriophage P22 infection of *Salmonella typhimurium* was investigated in the presence and in the absence of $C_{10}E_4$. The purpose of the study was to determine whether the presence of $C_{10}E_4$ would inhibit or slow down the normal bacteriophage P22 infection process due to the possible binding of the tailspikes of bacteriophage P22 to the $C_{10}E_4$ micelles.

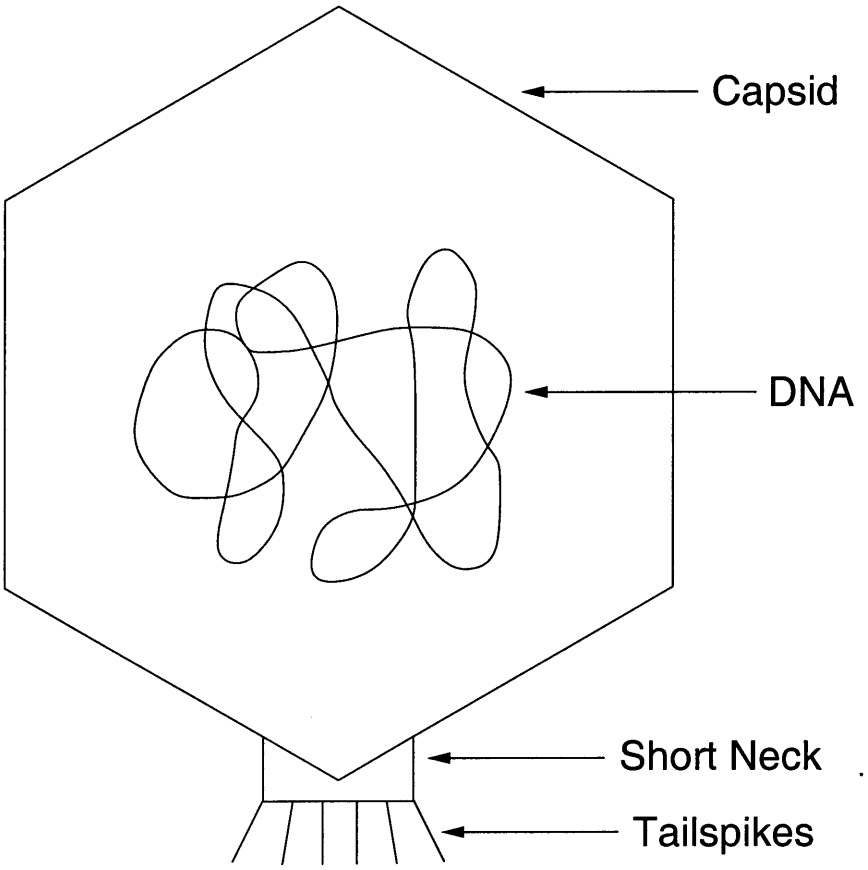

Figure 2-1: Schematic representation of bacteriophage P22.

The remainder of this chapter is organized as follows. Section 2.2 provides details of the materials and experimental methods utilized in this study. In Section 2.3, the experimental results are presented and discussed. Finally, concluding remarks are presented in Section 2.4.

2.2 Materials and Methods

2.2.1 Materials

Homogeneous *n*-decyl tetra(ethylene oxide) ($C_{10}E_4$) (lot no. 1006) was purchased from Nikko Chemicals (Tokyo, Japan). Bacteriophage P22 (5^-am/13^-am) and the host bacteria *Salmonella typhimurium* strains DB7136 and DB7155[86,94] were obtained from Professor Jonathan King's laboratory. Citric acid (lot no. 0616 KCXK) and magnesium sulfate ($MgSO_4$) (lot no. 6070 A31581) were purchased from Mallinckrodt (Paris, KY). Disodium phosphate (lot no. 896726) was obtained from Fisher Scientific (Fair Lawn, NJ). All these materials were used as received. All solutions were prepared using pH 7.2 McIlvaine's buffer consisting of 16.4 mM disodium phosphate and 1.82 mM citric acid in Milli-Q water. Milli-Q water is the product of passing deionized water through Millipore's (Bedford, MA) Milli-Q system. All glassware used in the experiments were subjected to washing in a 50:50 ethanol:1 M sodium hydroxide bath, washing in a 1 M nitric acid bath, rinsing copiously with Milli-Q water, and drying in an oven for at least one day.

The DNA of bacteriophage P22 (5^-am/13^-am) has two premature amber stop codons in genes 5 and 13, which prevent the complete synthesis of the coat protein (gene 5) and an enzyme necessary for cell lysis (gene 13), respectively. Therefore, once a bacteriophage P22 particle infects a DB7136 cell during the competitive inhibition experiment, it is not able to replicate into intact and infective particles, and it also cannot lyse the cell. Only incomplete bacteriophage parts accumulate in the infected DB7136 cells, and the original particle can no longer be detected. Therefore, only the bacteriophage P22 particles free in solution, that is, those which have not infected DB7136 cells, can be quantified in the plaque assay (described in Section 2.2.4 below). However, in order to implement the plaque assay, the free bacteriophage P22 particles must be able to replicate into intact and infective phage particles, and must also be able to lyse cells. Therefore, DB7155 cells were used in the plaque assay because, unlike the DB7136 cells, they are able to "read through" the amber (UAG) stop codons (their tRNA is mutated such that it inserts a glutamine amino acid for each amber stop codon) and allow complete synthesis of the proteins encoded by genes 5 and 13.

2.2.2 Stability of DB7136 Cells in $C_{10}E_4$ Solutions

During the actual competitive inhibition test (see Section 2.2.3 below), DB7136 cells were exposed to $C_{10}E_4$ concentrations ranging from 0 to 7.19 wt%. 7.19 wt% was chosen as the highest $C_{10}E_4$ concentration because it is comparable to the highest $C_{10}E_4$ concentration previously encountered by bacteriophage P22 in the top, micelle-rich phase of the two-phase aqueous $C_{10}E_4$ micellar system.[70] Since a viable population of DB7136 cells was required for the competitive inhibition test, the stability of DB7136 cells in the presence of $C_{10}E_4$ was investigated first.

The stability of DB7136 cells in five solutions, each containing a different concentration of $C_{10}E_4$, was examined. Specifically, for each solution, the concentration of viable bacteria was monitored over a 30 minute period, which corresponded to the duration of the competitive inhibition test. The competitive inhibition test is completed after 30 minutes because the cells double, or reproduce, in 30 minutes, thereby changing the experimental conditions. At the start of the stability experiment (t=0), 0.1 mL of a concentrated DB7136 cell solution was added to 0.9 mL of a buffered solution containing a certain concentration of $C_{10}E_4$. The resulting bacterium concentration in each solution was about 1×10^8 cells/mL. The resulting $C_{10}E_4$ concentrations in the five solutions were 0 wt% (the control), 0.891 wt%, 4.31 wt%, 5.97 wt%, and 7.51 wt% (which was greater than the highest concentration of $C_{10}E_4$ used in the competitive inhibition test). A 0.05 mL aliquot of each solution was then sampled at 30-second, 10-minute, and 30-minute intervals in order to monitor the viable bacterium concentration during the 30-minute period. The viable bacterium concentration in each 0.05 mL sample was determined by: (i) diluting each sample to an appropriate concentration of DB7136 cells, (ii) mixing a certain volume of the diluted sample with nutrients, such as, yeast extract and tryptone, (iii) pouring this mixture onto a petri dish containing agar, (iv) incubating the contents of the dish overnight, (v) counting the number of bacterial colonies that have formed, (vi) recognizing that each visible colony originated from a single intact or live cell, and (vii) multiplying the number of colonies by the dilution factor used in (i).

2.2.3 Competitive Inhibition Test

In the competitive inhibition test, four 0.9 mL buffered solutions were prepared containing bacteriophage P22 and varying concentrations of $C_{10}E_4$. The bacteriophage P22 particles were incubated in the $C_{10}E_4$ solutions at 25°C for at least one hour to allow any binding, if any, to occur between the bacteriophage P22 particles and the $C_{10}E_4$ micelles. During this incubation period and throughout the competitive inhibition test, the solutions were

maintained at 25°C in a NAPCO 220 water bath. A 0.05 mL sample was taken from each of these solutions prior to beginning the competitive inhibition test in order to determine the concentration of bacteriophage P22 present originally in each solution. To begin the competitive inhibition test (t=0), 0.1 mL of a concentrated DB7136 cell solution was added into each of the solutions. The resulting overall concentration of DB7136 cells in each solution was 4.9×10^8 cells/mL. The overall concentrations of $C_{10}E_4$ and bacteriophage P22 are summarized in Table 2-1. The concentrations of $C_{10}E_4$ were chosen to ensure the presence of micelles in the solutions, since the critical micelle concentration of $C_{10}E_4$ is 0.023 wt% at 25°C.[95] As discussed in Section 2.2.2, 7.19 wt% was selected as the highest $C_{10}E_4$ concentration because it was comparable to the highest surfactant concentration previously encountered by bacteriophage P22 in the top, micelle-rich phase of the two-phase aqueous $C_{10}E_4$ micellar system.[70] The concentrations of bacteriophage P22 were also chosen to be similar to those used in previous partitioning experiments.[70,78] It should also be noted that the overall concentration of Mg^{+2} (from $MgSO_4$ in the purified bacteriophage P22 solution, as well as from the added $MgSO_4$) was 2 mM in each solution. This divalent cation is required at this concentration to ensure the stability of bacteriophage P22. Specifically, the cation reduces the electrostatic repulsive interactions between the negatively-charged phosphate groups of the double-stranded DNA inside the capsid, which have the potential of repelling each other so strongly that they can burst open the capsid. Based on the concentrations of the DB7136 cells and the bacteriophage P22 particles in each solution, the multiplicity of infection, MOI, was evaluated for each solution. The MOI is defined as follows:

$$MOI \equiv \frac{initial\ viral\ concentration}{initial\ bacterium\ concentration} \tag{2.1}$$

The MOI values for the four solutions are also shown in Table 2-1. The MOI values were chosen to be close to unity so that there would be, on average, about one bacteriophage P22 particle per DB7136 cell, which in turn, implies that each bacteriophage P22 particle would not need to diffuse far in order to encounter and infect a DB7136 cell.

After beginning the competitive inhibition test with the addition of the DB7136 cells, a 0.05 mL aliquot from each of the solutions was withdrawn at the following time intervals: 1, 2, 4, 6, 8, 10, 15, and 30 minutes. As discussed in Section 2.2.2, the duration of the competitive inhibition test is 30 minutes. The concentrations of free bacteriophage P22 particles, that is, those that have not infected DB7136 cells, were determined for all the solutions at each time point using the plaque assay described in Section 2.2.4 below. Then, for each solution, the concentration of free bacteriophage P22 particles at each time point was normalized

Table 2-1: The conditions of the first competitive inhibition test.

Concentration of $C_{10}E_4$ (wt%)	Concentration of Bacteriophage P22 (particles/mL)	MOI
0	5.4×10^8	1.1
0.796	3.0×10^8	0.61
3.98	4.2×10^8	0.86
7.19	3.1×10^8	0.63

with respect to the initial concentration of bacteriophage P22 present in the solution just prior to beginning the competitive inhibition test. The fraction of free bacteriophage P22 particles was then plotted as a function of sampling time for each solution in order to examine the kinetics of the infection process. The fraction (or *normalized* concentration) of free bacteriophage P22 particles, instead of the *actual* concentration of free bacteriophage P22 particles, was used because the initial concentrations of bacteriophage P22 in the four solutions were different. Accordingly, by evaluating the fraction of free bacteriophage P22 particles, all the solutions were compared on an equal basis.

Another competitive inhibition test was conducted with lower MOI values. The lower MOI values were used to increase the average number of DB7136 cells per bacteriophage P22 particle, and therefore, to ensure that each bacteriophage P22 particle had the opportunity to easily diffuse and infect a DB7136 cell. In other words, lower MOI values were selected to ensure that any possible diffusional limitations were removed. Diffusional limitations were undesirable because they could lead to many bacteriophage P22 particles being free in the solution, which in turn, would prevent a good comparison of the kinetics of different infection processes. In this second competitive inhibition test, two 0.9 mL buffered solutions were prepared containing bacteriophage P22 and two different concentrations of $C_{10}E_4$. To begin this competitive inhibition test (t=0), 0.1 mL of a concentrated DB7136 cell solution was added into each of the solutions. The resulting overall concentration of DB7136 cells in each solution was 1.0×10^9 cells/mL. The overall concentrations of $C_{10}E_4$ and bacteriophage P22 in the two solutions, along with the MOI values, are shown in Table 2-2. Each solution also contained 2 mM Mg^{+2} (from $MgSO_4$ in the purified bacteriophage P22 solution, as well as from the added $MgSO_4$) in order to ensure the stability of bacteriophage P22.

Table 2-2: The conditions of the second competitive inhibition test.

Concentration of $C_{10}E_4$ (wt%)	Concentration of Bacteriophage P22 (particles/mL)	MOI
0	4.2×10^7	0.042
7.13	3.3×10^7	0.033

2.2.4 Plaque Assay

The plaque assay is used to quantify the concentration of viral particles in a particular solution. This assay is based on the concept that viral particles constantly infect cells, replicate inside them, and lyse them. Therefore, if viral particles are placed on a petri dish containing bacteria growing in agar, the above-mentioned process will continue until enough cells have been lysed such that a transparent circle, or plaque, will be visible in the yellowish, opaque background corresponding to the viable bacteria in the agar. Although many viral particles are responsible for one visible plaque, they all originated from a single infectious viral particle that was initially placed on the agar. Consequently, the concentration of biologically active viral particles in a solution can be determined by: (i) diluting the solution to an appropriate viral concentration, (ii) mixing a certain volume of the diluted solution with the host bacterium and nutrients, (iii) pouring this mixture onto a petri dish containing agar, (iv) incubating the contents of the dish overnight, (v) counting the number of plaques that have formed, and (iv) multiplying the number of plaques by the dilution factor used in (i).

The actual details of the plaque assay for bacteriophage P22 will now be given below. In preparation for the plaque assay, plates filled with agar are first made by pouring about 30 mL of a hot hard agar solution (see Appendix A for a description of the specific ingredients) into each sterile petri dish. On the next day, after the hard agar has solidified, 2.5 mL of soft agar (see Appendix A), 2 drops of a concentrated *Salmonella typhimurium* strain DB7155 cell solution, and a certain volume (0.05 to 0.5 mL) of the solution containing the bacteriophage P22 particles are mixed together and poured over the hard agar. This solution solidifies in about 15 to 30 minutes. The plates are then incubated at 30°C. The DB7155 cells begin reproducing quickly (the doubling time is about 30 minutes), and eventually all the agar in the dish contains bacteria. The DB7155 cells are used for the plaque assay because they are able to "read through" the stop codons in the mutant bacteriophage P22, and allow complete synthesis of the proteins required to generate intact particles and to lyse cells.

The bacteriophage P22 particles infect, replicate, and lyse the bacteria, and after only an incubation overnight, plaques are visible in the agar. The agar plays the important role of hindering the diffusion of bacteriophage P22 particles, and hence, the overlapping of plaques, which could cause difficulty in counting. It should also be noted that, in order to be able to count a statistically-meaningful number of plaques, generally 30 to 300 plaques should be present on each plate. Therefore, the solution of interest must first be diluted to ensure that only 30 to 300 bacteriophage P22 particles are present initially on a plate. Since the concentration of bacteriophage P22 in the solution is unknown *a priori*, a range of dilutions is necessary. The fluid used for these dilutions is referred to as the "dilution fluid", and its ingredients are listed in Appendix A.

2.3 Results and Discussion

2.3.1 Stability of DB7136 Cells in $C_{10}E_4$ Solutions

The results of the stability study are shown in Figure 2-2. For each solution containing a different concentration of $C_{10}E_4$ (0 wt%, 0.891 wt%, 4.31 wt%, 5.97 wt%, or 7.51 wt%), the concentration of the viable *Salmonella typhimurium* strain DB7136 cells remained, to within error, constant over the 30 minute period. Therefore, it can be concluded that, over a 30 minute period, the DB7136 cells are stable and remain viable in $C_{10}E_4$ solutions with concentrations lower than or equal to 7.51 wt%. Significant doubling of the DB7136 cells also did not occur over the 30 minute period. Consequently, the competitive inhibition tests were able to be conducted without concern for the stability and doubling of the DB7136 cells.

2.3.2 Competitive Inhibition Test

The results of the two competitive inhibition tests are shown in Figures 2-3 and 2-4. In these figures, the fraction of free bacteriophage P22 particles, that is, the fraction of bacteriophage P22 particles that have not infected DB7136 cells, is plotted as a function of the sampling time. The results of both competitive inhibition tests suggest that the presence of $C_{10}E_4$ does not influence the bacteriophage P22 infection process, since all the fractions decrease at approximately the same rates. Any type of binding between the tailspikes of bacteriophage P22 and the $C_{10}E_4$ micelles should have manifested itself in a lower infection rate. Although possible biospecific attractive interactions prompted this study, any type of attractive interaction between the tailspikes of bacteriophage P22 and the $C_{10}E_4$ micelles

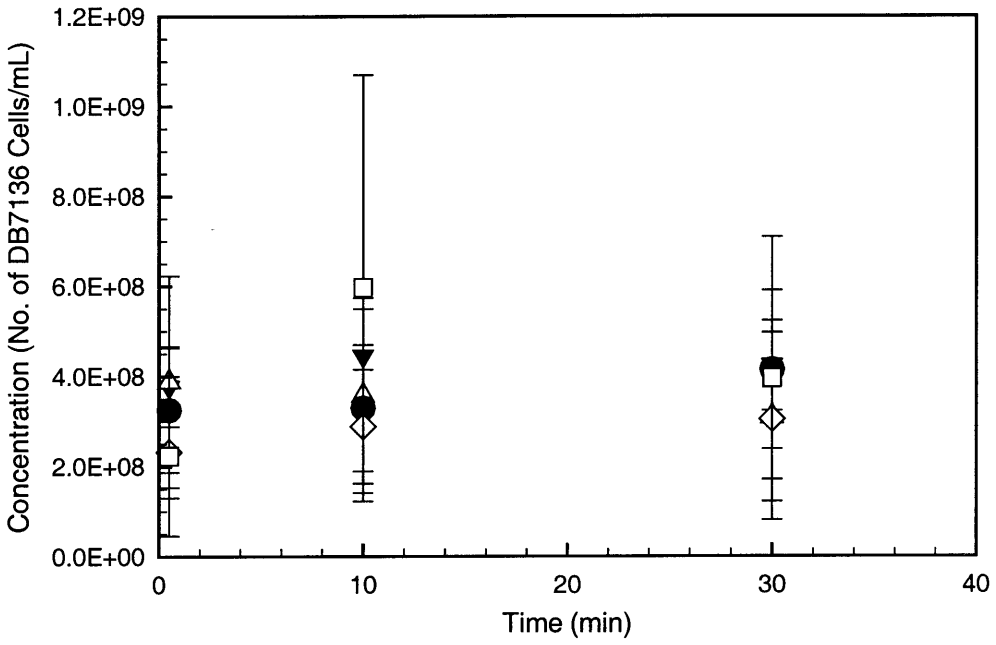

Figure 2-2: Experimental results corresponding to the stability study conducted on *Salmonella typhimurium* strain DB7136 cells in $C_{10}E_4$ solutions. The various symbols represent the concentrations of viable DB7136 cells in solutions containing five different concentrations of $C_{10}E_4$: 0 wt% (inverted black triangle), 0.890 wt% (white triangle), 4.31 wt% (black circle), 5.97 wt% (white diamond), and 7.51 wt% (white square). The error bars correspond to 95% confidence limits for the measurements.

should have inhibited bacteriophage P22 from infecting its host cells via steric hindrance. Therefore, it can be concluded that negligible or no attractive interactions operate between the tailspikes of bacteriophage P22 and the $C_{10}E_4$ micelles. However, a "cleaner", follow-up experimental study (see Chapter 3) was performed to further confirm this conclusion.

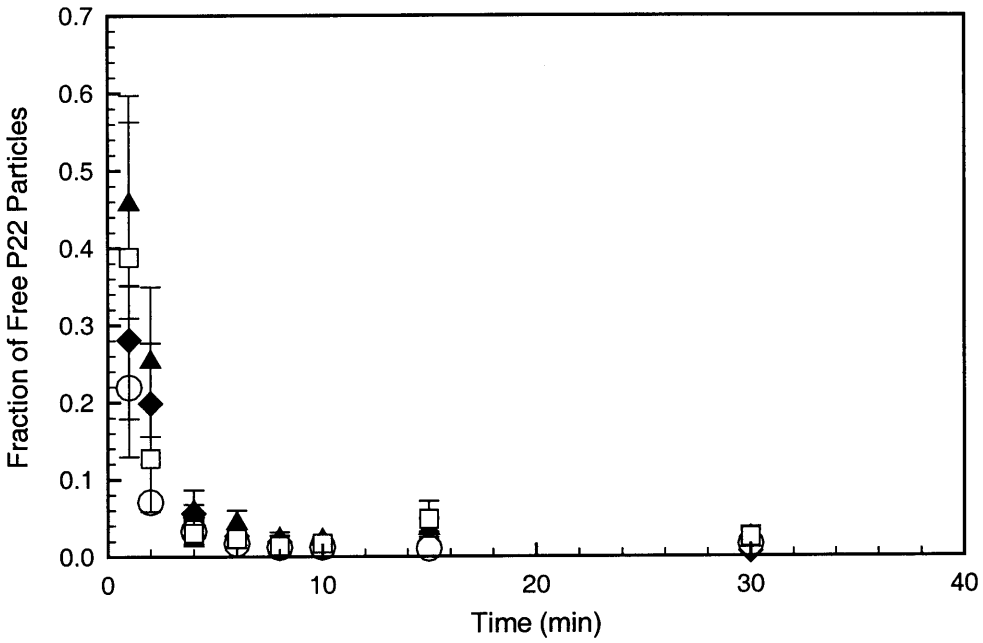

Figure 2-3: Experimental results corresponding to the first competitive inhibition test. The fraction of free bacteriophage P22 particles, that is, the fraction of bacteriophage P22 particles that have not infected DB7136 cells, is plotted as a function of the sampling time. The various symbols represent the P22 particle fractions in the solutions containing four different concentrations of $C_{10}E_4$: 0 wt% (black diamond), 0.796 wt% (black triangle), 3.98 wt% (white circle), and 7.19 wt% (white square). The MOI values in these solutions were 1.1, 0.61, 0.86, and 0.63, respectively. The error bars correspond to 95% confidence limits for the measurements.

2.4 Conclusions

In the competitive inhibition tests, bacteriophage P22 particles, *Salmonella typhimurium* strain DB7136 cells, and a certain concentration of $C_{10}E_4$ were incubated together for 30 minutes. During the 30 minute period, aliquots of the solutions containing different concentrations of $C_{10}E_4$ were taken at fixed time intervals to monitor the variation of the concentration of free bacteriophage P22 particles (those that have not infected DB7136 cells) with time. This experimental study essentially competed the DB7136 cells and the $C_{10}E_4$ micelles for the tailspikes of bacteriophage P22. The presence of $C_{10}E_4$ was found not to

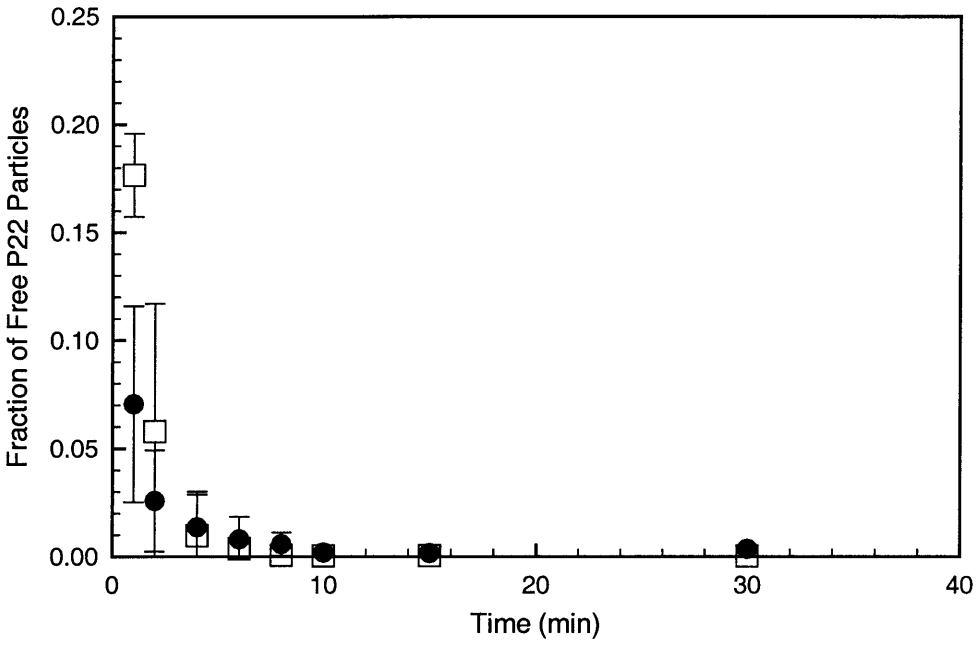

Figure 2-4: Experimental results corresponding to the second competitive inhibition test. The fraction of free bacteriophage P22 particles, that is, the fraction of bacteriophage P22 particles that have not infected DB7136 cells, is plotted as a function of the sampling time. The white square and black circle symbols represent the P22 particle fractions in the solutions containing 0 wt% $C_{10}E_4$ and 7.13 wt% $C_{10}E_4$, respectively. The corresponding MOI values in these solutions were 0.042 and 0.033, respectively. The error bars correspond to 95% confidence limits for the measurements.

interfere with the bacteriophage P22 infection process. Accordingly, it can be concluded that negligible or no attractive interactions operate between the tailspikes of bacteriophage P22 and the $C_{10}E_4$ micelles. This conclusion will be tested further in Chapter 3 with a "cleaner", follow-up experimental study.

Chapter 3

Partitioning the Capsids of Bacteriophage P22 without the Tailspikes

3.1 Introduction

The experimental study reported in this chapter was conducted to confirm the conclusion from the *Competitive Inhibition* study (see Chapter 2) that no attractive interactions exist between the tailspikes of bacteriophage P22 and the $C_{10}E_4$ micelles. This is a "cleaner," follow-up experimental study because the capsids of bacteriophage P22 were examined without the presence of the tailspikes. Specifically, the capsids of bacteriophage P22 without the tailspikes were partitioned in the two-phase aqueous $C_{10}E_4$ micellar system, and the resulting partition coefficient was compared to the one obtained previously[70] for intact bacteriophage P22 under the same conditions. It should be noted that the term "capsid" is used in this chapter to refer to the structure that includes the short neck in addition to the actual capsid (see Figure 2-1). Since the tailspikes comprise only a small fraction of the total size of an intact bacteriophage P22 particle, the capsids of bacteriophage P22 are approximately of the same size as the intact bacteriophage P22 particles (both are approximately 600 Å in diameter[85,87,96]). Accordingly, both the capsids and the intact bacteriophage P22 should experience similar excluded-volume interactions with the $C_{10}E_4$ micelles. Therefore, if a smaller partition coefficient is observed for the capsids than for the intact bacteriophage P22 particles, this would provide evidence that the tailspikes have considerable affinity towards the $C_{10}E_4$ micelles. These tailspikes would then be, at least partially, responsible for preventing the intact bacteriophage P22 particles from partitioning as predicted by the excluded-volume theory. However, if similar partitioning is observed for the capsids of bacteriophage P22 as well as for the intact bacteriophage P22 particles, it would further confirm the conclusion from the *Competitive Inhibition* study presented in Chapter 2 that negligible attractive interactions exist between the tailspikes of bacteriophage P22 and the $C_{10}E_4$ micelles.

The remainder of this chapter is organized as follows. In Section 3.2, the materials and experimental methods are detailed. Section 3.3 provides the definitions of the partition coefficients measured and/or compared in this study. In Section 3.4, the partitioning results are presented and discussed. Finally, concluding remarks are presented in Section 3.5.

3.2 Materials and Methods

3.2.1 Materials

Homogeneous *n*-decyl tetra(ethylene oxide) ($C_{10}E_4$) (lot no. 1006) was purchased from Nikko Chemicals (Tokyo, Japan). The purified tailspike solution (used for assaying the capsid concentrations) and the host bacteria *Salmonella typhimurium* strains DB7136 and DB7155[86,94] were obtained from Professor Jonathan King's laboratory. (For more details regarding the DB7136 and DB7155 cells, see Chapter 2 and Section 3.2.2 below.) The capsids of bacteriophage P22 (without their tailspikes) were synthesized using the DB7136 cells and purified in Professor King's laboratory (see Section 3.2.2 below). Citric acid (lot no. 0616 KCXK) and magnesium sulfate ($MgSO_4$) (lot no. 6070 A31581) were purchased from Mallinckrodt (Paris, KY). Disodium phosphate (lot no. 896726) was obtained from Fisher Scientific (Fair Lawn, NJ). All these materials were used as received. All solutions were prepared using pH 7.2 McIlvaine's buffer consisting of 16.4 mM disodium phosphate and 1.82 mM citric acid in Milli-Q water. Milli-Q water is the product of passing deionized water through Millipore's (Bedford, MA) Milli-Q system. All glassware used in the experiments were subjected to washing in a 50:50 ethanol:1 M sodium hydroxide bath, washing in a 1 M nitric acid bath, rinsing copiously with Milli-Q water, and drying in an oven for at least one day.

3.2.2 Synthesis of the Capsids of Bacteriophage P22 without the Tailspikes

The capsids of bacteriophage P22 were synthesized from mutant DB7136 cells. The DNA in the DB7136 cells contains the genes of bacteriophage P22 as a result of the lysogenic cycle of bacteriophage P22 (9^-am/13^-am). In the lysogenic cycle, the DNA of a viral particle becomes integrated into the cell's DNA, and therefore, is replicated along with the cell's genes.[97,98] The DNA of bacteriophage P22 (9^-am/13^-am) has two premature stop codons in genes 9 and 13, which prevent the complete synthesis of tailspikes (gene 9) and an enzyme necessary for cell lysis (gene 13), respectively.

As will now be described, growth of the DB7136 cells at the appropriate conditions

resulted in the production of cells containing many capsids of bacteriophage P22. First, the DB7136 cells were grown overnight at 34°C. This overnight solution was then diluted 1 to 500, and the DB7136 cells in this diluted solution were allowed to grow to a concentration of about 5 $\times 10^8$ cells/mL at 29°C. The solution temperature was then raised to 39°C to induce, or activate, the bacteriophage P22 genes in the cells and allow their expression to generate the capsids. Intact particles were not formed because complete tailspikes could not be produced. The cell solution was maintained at this condition for about 2.5 hours. The cells were also not lysed in this time period because of the mutation in gene 13 of bacteriophage P22. The cells containing the capsids of bacteriophage P22 were then harvested by centrifugation, and then lysed by the addition of chloroform and a freeze/thaw process. Deoxyribonuclease was then added to cleave DNA and decrease the viscosity of the solution after cell lysis. The cell debris was then removed by centrifugation at 10K rpm. The supernatant containing the capsids of bacteriophage P22 was collected and subsequently ultracentrifuged at 35K rpm to pellet the capsids. The capsids were then resuspended and filtered to remove residual cell debris. This was the purified capsid solution used for the partitioning experiments. The capsid concentration in this solution was measured to be 3×10^{11} capsids/mL using the tailing method described in Section 3.2.3. There were no intact bacteriophage P22 particles in the purified capsid solution, which was confirmed by performing the plaque assay (which is described in Section 2.2.4) with the purified capsid solution, and finding no plaques.

3.2.3 Partitioning the Capsids of Bacteriophage P22

In this partitioning experiment, five buffered solutions, each with a total volume of 3.0 mL, were prepared in graduated 10 mL test tubes. Four of the solutions contained 2.3×10^8 capsids/mL, 2 mM Mg^{+2} (from $MgSO_4$ in the purified capsid solution, as well as from the added $MgSO_4$) that was required to ensure the stability of the capsids, and 5.16 wt% $C_{10}E_4$. The fifth solution served as the control containing the same concentrations of $C_{10}E_4$ and $MgSO_4$, but no capsids. The solutions were then mixed, and equilibrated at 4°C in the refrigerator in order for each solution to exhibit a single, clear, homogeneous phase. The solutions were subsequently placed in the thermo-regulated device that is described in Section 3.2.4 below. The thermo-regulated device had already been set at the desired temperature of 21.0°C to initiate phase separation. This temperature was chosen because the experimentally measured partition coefficient of intact bacteriophage P22 was found to be orders of magnitude greater than the theoretically predicted one at 21.0°C (see Figure 1-11). Accordingly, if the tailspikes of bacteriophage P22 were responsible for this discrepancy,

a much lower partition coefficient should be measured for the capsids of bacteriophage P22 at 21.0°C. The initial $C_{10}E_4$ concentration of 5.16 wt% was selected because it yields a volume ratio (volume of the top phase divided by that of the bottom phase) of approximately 1 at the operating temperature of 21.0°C. A volume ratio of about 1 was chosen to be consistent with the partitioning experiments that were conducted previously.[70] The solutions were maintained at this condition for 17 hours before the two coexisting micellar phases were withdrawn with great care using 1 mL syringe and needle sets. All the partitioning experiments reported in this thesis were conducted for *at least* 14 hours, since it was shown previously[70] that partition coefficients measured after overnight partitioning did not differ from those measured after partitioning over at least three days. The capsid concentrations in the different phases were determined using the tailing method.[93] In the tailing method, a purified tailspike solution is first added to the solution containing the capsids in order to form intact and infective bacteriophage P22 particles. With these newly formed intact bacteriophage P22 particles, the plaque assay is conducted as described in Section 2.2.4. Essentially all the capsids are transformed into intact bacteriophage P22 particles because: (i) the concentration of the tailspikes is much greater than that of the capsids, and (ii) the tailspikes readily attach to the capsids.

3.2.4 The Thermo-Regulated Device

The thermo-regulated device is a transparent plastic or glass box connected to a NESLAB (Portsmouth, NH) water bath. At the top of the box, there is a plastic or cardboard lid with many slots available for inserting the tubes containing the surfactant solutions. Deionized water is used in the thermo-regulated device, and after allowing two hours for the system to equilibrate, the temperature of the water throughout the entire box is uniform. With this in mind, a tube containing deionized water and a thermocouple is placed in the box, and is used to represent the temperature of all the surfactant solutions present in the box. The thermocouple is connected to an Omega (Stamford, CT) Thermistor Thermometer temperature display that is capable of reporting the Celsius temperature to within two decimal points. The temperature inside the box can be controlled to within ±0.03°C during overnight partitioning.

Instead of placing the water bath on the lab bench, it is stored on the floor as a safety precaution. In this configuration, if there was a power failure during overnight partitioning, gravity will drive the water from the box into the water bath. The end result would only be an overflow of water out of the water bath onto the floor. On the other hand, if the water

bath was located on the lab bench, a power failure would cause water to flow from the water bath into the box. The end result would unfortunately be an overflow of water out of the box and onto other pieces of equipment on the lab bench, which then may become damaged. A schematic representation of the entire thermo-regulated device is shown in Figure 3-1.

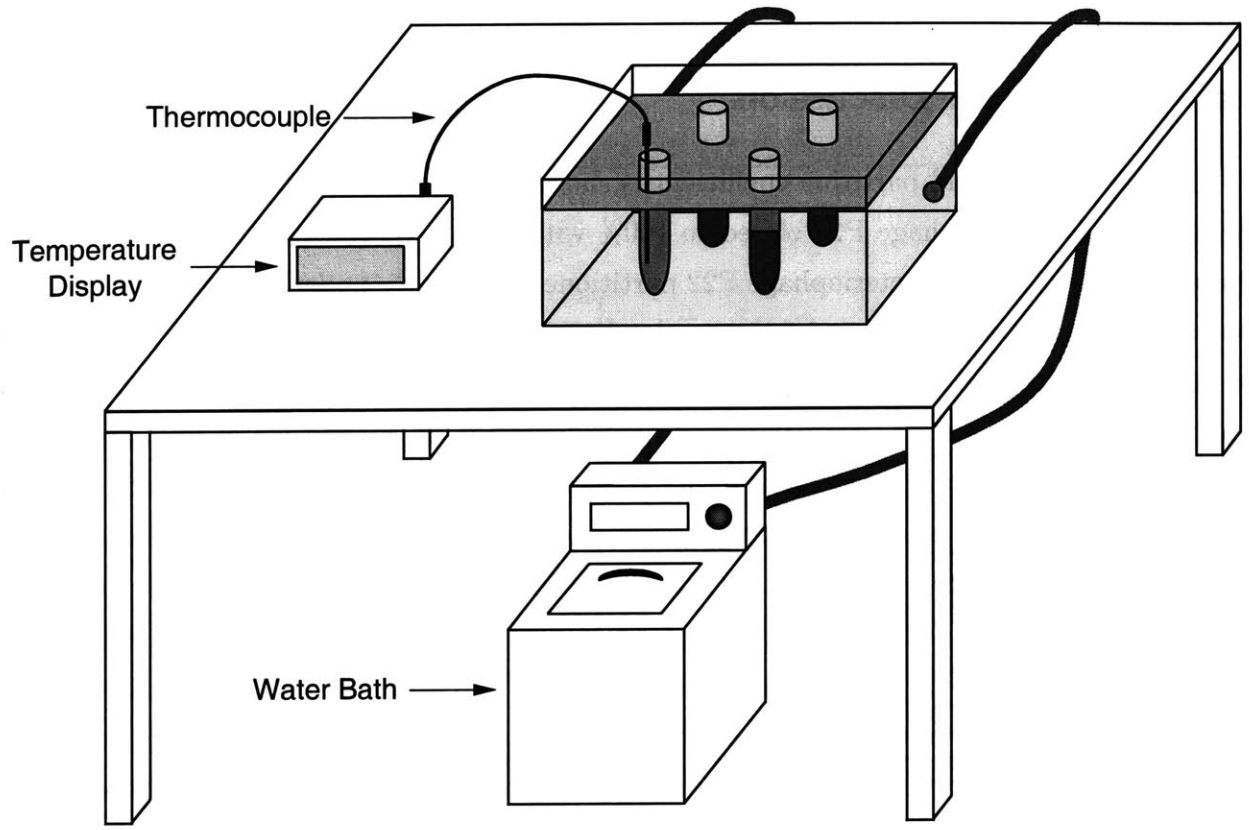

Figure 3-1: Schematic representation of the thermo-regulated device used in the partitioning experiments.

3.3 Theory

In order to quantify the distribution of the intact bacteriophage P22 and the capsid between the two coexisting micellar phases, their partition coefficients must be evaluated. The viral (or intact bacteriophage P22) and capsid partition coefficients, K_v and K_{cap}, are defined as follows:[75]

$$K_v \equiv \frac{C_{v,t}}{C_{v,b}} \tag{1.5}$$

and

$$K_{cap} \equiv \frac{C_{cap,t}}{C_{cap,b}} \tag{3.1}$$

where $C_{v,t}$ and $C_{v,b}$ are the concentrations of virus (or intact bacteriophage P22) in the top and bottom phases, respectively, and $C_{cap,t}$ and $C_{cap,b}$ are the concentrations of the capsid of bacteriophage P22 in the top and bottom phases, respectively.

3.4 Results and Discussion

The measured capsid partition coefficient is shown in Figure 3-2. The mass balances on the capsids of bacteriophage P22 closed to 100% within the experimental error. The partition coefficient of intact bacteriophage P22 partitioned previously under the same conditions (see the 21.0°C point in Figure 1-11) has also been included in Figure 3-2 for comparison purposes. As shown in Figure 3-2, the two partition coefficients are, to within error, essentially the same. In other words, the partitioning behavior of the capsids of bacteriophage P22 is essentially the same as that of intact bacteriophage P22 particles. Therefore, it can be concluded that significant attractive interactions between the tailspikes of bacteriophage P22 and the $C_{10}E_4$ micelles, which may hinder the intact bacteriophage P22 particles from attaining the predicted excluded-volume partitioning behavior, do not operate. Although possible biospecific interactions prompted the experimental studies conducted in this chapter and Chapter 2, the results from the two experimental studies indicate that any, and not only biospecific, attractive interactions between the tailspikes of bacteriophage P22 and the $C_{10}E_4$ micelles are negligible. Any type of attractive interaction would have manifested itself in inhibiting the bacteriophage P22 infection process in Chapter 2, as well as in causing the capsid and intact bacteriophage P22 partition coefficients to differ in this study. Therefore, if attractive interactions do exist between the bacteriophage P22 particles and the $C_{10}E_4$ micelles, they are associated with the capsids and not with the tailspikes of bacteriophage P22. Since bacteriophage P22 particles, like all biological particles, are part of a heterogeneous population, the capsids of some of the bacteriophage P22 particles may have surface properties that differ from the rest of the population. The surface properties of these capsids may, in turn, have a strong affinity for the $C_{10}E_4$ micelles. This possibility may account for the discrepancy between the experimentally measured and theoretically predicted viral partition coefficients, and therefore, this hypothesis was investigated in Chapter 4.

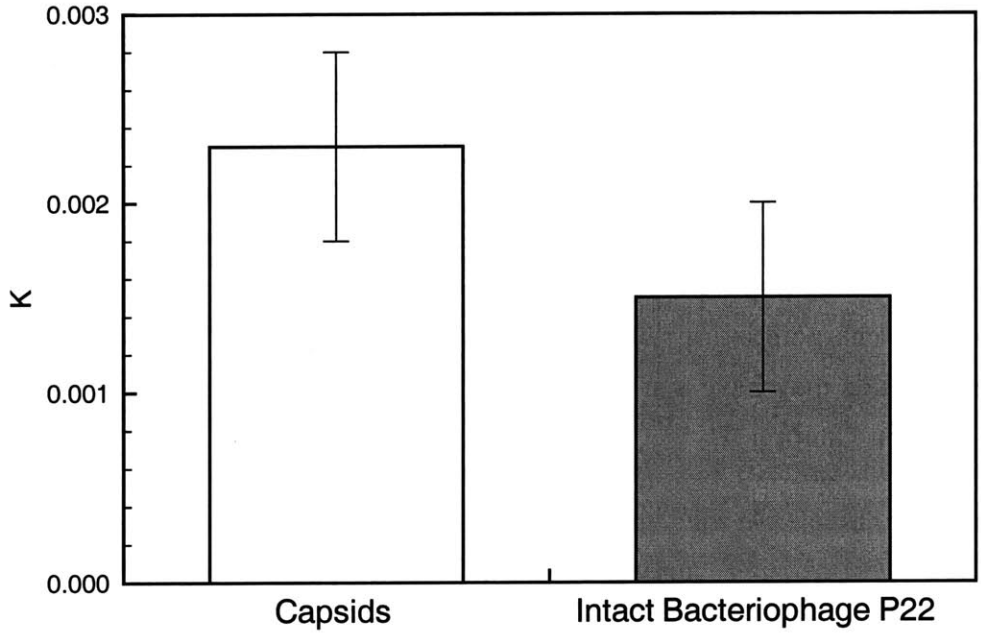

Figure 3-2: Experimentally measured capsid and intact bacteriophage P22 partition coefficients at 21.0°C in the two-phase aqueous $C_{10}E_4$ micellar system. The partition coefficient of intact bacteriophage P22 at 21.0°C (see Figure 1-11) was included in this figure for comparison. The white and gray bars correspond to the capsid and intact bacteriophage P22 partition coefficients, respectively. The error bars correspond to 95% confidence limits for the measurements.

3.5 Conclusions

In the experimental study reported in this chapter, the capsids of bacteriophage P22 without the tailspikes were first synthesized using *Salmonella typhimurium* strain DB7136 cells. The capsids were purified, and then partitioned in the two-phase aqueous $C_{10}E_4$ micellar system at a temperature of 21.0°C. The measured partition coefficient was then compared to the partition coefficient of intact bacteriophage P22 that was measured previously[70] in the two-phase aqueous $C_{10}E_4$ micellar system at 21.0°C. The partitioning behavior of the capsids of bacteriophage P22 was found to be essentially the same as that of the intact bacteriophage P22 particles. Accordingly, based on this result and the result of Chapter 2, it can be concluded that any, and not only biospecific, attractive interactions between the tailspikes of bacteriophage P22 and the $C_{10}E_4$ micelles are negligible. Any possible attractive interactions between the bacteriophage P22 particles and the $C_{10}E_4$ micelles must therefore be associated with the capsids of bacteriophage P22. Since bacteriophage P22 particles are part of a heterogeneous population, the capsids of some of the bacteriophage P22 particles may have surface characteristics that are different from the rest of the population. In particular, these capsids may have a strong affinity for the $C_{10}E_4$ micelles, and this hypothesis was investigated in Chapter 4.

Chapter 4

Investigating the Possible Existence of a Heterogeneous Population of Bacteriophage P22 Particles

4.1 Introduction

Although the experimental studies of Chapters 2 and 3 have shown that any attractive interactions between the tailspikes of bacteriophage P22 and the $C_{10}E_4$ micelles are negligible, the capsids of bacteriophage P22 may still have strong attractive interactions with the $C_{10}E_4$ micelles. If these attractive interactions exist, they may counter the excluded-volume interactions, and allow more of the bacteriophage P22 particles to remain in the top, micelle-rich phase of the two-phase aqueous $C_{10}E_4$ micellar system. This, in turn, would result in the measured partition coefficients of bacteriophage P22 being larger than those predicted based on the excluded-volume theory, which is what is observed experimentally. However, the mechanism for these possible attractive interactions with the capsids must not be applicable to the water-soluble proteins discussed in Chapter 1, since the excluded-volume theory already predicts reasonably well the partition coefficients of the water-soluble proteins.

The capsid of bacteriophage P22 is comprised of approximately 420 proteins.[85,87] Therefore, these capsids have a greater tendency of exhibiting heterogeneous surface properties than the previously studied water-soluble proteins. If different groups of capsids did exist with varying surface characteristics, they could cause the bacteriophage P22 particles to partition differently in the two-phase aqueous $C_{10}E_4$ micellar system due to their different affinities for each of the two coexisting micellar phases. Accordingly, Professor Jonathan King[99] and researchers in the field of two-phase aqueous *polymer* systems (including Dr. Harry Walter,[100] Dr. Donald Brooks,[101] and Dr. Göte Johansson[102]) have stressed the need to investigate the possible existence of a heterogeneous population of viral particles. In-

deed, this possible mechanism has the potential of significantly influencing the partitioning behavior of bacteriophage P22, while negligibly affecting the partitioning behavior of the previously studied water-soluble proteins.

Although hundreds of proteins comprise the capsid of bacteriophage P22, the number of different groups of capsids with varying affinities for the two coexisting micellar phases may still be very few. Consequently, as a first approximation, the population of bacteriophage P22 particles will be assumed to consist of two groups with two types of capsids. One of the groups will be assumed to have 100% affinity for the more abundant and larger micelles in the top, micelle-rich phase, while the other group will be assumed to partition according to the excluded-volume interactions. For such a bimodal population, it is shown theoretically in Section 4.3 that approximately *only* 2×10^{-3} of the total number of bacteriophage P22 particles need to have capsids with a strong affinity for the top, micelle-rich phase in order to yield a viral partition coefficient similar to those measured experimentally. If such a bimodal population of bacteriophage P22 particles did exist, then a single-stage partitioning would remove the first group entirely into the top phase, leaving most of the particles belonging to the second group in the bottom, micelle-poor phase. Accordingly, if the particles present in the bottom, micelle-poor phase were partitioned again, one would have eliminated the effect of the first group on the partitioning behavior of the second group. Therefore, the experimental study presented in this chapter tested the above-mentioned hypothesis by repartitioning the intact bacteriophage P22 particles from the bottom phase of a first partitioning stage in a second stage. According to the hypothesis, the bacteriophage P22 particles with capsids that have an affinity for the top, micelle-rich phase should have been removed in the first partitioning stage, and therefore, according to the excluded-volume theoretical prediction, a more extreme partition coefficient of bacteriophage P22 should be observed in the second stage. Intact bacteriophage P22 particles, and not just capsids, were partitioned because: (i) the tailspikes have already been shown to have negligible interactions with the $C_{10}E_4$ micelles, and (ii) the availability of intact bacteriophage P22 particles is greater, and they are easier to work with than the capsids.

4.2 Materials and Methods

4.2.1 Materials

The nonionic surfactant *n*-decyl tetra(ethylene oxide) ($C_{10}E_4$) (lot no. 6011) was purchased from Nikko Chemicals (Tokyo, Japan). Bacteriophage P22 (2^-am/13^-am) and

the host bacterium *Salmonella typhimurium* strain DB7155 were obtained from Professor Jonathan King's laboratory. The DNA of bacteriophage P22 (2^-am/13^-am) yields two premature stop codons in the mRNA (where a codon is a sequence of three mRNA bases) transcribed from genes 2 and 13, which prevent the complete synthesis of a pilot protein (gene 2) that aids in packaging the double-stranded DNA and an enzyme necessary for cell lysis (gene 13), respectively.[85,87] Citric acid (lot no. 0616 KCXK) and magnesium sulfate ($MgSO_4$) (lot no. 6070 A31581) were purchased from Mallinckrodt (Paris, KY). Disodium phosphate (lot no. 896726) was obtained from Fisher Scientific (Fair Lawn, NJ). All these materials were used as received. All solutions were prepared using pH 7.2 McIlvaine's buffer consisting of 16.4 mM disodium phosphate and 1.82 mM citric acid in Milli-Q water. Milli-Q water is the product of passing deionized water through Millipore's (Bedford, MA) Milli-Q system. All glassware used in the experiments were subjected to washing in a 50:50 ethanol:1 M sodium hydroxide bath, washing in a 1 M nitric acid bath, rinsing copiously with Milli-Q water, and drying in an oven for at least one day.

4.2.2 Mapping the Coexistence Curve of the Two-Phase Aqueous $C_{10}E_4$ Micellar System

The coexistence or binodal curve of the two-phase aqueous $C_{10}E_4$ micellar system delineates the two-phase region from the one-phase region in a temperature-$C_{10}E_4$ concentration phase diagram at constant pressure (see the schematic representation in Figure 1-3). Although the coexistence curve of the two-phase aqueous $C_{10}E_4$ micellar system was previously measured at 1 atm,[72] the coexistence curve was again mapped out at 1 atm because $C_{10}E_4$ from a new lot was used in this experimental study. In other words, the coexistence curve was mapped out to check for any $C_{10}E_4$ lot-to-lot variability. The cloud-point method was employed to measure the coexistence curve of the $C_{10}E_4$-buffer system. In this method, test tubes, each containing 1.0 mL of a buffered aqueous $C_{10}E_4$ solution, were placed in the thermo-regulated device described in Section 3.2.4. At least two cloud-point solutions were prepared for each $C_{10}E_4$ concentration to monitor the reproducibility of the measurements. Each solution was initially equilibrated at a temperature low enough that it exhibited a single, clear, homogeneous phase. The temperature of the solution was then raised at a rate of approximately 0.01°C/min until the solution became turbid and cloudy. The solution becomes turbid and cloudy at the onset of phase separation because of the formation of micelle-poor and micelle-rich domains that scatter visible light. Accordingly, the temperature at which the solution becomes turbid and cloudy is identified as the cloud-point temperature for that

particular $C_{10}E_4$ solution, and it corresponds to a point on the coexistence curve at that particular $C_{10}E_4$ concentration.

4.2.3 Double-Stage Partitioning of the Bacteriophage P22 Particles

Buffered solutions, each containing a total volume of 3 mL, were prepared in graduated 10 mL test tubes. In the preparation of each solution, $C_{10}E_4$ was first mixed with the buffer and 6 μL of a 1 M $MgSO_4$ solution. Subsequently, 0.1 mL of a concentrated bacteriophage P22 solution was added to each of the buffered solutions. The source of the concentrated bacteriophage P22 solution varied depending on the partitioning experiment being performed. For partitioning experiments Y1 and Z1, corresponding to the first partitioning stage, 0.1 mL of a stock solution from Professor King's laboratory was pipetted into the surfactant solutions. The stock solutions utilized for partitioning experiments Y1 and Z1 contained 4×10^9 and 4×10^{11} bacteriophage P22 particles/mL, respectively. For partitioning experiments Y2 and Z2, corresponding to the second partitioning stage, the sources of the bacteriophage P22 particles were the bottom phases of the solutions from partitioning experiments Y1 and Z1, respectively. Specifically, 0.1 mL of a bottom phase was diluted into a surfactant solution to yield the partitioning solutions utilized in partitioning experiments Y2 and Z2. For each partitioning experiment, at least two solutions were partitioned. The initial, overall concentrations of bacteriophage P22 particles, $C_{v,0}$, are reported in Table 4-1 for the various partitioning experiments. The initial, overall concentrations of $C_{10}E_4$ and $MgSO_4$ (from $MgSO_4$ in the purified bacteriophage P22 solution, as well as from the added $MgSO_4$) were 5.17 wt% and 2 mM, respectively. The 2 mM concentration of $MgSO_4$ was required to ensure the stability of the bacteriophage P22 particles.

Table 4-1: The initial, overall concentrations of bacteriophage P22 in the different partitioning experiments.

Partitioning Experiment	$C_{v,0}$ **(particles/mL)**
Y1 (1st Stage)	1×10^8
Y2 (2nd Stage)	7×10^6
Z1 (1st Stage)	2×10^{10}
Z2 (2nd Stage)	8×10^8

The solutions were then well-mixed, and equilibrated at 4°C in the refrigerator in order for each solution to exhibit a single, clear, homogeneous phase. The solutions were subsequently

placed in the thermo-regulated device, which was described in Section 3.2.4, to initiate phase separation at 21.0°C. This temperature was chosen for reasons given in Section 4.4.1. The initial, overall $C_{10}E_4$ concentration in all the solutions was chosen to be 5.17 wt% to yield two coexisting micellar phases having equal volumes at the operating temperature of 21.0°C. A volume ratio of 1 was chosen to be consistent with the partitioning experiments that were conducted previously.[70] The solutions were maintained at this condition for 15 hours prior to withdrawing the phases with great care using syringe and needle sets. All the partitioning experiments in this thesis were conducted for *at least* 14 hours, since it was shown previously[70] that partition coefficients measured after overnight partitioning did not differ from those measured after partitioning over at least three days. The concentration of bacteriophage P22 in each phase was measured with the plaque assay described in Section 2.2.4.

4.3 Theory

It will now be shown theoretically that a very small fraction of bacteriophage P22 particles with capsids which are different from those of the majority of the population can be responsible for the observed partitioning behavior of bacteriophage P22. The measured viral (bacteriophage P22) partition coefficient, K_v, will first be defined as follows:[75]

$$K_v \equiv \frac{C_{v,t}}{C_{v,b}} \tag{1.5}$$

where $C_{v,t}$ and $C_{v,b}$ are the concentrations of the virus in the top and bottom phases, respectively. The equation for the mass balance on the virus will also be required, and it is given by:

$$C_{v,0}\left(V_t + V_b\right) = C_{v,t}V_t + C_{v,b}V_b \tag{4.1}$$

where $C_{v,0}$ is the initial concentration of the virus, and V_t and V_b are the volumes of the top and bottom phases, respectively. In most of the experiments that have been conducted to date,[70] the volume ratio (V_t/V_b) has been maintained at approximately 1. In that case, the following equality applies:

$$V_t = V_b \tag{4.2}$$

Substituting Eq. (4.2) into Eq. (4.1), and rearranging yields:

$$2C_{v,0}V_t = \left(C_{v,t} + C_{v,b}\right)V_t \tag{4.3}$$

It then follows from Eq. (4.3) that the concentration of viral particles in the bottom phase is given by:

$$C_{v,b} = 2C_{v,0} - C_{v,t} \tag{4.4}$$

Substituting Eq. (4.4) into Eq. (1.5) yields the following expression for the viral partition coefficient:

$$K_v = \frac{C_{v,t}}{2C_{v,0} - C_{v,t}} \tag{4.5}$$

Equation (4.5) can now be used to express $C_{v,t}$ as a function of K_v and $C_{v,0}$. Specifically,

$$C_{v,t} = \frac{2K_v C_{v,0}}{1 + K_v} \tag{4.6}$$

Let us now define x as the fraction of the total number of bacteriophage P22 particles that have 100% affinity for the more abundant and larger micelles in the top, micelle-rich phase due to having capsids with different surface characteristics. Let us also define $C_{v,t}^{EV}$ as the concentration of bacteriophage P22 particles partitioning into the top phase as a result of experiencing only excluded-volume interactions with the $C_{10}E_4$ micelles. The total number of bacteriophage P22 particles in the top phase is then given by:

$$C_{v,t}V_t = C_{v,0}\left(V_t + V_b\right)x + C_{v,t}^{EV}V_t \tag{4.7}$$

As shown below, $C_{v,t}^{EV}$ is related to $C_{v,b}$ by K_v^{EV}, that is, the partition coefficient that results from only considering the excluded-volume interactions between the viral particles and the $C_{10}E_4$ micelles. Specifically,

$$K_v^{EV} = \frac{C_{v,t}^{EV}}{C_{v,b}^{EV}} = \frac{C_{v,t}^{EV}}{C_{v,b}} \tag{4.8}$$

where the equality

$$C_{v,b}^{EV} = C_{v,b} \tag{4.9}$$

is valid, since the viral particles partition into the bottom, micelle-poor phase due to solely experiencing the excluded-volume interactions with the $C_{10}E_4$ micelles. Solving for $C_{v,b}$ in Eq. (4.8), and using Eq. (4.4), yields the following relation:

$$C_{v,t}^{EV} = K_v^{EV}\left(2C_{v,0} - C_{v,t}\right) \tag{4.10}$$

Substituting Eqs. (4.10) and (4.2) in Eq. (4.7), and rearranging, yields:

$$x = \frac{C_{v,t}\left(1 + K_v^{EV}\right) - 2K_v^{EV}C_{v,0}}{2C_{v,0}} \tag{4.11}$$

Equation (4.6) will now be substituted into Eq. (4.11) to obtain an expression for x as a function of K_v and K_v^{EV}. Specifically,

$$x = \frac{K_v\left(1 + K_v^{EV}\right)}{1 + K_v} - K_v^{EV} = \frac{K_v - K_v^{EV}}{1 + K_v} \tag{4.12}$$

Note that if only a single population of bacteriophage P22 particles did exist, then $x = 0$, and Eq. (4.12) correctly yields $K_v = K_v^{EV}$. From Figure 1-11, $K_v \approx 2\times10^{-3}$, and $K_v^{EV} \ll 2\times10^{-3}$. Consequently, Eq. (4.12) simplifies to:

$$x \approx K_v - K_v^{EV} \approx K_v \approx 2 \times 10^{-3} \tag{4.13}$$

This result is very striking because it shows that only 2×10^{-3} of the total number of bacteriophage P22 particles need to have capsids with a particular affinity for the more abundant and larger micelles in the top, micelle-rich phase to yield the experimentally observed partition coefficients of bacteriophage P22. This hypothesis was tested in the experimental study reported here by repartitioning the bacteriophage P22 particles from the bottom phase of a first partitioning stage in a second stage.

4.4 Results and Discussion

4.4.1 Mapping the Coexistence Curve of the Two-Phase Aqueous $C_{10}E_4$ Micellar System

The measured coexistence curve of the two-phase aqueous $C_{10}E_4$ micellar system, which will also be referred to as the $C_{10}E_4$-buffer system, is shown in Figure 4-1. For comparison, the previously measured coexistence curve[72] has also been included. Although the $C_{10}E_4$ from the two different lots yielded similar coexistence curves, the coexistence curve should always be remeasured whenever $C_{10}E_4$ from a different lot is used. It should be noted that $C_{10}E_4$ (lot no. 6011) will be used for the remainder of this thesis.

Since similar coexistence curves were obtained, the partition coefficient of bacteriophage P22 at 21.0°C in the $C_{10}E_4$ (lot no. 6011)-buffer system was expected to be approximately the

same as the one measured in the $C_{10}E_4$ (lot no. 1006)-buffer system at the same temperature. This was indeed verified experimentally, and 21.0°C was chosen as the operating temperature in the double-stage partitioning experiments, since the experimentally measured partition coefficient of bacteriophage P22 at this temperature was orders of magnitude greater than the theoretically predicted one. Accordingly, if the heterogeneous surface properties of the capsids of bacteriophage P22 are indeed responsible for this discrepancy, a much lower partition coefficient should be measured in the second stage of the double-stage partitioning experiment.

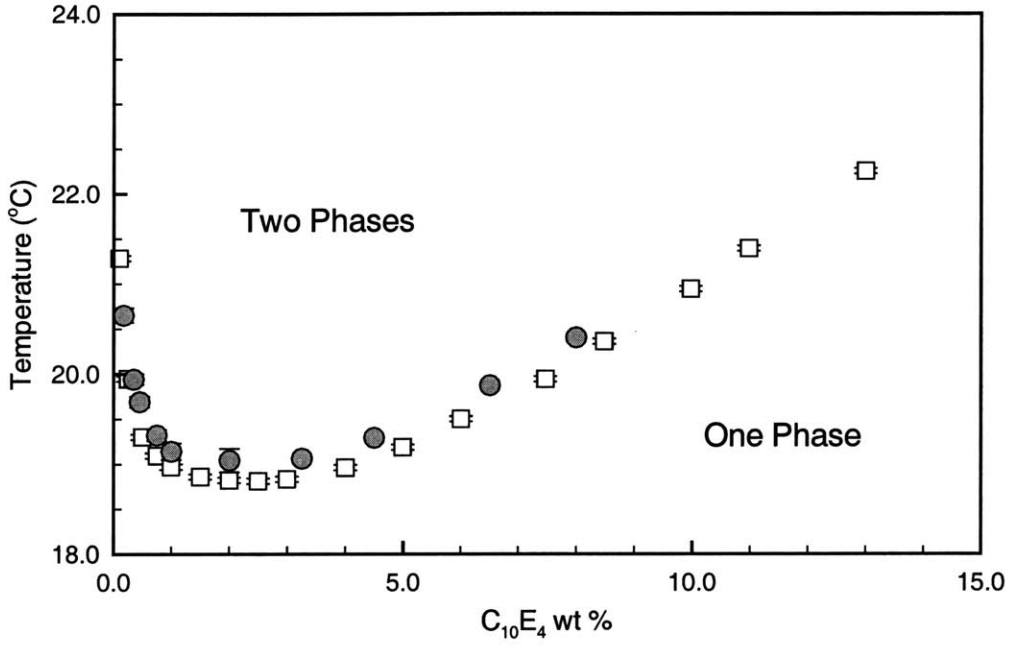

Figure 4-1: The coexistence curves of the two-phase aqueous $C_{10}E_4$ micellar system for $C_{10}E_4$ from two different lots. The coexistence curve measured in this study (lot no. 6011) consists of the gray circles. The coexistence curve measured in a previous study[72] (lot no. 1006) consists of the white squares. The error bars correspond to 95% confidence limits for the measurements.

4.4.2 Double-Stage Partitioning of the Bacteriophage P22 Particles

Two double-stage partitioning experiments were conducted with bacteriophage P22 in the two-phase aqueous $C_{10}E_4$ micellar system. Figure 4-2 summarizes the results of the double-stage partitioning experiments, for which the mass balances on bacteriophage P22 closed to 100% within the experimental error. Although the partition coefficients obtained after the first and second partitioning stages ($K_v(Y1) = 1.9 \times 10^{-3}$ vs. $K_v(Y2) = 7 \times 10^{-4}$, and $K_v(Z1) = 1.5 \times 10^{-3}$ vs. $K_v(Z2) = 2.5 \times 10^{-3}$) were not the same to within error, they

are still similar in value. Therefore, it can be concluded that, even if heterogeneities are present in the capsids of the bacteriophage P22 particles, they do not significantly influence the partitioning behavior of bacteriophage P22. More importantly, such heterogeneities cannot explain the orders of magnitude discrepancy between the theoretically predicted and experimentally measured partition coefficients of bacteriophage P22. This conclusion was also further tested by partitioning different mutants of bacteriophage P22 in the two-phase aqueous $C_{10}E_4$ micellar system, and measuring the same partition coefficients. Note that a few different mutants of bacteriophage P22, which were found to have the same partitioning behavior, have been used throughout this thesis.

In addition, since all four partition coefficients of bacteriophage P22 in Figure 4-2 were found to be fairly similar, it can also be concluded that partitioning in the two-phase aqueous $C_{10}E_4$ micellar system is independent of the initial concentration of bacteriophage P22 (see Section 4.2.3 for a description of the initial concentrations utilized in the experiments). This is a requirement if the two-phase aqueous $C_{10}E_4$ micellar system is to be used in a separation process, since reproducible viral partition coefficients must always be achieved, regardless of the initial viral concentration. Attaining reproducible viral partition coefficients is very important because the viral concentration in the fermentation broth will vary from one batch to another.

Based on the results obtained in this chapter and those obtained in Chapters 2 and 3, the only possible source of attractive interactions between the bacteriophage P22 particles and the $C_{10}E_4$ micelles are electromagnetic interactions between the capsids of bacteriophage P22 and the $C_{10}E_4$ micelles. These electromagnetic interactions include van der Waals, ion-dipole, and ion-induced dipole interactions,[42] where the ion refers to bacteriophage P22, since it is charged as opposed to the noncharged $C_{10}E_4$ micelles. However, when the partitioning behavior of all three bacteriophages discussed in Chapter 1 are considered together (see Figure 4-3), it seems highly unlikely that these possible attractive, electromagnetic interactions are responsible for the observed viral partitioning behavior. These three bacteriophages have very different sizes and properties, both external as well as internal. The external properties include the number and type of amino acids on the surface of each bacteriophage, while an important internal property is the dielectric constant inside each bacteriophage, since it can influence the strength of the van der Waals interactions with the micelles.[42] However, as shown in Figure 4-3, all three bacteriophages partition similarly as a function of temperature, and therefore, it is difficult to imagine that these three bacteriophages having very different sizes and properties would experience repulsive, excluded-volume and attractive,

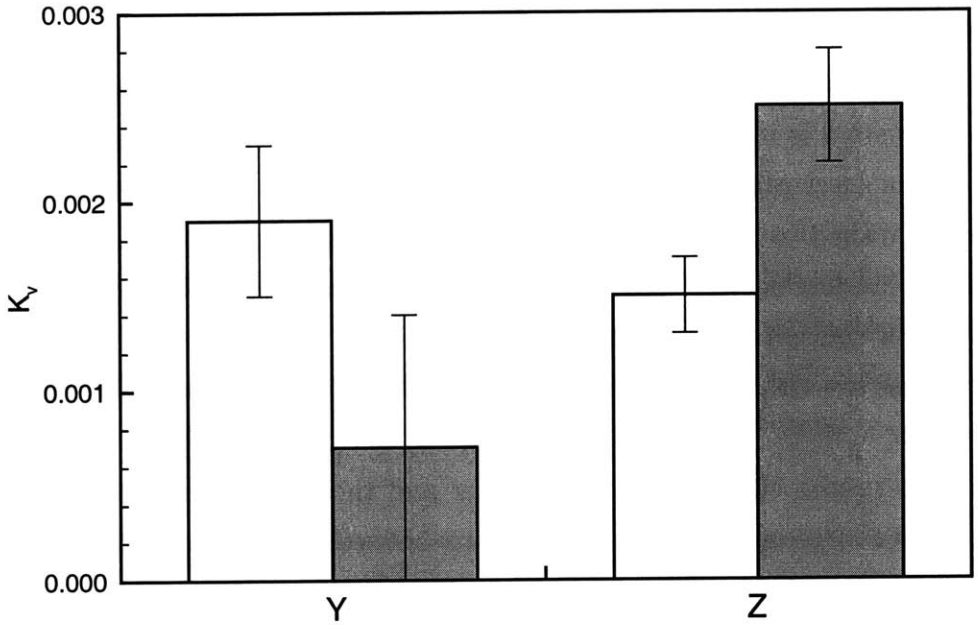

Figure 4-2: The partition coefficients of bacteriophage P22 from the double-stage partitioning experiments conducted in the two-phase aqueous $C_{10}E_4$ micellar system. For both double-stage partitioning experiments (Y and Z), the white and gray bars correspond to the partition coefficients measured in the first and second stages, respectively. The error bars correspond to 95% confidence limits for the measurements.

electromagnetic interactions with the $C_{10}E_4$ micelles that exactly cancel each other to yield similar partition coefficients. Accordingly, it was concluded that the observed viral partitioning behavior is most probably not a result of a balance between repulsive, excluded-volume and attractive, electromagnetic interactions. In view of this, other assumptions underlying the excluded-volume theory were challenged. In particular, the assumption that macroscopic phase separation equilibrium is achieved in the two-phase aqueous $C_{10}E_4$ micellar system was investigated, and the results of this investigation are reported in Chapter 5.

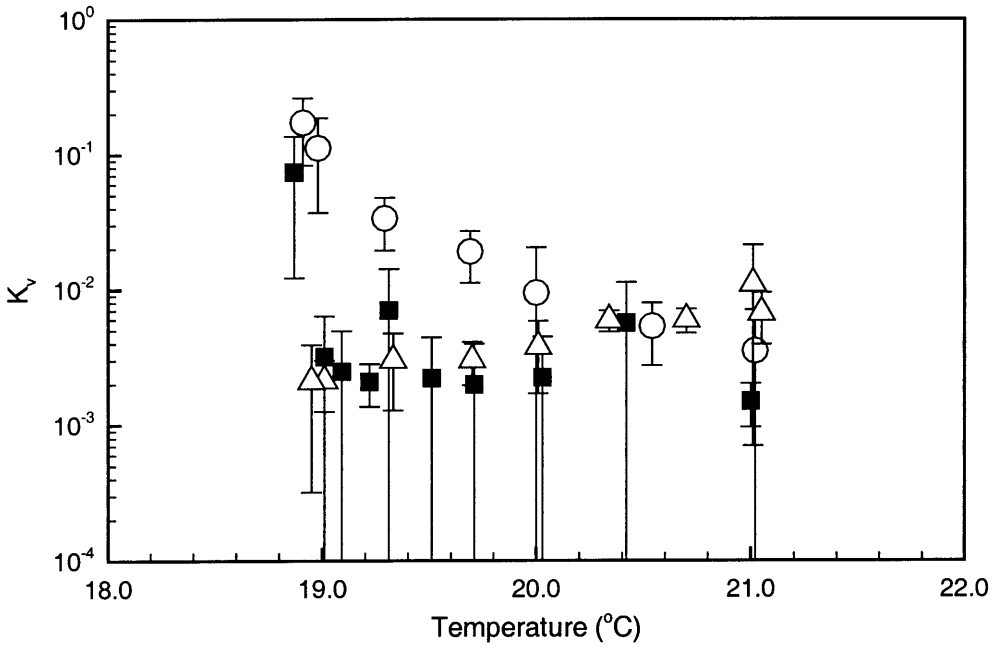

Figure 4-3: The partition coefficients of three bacteriophages as a function of temperature. This figure summarizes the partitioning data for the three bacteriophages discussed in Chapter 1 on a single plot. The various symbols represent the partition coefficients of the following three different bacteriophages: P22 (black squares), ϕX174 (white circles), and T4 (white triangles). The error bars correspond to 95% confidence limits for the measurements. Note that the error bars appear asymmetric due to the use of a semi-logarithmic plot.

4.5 Conclusions

Double-stage partitioning experiments were conducted with bacteriophage P22 in the two-phase aqueous $C_{10}E_4$ micellar system at 21.0°C. Since the measured partition coefficients of bacteriophage P22 before and after repartitioning were found to be similar, it was concluded that, even if heterogeneities do exist among the capsids of bacteriophage P22, they do not significantly influence the partitioning behavior of bacteriophage P22. In particular,

they cannot be invoked to rationalize the discrepancy between the theoretically predicted and experimentally measured partition coefficients of bacteriophage P22. Based on this conclusion and those from Chapters 2 and 3, the only remaining possible source of attractive interactions between the bacteriophage P22 particles and the $C_{10}E_4$ micelles are electromagnetic interactions between the capsids of bacteriophage P22 and the $C_{10}E_4$ micelles. However, since all three, very different bacteriophages discussed in Chapter 1 were found to partition similarly, these attractive, electromagnetic interactions are most probably not responsible for the observed viral partitioning behavior. Specifically, it is difficult to envision that the repulsive, excluded-volume and attractive, electromagnetic interactions associated with these three bacteriophages having very different sizes and properties (both external as well as internal) would precisely balance each other to yield similar partition coefficients. Therefore, these possible attractive, electromagnetic interactions were ruled out as "suspects", and the other assumption underlying the excluded-volume theory was challenged. In particular, in Chapter 5, we report our investigation of the assumption that the entire two-phase aqueous $C_{10}E_4$ micellar system attains macroscopic phase separation equilibrium.

Chapter 5

Investigating the Effect on the Viral Partition Coefficient of Micelle-Poor Domains Being Entrained in the Macroscopic, Top, Micelle-Rich Phase

5.1 Introduction

As discussed in Sections 4.4.2 and 4.5, attractive interactions between the viral particles and the $C_{10}E_4$ micelles are probably not responsible for the observed orders of magnitude discrepancy between the theoretically predicted and experimentally measured viral partition coefficients. Therefore, the other underlying assumptions of the excluded-volume theory must be challenged in order to identify other possible mechanisms, in addition to the excluded-volume interactions, that control viral partitioning. The biggest "clue" for identifying these other possible mechanisms is that they should significantly affect viral partitioning, while having little or no impact on protein partitioning, since the excluded-volume theory predicts reasonably well the experimentally observed partition coefficients of water-soluble proteins.

In addition to assuming that only repulsive, excluded-volume interactions operate between the viruses and the $C_{10}E_4$ micelles, the excluded-volume theory also assumes that macroscopic phase separation equilibrium, which is described below, is attained in the two-phase aqueous $C_{10}E_4$ micellar system. When phase separation is induced, micelle-rich and micelle-poor domains form in the solution. The micelle-rich domains must collide into each other, coalesce, and rise to form the macroscopic top phase. Similarly, the micelle-poor domains must also collide into each other, coalesce, and sediment to form the macroscopic bottom phase. Macroscopic phase separation equilibrium is being used to refer to the condition in which *all* the micelle-rich and micelle-poor domains are in their corresponding

macroscopic phases prior to withdrawing the top and bottom phases. However, this may not be true experimentally, since there could be micelle-poor domains entrained in the macroscopic, top, micelle-rich phase, as well as micelle-rich domains entrained in the macroscopic, bottom, micelle-poor phase. Consequently, the concentration of viral particles measured in each phase could be affected by the presence of these entrained domains. However, the concentration of water-soluble protein, on the other hand, should hopefully not be significantly affected by the entrained domains in either phase, since the excluded-volume theory already predicts reasonably well their partition coefficients.

The entrainment of micelle-poor domains in the macroscopic, top, micelle-rich phase is investigated theoretically in Section 5.3, along with the entrainment of micelle-rich domains in the macroscopic, bottom, micelle-poor phase. With regard to the entrained micelle-poor domains, it is shown theoretically in Section 5.3.1 that only a very small volume fraction of the macroscopic, top, micelle-rich phase needs to be comprised of micelle-poor domains in order to yield the currently measured viral partition coefficients. In accordance with the biggest "clue" concept put forward above, this effect is also shown theoretically in Section 5.3.1 to negligibly influence the partition coefficients of the previously studied water-soluble proteins. As will now be discussed, this difference regarding the effect of entrainment on viral and protein partition coefficients can be physically understood without invoking the equations of Section 5.3.1. If the viral particles are indeed partitioning according to the excluded-volume theory, the concentration of viral particles in the micelle-poor domains is orders of magnitude greater than that in the micelle-rich domains. Consequently, even if there are only a few micelle-poor domains entrained in the macroscopic, top, micelle-rich phase (see Figure 5-1a for a schematic representation of this scenario), the overall concentration of viral particles in the top phase will be measured as being much greater than if there were no entrained micelle-poor domains. Measuring a higher concentration of viral particles in the top phase will yield a partition coefficient that is larger than that predicted by the excluded-volume theory. On the other hand, in the case of the water-soluble proteins discussed in Chapter 1, the excluded-volume theory predicts protein partition coefficients that are between 0.1 and 1. The concentration of protein in the micelle-poor domains is therefore approximately equal to that in the micelle-rich domains. Accordingly, entrainment of a few micelle-poor domains in the macroscopic, top, micelle-rich phase should negligibly affect the measured overall concentration of protein in that top phase. The protein partition coefficient is therefore expected to be approximately equal to the one predicted by the excluded-volume theory, even in the presence of entrainment.

The opposite scenario, that is, having micelle-rich domains entrained in the macroscopic, bottom, micelle-poor phase (see Figure 5-1b), is shown theoretically in Section 5.3.2 to have a negligible effect on both viral and protein partition coefficients. For the water-soluble protein, this is again physically intuitive because the concentration of protein in the micelle-rich domains is similar to that in the micelle-poor domains. However, for the virus, the concentration of virus in the micelle-rich domains is expected to be orders of magnitude lower than that in the micelle-poor domains according to the excluded-volume theory. Consequently, a few entrained micelle-rich domains in the macroscopic, bottom, micelle-poor phase should only cause a slight dilution of the overall concentration of virus that is measured in the bottom phase. The viral partition coefficient in this case is therefore expected to be similar to the value predicted by the excluded-volume theory, even in the presence of entrainment.

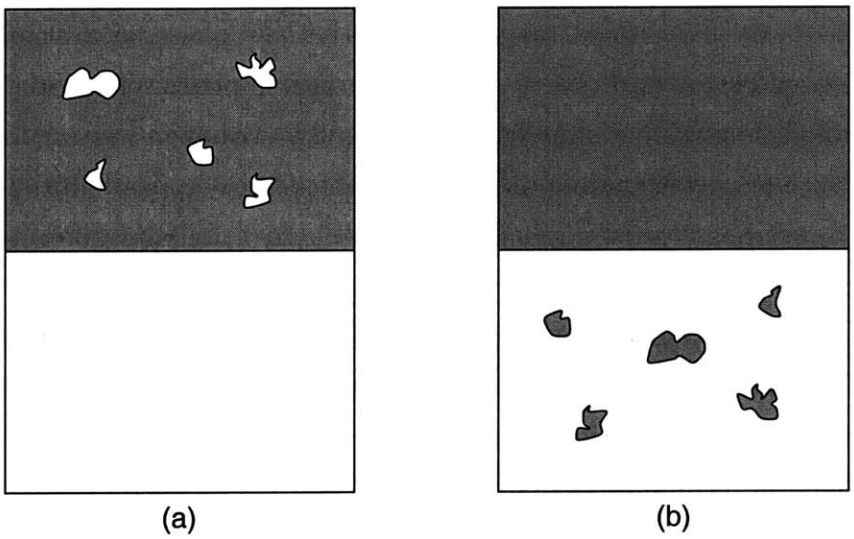

Figure 5-1: Schematic representation of: (a) the entrainment of micelle-poor (virus-rich) domains in the macroscopic, top, micelle-rich phase, and (b) the entrainment of micelle-rich (virus-poor) domains in the macroscopic, bottom, micelle-poor phase. The gray and white colors are used to denote the micelle-rich and micelle-poor domains, respectively. The concentration of virus in the micelle-poor domains, based on the excluded-volume theory, is predicted to be orders of magnitude larger than that in the micelle-rich domains. In contrast, according to the excluded-volume theory, the concentration of water-soluble protein in the micelle-poor domains is predicted to be approximately equal to that in the micelle-rich domains.

Based on the discussion above, the entrainment of micelle-rich (virus-poor) domains in the macroscopic, bottom, micelle-poor phase is not expected to be responsible for the experimentally observed viral partitioning behavior. In contrast, the entrainment of micelle-

poor (virus-rich) domains in the macroscopic, top, micelle-rich phase may be responsible for the observed orders of magnitude discrepancy between the experimentally measured and theoretically predicted viral partition coefficients. It can therefore be hypothesized that the entrainment of micelle-poor (virus-rich) domains in the macroscopic, top, micelle-rich phase may significantly influence the measured viral partition coefficients, while having little or no impact on the measured protein partition coefficients. In addition, entrainment should be investigated because it has already been shown to be present in two-phase aqueous *polymer* systems.[103]

The experimental study described in this chapter was conducted to test this hypothesis. Although centrifugation appears initially to be a good method for removing entrainment, preliminary experiments demonstrated that centrifugation leads to a slight increase in the temperature, which forces the system to undergo a new phase separation process. As a result, new micelle-rich and micelle-poor domains form, and it becomes difficult to decouple the domains that have just formed (as a result of the new phase separation process) from those that have been entrained (as a result of the previous phase separation process). Consequently, centrifugation was not employed in this study. Although waiting for the entrained domains to reach their corresponding macroscopic phases also appears initially to be a good method, previous studies in the two-phase aqueous $C_{10}E_4$ micellar system have shown that the partition coefficient of bacteriophage P22 does not change even after 2 weeks of partitioning.[70] This is not surprising, because domains can remain entrained for very long periods of time even in oil-water-surfactant systems where the two phases are more dissimilar. Consequently, centrifuging and partitioning over a long period of time were not exploited, and a different experimental technique was pursued.

A systematic and simple experimental method was developed previously to demonstrate the existence of entrainment in two-phase aqueous *polymer* systems.[103] In this experimental method, the volume ratio is varied from being much less than 1 to being much greater than 1. As explained below, if this experimental method is applied to the two-phase aqueous $C_{10}E_4$ micellar system, a volume ratio that is much less than 1 ($V_t/V_b << 1$) is expected to entrain micelle-rich domains in the macroscopic, bottom, micelle-poor phase, whereas a volume ratio that is much greater than 1 ($V_t/V_b >> 1$) is expected to entrain micelle-poor domains in the macroscopic, top, micelle-rich phase. For a volume ratio that is much less than 1 at the end of the phase separation process, there are more micelle-poor (virus-rich) domains than micelle-rich (virus-poor) domains when phase separation is induced. Accordingly, the micelle-rich (virus-poor) domains experience difficulty in finding each other and coalescing,

since each micelle-rich (virus-poor) domain is surrounded primarily by micelle-poor (virus-rich) domains at the onset of the phase separation process (see Figure 5-2a for a schematic representation). Consequently, some micelle-rich (virus-poor) domains can get entrained in the macroscopic, bottom, micelle-poor phase. On the other hand, when the final volume ratio is much greater than 1, the onset of the phase separation process can be viewed as shown schematically in Figure 5-2b. In this scenario, there are more micelle-rich (virus-poor) domains than micelle-poor (virus-rich) domains. Consequently, the micelle-poor (virus-rich) domains experience difficulty in finding each other and coalescing, since each micelle-poor (virus-rich) domain is surrounded primarily by micelle-rich (virus-poor) domains. Therefore, some micelle-poor domains can get entrained in the macroscopic, top, micelle-rich phase.

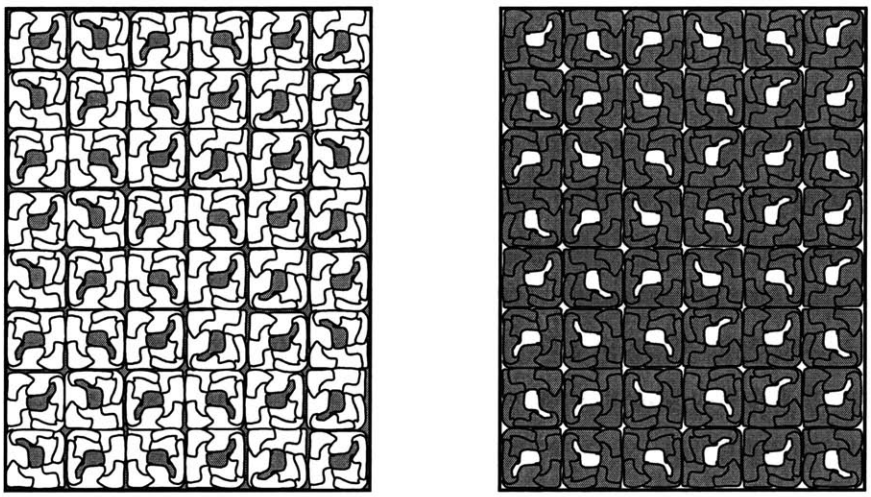

Figure 5-2: Schematic representation of the onset of the phase separation process when employing a volume ratio that is: (a) much less than one, and (b) much greater than one. The gray and white colors are used to denote the micelle-rich (virus-poor) and micelle-poor (virus-rich) domains, respectively.

Although utilizing a volume ratio that is much less than 1 does not guarantee the removal of all the micelle-poor (virus-rich) domains in the macroscopic, top, micelle-rich phase, the fraction of entrained micelle-poor (virus-rich) domains in the top phase is expected to decrease when the volume ratio is decreased from being much greater than 1 to being much less than 1. As a result, if the entrainment hypothesis is correct, the concentration of virus in the top phase should decrease when the volume ratio is decreased from being much greater than 1 to being much less than 1. The concentration of virus in the bottom phase, however, will remain essentially constant, since, as explained above, entraining micelle-rich (virus-poor) domains in the bottom phase has a negligible effect on the measured concentration of virus

in the bottom phase. Therefore, based on this hypothesis, the viral partition coefficient is expected to decrease as the volume ratio is decreased from being much greater than 1 to being much less than 1.

As an initial, more qualitative test of the proposed experimental method which exploits varying the volume ratio, photographs of the two-phase aqueous $C_{10}E_4$ micellar system, which will also be referred to as the $C_{10}E_4$-buffer system, were taken for volume ratios that were much less than 1 and much greater than 1. Photographs were taken because the entrained domains in a macroscopic phase were expected to scatter visible light, similar to when an oil-water mixture appears "milky" and turbid after vigorous shaking. Although taking photographs through a microscope to actually see the domains would be more desirable, preliminary attempts to obtain these microscale photographs have shown that the temperature cannot be controlled well enough to prevent the onset of phase separation. In particular, the radiative heat from the light source of the microscope was enough to slightly increase the temperature and force the system to undergo a new phase separation process. Since the onset of phase separation is associated with the formation of new micelle-rich and micelle-poor domains, it became difficult to decouple the domains that had just formed (as a result of the new phase separation process) from those that had been entrained (as a result of the previous phase separation process). Consequently, only photographs on a macroscopic scale were taken of the two-phase aqueous $C_{10}E_4$ micellar system.

A more precise, quantitative experimental test of the hypothesis put forward, however, involved the partitioning of a model protein and a model virus in the two-phase aqueous $C_{10}E_4$ micellar system with volume ratios that were much greater than 1 and much less than 1. Cytochrome *c* was chosen as the model protein because its partitioning behavior is already predicted reasonably well by the excluded-volume theory (see Figure 1-6), and it is also: (i) water-soluble, (ii) available in high purity, and (iii) easy to assay using visible absorbance measurements. Bacteriophage P22 was selected as the model virus because: (i) its experimentally measured partition coefficients differ significantly from its predicted ones (see Chapter 1), (ii) it is readily available in high purity from Professor Jonathan King's laboratory, (iii) it is safer to use than mammalian viruses, and (iv) its concentration can be measured with reasonable accuracy using the plaque assay described in Section 2.2.4. If the proposed hypothesis is correct, the partition coefficient of cytochrome *c* is expected to remain constant as the volume ratio is decreased from a value that is much greater than 1 to a value that is much less than 1, while the partition coefficient of bacteriophage P22 is expected to decrease with the decrease in the volume ratio.

The remainder of this chapter is organized as follows. In Section 5.2, the materials and experimental methods are detailed. Section 5.3 provides a theoretical analysis of entrainment. In Section 5.4, the experimental and theoretical results are presented and discussed. Finally, concluding remarks are presented in Section 5.5.

5.2 Materials and Methods

5.2.1 Materials

The nonionic surfactant *n*-decyl tetra(ethylene oxide) ($C_{10}E_4$) (lot no. 6011) was obtained from Nikko Chemicals (Tokyo, Japan). Cytochrome *c* (lot no. 77H7052) and sodium L-ascorbate (lot no. 46H02965) were purchased from Sigma (St. Louis, MO). Bacteriophage P22 (5^-am/13^-am) and the bacteriophage P22 host bacterium, *Salmonella typhimurium* strain DB7155, were provided by Professor Jonathan King's laboratory. Citric acid (lot no. 0616 KCXK) and magnesium sulfate ($MgSO_4$) (lot no. 6070 A31581) were purchased from Mallinckrodt (Paris, KY). Disodium phosphate (lot no. 896726) was obtained from Fisher Scientific (Fair Lawn, NJ). All these materials were used as received. All solutions were prepared using pH 7.2 McIlvaine's buffer consisting of 16.4 mM disodium phosphate and 1.82 mM citric acid in Milli-Q water. Milli-Q water is the product of passing deionized water through Millipore's (Bedford, MA) Milli-Q system. All glassware used in the experiments were subjected to washing in a 50:50 ethanol:1 M sodium hydroxide bath, washing in a 1 M nitric acid bath, rinsing copiously with Milli-Q water, and drying in an oven for at least one day.

5.2.2 Photographing the Two-Phase Aqueous $C_{10}E_4$ Micellar System with Different Volume Ratios

Two buffered solutions, each with a total volume of 5.7 mL, were prepared in test tubes. One solution, containing 1.50 wt% $C_{10}E_4$ and 2 mM $MgSO_4$, yielded a volume ratio that was much less than 1 at room temperature. The other solution, containing 9.80 wt% $C_{10}E_4$ and 2 mM $MgSO_4$, yielded a volume ratio that was much greater than 1 at room temperature. Graduated test tubes were not used to hold these solutions because the graduations, or markings, made the photographs less clear. These solutions were first mixed and equilibrated at 4°C in order for each solution to exhibit a single phase. The test tubes containing the solutions were subsequently clamped to a test tube stand, and allowed to equilibrate with the surrounding air at room temperature. The solutions were not placed in the thermo-regulated

device described in Section 3.2.4 because preliminary photographs that were taken of the solutions in the device appeared blurry. The photographs of the solutions in the device had less clarity because of the additional changes in the index of refraction associated with the light passing through the glass box and then through the water in the box. A white piece of paper filled with the letter "X" was then placed behind the tubes to aid in visualizing the turbidity of each phase. Specifically, if the "X" was not visible, the macroscopic phase was definitely turbid and "milky". On the other hand, if the "X" was visible, the macroscopic phase was more clear and less turbid. Since the entrained domains can scatter visible light, the turbidity in a macroscopic phase was used as an indicator to qualitatively determine the extent of entrainment. In other words, a less turbid macroscopic phase corresponded to less entrainment of domains, and vice versa. The photographs were taken after the solutions were allowed to sit at room temperature for 3 to 4 hours. The reasons for choosing a duration of 3 to 4 hours are given in Section 5.4.1.

5.2.3 Partitioning Bacteriophage P22 and Cytochrome *c* with Different Volume Ratios

For every partitioning experiment, five buffered solutions, each having a total volume of 5.5 mL, were prepared in graduated 10 mL test tubes. For the bacteriophage P22 partitioning experiments, four of the solutions contained $C_{10}E_4$, bacteriophage P22, and 2 mM $MgSO_4$ (which was required to ensure the stability of bacteriophage P22), while the fifth solution served as the control containing the same concentrations of $C_{10}E_4$ and $MgSO_4$ but no bacteriophage P22. Similarly, for the cytochrome *c* partitioning experiments, four of the solutions contained $C_{10}E_4$ and cytochrome *c*, while the fifth solution served as the control containing the same concentration of $C_{10}E_4$ but no cytochrome *c*. Since 2 mM $MgSO_4$ was only required for the stability of bacteriophage P22, it was not utilized in the cytochrome *c* partitioning experiments. The initial, overall concentrations of $C_{10}E_4$, bacteriophage P22, and cytochrome *c* in the twelve different partitioning experiments are provided in Table 5-1. The solutions were first mixed, and then equilibrated at 4°C in order for each solution to exhibit a single phase. The solutions were subsequently placed in the thermo-regulated device described in Section 3.2.4 to initiate phase separation at a particular temperature. The various partitioning temperatures are also listed in Table 5-1, along with the volume ratios attained in the experiments. Solutions were maintained at this condition for 24 hours before the two coexisting micellar phases were withdrawn with great care using 1 mL syringe and needle sets. All the partitioning experiments in this thesis were conducted for *at least* 14

Table 5-1: The conditions of the six bacteriophage P22 and the six cytochrome *c* partitioning experiments in the two-phase aqueous $C_{10}E_4$ micellar system.

Initial Concentration of $C_{10}E_4$ (wt%)	**Initial Concentration of Bacteriophage P22 (particles/mL)**	**Initial Concentration of Cytochrome *c* (g/L)**	**Partitioning Temperature (°C)**	**Volume Ratio (V_t/V_b)**
0.970	9.6×10^7	0	19.6	0.1
0.970	0	0.32	19.6	0.1
4.65	6.5×10^7	0	19.6	10
4.65	0	0.32	19.6	10
0.991	9.2×10^7	0	20.2	0.1
0.991	0	0.32	20.2	0.1
6.14	6.4×10^7	0	20.2	10
6.14	0	0.32	20.2	10
1.10	9.6×10^7	0	21.0	0.1
1.10	0	0.32	21.0	0.1
8.25	8.4×10^7	0	21.0	10
8.25	0	0.32	21.0	10

hours, since it was previously shown[70] that partition coefficients measured after overnight partitioning were similar to those measured after partitioning over at least three days. The concentration of bacteriophage P22 in each phase was measured with the plaque assay described in Section 2.2.4. The concentration of cytochrome *c* in each phase was determined as described in Section 5.2.4 below.

The partitioning temperatures of 19.6°C and 21.0°C were chosen because they were close to the minimum and maximum operating temperatures that had already been used.[70] The temperature of 20.2°C was chosen because it was approximately in the middle of the range defined by the temperatures of 19.6°C and 21.0°C. These three partitioning temperatures were also selected because the experimentally measured partition coefficients of bacteriophage P22 were found to be orders of magnitude greater than the theoretically predicted ones at these temperatures. Accordingly, if the entrainment of micelle-poor domains in the macroscopic, top, micelle-rich phase was responsible for this discrepancy between experiment and theory, a significant decrease in the partition coefficient was expected to be observed for bacteriophage P22 when the volume ratio was decreased from being much greater than 1 to being much less than 1. After selecting the partitioning temperatures, the initial, overall concentrations of $C_{10}E_4$ were chosen for the different experiments to yield volume ratios that were approximately equal to 10 and 0.1. These volume ratios were chosen because they differed by a factor of 100. More extreme volume ratios, such as, 100 and 0.01, were not utilized because of the difficulties associated with using a syringe to withdraw a very small sample volume. Indeed, even for volume ratios that are approximately equal to 10 and 0.1, the volume of the small phase is only 0.5 mL. Although the volume of the small phase could be increased by increasing the total solution volume and increasing the size of the test tubes, different test tubes were not used, and the same graduated 10 mL test tubes were utilized to ensure consistency between all the partitioning experiments.

5.2.4 Experimentally Evaluating the Partition Coefficient of Cytochrome *c*

The partition coefficient of cytochrome *c* was determined by measuring the concentrations of cytochrome *c* in the top and bottom phases of a partitioning solution. The concentration of cytochrome *c* in each phase was determined as described below. After first adding sodium L-ascorbate to each phase to reduce cytochrome *c*, the phases were transferred to cuvettes and placed in a cuvette holder that was maintained at a temperature of 14 to 15°C to prevent the onset of phase separation. Visible absorbance readings of the sample and the control were then taken at 549.5 nm (where cytochrome *c* absorbs visible light) and 600 nm

(to define the zero absorbance for each solution) using a Shimadzu UV-160U UV-Visible Recording Spectrophotometer (Columbia,MD). Note that the absorbances of the sample and the control at 600 nm were measured to ensure that the same baseline was employed for all the different solutions. Specifically, the absorbance at 600 nm was measured and set equal to zero to remove any constant offsets or systematic errors associated with comparing absorbance readings from different cuvettes. Although quartz cuvettes of the same type were purchased from the same manufacturer to minimize this source of systematic error, the error was not negligible for the absorbance readings in our experiments. The wavelength of 600 nm was selected to define the zero absorbance because it corresponded to a wavelength where there was little or no measured absorbance in all the solutions. Absorbance readings of a particular sample at 549.5 nm and 600 nm were then taken and referenced to those obtained from the control to eliminate the contribution due to scattering from the micelles present in the solutions. This is shown in the following two equations:

$$A_{s,t,549.5nm,cor} = (A_{s,t,549.5nm} - A_{s,t,600nm}) - (A_{c,t,549.5nm} - A_{c,t,600nm}) \tag{5.1}$$

and

$$A_{s,b,549.5nm,cor} = (A_{s,b,549.5nm} - A_{s,b,600nm}) - (A_{c,b,549.5nm} - A_{c,b,600nm}) \tag{5.2}$$

where $A_{s,t,549.5nm,cor}$ and $A_{s,b,549.5nm,cor}$ are the *corrected* absorbance readings at 549.5 nm for the sample's top and bottom phases, respectively, $A_{s,t,549.5nm}$ and $A_{s,b,549.5nm}$ are the *actual* absorbance readings at 549.5 nm for the sample's top and bottom phases, respectively, $A_{s,t,600nm}$ and $A_{s,b,600nm}$ are the *actual* absorbance readings at 600 nm for the sample's top and bottom phases, respectively, $A_{c,t,549.5nm}$ and $A_{c,b,549.5nm}$ are the *actual* absorbance readings at 549.5 nm for the control's top and bottom phases, respectively, and $A_{c,t,600nm}$ and $A_{c,b,600nm}$ are the *actual* absorbance readings at 600 nm for the control's top and bottom phases, respectively. The absorbance readings of the top and bottom phases of the control were required to account for the light scattering from the micelles. The control's top phase contains the same concentration of micelles as the sample's top phase, but contains no protein. The same is true with regard to the bottom phases of the control and the sample. The micelles in each sample phase scatter some of the incident light in many directions, which causes a decrease in the intensity of light that actually reaches the detector. Accordingly, the measured absorbance of each sample phase will be greater than that due to a sample

phase containing cytochrome c alone, since the absorbance of the solution is defined as:[104]

$$A \equiv log\left(\frac{I_0}{I}\right) \tag{5.3}$$

where I is the intensity of light transmitted by the absorbing solution (the intensity of light that actually reaches the detector), and I_0 is the intensity of incident light (the intensity that leaves the source). Therefore, in order to subtract the contribution to the absorbance due to the micelles, absorbance measurements of the control's top and bottom phases were conducted, and Eqs. (5.1) and (5.2) were used. The *corrected* absorbance readings evaluated using Eqs. (5.1) and (5.2) were found to be directly proportional to the concentrations of cytochrome c, which was in agreement with the following Beer-Lambert law:[104]

$$A = \epsilon d_p C \tag{5.4}$$

where ϵ is the absorption coefficient of the solution, d_p is the path length of the cuvette, and C is the concentration of the absorbing species (cytochrome c) in the solution.

Recall that the protein partition coefficient, K_p, is defined as follows:[75]

$$K_p \equiv \frac{C_{p,t}}{C_{p,b}} \tag{1.3}$$

where $C_{p,t}$ and $C_{p,b}$ are the concentrations of protein in the top and bottom phases, respectively. The protein partition coefficient quantifies the distribution of a particular protein between the two coexisting phases. Since the Beer-Lambert law (Eq. (5.4)) was found to apply for cytochrome c, the partition coefficient of cytochrome c was evaluated as follows:

$$K_p = \frac{\left[\frac{A_{s,t,549.5nm,cor}}{\epsilon_t}\right]}{\left[\frac{A_{s,b,549.5nm,cor}}{\epsilon_b}\right]} \tag{5.5}$$

where ϵ_t and ϵ_b are the absorption coefficients of the top and bottom phases, respectively. Note that the path length, d_p, does not appear in Eq. (5.5), since it has the same value for all the cuvettes, and therefore, cancels out in the ratio (see Eqs. (1.3) and (5.4)). The absorption coefficient, on the other hand, is a weak function of the temperature and the environment surrounding the protein.[104] Although the temperature was maintained constant, it was not clear if the presence of more micelles in the top phase would give rise to a different solvent effect with regard to absorbance when compared to the bottom phase. However,

after measuring standard curves of absorbance as a function of protein concentration at different concentrations of $C_{10}E_4$, the absorption coefficient was experimentally found to be the same between the top and bottom phases. Therefore, Eq. (5.5) can be rewritten as follows:

$$K_p = \frac{A_{s,t,549.5nm,cor}}{A_{s,b,549.5nm,cor}} \tag{5.6}$$

Accordingly, the protein partition coefficient was evaluated by taking the ratio of the *corrected* absorbance reading of the top phase and that of the bottom phase.

5.2.5 Measuring the Viscosities of Buffered $C_{10}E_4$ Solutions

In Section 5.3.3, the viscosity of the macroscopic, top, micelle-rich phase is shown to be a possible factor influencing the entrainment of micelle-poor domains in the macrocopic, top, micelle-rich phase. In particular, it is shown that increasing the viscosity of the macrocopic, top, micelle-rich phase can decrease the settling velocity of a sedimenting micelle-poor domain by increasing the Stokes drag force on the micelle-poor domain. This decrease in the settling velocity can then give rise to more micelle-poor domains being entrained in the macroscopic, top, micelle-rich phase when the top phase is withdrawn. The viscosity of the macroscopic, top, micelle-rich in the $C_{10}E_4$-buffer system is also expected to increase with an increase in the temperature, since the $C_{10}E_4$ concentration in the macroscopic, top, micelle-rich phase increases with an increase in temperature (see Figure 4-1). Since viral partitioning experiments were already being conducted as a function of temperature (see Section 5.2.3), viscosity measurements of buffered $C_{10}E_4$ solutions were also performed to identify any correlation between the measured viral partition coefficients and the measured viscosities. For the partitioning experiments conducted at 19.6°C, 20.2°C, and 21.0°C, the concentrations of $C_{10}E_4$ in the macroscopic, top, micelle-rich phase were 5.37 wt%, 7.46 wt%, and 10.2 wt%, respectively (see the coexistence curve for the $C_{10}E_4$ (lot no. 6011)-buffer system in Figure 4-1). Therefore, in order to identify a trend in the viscosities of the macroscopic, top, micelle-rich phases encountered in the partitioning experiments, the viscosities of buffered $C_{10}E_4$ solutions containing 5 wt% and 10 wt% $C_{10}E_4$ were measured as described below.

The solution viscosity was measured using a Cannon (State College, PA) capillary viscometer (Cannon-Ubbelhode semi-micro dilution viscometer, no. 100 K888). In these experiments, the time required for a fixed volume of the solution to flow through the vertical capillary tube is measured, and the solution viscosity can then be calculated from this time period. A 10 wt% $C_{10}E_4$ solution was first poured into the viscometer. The viscometer was then vertically held in a water tank connected to a water bath. This set-up was similar to

that of the thermo-regulated device described in Section 3.2.4, except that a very large water tank was used in place of the smaller plastic or glass box. A large water tank was required in order for the viscometer to be completely immersed in the water. The temperature of the water throughout the entire tank was maintained constant at 16.0°C. This temperature was chosen to ensure that both the 10 wt% and 5 wt% $C_{10}E_4$ solutions exhibited a single phase during the measurements. Before taking any measurements, the solution was kept in the viscometer in the water tank for at least 20 minutes to ensure the attainment of thermal equilibrium. After allowing the solution to thermally equilibrate, the solution was drawn up through the capillary tube to position the meniscus of the solution at a prescribed horizontal position marked on the viscometer. The time required for a fixed volume of the solution to flow through the capillary, as denoted by the solution meniscus passing through two horizontal marks on the viscometer (the original one and a lower one), was measured. This procedure was repeated at least three times.

Following the viscosity measurement of the 10 wt% $C_{10}E_4$ solution, buffer was added directly into the viscometer to dilute the solution to half of its original concentration, that is, to 5 wt%. The viscometer was then shaken gently to ensure that the solution inside was uniformly mixed. As in the case of the 10 wt% $C_{10}E_4$ solution, the 5 wt% $C_{10}E_4$ solution was kept in the viscometer in the water tank for at least 20 minutes before taking any measurements to ensure the attainment of thermal equilibrium.

5.3 Theory

5.3.1 Estimation of the Effect of Micelle-Poor (Virus-Rich) Domains Being Entrained in the Macroscopic, Top, Micelle-Rich Phase

It will now be shown theoretically that only a very small volume fraction of the macroscopic, top, micelle-rich phase needs to be comprised of micelle-poor (virus-rich) domains in order to yield the experimentally measured viral partition coefficients. In accordance with the biggest "clue" concept described in Section 5.1, this effect will also be shown theoretically to negligibly influence the partition coefficients of the previously studied water-soluble proteins.

The measured viral partition coefficient, K_v, will first be defined as follows:[75]

$$K_v \equiv \frac{C_{v,t}}{C_{v,b}} \tag{1.5}$$

where $C_{v,t}$ and $C_{v,b}$ are the concentrations of the virus in the top and bottom phases, respectively. Let us now define x to be the volume fraction of the macroscopic, top, micelle-rich phase that corresponds to the micelle-poor domains. Let us also define $C^{EV}_{v,rich}$ and $C^{EV}_{v,poor}$ to be the concentrations of virus in the micelle-rich and micelle-poor domains, respectively. Note that, in the derivation that follows, it is assumed that the virus, and also the protein (see below), partition between the micelle-rich and micelle-poor domains according to the excluded-volume theory. The overall concentration of virus that is measured in the top phase is therefore given by:

$$C_{v,t} = \frac{(1-x)\,V_t C^{EV}_{v,rich} + x V_t C^{EV}_{v,poor}}{V_t} \tag{5.7}$$

where V_t is the volume of the macroscopic, top phase. Cancelling the V_t terms in Eq. (5.7) yields:

$$C_{v,t} = (1-x)\,C^{EV}_{v,rich} + x C^{EV}_{v,poor} \tag{5.8}$$

As shown below, $C^{EV}_{v,rich}$ is related to $C^{EV}_{v,poor}$ by K^{EV}_v, that is, by the partition coefficient that results from only considering the excluded-volume interactions between the virus and the $C_{10}E_4$ micelles. Specifically,

$$K^{EV}_v = \frac{C^{EV}_{v,rich}}{C^{EV}_{v,poor}} \tag{5.9}$$

Solving Eq. (5.9) for $C^{EV}_{v,rich}$ yields:

$$C^{EV}_{v,rich} = K^{EV}_v C^{EV}_{v,poor} \tag{5.10}$$

Substituting Eq. (5.10) in Eq. (5.8), and rearranging yields:

$$C_{v,t} = C^{EV}_{v,poor}\left[K^{EV}_v + x\left(1 - K^{EV}_v\right)\right] \tag{5.11}$$

Combining Eqs. (1.5) and (5.11) then yields:

$$K_v = \frac{C^{EV}_{v,poor}\left[K^{EV}_v + x\left(1 - K^{EV}_v\right)\right]}{C_{v,b}} \tag{5.12}$$

Since only the entrainment of micelle-poor (virus-rich) domains in the macroscopic, top, micelle-rich phase is being considered in this derivation, the entrainment of micelle-rich (virus-poor) domains in the macrocopic, bottom, micelle-poor phase will be neglected in this derivation. (Note, however, that Section 5.3.2 examines theoretically the entrainment of micelle-rich (virus-poor) domains.) Assuming no entrainment of micelle-rich (virus-poor)

domains, the following equation also applies:

$$C_{v,b} = C_{v,poor}^{EV} \tag{5.13}$$

Substituting Eq. (5.13) in Eq. (5.12) yields:

$$K_v = K_v^{EV} + x\left(1 - K_v^{EV}\right) \tag{5.14}$$

Note that if there was no entrainment of micelle-poor domains, then $x = 0$, and Eq. (5.14) correctly yields $K_v = K_v^{EV}$. For bacteriophage P22, $K_v \approx 2 \times 10^{-3}$, and $K_v^{EV} \ll 2 \times 10^{-3}$ based on Figure 1-11. Consequently, Eq. (5.14) simplifies to:

$$K_v \approx 2 \times 10^{-3} \approx x \tag{5.15}$$

This result is very striking because it shows that only 2×10^{-3} of the total top phase volume needs to be comprised of micelle-poor domains in order to yield the observed viral partition coefficient. As will now be shown, this effect is negligible for the partition coefficients of water-soluble proteins. The derivation of Eq. (5.14) is also valid for a water-soluble protein, where "p" for protein replaces "v" for virus in the subscripts. Accordingly, Eq. (5.14) for a water-soluble protein is given by:

$$K_p = K_p^{EV} + x\left(1 - K_p^{EV}\right) \tag{5.16}$$

In contrast to viral partitioning, K_p^{EV} is between 0.1 and 1. However, the worst case scenario will be investigated to demonstrate that the entrainment of micelle-poor domains in the macroscopic, top, micelle-rich phase can only have a small effect on the experimentally measured protein partition coefficients. With regard to x, $x = 0.1 \gg 2 \times 10^{-3}$ corresponds to a highly unlikely situation, since some of the entrained micelle-poor domains should be able to coalesce and sediment if one-tenth of the total top phase volume is comprised of the micelle-poor domains. With regard to K_p, $K_p^{EV} = 0.1$ represents the worst case scenario, since the difference in protein concentrations between the two domains is the largest. For $x = 0.1$ and $K_p^{EV} = 0.1$, K_p would only be 0.19, which is less than twice the value of $K_p^{EV} = 0.1$. Therefore, even in this very unlikely case where one-tenth of the total top phase volume is comprised of micelle-poor domains, K_p and K_p^{EV} are not orders of magnitude different. Therefore, the hypothesis put forward regarding the possible entrainment of micelle-poor domains in the macroscopic, top, micelle-rich phase is one that can significantly affect viral

partitioning, while negligibly affecting protein partitioning. As discussed in Section 5.1, this hypothesis was investigated in this experimental study by partitioning cytochrome c and bacteriophage P22 with different volume ratios.

5.3.2 Estimation of the Effect of Micelle-Rich (Virus-Poor) Domains Being Entrained in the Macroscopic, Bottom, Micelle-Poor Phase

It will now be shown theoretically that, unlike the scenario described in Section 5.3.1, the entrainment of micelle-rich (virus-poor) domains in the macrocopic, bottom, micelle-poor phase has a negligible effect on *both* the viral and protein partition coefficients.

Let us define y to be the volume fraction of the macroscopic, bottom, micelle-poor phase that corresponds to the micelle-rich (virus-poor) domains. The overall concentration of virus that is measured in the bottom phase is therefore given by:

$$C_{v,b} = \frac{(1-y)\,V_b C^{EV}_{v,poor} + y V_b C^{EV}_{v,rich}}{V_b} \tag{5.17}$$

where V_b is the volume of the macroscopic, bottom phase. Cancelling the V_b terms in Eq. (5.17) yields:

$$C_{v,b} = (1-y)\,C^{EV}_{v,poor} + y C^{EV}_{v,rich} \tag{5.18}$$

Solving Eq. (5.9) for $C^{EV}_{v,poor}$ yields:

$$C^{EV}_{v,poor} = \frac{C^{EV}_{v,rich}}{K^{EV}_v} \tag{5.19}$$

Substituting Eq. (5.19) in Eq. (5.18), and rearranging yields the following relation:

$$C_{v,b} = C^{EV}_{v,rich}\left[\frac{1}{K^{EV}_v} + y\left(1 - \frac{1}{K^{EV}_v}\right)\right] \tag{5.20}$$

Multiplying Eq. (5.20) by 1 in the form of (K^{EV}_v/K^{EV}_v) then yields:

$$C_{v,b} = \left(\frac{C^{EV}_{v,rich}}{K^{EV}_v}\right)\left[1 + y\left(K^{EV}_v - 1\right)\right] \tag{5.21}$$

Combining Eqs. (1.5) and (5.21) yields:

$$K_v = \frac{C_{v,t} K^{EV}_v}{C^{EV}_{v,rich}\left[1 + y\left(K^{EV}_v - 1\right)\right]} \tag{5.22}$$

Since only the entrainment of micelle-rich (virus-poor) domains in the macroscopic, bottom, micelle-poor phase is being considered in this derivation, the entrainment of micelle-poor (virus-rich) domains in the macrocopic, top, micelle-rich phase will be neglected in this derivation. Accordingly, the following equation also applies:

$$C_{v,t} = C_{v,rich}^{EV} \tag{5.23}$$

Substituting Eq. (5.23) in Eq. (5.22) yields:

$$K_v = \frac{K_v^{EV}}{1 + y\left(K_v^{EV} - 1\right)} \tag{5.24}$$

Note that if there was no entrainment of micelle-rich (virus-poor) domains, then $y = 0$, and Eq. (5.24) correctly yields $K_v = K_v^{EV}$. From Figure 1-11, $K_v^{EV} \ll 1$. In addition, for the highly unlikely situation where $y = 0.1$, Eq. (5.24) simplifies to:

$$K_v \approx 1.1 K_v^{EV} \tag{5.25}$$

Hence, even in this highly unlikely case where one-tenth of the total bottom phase volume is comprised of micelle-rich (virus-poor) domains, K_v and K_v^{EV} are similar. In other words, the entrainment of micelle-rich (virus-poor) domains in the macroscopic, bottom, micelle-poor phase should negligibly affect the partitioning behavior of the virus. This effect, as will now be shown, is also negligible for the partition coefficients of water-soluble proteins. The derivation of Eq. (5.24) is also valid for a water-soluble protein, where "p" for protein replaces "v" for virus in the subscripts. Accordingly, Eq. (5.24) for a water-soluble protein is given by:

$$K_p = \frac{K_p^{EV}}{1 + y\left(K_p^{EV} - 1\right)} \tag{5.26}$$

Even in the highly unlikely situation of $y = 0.1$, and the worst case scenario of $K_p^{EV} = 0.1$ (where the difference in protein concentrations between the two domains is the largest), K_p would only be 0.11, which is very close to the value of $K_p^{EV} = 0.1$. Accordingly, contrary to the scenario where micelle-poor (virus-rich) domains are entrained in the macroscopic, top, micelle-rich phase, entrainment of micelle-rich (virus-poor) domains in the macroscopic, bottom, micelle-poor phase has a negligible effect on *both* viral and protein partitioning. Consequently, the entrainment of micelle-rich (virus-poor) domains in the bottom phase will not be the focus of this study.

5.3.3 The Settling Velocity of a Micelle-Poor Domain Entrained in the Macroscopic, Top, Micelle-Rich Phase

It will now be shown theoretically that an increase in the viscosity of the macroscopic, top, micelle-rich phase may cause an increase in the entrainment of micelle-poor domains in the top phase. The entrained micelle-poor domains will be modeled as dispersed spherical droplets within a continuous macroscopic, top, micelle-rich phase. These entrained domains sediment due to the density difference between the macroscopic, micelle-rich phase and the micelle-poor domains. The micelle-poor domains will be assumed to be sufficiently far from each other so that the streamlines associated with one domain are independent of the streamlines associated with the other domains, that is, the flow patterns around each domain can be viewed as being independent. This is a reasonable assumption, because the number of entrained micelle-poor domains, or the volume fraction of the top phase associated with the micelle-poor domains, is expected to be low. Creeping flow ($Re \ll 1$, where Re is the Reynolds number) will first be assumed to obtain an expression for the settling velocity. This assumption, however, will be justified later by showing that the resulting settling velocity does indeed yield a Reynolds number that is much less than 1. In the creeping flow regime, the drag force, F_D, on a spherical droplet (micelle-poor microdomain) is given by:

$$F_D = 6\pi\eta_{out}Rv\frac{2\eta_{out} + 3\eta_{in}}{3\eta_{out} + 3\eta_{in}} \tag{5.27}$$

where R is the radius of the spherical, micelle-poor domain, η_{out} and η_{in} are the viscosities of the fluid outside (micelle-rich) and inside (micelle-poor) the sphere, respectively, and v is the settling velocity of the sphere. A force balance on the spherical, micelle-poor domain is also necessary, and is given by Newton's second law of motion, that is, by:

$$m_{in}\frac{dv}{dt} = F_G - F_B - F_D \tag{5.28}$$

where m_{in} is the mass of the spherical, micelle-poor domain, t is time, F_B is the buoyant force on the spherical domain, and F_G is the gravitational force on the spherical domain. Equation (5.28) can also be rewritten as follows:

$$(4/3)\,\pi R^3\rho_{in}\frac{dv}{dt} = (4/3)\,\pi R^3 g\,(\rho_{in} - \rho_{out}) - 6\pi\eta_{out}Rv\frac{2\eta_{out} + 3\eta_{in}}{3\eta_{out} + 3\eta_{in}} \tag{5.29}$$

where ρ_{in} and ρ_{out} are the mass densities of the fluid inside (micelle-poor) and outside (micelle-rich), respectively, and g is the gravitational acceleration. Assuming that the spher-

ical domains are initially at rest, the solution of Eq. (5.29) is given by:

$$v = \left(1 - \frac{\rho_{out}}{\rho_{in}}\right)\left(\frac{g}{\varsigma}\right)[1 - \exp(-\varsigma t)] \tag{5.30}$$

where

$$\varsigma = \frac{9\eta_{out}\,(2\eta_{out} + 3\eta_{in})}{2\rho_{in}R^2\,(3\eta_{out} + 3\eta_{in})} \tag{5.31}$$

Equation (5.30) is an expression for the settling velocity. Based on Eqs. (5.30) and (5.31), the settling velocity decreases as the viscosity of the macroscopic, top, micelle-rich phase increases (η_{out} increases). This decrease in the settling velocity can then allow more of the micelle-poor domains to remain entrained in the macroscopic, top, micelle-rich phase for a longer period of time. Consequently, when the top phase is withdrawn with a syringe, a higher concentration of viral particles may be measured in the macroscopic, top phase, which will in turn yield a higher viral partition coefficient. Although Eq. (5.30) is an expression for the settling velocity as a function of time, a value is required for v to check the creeping flow assumption ($Re \ll 1$), where the Reynolds number is given by:

$$Re = \frac{(\rho_{out})\,(v)\,(2R)}{\eta_{out}} \tag{5.32}$$

The worst case scenario should be applied in verifying the creeping flow assumption. According to Eq. (5.32), the worst case scenario corresponds to using the highest settling velocity, which happens to be the terminal velocity, v_{ter}, (Eq. (5.30) when t$\rightarrow \infty$). Note that v_{ter} is equivalent to solving for the velocity when the gravitational force equals the sum of the drag and buoyant forces, that is,

$$v_{ter} = \frac{g}{\varsigma}\left(1 - \frac{\rho_{out}}{\rho_{in}}\right) \tag{5.33}$$

According to Eqs. (5.31) and (5.33), the terminal velocity is also the largest value when the viscosity of the micelle-rich phase (η_{out}) is equal to the lowest possible value, which is the viscosity of pure water (1 cP). This value for η_{out} also aids in providing the worst case scenario by decreasing the denominator in Eq. (5.32), and therefore, increasing the Reynolds number. Since the viscosity of the micelle-poor domains (η_{in}) cannot be higher than that of the macroscopic, top, micelle-rich phase, the following approximation will be used.

$$\eta_{out} \approx \eta_{in} \approx 1cP \tag{5.34}$$

With regard to R, the radius of a spherical, micelle-poor domain, it will be assumed to be 10

μm, since particles of that size can scatter light. Only the mass densities, ρ_{out} and ρ_{in}, remain to be estimated. However, they both cannot be approximated as 1 g/mL because then v_{ter} would be 0 according to Eq. (5.33). Since these density values are unavailable, they were estimated as shown in Appendix B. The mass densities were evaluated to be $\rho_{in} = 0.99995$ g/mL and $\rho_{out} = 0.99539$ g/mL. With all these estimates for the parameters and $g = 9.8$ m/s^2, the Reynolds number was found to be $Re = 2.4 \times 10^{-5}$. Since the Reynolds number was found to be orders of magnitude less than 1, the creeping flow assumption is indeed valid.

The estimates of ρ_{in} and ρ_{out} also indicate that entrainment is likely because of the small difference between ρ_{in} and ρ_{out}, or more specifically, between the gravitational and buoyant forces. Since the viscosity of the macroscopic, top, micelle-rich phase is also expected to be higher than that of pure water, the higher viscosity can also increase the entrainment by increasing the drag force on the micelle-poor domains. In addition, the energetic penalty associated with the interfacial area between the entrained micelle-poor domains and the macroscopic, top, micelle-rich phase is also expected to be relatively small, since the interfacial tension between two micellar phases is estimated to be only about 0.01 erg/cm^2.[105] This is a very low interfacial tension when compared to a heptane-water interfacial tension of 51 erg/cm^2.[106]

5.4 Results and Discussion

5.4.1 Photographing the Two-Phase Aqueous $C_{10}E_4$ Micellar System with Different Volume Ratios

The photographs of the two-phase aqueous $C_{10}E_4$ micellar system with volume ratios that are much less than 1 and much greater than 1 are presented in Figure 5-3. As shown in Figure 5-3, the top phase becomes clear when the volume ratio is decreased from being much greater than 1 to being much less than 1. Specifically, the letter "X" behind the top phase becomes visible as the volume ratio is decreased. Since the entrained domains can scatter visible light, the turbidity of each macroscopic phase can be used as an indicator to qualitatively asses the extent of entrainment. Therefore, the photographs shown in Figure 5-3 indicate that the entrainment of micelle-poor domains in the macroscopic, top, micelle-rich phase decreases as the volume ratio is decreased from being much greater than 1 to being much less than 1.

Although the duration of a typical partitioning experiment is greater than or equal to 14

hours, the photographs shown in Figure 5-3 were taken 3 to 4 hours after phase separation was initiated. Preliminary photographs, however, were first taken after letting the phases settle overnight, but they were not able to capture the slight turbidity of the top phase (in the case corresponding to $V_t/V_b \gg 1$) and of the bottom phase (in the case corresponding to $V_t/V_b \ll 1$). The phases were less turbid after letting the phases settle overnight because some of the entrained domains reached their corresponding macroscopic phases. However, in order to qualitatively identify a trend between entrainment and the volume ratio, pictures of the phases were taken after a shorter time period of 3 to 4 hours. Even though a shorter duration of 3 to 4 hours was utilized, the entrainment of micelle-poor domains in the macroscopic, top, micelle-rich phase was still expected to be less for the $V_t/V_b \ll 1$ case than for the $V_t/V_b \gg 1$ case after an overnight partitioning experiment. In addition, it should be noted that the more precise, quantitative experimental test of the hypothesis proposed in Section 5.1 was the partitioning study conducted with a model protein and a model virus in the two-phase aqueous $C_{10}E_4$ micellar system with volume ratios that were much greater than 1 and much less than 1 (see Section 5.4.2).

5.4.2 Partitioning Bacteriophage P22 and Cytochrome *c* with Different Volume Ratios

The results of the bacteriophage P22 and cytochrome *c* partitioning experiments are shown in Figures 5-4 and 5-5, respectively. The mass balances on both bacteriophage P22 and cytochrome *c* closed to 100% within the experimental error for all the partitioning experiments. As shown in Figure 5-4, the partition coefficient of bacteriophage P22 at each temperature decreased by about an order of magnitude when the volume ratio was decreased from 10 to 0.1. Since the entrainment of micelle-poor domains in the macroscopic, top, micelle-rich phase was also expected to decrease as the volume ratio was decreased from 10 to 0.1, it was concluded that the entrainment of micelle-poor domains in the top phase does significantly affect viral partitioning. It should also be noted that this was the first time that partition coefficients as low as 1.0×10^{-4} were observed for bacteriophage P22, since in previous partitioning experiments, the partition coefficients of bacteriophage P22 were approximately 2×10^{-3} for a volume ratio of 1 (see Figures 1-11 and 4-2). Therefore, the decrease in the partition coefficient of bacteriophage P22 from 2×10^{-3} to 1×10^{-4} indicates that some of the entrainment of micelle-poor domains in the top phase was also reduced when the volume ratio was reduced from 1 to 0.1. This was expected since the entrainment of micelle-poor domains in the top phase decreases as the volume ratio decreases, and therefore,

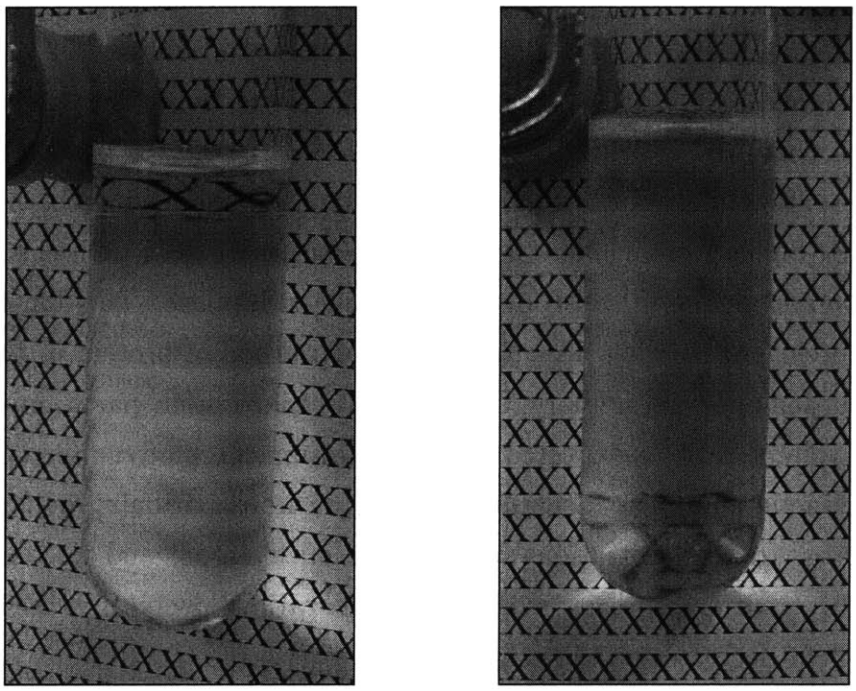

Figure 5-3: The two-phase aqueous $C_{10}E_4$ micellar system three to four hours after initiating phase separation for a volume ratio: (a) much less than 1, and (b) much greater than 1. Since the entrained domains can give rise to light scattering, the turbidity of each macroscopic phase can be used as an indicator to qualitatively assess the extent of entrainment. The white piece of paper filled with the letter "X" was placed behind the tubes to aid in visualizing the turbidity of each phase.

reducing the volume ratio below 0.1 in the future may further reduce the entrainment. In addition, the partition coefficient of 2×10^{-3} was slightly lower than those measured for a volume ratio of 10, which further corroborates the idea that decreasing the volume ratio (in this case, from 10 to 1) reduces the entrainment.

On the other hand, as shown in Figure 5-5, for cytochrome *c*, the entrainment of micelle-poor domains in the macroscopic, top, micelle-rich phase has a negligible effect on its partitioning behavior. Accordingly, the protein partition coefficients are independent of volume ratio, which is what is expected based on equilibrium thermodynamics. Varying the volume ratio at a given temperature does not change the intensive properties of the two phases in the $C_{10}E_4$-buffer system, namely, the concentrations of $C_{10}E_4$ in the two phases. Therefore, the interactions of a partitioning solute with the micelles in the two phases should not change with the volume ratio, and the partition coefficient should remain constant. However, in the case of the $C_{10}E_4$-buffer system, there is a kinetic effect associated with the entrainment of micelle-poor domains in the macroscopic, top, micelle-rich phase. This kinetic effect negligibly affects protein partitioning because the concentrations of protein in the micelle-poor and micelle-rich domains are similar. Consequently, the protein partition coefficients are independent of volume ratio as expected from equilibrium thermodynamics. With regard to the virus, this kinetic effect has a significant effect on its partitioning behavior due to the large difference in viral concentrations between the micelle-poor and micelle-rich domains. As a result, viral partitioning varies with the volume ratio. Specifically, the measured viral partition coefficient decreases as the volume ratio decreases.

In addition, as shown in Figure 5-5, the partition coefficient of cytochrome *c* decreases as the temperature increases in accordance with equilibrium thermodynamics dictated by excluded-volume interactions (see the theoretical predictions in Figures 1-6 and 1-11). In contrast, the partition coefficient of bacteriophage P22 slightly increases as the temperature increases in Figure 5-4. This opposite trend may be rationalized if the entrainment of the micelle-poor domains in the macroscopic, top, micelle-rich phase was found to increase as the temperature increased. Since increasing the viscosity of the macroscopic, top, micelle-rich phase may increase the entrainment of micelle-poor domains in the top phase (see the theoretical discussion in Section 5.3.3), it is indeed possible that an increase in temperature, which is expected to increase the viscosity of the top phase, could give rise to a slight increase in the partition coefficient of bacteriophage P22. The viscosities of buffered $C_{10}E_4$ solutions were therefore measured, and the results are presented in Section 5.4.3.

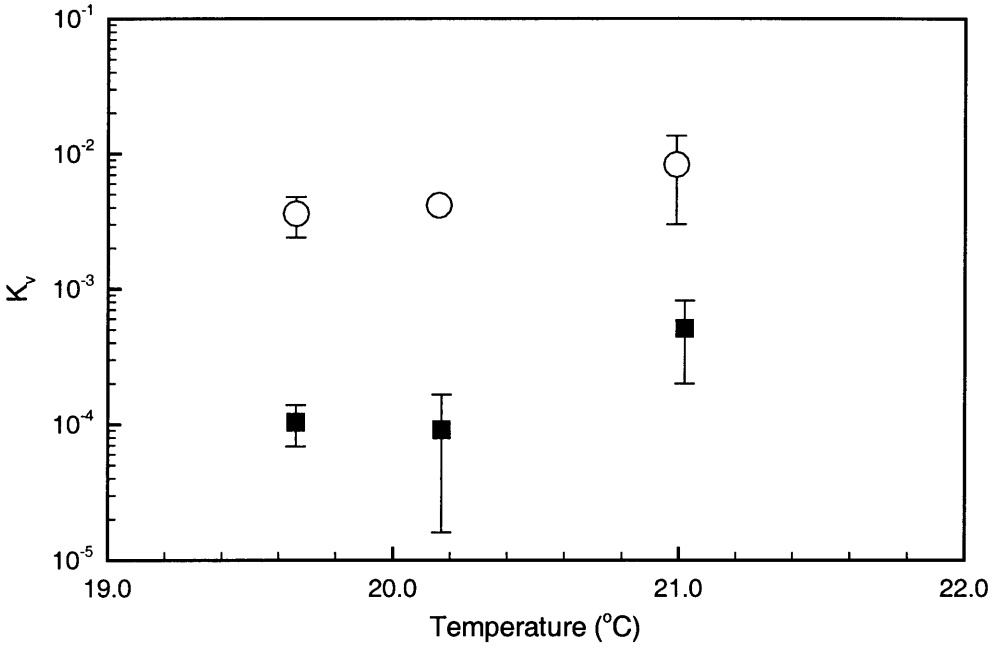

Figure 5-4: Experimentally measured partition coefficients of bacteriophage P22 as a function of temperature for different volume ratios. The black square and white circle symbols represent the partition coefficients of bacteriophage P22 that were measured using a volume ratio of 0.1 and 10, respectively. The error bars correspond to 95% confidence limits for the measurements. Note that the error bars appear asymmetric due to the use of a semi-logarithmic plot.

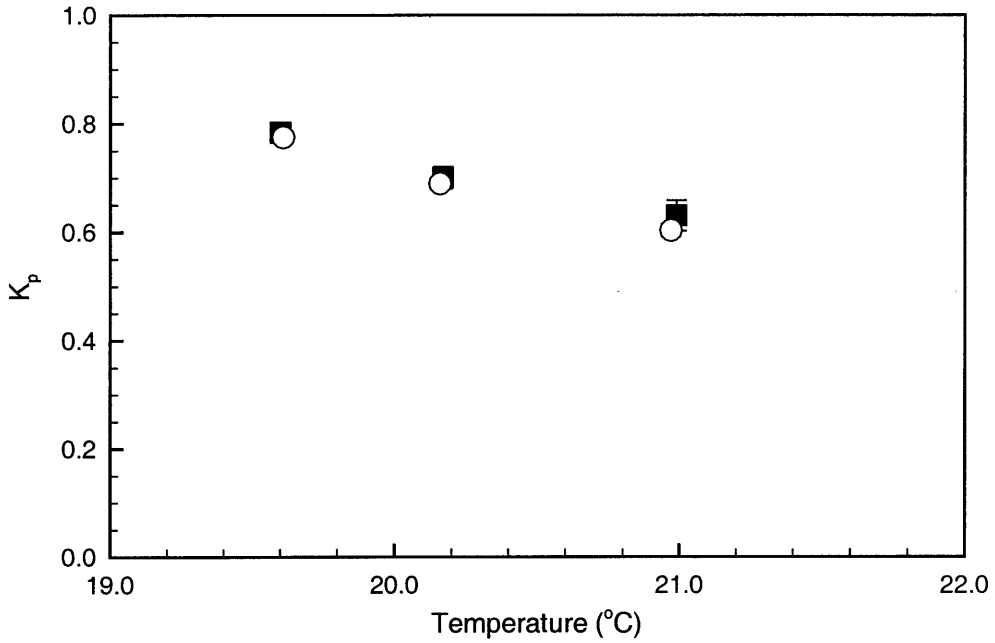

Figure 5-5: Experimentally measured partition coefficients of cytochrome *c* as a function of temperature for different volume ratios. The black square and white circle symbols represent the partition coefficients of cytochrome *c* that were measured using a volume ratio of 0.1 and 10, respectively. The error bars correspond to 95% confidence limits for the measurements.

5.4.3 Measuring the Viscosities of Buffered $C_{10}E_4$ Solutions

The viscosity of the macroscopic, top, micelle-rich phase in the $C_{10}E_4$-buffer system is expected to increase with an increase in the temperature, since the concentration of $C_{10}E_4$ in the top phase increases with an increase in temperature (see Figure 4-1). For the temperatures of 19.6°C, 20.2°C, and 21.0°C used in the partitioning experiments of Section 5.4.2, the concentrations of $C_{10}E_4$ in the macroscopic, top, micelle-rich phase were 5.37 wt%, 7.46 wt%, and 10.2 wt%, respectively (see the coexistence curve for the $C_{10}E_4$ (lot no. 6011)-buffer system in Figure 4-1). Therefore, in order to identify a trend in the viscosities of the macroscopic, top, micelle-rich phases encountered in the partitioning experiments, the viscosities of buffered $C_{10}E_4$ solutions containing 5 wt% and 10 wt% $C_{10}E_4$ were measured, and the results are summarized in Table 5-2.

As expected, the viscosity of the 10 wt% $C_{10}E_4$ solution was higher than that of the 5 wt% $C_{10}E_4$ solution. Although these micellar solutions with fairly high concentrations of $C_{10}E_4$ may no longer be Newtonian, the results reported here clearly verify the trend that increasing the concentration of $C_{10}E_4$ in the macroscopic, top, micelle-rich phase increases its viscosity. More importantly, these viscosity results can be used along with the coexistence

Table 5-2: Experimentally measured viscosities of buffered $C_{10}E_4$ solutions. The errors correspond to 95% confidence limits for the measurements.

Concentration of $C_{10}E_4$ (wt%)	Viscosity (cP)
5	7.7 ± 0.1
10	18.9 ± 0.1

curve of the $C_{10}E_4$-buffer system to rationalize the increase in the partition coefficient of bacteriophage P22 with an increase in the temperature.

Although partitioning over longer periods of time should allow more of the entrained micelle-poor domains to sediment into the bottom phase (especially for the partitioning experiments conducted at higher temperatures), some micelle-poor domains will remain entrained. For example, as discussed in Section 5.1, previous partitioning experiments, which were conducted with a volume ratio of 1, demonstrated that the partition coefficients of bacteriophage P22 measured after 2 weeks of partitioning were similar to those measured after overnight partitioning.[70] This result is not surprising, because domains can remain entrained for very long periods of time even in oil-water-surfactant systems where the two phases are more dissimilar.

5.4.4 Comparison between the Experimentally Measured and Theoretically Predicted Partition Coefficients

In this section, the measured partition coefficients of bacteriophage P22 and cytochrome *c* from Section 5.4.2 are compared to the predicted values based on the excluded-volume theory. Accordingly, a brief review of the excluded-volume theory will now be provided to discuss the parameters in the theory. Recall that the partition coefficient of solute (s) predicted by the excluded-volume theory is given by the following expression:[71,74]

$$K_s = \exp\left[-(\phi_t - \phi_b)\left(1 + \frac{R_s}{R_0}\right)^2\right] \tag{5.35}$$

where ϕ_t and ϕ_b are the surfactant volume fractions in the top and bottom phases, respectively, R_s is the hydrodynamic radius of the partitioning solute, and R_0 is the cross-sectional radius of each $C_{10}E_4$ cylindrical micelle (modeled as a spherocylindrical entity). In order to predict the partition coefficients of bacteriophage P22 and cytochrome *c* at each partitioning temperature, the hydrodynamic radii of bacteriophage P22 and cytochrome *c*, the

cross-sectional radius of each $C_{10}E_4$ cylindrical micelle, and the surfactant volume fractions in the two coexisting phases are required. The hydrodynamic radii of bacteriophage P22 and cytochrome *c* are 300 Å[85,87,96] and 16 Å,[76,77] respectively, while the cross-sectional radius of each $C_{10}E_4$ cylindrical micelle is 21 Å.[70–74] As will now be described, the difference in surfactant volume fractions in the two coexisting phases ($\phi_t - \phi_b$) at a given temperature was obtained from the coexistence curve of the two-phase aqueous $C_{10}E_4$ micellar system. The coexistence or binodal curve of the $C_{10}E_4$-buffer system delineates the two-phase region from the one-phase region in a temperature-$C_{10}E_4$ concentration phase diagram at constant pressure. In this two-dimensional phase diagram, tie lines correspond to the intersections of constant temperature horizontal lines with the coexistence curve. Consequently, once the partitioning temperature is fixed, the wt% concentrations of $C_{10}E_4$ in the two phases are fixed. Since the surfactant volume fractions can be approximated as being equal to the weight fractions due to the densities of both phases being close to 1 g/mL, the surfactant volume fractions in the two phases can be obtained from the tie lines. Specifically, $(\phi_t - \phi_b)\times 100$ is the tie line length at a given temperature, where the multiplication by 100 is necessary to convert between percents and fractions.

Although it was not discussed earlier, the coexistence curves in Figure 4-1 correspond to those for binary systems even though the $C_{10}E_4$-buffer systems shown in this figure actually consist of four components, namely, water, $C_{10}E_4$, disodium phosphate, and citric acid. The justification for approximating the $C_{10}E_4$-buffer system in Chapter 4 as a pseudo-binary system is provided in Appendix C.1. Even though an additional component, namely, protein, is added to these four components in the protein partitioning experiments, the coexistence curves in Figure 4-1 were also found to apply to these five-component systems (see Appendix C.1 for details). With regard to the bacteriophage P22 partitioning experiments, $MgSO_4$ and the virus are two components that are present in addition to water, $C_{10}E_4$, disodium phosphate, and citric acid. However, it is also shown in Appendix C.1 that the concentrations of $MgSO_4$ and bacteriophage P22 are low enough to not perturb the phase separation process of the $C_{10}E_4$-buffer system. Accordingly, the coexistence curves in Figure 4-1 apply to both the protein and viral partitioning experiments, and therefore, the coexistence curve of the $C_{10}E_4$ (lot no. 6011)-buffer system was used to determine ($\phi_t - \phi_b$) in the following predictions for cytochrome *c* and bacteriophage P22.

As indicated in Figure 5-6, the experimentally measured partition coefficients of cytochrome *c* are similar to those predicted according to the excluded-volume theory. This agreement was already demonstrated previously by our group.[70–74,78] In the case of bacterio-

phage P22 (see Figure 5-7), the discrepancy between the experimentally measured partition coefficients and the excluded-volume predictions decreases as the volume ratio decreases. However, the measured partition coefficients for the volume ratio of 0.1 (black square symbols) are still orders of magnitude higher than the theoretically predicted ones based on the excluded-volume theory. One highly probable reason for this discrepancy is that there are still entrained micelle-poor (virus-rich) domains in the macroscopic, top, micelle-rich phase. To test this possibility, the volume fraction, x, of entrained micelle-poor (virus-rich) domains still remaining in the macroscopic, top, micelle-rich phase was fitted using the experimentally measured partition coefficient of bacteriophage P22 at 20.2°C for the V_t/V_b=0.1 case ($K_v = 9.1 \times 10^{-5}$) in Eq. (5.14) with K_v^{EV} given by Eq. (5.35). Although the volume fraction of entrained micelle-poor (virus-rich) domains is most probably increasing with an increase in temperature (see the discussion in Section 5.4.3), x will be assumed to be independent of temperature. With $x = 9.1 \times 10^{-5}$, the fitted value for the volume fraction of entrained micelle-poor (virus-rich) domains in the top phase, Eqs. (5.14) and (5.35) were used to predict new partition coefficients of bacteriophage P22 for the V_t/V_b=0.1 case. These newly predicted partition coefficients of bacteriophage P22 are represented in Figure 5-7 by the dashed line. As shown in Figure 5-7, the predictions improved by orders of magnitude in comparison to the excluded-volume predictions. A similar improvement in the theoretical predictions for the V_t/V_b=10 case was also observed when Eqs. (5.14) and (5.35) were utilized after the volume fraction of entrained micelle-poor (virus-rich) domains was fitted using the partition coefficient of bacteriophage P22 at 20.2°C for the V_t/V_b=10 case ($K_v = 4.2 \times 10^{-3}$). Note that the fitted value for the volume fraction of entrained micelle-poor domains from the V_t/V_b=0.1 case could not be applied to the V_t/V_b=10 case because the amount of entrainment differed for the two volume ratios. As indicated by Eq. (5.14), the measured partition coefficient of bacteriophage P22 is basically determined by the volume fraction of entrained domains, since the predicted value for the partition coefficient based on the excluded-volume theory is generally orders of magnitude smaller than 1. Therefore, accounting for entrainment, albeit with one fitted parameter, can explain the almost constant partition coefficient of bacteriophage P22 that accompanies an increase in the temperature. In addition, when the two fitted values for the volume fraction of entrained micelle-poor domains ($x = 9.1 \times 10^{-5}$ for V_t/V_b=0.1, and $x = 4.1 \times 10^{-3}$ for V_t/V_b=10) were applied to the protein partition coefficients using Eqs. (5.16) and (5.35), no changes in the predicted protein partition coefficients were observed (see dashed and dotted lines in Figure 5-6) as expected from the discussion in Section 5.3.1. Essentially all the predictions lie on top of each other in Figure 5-6.

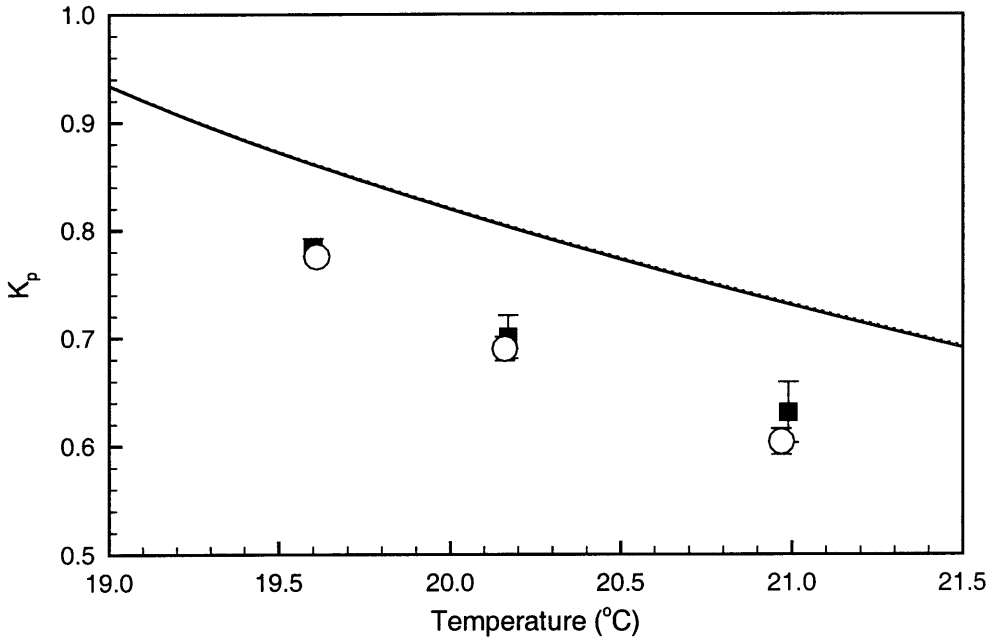

Figure 5-6: Comparison between the theoretically predicted and experimentally measured partition coefficients of cytochrome *c*. The solid line corresponds to the partition coefficients predicted based on the excluded-volume theory (Eq. (5.35)). The dashed and dotted lines correspond to the partition coefficients predicted after accounting for both the entrainment (Eq. (5.16)) and the excluded-volume interactions (Eq. (5.35)) for the $V_t/V_b = 0.1$ and $V_t/V_b = 10$ cases, respectively. The dashed and dotted lines are difficult to see because all three predictions lie on top of each other. The black square and white circle symbols represent the partition coefficients of cytochrome *c* that were measured using a volume ratio of 0.1 and 10, respectively. The error bars correspond to 95% confidence limits for the measurements.

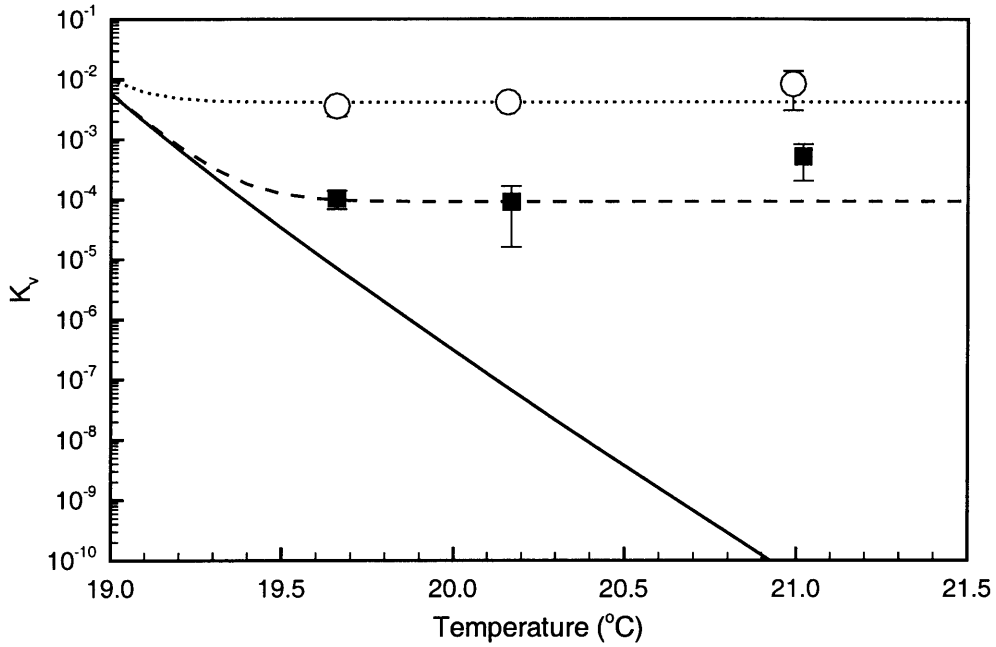

Figure 5-7: Comparison between the theoretically predicted and experimentally measured partition coefficients of bacteriophage P22. The solid line corresponds to the partition coefficients predicted based on the excluded-volume theory (Eq. (5.35)). The dashed and dotted lines correspond to the partition coefficients predicted after accounting for both the entrainment (Eq. (5.14)) and the excluded-volume interactions (Eq. (5.35)) for the $V_t/V_b = 0.1$ and $V_t/V_b = 10$ cases, respectively. The black square and white circle symbols represent the partition coefficients of bacteriophage P22 that were measured using a volume ratio of 0.1 and 10, respectively. The error bars, which correspond to 95% confidence limits for the measurements, appear asymmetric due to the use of a semi-logarithmic plot.

Since the agreement between the experimentally measured and theoretically predicted partition coefficients of bacteriophage P22 drastically improved after incorporating entrainment into the theory, viral partition coefficients measured previously by our group[70] (see Figures 1-11, 1-10, and 1-12) were revisited. Specifically, the volume fraction of entrained micelle-poor domains was again assumed to be a constant for all the temperatures and all the partitioning experiments, independent of the bacteriophage, in Figures 1-11, 1-10, and 1-12. This constant was fitted using the partition coefficient of bacteriophage P22 at 22°C ($K_v = 2.2 \times 10^{-3}$), and Eqs. (5.14) and (5.35). A new fitted value for the volume fraction of entrained micelle-poor domains was required, since the results in Figures 1-11, 1-10, and 1-12 were obtained with an experimental volume ratio of 1, which was expected to have a different degree of entrainment than the $V_t/V_b = 0.1$ and $V_t/V_b = 10$ cases. In fact, as expected, the fitted volume fractions of entrained micelle-poor domains increased from 9.1×10^{-5} to 2.2×10^{-3} to 4.1×10^{-3} as the volume ratio increased from 0.1 to 1 to 10. The comparisons between the newly predicted viral partition coefficients and the measured ones are provided in Figures 5-8, 5-9, and 5-10. As shown in these figures, there is an orders of magnitude improvement in the predictions for bacteriophages P22 and T4, when entrainment is accounted for in the theory. Considerable improvement is also observed for bacteriophage ϕX174, especially at the higher temperatures where the excluded-volume predictions begin to decrease beyond 2×10^{-3}. It should be noted that the newly predicted partition coefficients of bacteriophage ϕX174 still decrease as a function of temperature, and are not fixed at a constant value equal to the fitted volume fraction of entrained micelle-poor domains. Such partitioning behavior is predicted for bacteriophage ϕX174, even with the incorporation of entrainment, because the predicted partition coefficients based on the excluded-volume theory are all 10^{-3} and higher, and therefore, the volume fraction of entrained micelle-poor domains does not dictate solely the value of the predicted partition coefficient in Eq. (5.14).

Based on the experimental and theoretical results in this chapter, it can be concluded that the observed viral partitioning in the two-phase aqueous $C_{10}E_4$ micellar system is primarily governed by only the excluded-volume interactions with the micelles and the entrainment of micelle-poor (virus-rich) domains in the macroscopic, top, micelle-rich phase. Incorporation of entrainment into the theory has yielded very good agreement between experiment and theory for the viral partition coefficients. In addition, although the results are not shown, this agreement is insensitive to the actual experimental viral partition coefficient that is used to fit the volume fraction of entrained domains.

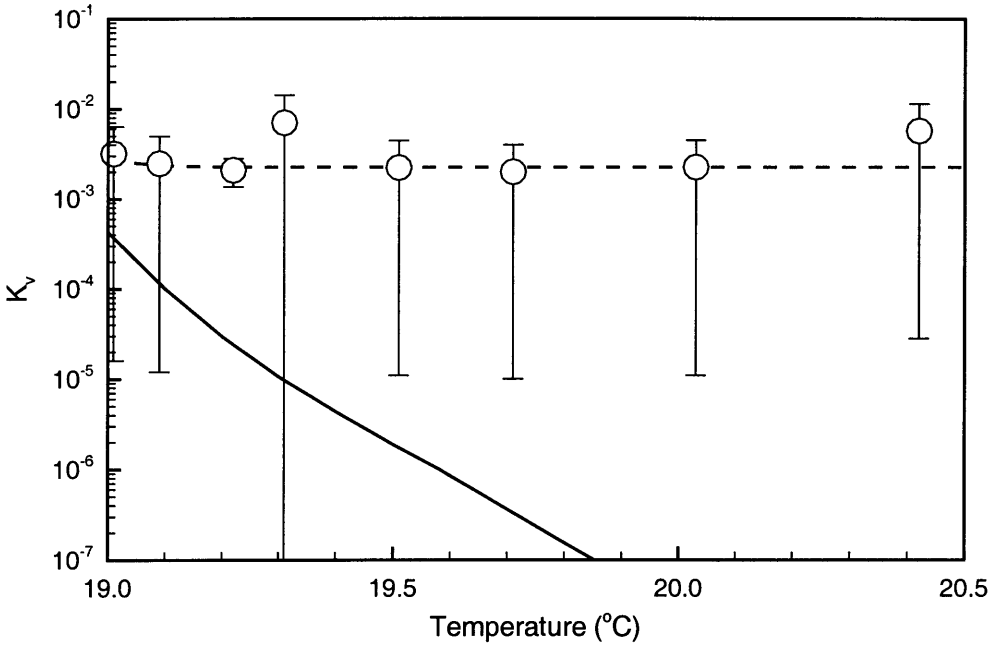

Figure 5-8: Comparison between the theoretically predicted and experimentally measured partition coefficients of bacteriophage P22 for a volume ratio of 1. The solid line corresponds to the partition coefficients predicted based on the excluded-volume theory (Eq. (5.35)). The dashed line corresponds to the partition coefficients predicted after accounting for both the entrainment (Eq. (5.14)) and the excluded-volume interactions (Eq. (5.35)). The white circle symbols represent the partition coefficients of bacteriophage P22 that were previously measured[70] using a volume ratio of 1. The error bars, which correspond to 95% confidence limits for the measurements, appear asymmetric due to the use of a semi-logarithmic plot.

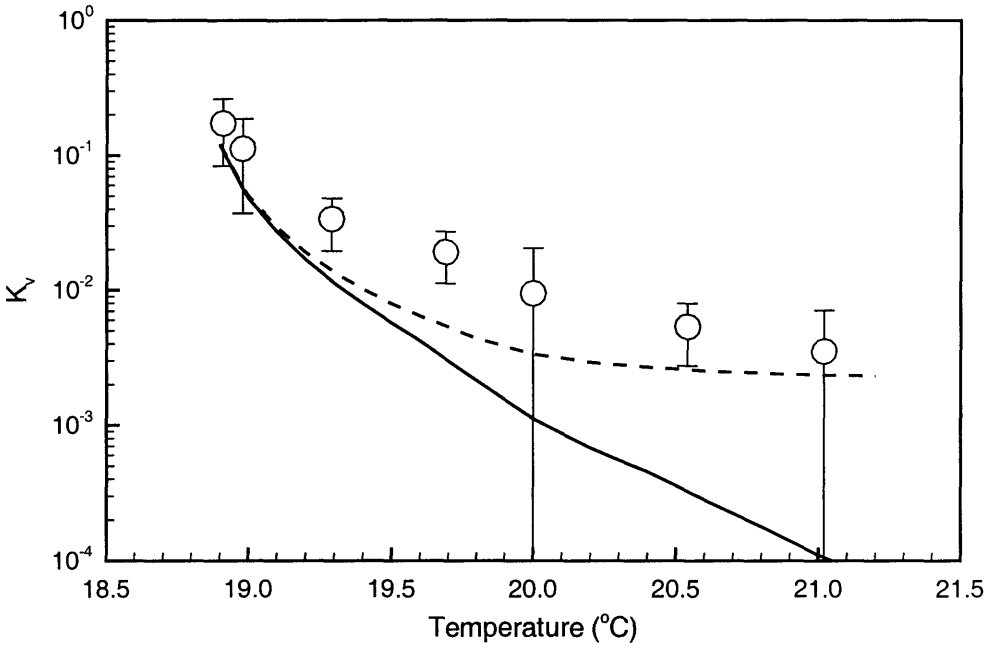

Figure 5-9: Comparison between the theoretically predicted and experimentally measured partition coefficients of bacteriophage ϕX174 for a volume ratio of 1. The solid line corresponds to the partition coefficients predicted based on the excluded-volume theory (Eq. (5.35)). The dashed line corresponds to the partition coefficients predicted after accounting for both the entrainment (Eq. (5.14)) and the excluded-volume interactions (Eq. (5.35)). The white circle symbols represent the partition coefficients of bacteriophage ϕX174 that were previously measured[70] using a volume ratio of 1. The error bars, which correspond to 95% confidence limits for the measurements, appear asymmetric due to the use of a semi-logarithmic plot.

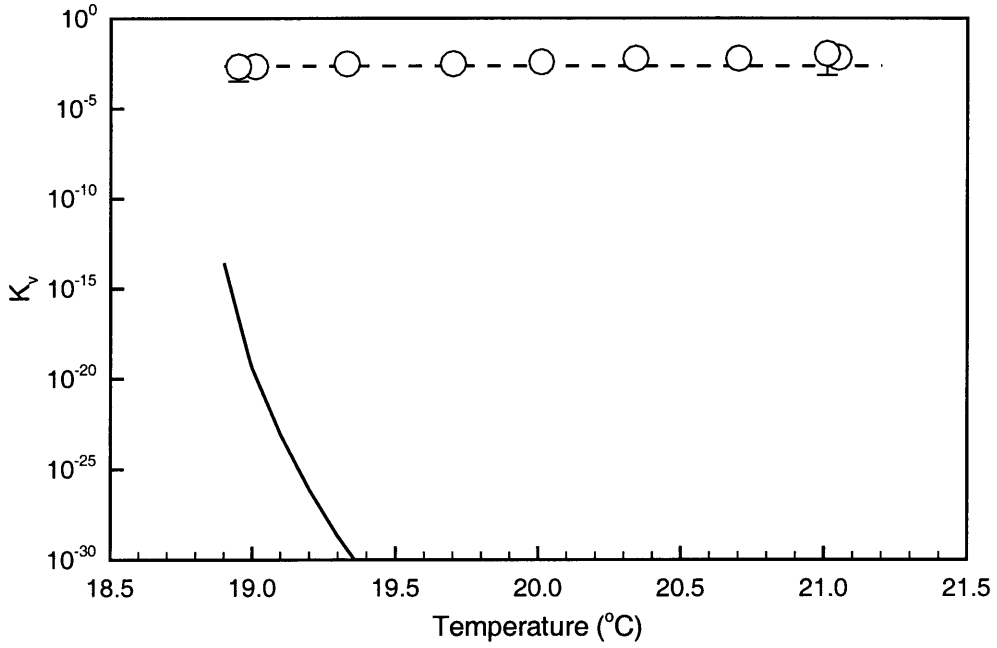

Figure 5-10: Comparison between the theoretically predicted and experimentally measured partition coefficients of bacteriophage T4 for a volume ratio of 1. The solid line corresponds to the partition coefficients predicted based on the excluded-volume theory (Eq. (5.35)). The dashed line corresponds to the partition coefficients predicted after accounting for both the entrainment (Eq. (5.14)) and the excluded-volume interactions (Eq. (5.35)). The white circle symbols represent the partition coefficients of bacteriophage T4 that were previously measured[70] using a volume ratio of 1. The error bars, which correspond to 95% confidence limits for the measurements, appear asymmetric due to the use of a semi-logarithmic plot.

5.5 Conclusions

The experimental and theoretical study described in this chapter has shown that the entrainment of micelle-poor (virus-rich) domains in the macroscopic, top, micelle-rich phase is indeed the key factor influencing the partitioning behavior of viruses. Photographs that were taken of the two-phase aqueous $C_{10}E_4$ micellar system demonstrated that the entrainment of micelle-poor (virus-rich) domains in the macroscopic, top; micelle-rich phase decreases with a decrease in the volume ratio. Bacteriophage P22 and cytochrome *c* were then partitioned at three different operating temperatures with volume ratios of 10 and 0.1. For bacteriophage P22, the measured viral partition coefficient at each temperature decreased by about an order of magnitude when the volume ratio was decreased from 10 to 0.1, which clearly demonstrated that entrainment is indeed the key factor influencing viral partitioning. For cytochrome *c*, the measured protein partition coefficient did not change, which indicated that this entrainment effect negligibly influences protein partitioning. This was a desired outcome, since this observed behavior was in accordance with the biggest "clue" concept in our search for identifying other possible mechanisms that govern viral partitioning. Specifically, these possible mechanisms must significantly influence viral partitioning, while having little or no impact on protein partitioning. The entrainment of micelle-poor domains in the macroscopic, top, micelle-rich phase was expected to strongly influence viral partitioning because the concentration of virus in the micelle-poor domains is much larger than that in the micelle-rich domains. In contrast, the concentrations of protein in the micelle-poor and micelle-rich domains are similar, and therefore, the effect of the entrainment on protein partitioning was expected *a priori* to be negligible. It should also be noted that the partition coefficients of bacteriophage P22 that were previously measured for a volume ratio of 1 had values that were between those measured for the volume ratios of 10 and 0.1, which is consistent with the notion that the entrainment decreased as the volume ratio decreased from 10 to 1 to 0.1. The volume ratio may be reduced below 0.1 in the future to further reduce entrainment. Other equipment should also be investigated in which the entrainment can be reduced.

In this study, a new theoretical description of partitioning was also developed that combines the excluded-volume theory with the entrainment of micelle-poor (virus-rich) domains in the macroscopic, top, micelle-rich phase. To account for the entrainment, one fitted parameter, namely, the volume fraction of entrained micelle-poor domains in the macroscopic, top, micelle-rich phase, was incorporated into the theory. This volume fraction was assumed to be a constant for all the partitioning temperatures and partitioning solutes at a fixed

volume ratio. Consequently, for a given volume ratio, only a single partitioning experiment is required to fit this volume fraction of entrained micelle-poor domains. With this fitted parameter and the excluded-volume theory, very good agreement between the measured and predicted viral partition coefficients was achieved. An orders of magnitude improvement was attained for the predicted partition coefficients of bacteriophages P22 and T4. Even for bacteriophage ϕX174, a considerable improvement in its predicted viral partition coefficients was achieved with the incorporation of entrainment. Therefore, it can be concluded that the primary mechanisms governing viral partitioning in the two-phase aqueous $C_{10}E_4$ micellar system are only the entrainment of micelle-poor (virus-rich) domains in the macroscopic, top, micelle-rich phase and the excluded-volume interactions between the viruses and the micelles.

PART III

MANIPULATING THE VOLUME RATIO AND EXPLOITING ELECTROSTATIC INTERACTIONS BETWEEN MIXED MICELLES AND PROTEINS

Chapter 6

Manipulating the Volume Ratio in the $C_{10}E_4$-Buffer Two-Phase System to Achieve Good Separation of Protein from Virus

6.1 Introduction

While the mechanisms governing viral partitioning were being investigated in the context of *Direction A*, *Direction B* of this thesis was being simultaneously pursued. As discussed in Chapter 1, *Direction B* centered around the less optimistic point-of-view that the viral partition coefficients would not decrease below the experimentally observed values of 10^{-3} to 10^{-2} in the two-phase aqueous $C_{10}E_4$ micellar system, which will also be referred to as the $C_{10}E_4$-buffer system. In addition, as described in Chapter 1, the partition coefficients of water-soluble proteins in this system were all measured to be about 0.5. Accordingly, the selectivity of this system for protein versus virus,[107]

$$S_{pv} \equiv \frac{K_p}{K_v} \tag{6.1}$$

is between 50 and 500, which quantitatively indicates that a good separation of protein from virus may be already achieved without further reducing the viral partition coefficient.

Since the virus is generally excluded more strongly than the protein into the bottom, micelle-poor phase, a liquid-liquid extraction was performed where the protein was recovered in the top, micelle-rich phase, while the virus was recovered in the bottom, micelle-poor phase. However, prior to conducting the extraction, an analysis of liquid-liquid extraction theory was performed to determine a desirable volume ratio, which is an important operating parameter in extraction processes. Lysozyme was used as the model protein, since it is: (i) water-soluble, (ii) available in high purity, and (iii) easy to assay with ultraviolet absorbance

measurements. Bacteriophage P22 was used as the model virus, since: (i) it is readily available in high purity from Professor Jonathan King's laboratory, (ii) it is safer to employ than mammalian viruses, (iii) its concentration can be measured with good accuracy using the plaque assay, and (iv) it is used in the experiments associated with *Direction A*.

The remainder of this chapter is organized as follows. In Section 6.2, the materials and experimental methods are detailed. Section 6.3 provides an analysis of the equations that are important in determining the performance of the extraction process. In Section 6.4, the liquid-liquid extraction results are presented and discussed. Finally, concluding remarks are presented in Section 6.5.

6.2 Materials and Methods

6.2.1 Materials

Homogeneous *n*-decyl tetra(ethylene oxide) ($C_{10}E_4$) (lot no. 6011) was obtained from Nikko Chemicals (Tokyo, Japan). Lysozyme (lot no. 57H7045) was purchased from Sigma (St. Louis, MO). Bacteriophage P22 (5^-am/13^-am) and the bacteriophage P22 host bacterium, *Salmonella typhimurium* strain 7155, were provided by Professor Jonathan King's laboratory. Citric acid (lot no. 0616 KCXK) and magnesium sulfate ($MgSO_4$) (lot no. 6070 A31581) were purchased from Mallinckrodt (Paris, KY). Disodium phosphate (lot no. 896726) was obtained from Fisher Scientific (Fair Lawn, NJ). All these materials were used as received. All solutions were prepared using pH 7.2 McIlvaine's buffer consisting of 16.4 mM disodium phosphate and 1.82 mM citric acid in Milli-Q water. Milli-Q water is the product of passing deionized water through Millipore's (Bedford, MA) Milli-Q system. All glassware used in the experiments were subjected to washing in a 50:50 ethanol:1 M sodium hydroxide bath, washing in a 1 M nitric acid bath, rinsing copiously with Milli-Q water, and drying in an oven for at least one day.

6.2.2 Separating Lysozyme from Bacteriophage P22 in the $C_{10}E_4$-Buffer System

In this experimental study, five 7.0 mL buffered solutions were prepared in graduated 10 mL test tubes. Four of the solutions contained 9.3×10^7 particles/mL of bacteriophage P22, 0.10 g/L of lysozyme, 2 mM $MgSO_4$ (which was required to ensure the stability of the bacteriophage P22), and 4.13 wt% $C_{10}E_4$. The fifth solution served as the control containing the same concentrations of $C_{10}E_4$ and $MgSO_4$ but no protein or virus. The solutions were then gently mixed, and equilibrated at 4°C in the refrigerator in order for each solution to

exhibit a single, clear, homogeneous phase. The solutions were subsequently placed in the thermo-regulated device, which was described in Section 3.2.4, to initiate phase separation at 19.4°C. This temperature was chosen because the difference in surfactant volume fractions between the two phases ($\phi_t - \phi_b$) is 0.040, and at this value of ($\phi_t - \phi_b$), bacteriophage P22 had been previously found to partition strongly into the bottom, micelle-poor phase. The initial $C_{10}E_4$ concentration of 4.13 wt% was selected because it yields a volume ratio (volume of the top phase divided by that of the bottom phase) of 4.0 at the operating temperature of 19.4°C. The choice of this volume ratio is explained in Section 6.3.4. The solutions were maintained at this condition for 17 hours prior to withdrawing the phases with great care using 1 mL syringe and needle sets. All the partitioning experiments in this thesis were conducted for *at least* 14 hours, since it was shown previously[70] that partition coefficients measured after overnight partitioning were similar to those measured after partitioning over at least three days. The concentration of bacteriophage P22 in each phase was measured with the plaque assay described in Section 2.2.4. The concentration of lysozyme in each phase was determined by utilizing a procedure similar to the one discussed for cytochrome *c* in Section 5.2.4. The only differences were: (i) lysozyme did not need to be reduced with sodium L-ascorbate prior to measuring its absorbance, and (ii) the wavelength for absorption was 280 nm.

6.3 Theory

6.3.1 Protein and Viral Partition Coefficients

In order to quantify the distribution of the protein and the virus between the two coexisting micellar phases, their partition coefficients must be evaluated. The protein and viral partition coefficients, K_p and K_v, are defined as follows:[75]

$$K_p \equiv \frac{C_{p,t}}{C_{p,b}} \tag{1.3}$$

and

$$K_v \equiv \frac{C_{v,t}}{C_{v,b}} \tag{1.5}$$

where $C_{p,t}$ and $C_{p,b}$ are the concentrations of protein in the top and bottom phases, respectively, and $C_{v,t}$ and $C_{v,b}$ are the concentrations of virus in the top and bottom phases, respectively. Once the experimentally measured protein and viral partition coefficients are available, the yield (or recovery) of the protein, as well as the yield (or recovery) of the virus,

in a particular phase can be subsequently calculated as shown in Section 6.3.2 below.

6.3.2 Protein and Viral Yields

The protein will be recovered in the top, micelle-rich phase, while the virus will be recovered in the bottom, micelle-poor phase. To determine the performance of the extraction process, the yield of the protein in the top phase and the yield of the virus in the bottom phase will be evaluated. The yield of the protein in the top phase, $Y_{p,t,C_{10}E_4}$, is the percentage of the total amount of protein fed into the extraction step that is recovered in the top phase. ("$C_{10}E_4$" has been included in the subscript to distinguish quantities evaluated in the $C_{10}E_4$ micellar systems from those evaluated in Chapter 9 in the C_8-lecithin micellar systems.) $Y_{p,t,C_{10}E_4}$ is therefore given by:[75]

$$Y_{p,t,C_{10}E_4} = \frac{C_{p,t}V_t}{C_{p,t}V_t + C_{p,b}V_b} \times 100\% \tag{6.2}$$

where V_t and V_b are the volumes of the top and bottom phases, respectively. Similarly, the yield of the virus in the bottom phase, $Y_{v,b,C_{10}E_4}$, can be written as follows:[75]

$$Y_{v,b,C_{10}E_4} = \frac{C_{v,b}V_b}{C_{v,t}V_t + C_{v,b}V_b} \times 100\% \tag{6.3}$$

Combining Eqs. (1.3) and (6.2), and combining Eqs. (1.5) and (6.3), results in the following expressions:

$$Y_{p,t,C_{10}E_4} = \frac{K_p\left(\frac{V_t}{V_b}\right)}{1 + K_p\left(\frac{V_t}{V_b}\right)} \times 100\% \tag{6.4}$$

and

$$Y_{v,b,C_{10}E_4} = \frac{1}{1 + K_v\left(\frac{V_t}{V_b}\right)} \times 100\% \tag{6.5}$$

These last two expressions for $Y_{p,t,C_{10}E_4}$ and $Y_{v,b,C_{10}E_4}$ are more useful than Eqs. (6.2) and (6.3) because they are related to an operating parameter—the volume ratio (V_t/V_b)—and to measurable quantities—the partition coefficients, K_p and K_v. This capability to predict yields once the partition coefficients are known is a requirement if two-phase aqueous micellar systems are to be competitive with membranes, for which yields can be predicted as well.[14]

6.3.3 Viral Concentration Factor

Another quantity of interest related to the extraction process is the viral concentration factor, which quantifies the extent to which the virus has been concentrated in a particular phase. Since the virus will be recovered in the bottom phase, the concentration factor of the virus in the bottom phase, $CF_{v,b,C_{10}E_4}$, is given by:[75]

$$CF_{v,b,C_{10}E_4} = \frac{C_{v,b}}{C_{v,0}} \tag{6.6}$$

where $C_{v,0}$ is the initial concentration of the virus prior to the extraction. This expression for the concentration factor can also be written in terms of the volume ratio and the viral partition coefficient. However, the mass balance on the virus must first be written as follows:

$$C_{v,0}\left(V_t + V_b\right) = C_{v,t}V_t + C_{v,b}V_b \tag{4.1}$$

Then, combining Eqs. (1.5), (6.6), and (4.1) yields:

$$CF_{v,b,C_{10}E_4} = \frac{1 + \frac{V_t}{V_b}}{1 + K_v\left(\frac{V_t}{V_b}\right)} \tag{6.7}$$

6.3.4 Analysis of the Protein and Viral Yields and the Viral Concentration Factor

Equations (6.4) and (6.5) for the protein and viral yields, respectively, and Eq. (6.7) for the viral concentration factor can now be analyzed to determine a desirable volume ratio, which is a key operating parameter in liquid-liquid extraction. As discussed in Section 6.1, the protein and viral partition coefficients have been experimentally measured to be about 0.5 and 10^{-3} to 10^{-2}, respectively. Using a value of K_p=0.5 in Eq. (6.4), and a value of K_v=10^{-3} to 10^{-2} in Eqs. (6.5) and (6.7), it follows that an increase in the volume ratio, V_t/V_b, results in an *increase* in $Y_{p,t,C_{10}E_4}$, a *decrease* in $Y_{v,b,C_{10}E_4}$, and an *increase* in $CF_{v,b,C_{10}E_4}$. Regarding the yield of the protein in the top phase, $Y_{p,t,C_{10}E_4}$, as V_t/V_b increases, the denominator begins to approach the numerator, and therefore, $Y_{p,t,C_{10}E_4}$ increases towards 100%. Regarding the yield of the virus in the bottom phase, $Y_{v,b,C_{10}E_4}$, as V_t/V_b increases, the denominator becomes larger, and $Y_{v,b,C_{10}E_4}$ decreases from 100%. However, since the viral partition coefficient is approximately 10^{-3} to 10^{-2}, and therefore much less than 1, the yield of the virus in the bottom phase is only a weak function of the volume ratio for the experimentally accessible values of V_t/V_b. This small value of the viral partition coefficient also allows the concentration

factor of the virus in the bottom phase to be approximated as follows (see Eq. (6.7)):

$$CF_{v,b,C_{10}E_4} \approx 1 + \frac{V_t}{V_b} \tag{6.8}$$

Therefore, it is clear that increasing the volume ratio increases $CF_{v,b,C_{10}E_4}$. In addition, Eq. (6.8) indicates that the concentration factor of virus in the bottom phase is only limited by the magnitude of the volume ratio that can be attained experimentally.

The above analysis is also physically intuitive. Indeed, increasing the volume ratio implies that the volume of the top phase is becoming proportionately larger than that of the bottom phase. Accordingly, more of the protein molecules will be recovered in the top phase, and the yield of the protein in the top phase should therefore increase as V_t/V_b increases. However, more of the viral particles will be recovered in the top phase as well, and therefore, the yield of the virus in the bottom phase should decrease as V_t/V_b increases. Although the yield of the virus in the bottom phase decreases, it is only weakly dependent on the volume ratio, since the virus really "wants to be" in the bottom phase as reflected in its partition coefficient being much less than 1. An increase in the volume ratio can also be interpreted in terms of the volume of the bottom phase becoming proportionately smaller than that of the top phase. Therefore, there is less dilution of the virus in the bottom phase, and the concentration factor of the virus in the bottom phase should increase as V_t/V_b increases.

Based on this analysis, a volume ratio that is larger than one is desirable to attain good recovery of the protein in the top phase, while still maintaining a good recovery of the virus in the bottom phase. Such a volume ratio would also give rise to a higher concentration factor of the virus in the bottom phase. In this experimental study, a volume ratio of approximately four was utilized. Note that this volume ratio was not expected to reduce the entrainment effect discussed in Chapter 5. Accordingly, in this analysis, a viral partition coefficient of 10^{-3} to 10^{-2} was assumed.

6.4 Results and Discussion

The results of the separation experiment are summarized in Figure 6-1. The measured partition coefficient of lysozyme (K_p=0.78) was similar to the partition coefficients of other water-soluble proteins investigated in the $C_{10}E_4$-buffer system. The measured partition coefficient of bacteriophage P22 (K_v=6.1×10^{-3}) was similar to those observed in Chapter 5 because of the entrainment effects associated with using a volume ratio that is larger than 1. The mass balances on both lysozyme and bacteriophage P22 closed to 100% within the

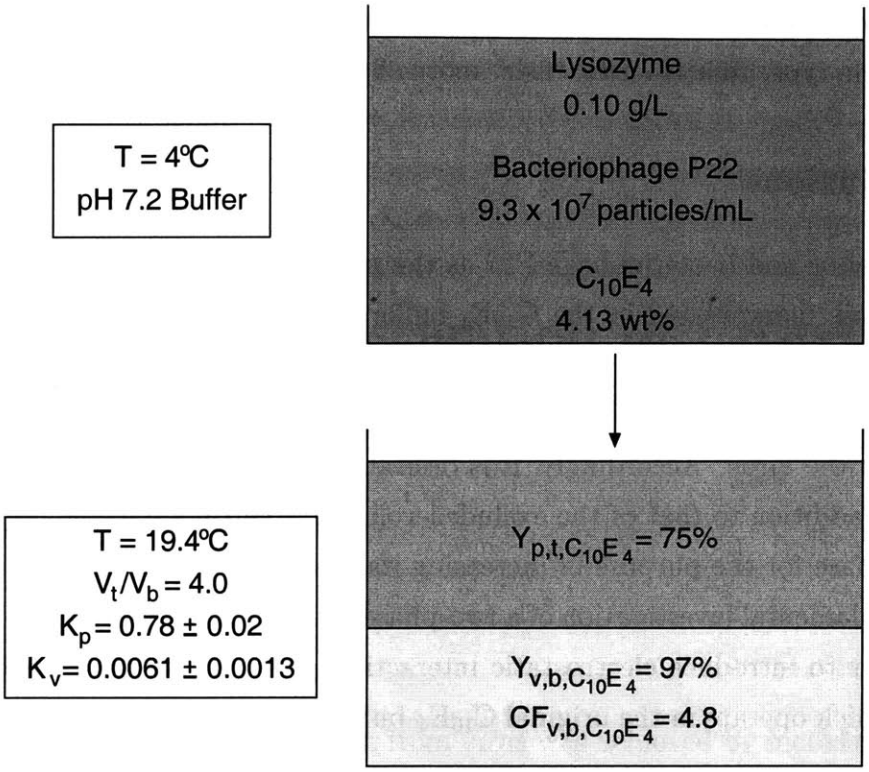

Figure 6-1: The results of separating lysozyme from bacteriophage P22 in the $C_{10}E_4$-buffer system. The buffered solutions were first equilibrated at 4°C in order for each solution to exhibit a single phase. The solutions were then placed in the thermo-regulated device to initiate phase separation at 19.4°C. The solutions were maintained at this condition for 17 hours. With a volume ratio of 4.0, a good separation of protein from virus was achieved. The errors correspond to 95% confidence limits for the measurements.

experimental error. As expected from the analysis presented in Section 6.3, a good separation of protein from virus was achieved by using a volume ratio that was larger than 1. With a volume ratio of 4.0, the protein yield in the top phase was $Y_{p,t,C_{10}E_4}$=75%, the viral yield in the bottom phase was $Y_{v,b,C_{10}E_4}$=97%, and the concentration factor of virus in the bottom phase was $CF_{v,b,C_{10}E_4}$=4.8. A higher protein yield in the top phase is desirable, however, since a significant amount of the protein is still being lost to the bottom phase. Although a higher volume ratio may be used to increase the yield of the protein in the top phase (and also to increase the concentration factor of the virus in the bottom phase), there will be a maximum value of the volume ratio beyond which the contamination of the top phase with virus will be unacceptable. An increase in the contamination of the top phase with virus corresponds to a decrease in the yield of the virus in the bottom phase. Therefore, another method for achieving a higher yield of protein in the top phase, while still maintaining a good yield of virus in the bottom phase, is desirable. One such method involves introducing

another mode of interaction between the protein and the micelles, in addition to that of the excluded-volume type, to attract or "fish" more of the protein into the top phase.

6.5 Conclusions

Using lysozyme and bacteriophage P22 as the model protein and virus, respectively, the volume ratio was manipulated in the $C_{10}E_4$-buffer system to achieve a good separation of protein from virus. Although the volume ratio can be increased further to increase the yield of the protein in the top phase beyond 75%, this will also increase the contamination of the top phase with the virus. Accordingly, it is desirable instead to introduce another mode of interaction, in addition to that of the excluded-volume type, to attract or "fish" the protein into the top phase for the purpose of increasing its yield. The next chapter, Chapter 7, describes our fundamental investigation of a two-phase aqueous mixed (nonionic/ionic) micellar system in order to introduce electrostatic interactions, in addition to the excluded-volume interactions which operate in the original $C_{10}E_4$-buffer system, between the proteins and the micelles.

Chapter 7

A Fundamental Investigation of Protein Partitioning in the $C_{10}E_4$-SDS-Buffer Two-Phase System

7.1 Introduction

Although a good separation of protein from virus was achieved by increasing the volume ratio (see Chapter 6), a significant amount of protein was still lost to the bottom, micelle-poor phase in the $C_{10}E_4$-buffer system. Since only steric, excluded-volume interactions between the proteins and the micelles have been exploited until now, introducing another mode of interaction to attract or "fish" the proteins into the top, micelle-rich phase may aid in increasing the yield of proteins in the top phase. Although biospecific affinity interactions could be introduced, electrostatic interactions were instead chosen because they can be exploited with a wide variety of proteins. This concept of combining excluded-volume and electrostatic interactions in two-phase aqueous micellar systems is analogous, in the language of liquid chromatography, to combining size-exclusion chromatography and ion-exchange chromatography.

A two-phase aqueous mixed micellar system composed of the nonionic surfactant $C_{10}E_4$ and the anionic surfactant sodium dodecyl sulfate SDS was investigated because of its potential for modulating both excluded-volume and electrostatic interactions between the proteins and the micelles. Similar to the $C_{10}E_4$-buffer system, this system also exhibits a single, homogeneous micellar solution at low temperatures. Increasing the temperature also induces a macroscopic phase separation to form a top, micelle-rich phase and a bottom, micelle-poor phase. The micelles in the micelle-rich phase are larger and more abundant than those in the micelle-poor phase. Every micelle in the two-phase system is a mixed micelle, that is, a micelle composed of both surfactants. As in the case of the $C_{10}E_4$-buffer system, both

phases contain cylindrical micelles, which can be modeled as micelles having a cylindrical body capped by two hemispherical micelles at the ends.[108] The water content in both phases is also very high. There is at least 80 wt% and 99 wt% water in the top and bottom phases, respectively. A schematic representation of the two-phase aqueous mixed ($C_{10}E_4$/SDS) micellar system, which will also be referred to as the $C_{10}E_4$-SDS-buffer system, is shown in Figure 7-1.

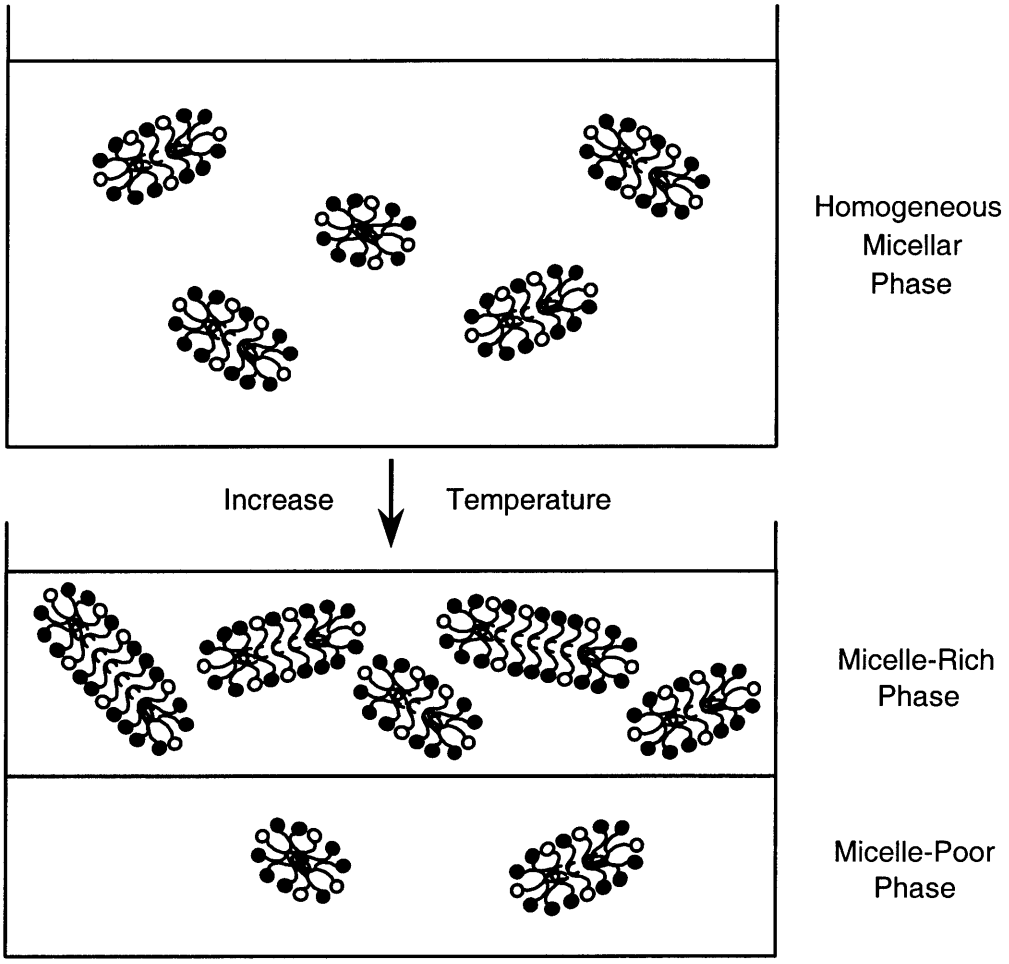

Figure 7-1: Schematic representation of the two-phase aqueous mixed ($C_{10}E_4$/SDS) micellar system. This system will also be referred to as the $C_{10}E_4$-SDS-buffer system. The black and white circles represent the hydrophilic heads of the $C_{10}E_4$ and the SDS molecules, respectively. As in the case of the $C_{10}E_4$-buffer system, this system exhibits a single phase at low temperatures, and phase separates at high temperatures. Another similarity with the $C_{10}E_4$-buffer system is that the top phase is micelle-rich, while the bottom phase is micelle-poor. However, unlike the $C_{10}E_4$-buffer system, every micelle in the $C_{10}E_4$-SDS-buffer system is a mixed micelle composed of both $C_{10}E_4$ and SDS.

The negatively-charged mixed micelles are expected to influence the partitioning behavior

of any protein having a net charge. If a net positively-charged protein is placed in the $C_{10}E_4$-SDS-buffer system, it is expected to be attracted electrostatically into the top, micelle-rich phase where there are a greater number of negatively-charged mixed micelles. On the other hand, if a net negatively-charged protein is placed in this system, it is expected to be repelled electrostatically into the bottom, micelle-poor phase where there are fewer negatively-charged mixed micelles. In addition to being applicable to a wide range of proteins, these charged mixed micelles are relatively easy to generate. Due to the self-assembling nature of micelles, these mixed micelles can be formed *in situ* by just mixing the two surfactants in an aqueous medium. No synthesis is therefore required, and this is a key advantage when comparing these systems to two-phase aqueous polymer systems composed of at least one polyelectrolyte. Another attractive feature of the two-phase aqueous mixed (nonionic/ionic) micellar system is that solution conditions, such as pH and ionic strength, can be varied to: (i) reverse the electrostatic interactions and separate the desired proteins from the mixed micelles, and (ii) manipulate the shapes and sizes of the self-assembling micelles, which can have an effect on the excluded-volume and electrostatic interactions between the proteins and the micelles.

Both experimental and theoretical studies were conducted in this fundamental investigation. The purpose of the experimental study was to demonstrate proof-of-principle that two-phase aqueous mixed (nonionic/ionic) micellar systems can indeed be used to modulate both electrostatic and excluded-volume interactions between the proteins and the charged mixed micelles. The effects of any electrostatic interactions were probed by partitioning two net positively-charged proteins and two net negatively-charged proteins in the $C_{10}E_4$-buffer and the $C_{10}E_4$-SDS-buffer systems at conditions where the excluded-volume interactions between the proteins and the micelles were maintained constant. By maintaining the excluded-volume interactions constant, any difference in the partitioning behavior of the proteins between the two systems could be attributed to the electrostatic interactions between the proteins and the mixed ($C_{10}E_4$/SDS) micelles. At the pH of the buffer used in this study (pH=7.2), lysozyme and cytochrome *c* were net positively-charged, while ovalbumin and catalase were net negatively-charged. Some useful relevant characteristics of these four proteins are shown in Table 7-1.

The theoretical study was conducted to gain a deeper understanding of protein partitioning in two-phase aqueous mixed (nonionic/ionic) micellar systems. In particular, a theory was developed that incorporates the dominant interactions, namely, the excluded-volume and the electrostatic interactions, between the proteins and the mixed micelles. Since certain properties of the mixed micelles (such as the molar ratio of the ionic surfactant to the

Table 7-1: Proteins partitioned in the $C_{10}E_4$-buffer and $C_{10}E_4$-SDS-buffer systems. The hydrodynamic radii, R_p, and isoelectric points, pI, were obtained from various sources.[76,77,109]

Protein	R_p (Å)	pI	Net Charge at pH 7.2
Lysozyme	19	11.0	Positive
Cytochrome *c*	16	10.6	Positive
Ovalbumin	29	4.6	Negative
Catalase	52	5.6	Negative

nonionic surfactant in the mixed micelles) were required in the modeling, SDS was chosen as the ionic surfactant because of the capability of our group to predict many properties of mixed micelles composed of $C_{10}E_4$ and SDS. To test the ability of the theory to capture the underlying physics involved in protein partitioning, the theoretically predicted protein partition coefficients were compared to the experimentally measured ones.

It is also desirable to develop a predictive theory because it can decrease some of the time and effort associated with performing experiments. A predictive theory allows the scientist or engineer to identify the majority of the factors that can influence protein partitioning. The theory can also indicate if an increase in a particular factor will result in an increase or a decrease in the protein partition coefficient. Accordingly, this deeper understanding of protein partitioning, that is provided by the predictive theory, can aid the scientist or engineer in determining the pH and ionic strength of the solution, the type and concentration of surfactants to use, and other operating conditions, that will result in the optimal separation efficiency.

The remainder of this chapter is organized as follows: Section 7.2 provides details of the materials and experimental methods used in this study. In Section 7.3, the theory for predicting protein partition coefficients in two-phase aqueous mixed (nonionic/ionic) micellar systems is developed. In Section 7.4, the experimental and theoretical results are presented and discussed. Finally, concluding remarks are presented in Section 7.5.

7.2 Materials and Methods

7.2.1 Materials

The nonionic surfactant *n*-decyl tetra(ethylene oxide) ($C_{10}E_4$) (lot no. 6011) was obtained from Nikko Chemicals (Tokyo, Japan). Sodium dodecyl sulfate (SDS) (lot no. 64H02972),

cytochrome *c* (lot no. 77H7052), lysozyme (lot no. 57H7045), catalase (lot no. 106H7055), ovalbumin (lot no. 40H8060), and sodium L-ascorbate (lot no. 46H02965) were purchased from Sigma (St. Louis, MO). Disodium phosphate (lot no. 896726) and citric acid (lot no. 0616 KCXK) were obtained from Fisher Scientific (Fair Lawn, NJ) and Mallinckrodt (Paris, KY), respectively. All these materials were used as received. Although SDS was also recrystallized 3 times in ethanol prior to use for the removal of impurities which may be present, the experimental results were found to be insensitive to the use of the recrystallized or the untreated SDS. All solutions were prepared using pH 7.2 McIlvaine's buffer consisting of 16.4 mM disodium phosphate and 1.82 mM citric acid in Milli-Q water. Milli-Q water is the product of passing deionized water through Millipore's (Bedford, MA) Milli-Q system. All glassware used in the experiments were subjected to washing in a 50:50 ethanol:1 M sodium hydroxide bath, washing in a 1 M nitric acid bath, rinsing copiously with Milli-Q water, and drying in an oven for at least one day.

7.2.2 Mapping the Three-Dimensional Phase Diagram of the $C_{10}E_4$-SDS-Buffer System between 19.8°C and 23.1°C

The addition of SDS to the $C_{10}E_4$-buffer system increases the number of degrees of freedom, or number of independent intensive variables, by one. Accordingly, the $C_{10}E_4$-SDS-buffer phase diagram is three-dimensional instead of two-dimensional. Since some knowledge of the two-phase region is required in order to perform protein partitioning experiments, the three-dimensional phase diagram was mapped out between 19.8°C and 23.1°C to get an idea of its structure. This temperature range was chosen because proteins are fairly stable at around room temperature.

For this purpose, a 0.5 mL buffered aqueous solution containing low concentrations of SDS and $C_{10}E_4$ was first equilibrated at 19.8°C in the thermo-regulated device, where it was turbid. A 1.0 wt% buffered solution of SDS was then added one drop at a time with a 1 mL syringe and needle set until the solution cleared. The concentrations of SDS and $C_{10}E_4$ were then calculated based on the initial concentrations of the two surfactants and the amount of SDS solution added. The resulting concentrations of SDS and $C_{10}E_4$ correspond to the coordinates of one point on the coexistence curve at 19.8°C, since it represents one point where the solution can change from being turbid to being clear. Known masses of pH 7.2 buffer and pure $C_{10}E_4$ were then added until the solution again became turbid. The above-mentioned procedure was then repeated, beginning with the addition of the 1.0 wt% buffered solution of SDS. This process was continued until many points on the coexistence

curve at 19.8°C were determined. In a similar manner, the coexistence curves at 20.0, 20.2, 21.2, 22.1, and 23.1°C were subsequently mapped out.

7.2.3 Mapping the Coexistence Curve of the $C_{10}E_4$-SDS-Buffer System at a Temperature of 25.2°C

To attain a measurable effect of the electrostatic interactions in the protein partitioning experiments, it is desirable to form a two-phase system with the top, micelle-rich phase containing a relatively high concentration of SDS. The concentration of SDS in the bottom, micelle-poor phase, on the other hand, will generally always be very low, since the surfactant concentration in the micelle-poor phase has been close to zero in past partitioning experiments. After mapping out the three-dimensional phase diagram between 19.8°C and 23.1°C (see Figure 7-2), it was concluded that higher concentrations of SDS could be attained by increasing the temperature. However, an operating temperature of only 25.2°C was selected because: (i) proteins are generally still thermally stable at 25.2°C, and (ii) the purpose of this experimental study was only to demonstrate proof-of-principle that these two-phase aqueous mixed (nonionic/ionic) micellar systems have the ability to modulate both electrostatic and excluded-volume interactions. The coexistence curve was mapped out at 25.2°C using the procedure described in Section 7.2.2.

The location of an operating tie line on this $C_{10}E_4$-SDS-buffer phase diagram was also required, since protein partitioning experiments were to be conducted at this temperature. An operating tie line was located by finding several (SDS wt%, $C_{10}E_4$ wt%) points along a line for which the experimentally measured volume ratios were approximately equal to the predicted volume ratios based on the lever rule (see Eq. (7.3) in Section 7.3.1). The volume ratios were measured experimentally by preparing 3.0 mL solutions containing $C_{10}E_4$ and SDS in graduated 10 mL test tubes, phase separating them in the thermo-regulated device at 25.2°C, and reading the volumes of the top and bottom phases.

7.2.4 Partitioning Proteins in the $C_{10}E_4$-Buffer and the $C_{10}E_4$-SDS-Buffer Systems

For every protein partitioning experiment conducted in the $C_{10}E_4$-buffer system, four buffered solutions, each with a total volume of 3.4 mL, were prepared in graduated 10 mL test tubes. Three of the solutions contained 2.67 wt% $C_{10}E_4$ and 0.2 g/L of a particular protein. The fourth solution served as the control containing the same concentration of $C_{10}E_4$ but no protein. The proteins that were investigated included lysozyme, cytochrome *c*, ovalbumin,

and catalase. In addition to their desirable net charges (see Section 7.1), these proteins were selected because they are: (i) water-soluble, (ii) available in high purity, and (iii) easy to assay with ultraviolet or visible absorbance measurements. The solutions were first gently mixed to ensure uniform mixing, and then equilibrated at 4°C in order for each solution to exhibit a single phase. The solutions were subsequently placed in the thermo-regulated device, which had already been set at the desired temperature of 19.3°C, to initiate phase separation. At 19.3°C, approximately equal phase volumes were obtained for the initial $C_{10}E_4$ concentration of 2.67 wt%. Since it was shown in Chapter 5 that most protein partition coefficients can be measured at any volume ratio due to negligible entrainment effects, a volume ratio of about 1 was chosen to be consistent with the protein partitioning experiments that were conducted previously.[70] Solutions were maintained at this condition for at least 14 hours before the two coexisting micellar phases were withdrawn with great care using syringe and needle sets. All the partitioning experiments reported in this thesis were conducted for *at least* 14 hours, since it was shown previously[70] that partition coefficients measured after overnight partitioning did not differ from those measured after partitioning over at least three days. The protein concentrations were determined as described in Section 5.2.4. Although absorbance measurements were conducted at 549.5 nm for cytochrome *c* (after it had been reduced by the addition of sodium L-ascorbate), different wavelengths were used for catalase, lysozyme, and ovalbumin. Specifically, absorbances were measured at 405 nm for catalase and 280 nm for lysozyme and ovalbumin. It should be noted that, unlike cytochrome *c*, the other proteins did not need to be reduced with sodium L-ascorbate prior to measuring their absorbances.

With regard to the protein partitioning experiments conducted in the $C_{10}E_4$-SDS-buffer system, the procedure was similar to the one described for the $C_{10}E_4$-buffer system. However, these solutions contained 2.02 wt% $C_{10}E_4$ and 0.0970 wt% SDS, and the partitioning temperature was 25.2°C. At this temperature, approximately equal phase volumes were obtained for the above-mentioned, initial $C_{10}E_4$ and SDS concentrations.

7.3 Theory

7.3.1 Review of Expressions for the Volume Ratio in Two-Phase Aqueous Micellar Systems

The volume ratio, V_t/V_b, is defined as the volume of the top phase divided by that of the bottom phase, and can be measured experimentally by reading the volumes of the top

and bottom phases in graduated 10 mL test tubes. The volume ratio can also be calculated using the lever rule.[75,110] For the $C_{10}E_4$-buffer system, the lever rule states that:

$$\frac{V_t}{V_b} = \frac{\nu_{C_{10}E_4,0} - \nu_{C_{10}E_4,b}}{\nu_{C_{10}E_4,t} - \nu_{C_{10}E_4,0}} \tag{7.1}$$

where $\nu_{C_{10}E_4,0}$ is the initial concentration of $C_{10}E_4$ in g/mL prior to phase separation, and $\nu_{C_{10}E_4,t}$ and $\nu_{C_{10}E_4,b}$ are the concentrations of $C_{10}E_4$ in g/mL in the top and bottom phases, respectively. Since the densities of the initial, single phase solution and the two resulting top and bottom phases are all approximately 1 g/mL, the volume ratio can be rewritten as follows:

$$\frac{V_t}{V_b} = \frac{\omega_{C_{10}E_4,0} - \omega_{C_{10}E_4,b}}{\omega_{C_{10}E_4,t} - \omega_{C_{10}E_4,0}} \tag{7.2}$$

where $\omega_{C_{10}E_4,0}$ is the initial weight fraction of $C_{10}E_4$ prior to phase separation, and $\omega_{C_{10}E_4,t}$ and $\omega_{C_{10}E_4,b}$ are the weight fractions of $C_{10}E_4$ in the top and bottom phases, respectively. According to Eq. (7.2), the volume ratio can be calculated using tie lines on the coexistence curve of the $C_{10}E_4$-buffer system. Similarly, the volume ratio in the $C_{10}E_4$-SDS-buffer system can be calculated using tie lines on the coexistence curve of the $C_{10}E_4$-SDS-buffer system using the following lever rule result:

$$\frac{V_t}{V_b} = \frac{\sqrt{\left(\omega_{C_{10}E_4,0} - \omega_{C_{10}E_4,b}\right)^2 + \left(\omega_{SDS,0} - \omega_{SDS,b}\right)^2}}{\sqrt{\left(\omega_{C_{10}E_4,t} - \omega_{C_{10}E_4,0}\right)^2 + \left(\omega_{SDS,t} - \omega_{SDS,0}\right)^2}} \tag{7.3}$$

where $\omega_{SDS,0}$ is the initial weight fraction of SDS prior to phase separation, and $\omega_{SDS,t}$ and $\omega_{SDS,b}$ are the weight fractions of SDS in the top and bottom phases, respectively.

7.3.2 Brief Review of the Excluded-Volume Theory

In order to quantify the distribution of a protein between the two coexisting micellar phases, the protein partition coefficient must be evaluated. The protein partition coefficient, K_p, is experimentally measured and theoretically predicted in this study, and it is defined as follows:[75]

$$K_p \equiv \frac{C_{p,t}}{C_{p,b}} \tag{1.3}$$

where $C_{p,t}$ and $C_{p,b}$ are the number densities (molecules/mL) of protein in the top and bottom phases, respectively. Experimentally, the protein partition coefficient is evaluated by taking the ratio of the measured absorbances in the top and bottom phases, since the protein concentrations are directly proportional to the measured absorbances (see Section 5.2.4).

Theoretically, an expression capable of reasonably predicting hydrophilic, water-soluble protein partition coefficients in two-phase aqueous "non-charged" (nonionic or zwitterionic) micellar systems composed of cylindrical micelles was developed by our group, and is repeated below:[71,74]

$$K_p = \exp\left[-(\phi_t - \phi_b)\left(1 + \frac{R_p}{R_0}\right)^2\right] \tag{1.4}$$

where ϕ_t and ϕ_b are the surfactant volume fractions in the top and bottom phases, respectively, R_p is the hydrodynamic radius of the protein, and R_0 is the cross-sectional radius of each cylindrical micelle (modeled as a spherocylindrical entity). This theory only incorporates steric, excluded-volume interactions that operate between the proteins and the micelles,[74] and is able to predict the preferential partitioning of proteins into the micelle-poor phase where they experience fewer excluded-volume interactions with the micelles. This theory can be derived from purely entropic arguments as well,[71] and is also able to predict the preferential partitioning of proteins into the micelle-poor phase where they can sample a greater number of configurations due to the larger available volume. Based on Eq. (1.4), for given R_p and R_0 values, the excluded-volume interactions between the proteins and the micelles are determined solely by the difference in the surfactant volume fractions in the two phases, $(\phi_t - \phi_b)$. As further described in Section 7.4.3, this feature was exploited to maintain the excluded-volume interactions between the proteins and the micelles constant for the partitioning experiments in the $C_{10}E_4$-buffer and the $C_{10}E_4$-SDS-buffer systems. By maintaining the excluded-volume interactions constant, the strength of the electrostatic interactions between the proteins and the mixed ($C_{10}E_4$/SDS) micelles were examined. The surfactant volume fractions in the two phases were obtained from the intersections of the tie lines with the coexistence curves, since the volume fractions were approximated as being equal to the weight fractions due to the densities of both phases being close to 1 g/mL.

7.3.3 Development of a Theory Incorporating Electrostatic Interactions

Protein partitioning in two-phase aqueous mixed (nonionic/ionic) micellar systems cannot be fully explained by the excluded-volume theory because electrostatic interactions between the proteins and the charged micelles are also expected to play a significant role. In this section, a theory that incorporates both excluded-volume and electrostatic interactions is developed. Since the proteins are allowed to partition over at least 14 hours in the experiments, the establishment of diffusional equilibrium of the proteins between the two coexisting

phases will be assumed. At equilibrium,[111]

$$\mu_{p,t} = \mu_{p,b} \tag{7.4}$$

where $\mu_{p,t}$ and $\mu_{p,b}$ are the chemical potentials of the protein in the top and bottom phases, respectively. After some simplification (see details in Appendix D), the chemical potential of the protein in each phase α can be written as follows:[112]

$$\mu_{p,\alpha} = \mu_p^\circ + k_B T \ln C_{p,\alpha} + \mu_{p,\alpha}^{ex} + z_{p,\alpha} e \psi_\alpha \tag{7.5}$$

where α denotes either top or bottom, μ_p° is the standard-state chemical potential of the protein, k_B is the Boltzmann constant, T is the absolute temperature, $C_{p,\alpha}$ is the number density (molecules/mL) of the protein in phase α, $\mu_{p,\alpha}^{ex}$ is the excess chemical potential of the protein in phase α, $z_{p,\alpha}$ is the valence or net charge of the protein in phase α, e is the electronic charge, and ψ_α is the electrostatic or electrical potential of phase α. The standard-state chemical potential of the protein, μ_p°, does not have the index α because the same standard state was chosen for the protein in both phases. This standard-state chemical potential of the protein corresponds to a standard state in which: (i) the protein and the solvent are the only two components present, (ii) the protein molecules interact with the solvent molecules but not with each other, (iii) the solvent molecules interact with each other, and (iv) the concentration of the protein is 1 molecule/mL, and therefore, has an ideal entropy corresponding to this concentration (see Appendix D). The interactions, as well as the ideal entropy of 1 protein molecule/mL included in μ_p°, are all accounted for at the temperature and pressure of the system. Most of the protein's ideal entropy, however, is accounted for in the $k_B T \ln C_{p,\alpha}$ term (see Appendix D). The excess chemical potential of the protein in phase α accounts for any interactions not accounted for in the standard-state chemical potential, such as, the protein-micelle interactions, and any non-idealities in the entropy. The $z_{p,\alpha} e \psi_\alpha$ term is the electrostatic potential energy of the protein in phase α. It is analogous to the gravitational potential energy, where the charge of the protein ($z_{p,\alpha} e$) is analogous to the mass of an object (m), and the electrostatic potential of phase α (ψ_α) is analogous to the gravitational acceleration (g). Only the valence or the net charge of the protein is required to evaluate the electrostatic potential energy, because summing the electrostatic potential energy of each charge on the protein is equivalent to evaluating the electrostatic potential energy associated with only the net charge of the protein as shown

below:

$$\begin{aligned}\sum_{aa,i} N_{aa,i} z_{aa,i} e\psi_\alpha + N_{ag} z_{ag} e\psi_\alpha + N_{cg} z_{cg} e\psi_\alpha &= \left(\sum_{aa,i} N_{aa,i} z_{aa,i} + N_{ag} z_{ag} + N_{cg} z_{cg}\right) e\psi_\alpha \\ &= z_p e\psi_\alpha \end{aligned} \tag{7.6}$$

where $N_{aa,i}$ is the number of amino acids of type i in the protein, $z_{aa,i}$ is the valence of the amino acid of type i, N_{ag} is the number of terminal amino groups in the protein (if the protein is comprised of multiple subunits), z_{ag} is the valence of the terminal amino group, N_{cg} is the number of terminal carboxyl groups in the protein (if the protein is comprised of multiple subunits), and z_{cg} is the valence of the terminal carboxyl group.

Substituting Eq. (7.5) in Eq. (7.4), recognizing that $z_{p,t} = z_{p,b} = z_p$ since both phases have approximately equal pH values (which was later confirmed experimentally), and rearranging yields:

$$K_p = \exp\left[\frac{-\left(\mu_{p,t}^{ex} - \mu_{p,b}^{ex}\right) - z_p e\left(\psi_t - \psi_b\right)}{k_B T}\right] \tag{7.7}$$

The electrostatic potentials of both phases will be assumed to be approximately equal, that is, $(\psi_t - \psi_b) \approx 0$. This is a reasonable first approximation, since the electrostatic potential difference was shown in Appendix E to be approximately 0 for the $C_{10}E_4$-buffer system considered in this thesis. Equation (7.7) therefore simplifies to:

$$K_p = \exp\left[\frac{-\left(\mu_{p,t}^{ex} - \mu_{p,b}^{ex}\right)}{k_B T}\right] \tag{7.8}$$

Accordingly, an expression for the excess chemical potential of the protein in each phase is required, and can be obtained from an expression for the excess Gibbs free energy of each phase by taking the following partial derivative:[111]

$$\mu_{p,\alpha}^{ex} = \left(\frac{\partial G_\alpha^{ex}}{\partial N_{p,\alpha}}\right)_{T,P,N_{k,\alpha\neq p,\alpha}} \tag{7.9}$$

where G_α^{ex} is the excess Gibbs free energy in phase α, $N_{p,\alpha}$ is the number of protein molecules in phase α, $N_{k,\alpha\neq p,\alpha}$ is the number of non-protein molecules of type k in phase α, and T and P are the absolute temperature and pressure in both phases. The excess Gibbs free energy in phase α will be approximated as follows:

$$G_\alpha^{ex} = G_\alpha^{ex,EV} + G_\alpha^{ex,elec} \tag{7.10}$$

where $G_\alpha^{ex,EV}$ and $G_\alpha^{ex,elec}$ are the excluded-volume and electrostatic contributions to the excess Gibbs free energy in phase α, respectively. Other interactions, such as those of the van der Waals and hydrophobic type, were not considered because they were shown to be negligible in the $C_{10}E_4$-buffer system without the ionic surfactant. Combining Eqs. (7.8), (7.9), and (7.10) yields:

$$K_p = \exp\left[\frac{-\left(\mu_{p,t}^{ex,EV} - \mu_{p,b}^{ex,EV}\right)}{k_B T}\right] \exp\left[\frac{-\left(\mu_{p,t}^{ex,elec} - \mu_{p,b}^{ex,elec}\right)}{k_B T}\right] \tag{7.11}$$

where

$$\mu_{p,\alpha}^{ex,EV} = \left(\frac{\partial G_\alpha^{ex,EV}}{\partial N_{p,\alpha}}\right)_{T,P,N_{k,\alpha\neq p,\alpha}} \tag{7.12}$$

and

$$\mu_{p,\alpha}^{ex,elec} = \left(\frac{\partial G_\alpha^{ex,elec}}{\partial N_{p,\alpha}}\right)_{T,P,N_{k,\alpha\neq p,\alpha}} \tag{7.13}$$

Equation (7.11) can also be rewritten in the following useful form:

$$K_p = K_p^{EV} K_p^{elec} \tag{7.14}$$

where

$$K_p^{EV} = \exp\left[\frac{-\left(\mu_{p,t}^{ex,EV} - \mu_{p,b}^{ex,EV}\right)}{k_B T}\right] \tag{7.15}$$

is the excluded-volume contribution to the protein partition coefficient, and

$$K_p^{elec} = \exp\left[\frac{-\left(\mu_{p,t}^{ex,elec} - \mu_{p,b}^{ex,elec}\right)}{k_B T}\right] \tag{7.16}$$

is the electrostatic contribution to the protein partition coefficient. With regard to K_p^{EV}, an expression has already been derived by our group (see Eq. (1.4) above). An expression for K_p^{elec} will now be derived by developing an expression for $G_\alpha^{ex,elec}$.

In order to derive an expression for $G_\alpha^{ex,elec}$, we first derive an expression for the electrostatic contribution to the excess internal energy in phase α, $U_\alpha^{ex,elec}$. Once an expression for $U_\alpha^{ex,elec}$ is obtained, the electrostatic contribution to the excess Helmholtz free energy in

phase α, $A_\alpha^{ex,elec}$, can then be evaluated as follows:[111]

$$A_\alpha^{ex,elec} = U_\alpha^{ex,elec} - TS_\alpha^{ex,elec} \tag{7.17}$$

where $S_\alpha^{ex,elec}$ is the electrostatic contribution to the excess entropy. In addition, as a first approximation, the electrostatic contribution to the excess entropy will be assumed to be zero, since the excess entropic effects associated with the sizes of the micelles and the proteins were primarily incorporated in the excluded-volume contribution to the protein partition coefficient, K_p^{EV}. Once an expression for $A_\alpha^{ex,elec}$ is obtained, $G_\alpha^{ex,elec}$ can then be evaluated as follows:[111]

$$G_\alpha^{ex,elec} = A_\alpha^{ex,elec} + PV_\alpha^{ex,elec} \tag{7.18}$$

A model for the total volume of the solution in phase α, V_α, is then required to evaluate $V_\alpha^{ex,elec}$ in Eq. (7.18). Partial molecular volumes of dilute solutions, where mixing volume effects are negligible, are commonly assumed to be independent of the solution composition and to be only a function of temperature and pressure.[55,74,113] Accordingly, the total volume of the solution in phase α will be modeled as follows:

$$V_\alpha = N_{w,\alpha}\Omega_w + N_{p,\alpha}\Omega_p + \sum_{n_\alpha=n^\circ_{cyl,\alpha}}^{\infty} N_{n_\alpha}\Omega_{n_\alpha} \tag{7.19}$$

where $N_{w,\alpha}$ is the number of solvent molecules in phase α, N_{n_α} is the number of micelles of aggregation number n in phase α, $n^\circ_{cyl,\alpha}$ is the aggregation number of the smallest cylindrical micelle in phase α, Ω_w is the volume of a solvent molecule, Ω_p is the volume of a protein molecule, and Ω_{n_α} is the volume of a cylindrical micelle of aggregation number n in phase α. Note that Ω_i $(i = w, p, n_\alpha)$ is only a function of temperature and pressure because it is the pure molecular volume of component i. The index α is required in Ω_{n_α} because Ω_{n_α} is equal to the sum of all the pure molecular volumes of the individual monomers that comprise the micelle, and the micelle composition (the molar ratio of ionic surfactant to total surfactant in each micelle) can depend on whether the micelle is in the top or bottom phase. The micelle composition, however, can be approximated as a constant equal to the optimum value for all the mixed micelles in each phase α regardless of the aggregation number,[114] and therefore, the micelle composition is not considered as a variable in Eq. (7.19). Note also that the buffer salt ions have been lumped along with the water molecules to form the hypersolvent. The monomers of $C_{10}E_4$ and SDS free in the solution, and not in the micelles, have been neglected in the theoretical development because they are present at essentially the same

concentrations at the critical micelle concentration in the top and bottom phases, and their effects on protein partitioning cancel between the two phases. In addition, including the volumes of the free monomers in Eq. (7.19) will not change the expression obtained for ($\mu_{p,t}^{ex,elec}$ - $\mu_{p,b}^{ex,elec}$) (see Appendix G). With this model for the total volume of the solution in phase α, the contributions of V_t^{ex} and V_b^{ex} to ($\mu_{p,t}^{ex} - \mu_{p,b}^{ex}$) cancel each other (see Appendix G), and therefore, the difference in excess chemical potentials due to electrostatic interactions simplifies to:

$$\mu_{p,t}^{ex,elec} - \mu_{p,b}^{ex,elec} = \left(\frac{\partial U_t^{ex,elec}}{\partial N_{p,t}}\right)_{T,P,N_{w,t},N_{n_t}} - \left(\frac{\partial U_b^{ex,elec}}{\partial N_{p,b}}\right)_{T,P,N_{w,b},N_{n_b}} \tag{7.20}$$

Once an expression for $U_\alpha^{ex,elec}$ is derived, an expression for K_p^{elec} can be obtained by combining Eqs. (7.16) and (7.20). Therefore, the main challenge in our theoretical approach involves deriving an expression for $U_\alpha^{ex,elec}$, which can be written as follows:[115,116]

$$U_\alpha^{ex,elec} = \sum_{n_\alpha = n_{cyl,\alpha}^\circ}^{\infty} \int_{R_0}^{\infty} [N_{n_\alpha}] \left[u_{np,\alpha}(r)\right] [C_{p,\alpha} 2\pi r L_{n_\alpha} dr] \tag{7.21}$$

where r is the radial distance from the cylindrical micelle axis of symmetry, $u_{np,\alpha}(r)$ is the interaction potential between a micelle of aggregation number n and a protein in phase α, $C_{p,\alpha}$ is the number density (molecules/mL) of protein in phase α, N_{n_α} is the number of micelles of aggregation number n in phase α, and L_{n_α} is the length of a cylindrical micelle of aggregation number n in phase α. Equation (7.21) can be rationalized physically as follows. A cylindrical micelle of aggregation number n is first chosen at random in phase α. The z-axis of a cylindrical coordinate system is then placed along the axis of symmetry of the cylindrical micelle. The micelle will be modeled as a cylinder having all its charges smeared uniformly on its surface of charge, that is, on the cylindrical surface with a radius equal to the length of the charged SDS molecules in the mixed micelle. This assumption is reasonable, since the positions of the charged SDS molecules are not fixed due to the micelles continually exchanging surfactant molecules with the other micelles and the free monomers in the solution. Therefore, the micelles appear, on a time-averaged basis, to have a uniform charge density.[114] Accordingly, the electric field is radially symmetric, and independent of the θ direction. In addition, since even the smallest cylindrical micelle in phase α with aggregation number $n_{cyl,\alpha}^\circ$ is infinitely long on the length scale of a protein, the electric field is also not a function of the z direction, and is only a function of the radial distance. This

micelle therefore interacts with all the proteins located at a radial distance r away from it with an interaction potential $u_{np,\alpha}(r)$. The number of proteins located at a radial distance r away from the micelle, in a mean-field approach, is equal to the concentration of proteins in phase α, $C_{p,\alpha}$, multiplied by the differential volume, $2\pi r L_{n_\alpha} dr$. The same analysis is then performed for all the micelles of aggregation number n in phase α, and therefore, a factor of N_{n_α} appears in Eq. (7.21). Then, an integration over the entire volume of phase α is performed from R_0 (the choice of this lower limit will be discussed later) to infinity. The aggregation number is then varied from $n^\circ_{cyl,\alpha}$ to infinity, while the above analysis is performed at each aggregation number. Although electrostatic interactions are generally long-ranged, considering only pairwise interactions is reasonable since the electrostatic potentials of the micelles are effectively screened by the hypersolvent, which contains the buffer salt ions. In particular, the Debye-Hückel screeening length is only 13.9 Å, and the electrostatic interactions are indeed short-ranged. Protein-protein interactions have been neglected, since the solutions are infinitely dilute in protein. With regard to micelle-micelle interactions, they are present in these systems, since they are required in order to have phase separation. However, their contribution to the protein partition coefficient has been found to be negligible in the past,[71] and therefore, they will also be neglected in this derivation.

Based on Eq. (7.21), an expression for the interaction potential between a micelle and a protein in phase α, $u_{np,\alpha}(r)$, is required to derive an expression for $U_\alpha^{ex,elec}$. Since the micelles are infinitely long on the length scale of the protein, their end effects due to their hemispherical caps will be ignored. The Debye-Hückel approximation to the Poisson-Boltzmann equation will also be used, and its validity in this system will be verified later. In the Debye-Hückel approximation, the electrostatic potential of an infinitely long cylinder in the hypersolvent (in the cgs system of units) is given by:[117,118]

$$\psi_{cyl}(r) = \frac{4\pi\sigma K_0(\kappa r)}{\kappa\epsilon_w K_1(\kappa R_{cyl})} \tag{7.22}$$

where r is the radial distance from the cylinder's axis of symmetry, σ is the surface charge density of the cylinder (charge/area), κ is the inverse Debye-Hückel screening length based on the buffer salt ions in the hypersolvent, ϵ_w is the dielectric constant of water, R_{cyl} is the radius of the cylinder, and K_0 and K_1 are modified Bessel functions of the second kind of order 0 and 1, respectively.

The surface charge density can be evaluated because, as discussed above, all the charges will be modeled as being uniformly distributed on the cylindrical surface of charge. This

assumption of a uniform charge density was required in order to use the Poisson-Boltzmann equation,[119] which was used to derive the electrostatic potential in Eq. (7.22).[117,118] In Appendix H, the surface charge density of every micelle in phase α is shown to be a constant. In addition, R_{cyl} is the radius of the surface of charge of the mixed micelles, which is equal to the length of a SDS molecule in the micelle, l_{SDS}. With Program MIX2 (a program developed by our group to predict fundamental properties of mixed surfactant systems),[54,108,114] l_{SDS} was shown to be essentially constant for all the micelles in the top and bottom phases. κ is also a constant for the two phases, since the concentrations of the buffer salt ions are essentially the same in both phases (see Appendix C). Accordingly, the electrostatic potential of any micelle in phase α can be rewritten as follows:

$$\psi_{mic,\alpha}(r) = \frac{4\pi\sigma_\alpha K_0(\kappa r)}{\kappa\epsilon_w K_1(\kappa l_{SDS})} \tag{7.23}$$

For the electrostatic potential in Eq. (7.23), the quantity that will be referred to as ξ can be evaluated as follows:

$$\xi \equiv \left| \frac{z_{ion} e \psi_{mic,\alpha}}{k_B T} \right| \tag{7.24}$$

where z_{ion} is the valence of a buffer salt ion. ξ is an important quantity to calculate because the Debye-Hückel approximation is valid when ξ is much less than 1. It can be shown that ξ is indeed much less than 1 for r values between 45 Å and ∞. Even at r=21 Å (the lower limit of integration in Eq. (7.21)), where the magnitude of $\psi_{mic,\alpha}$ is the highest, ξ is only 0.9, which indicates that the Debye-Hückel approximation should not give rise to large errors. This is expected, since the surface charge density of the micelles, and therefore, $\psi_{mic,\alpha}$, is low due to the molar ratio of charged surfactant to non-charged surfactant being only about 1 to 20 in each phase.

In order to obtain an analytical expression for the electrostatic contribution to the protein partition coefficient, each protein will be modeled as a point ion with a charge equal to its net charge. The estimation of the net charge of each protein is described in Section 7.3.4. Treating the proteins as point ions should also not give rise to large errors, since the net charges on the proteins considered in this study are all fairly low (see Section 7.3.4). With this model for the micelles and the proteins, the interaction potential, $u_{np,\alpha}(r)$, is given by:[120]

$$u_{np,\alpha}(r) = \psi_{mic,\alpha}(r) z_p e \tag{7.25}$$

Since the proteins are treated as point ions, the shortest distance between the micelle's

axis of symmetry and each ion is the length of the $C_{10}E_4$ molecule in the micelle. The length of the $C_{10}E_4$ molecule (R_0), and not the length of the SDS molecule (l_{SDS}), determines this distance because about 95% of each micelle is composed of the $C_{10}E_4$ molecules. Accordingly, R_0 defines the lower limit of integration in Eq. (7.21). Although the electrical double-layer interaction between a sphere and a cylinder has been modeled more rigorously,[121,122] an analytical solution cannot be obtained. The expression of Hogg *et al.* was also not used for the double layer interaction between a sphere and a cylinder because their expression also requires approximations, such as modeling the cylinder as a flat plate.[121]

Combining Eqs. (7.21), (7.23), and (7.25) yields the following expression for $U_\alpha^{ex,elec}$:

$$U_\alpha^{ex,elec} = \frac{8\pi^2\sigma_\alpha z_p e N_{p,\alpha} R_0 K_1(\kappa R_0)}{\kappa^2 \epsilon_w V_\alpha K_1(\kappa l_{SDS})} \sum_{n_\alpha = n^\circ_{cyl,\alpha}}^{\infty} L_{n_\alpha} N_{n_\alpha} \tag{7.26}$$

Taking the partial derivative of $U_\alpha^{ex,elec}$ with respect to $N_{p,\alpha}$ then yields:

$$\left(\frac{\partial U_\alpha^{ex,elec}}{\partial N_{p,\alpha}}\right)_{T,P,N_{w,\alpha},N_{n_\alpha}} = \frac{8\pi^2\sigma_\alpha z_p e R_0 K_1(\kappa R_0)}{\kappa^2 \epsilon_w K_1(\kappa l_{SDS})} \left(\frac{1}{V_\alpha} - C_{p,\alpha}\frac{\Omega_p}{V_\alpha}\right) \left(\sum_{n_\alpha = n^\circ_{cyl,\alpha}}^{\infty} L_{n_\alpha} N_{n_\alpha}\right) \tag{7.27}$$

The term $(C_{p,\alpha}\Omega_p/V_\alpha)$ is negligible because each phase is infinitely dilute in protein, and the ratio of the protein's molecular volume to the volume of the entire α phase (Ω_p/V_α) is much less than 1. In addition, the protein partition coefficient, in the strict sense, should be independent of protein concentration, since it is truly defined in the limit of infinite dilution of the protein. Accordingly, Eq. (7.27) simplifies to:

$$\left(\frac{\partial U_\alpha^{ex,elec}}{\partial N_{p,\alpha}}\right)_{T,P,N_{w,\alpha},N_{n_\alpha}} = \frac{8\pi^2\sigma_\alpha z_p e R_0 K_1(\kappa R_0)}{\kappa^2 \epsilon_w K_1(\kappa l_{SDS})} \frac{1}{V_\alpha} \left(\sum_{n_\alpha = n^\circ_{cyl,\alpha}}^{\infty} L_{n_\alpha} N_{n_\alpha}\right) \tag{7.28}$$

Equation (7.28) can also be rewritten in terms of the total surfactant volume fraction in phase α, ϕ_α. The total surfactant volume fraction in phase α is approximately equal to the volume fraction of the micelles in phase α, since the volume fraction of the monomers is orders of magnitude lower that of the micelles in each phase. The total surfactant volume fraction in phase α is therefore essentially given by:

$$\phi_\alpha = \frac{\sum_{n_\alpha = n^\circ_{cyl,\alpha}}^{\infty} (N_{n_\alpha})(\pi R_0^2 L_{n_\alpha})}{V_\alpha} \tag{7.29}$$

where R_0, and not l_{SDS}, defines the radius of each micelle, since about 95% of each micelle is composed of the $C_{10}E_4$ molecules. Combining Eqs. (7.28) and (7.29) yields:

$$\left(\frac{\partial U_{\alpha}^{ex,elec}}{\partial N_{p,\alpha}}\right)_{T,P,N_{w,\alpha},N_{n_\alpha}} = \frac{8\pi\sigma_\alpha z_p e K_1(\kappa R_0)}{\kappa^2 \epsilon_w R_0 K_1(\kappa l_{SDS})}\phi_\alpha \tag{7.30}$$

Combining Eqs. (7.16), (7.20), and (7.30) then yields:

$$K_p^{elec} = \exp\left[\frac{-8\pi z_p e K_1(\kappa R_0)}{\kappa^2 \epsilon_w R_0 k_B T K_1(\kappa l_{SDS})}(\sigma_t\phi_t - \sigma_b\phi_b)\right] \tag{7.31}$$

An analytical expression for the electrostatic contribution to the protein partition coefficient has therefore been derived. This expression, given by Eq. (7.31), will be used to predict protein partition coefficients in the $C_{10}E_4$-SDS-buffer system in Section 7.4.4.

7.3.4 Estimation of the Net Charges of the Proteins

The expressions used for estimating the net charges or valences of the proteins will now be derived. Focusing on the terminal carboxyl unit and the amino acids that can have side chains with negative charges (that is, aspartic acid, glutamic acid, cysteine, and tyrosine), the Henderson-Hasselbalch equation[123] can be applied as follows:

$$pH = pK_a + \log\left(\frac{[A^-]}{[HA]}\right) \tag{7.32}$$

where $[HA]$ is the molar concentration of the amino acid, $[A^-]$ is the molar concentration of the unprotonated form of the amino acid, and the pK_a of the amino acid is given by:

$$pK_a = -\log K_a = -\log\left(\frac{[H^+][A^-]}{[HA]}\right) \tag{7.33}$$

where $[H^+]$ is the molar concentration of H^+. Equation (7.32) can be rearranged to yield:

$$[HA] = [A^-]\frac{1}{10^{(pH-pK_a)}} \tag{7.34}$$

A mole balance on the unprotonated and protonated forms yields the following relation that involves $[A^-]$ and $[HA]$:

$$[A^-] + [HA] = N_A[P] \tag{7.35}$$

where N_A is the number of amino acids per protein or the number of terminal carboxyl units per protein (if the protein is composed of more than one subunit), and $[P]$ is the molar concentration of the protein. Substituting Eq. (7.34) in Eq. (7.35) and rearranging yields:

$$[A^-] = \frac{N_A[P]}{1 + \frac{1}{10^{(pH-pK_a)}}} \tag{7.36}$$

Equation (7.36) can be simplified to:

$$[A^-] = \frac{N_A[P]}{1 + \frac{1}{10^{(pH-pK_a)}}} \frac{10^{(pH-pK_a)}}{10^{(pH-pK_a)}} = \frac{N_A 10^{(pH-pK_a)}}{1 + 10^{(pH-pK_a)}}[P] \tag{7.37}$$

Equation (7.37) can be applied to the terminal carboxyl unit, aspartic acid, glutamic acid, cysteine, and tyrosine with knowledge of the N_A, pH, and the pK_a values. The N_A value can be determined from the amino acid sequence. The pH of the solution can be measured. The pK_a of the amino acid or the terminal carboxyl unit can be estimated based on typical values in the literature (see Table 7-2). After applying Eq. (7.37) to the terminal carboxyl unit and the different amino acids, the resulting $[A^-]$ values can then be summed to obtain a relation for the molar concentration of negative charges, $[Neg\ Charge]$, in terms of $[P]$.

For some amino acids, however, the protonated form is positively charged, while the unprotonated form is neutral. Focusing on these amino acids that can have side chains with positive charges (that is, histidine, lysine, and arginine) and the terminal amino unit, Eq. (7.32) can be rewritten as follows:

$$pH = pK_a + \log\left(\frac{[A]}{[HA^+]}\right) \tag{7.38}$$

where $[HA^+]$ is the molar concentration of the amino acid, $[A]$ is the molar concentration of the unprotonated form of the amino acid, and the pK_a of the amino acid is given by:

$$pK_a = -\log K_a = -\log\left(\frac{[H^+][A]}{[HA^+]}\right) \tag{7.39}$$

Equation (7.38) can be rearranged to yield:

$$[A] = [HA^+]10^{(pH-pK_a)} \tag{7.40}$$

A mole balance on the unprotonated and protonated forms yields the following relation that

involves $[A]$ and $[HA^+]$:

$$[A] + [HA^+] = N_A[P] \tag{7.41}$$

where N_A is the number of amino acids per protein or the number of terminal amino units per protein (if the protein is composed of more than one subunit), and $[P]$ is the molar concentration of the protein. Substituting Eq. (7.40) in Eq. (7.41), and rearranging yields:

$$[HA^+] = \frac{N_A}{1 + 10^{(pH - pK_a)}}[P] \tag{7.42}$$

Equation (7.42) can be applied to the terminal amino unit, histidine, lysine, and arginine with knowledge of the N_A (from the amino acid sequence), pH (which is measured), and pK_a values (see Table 7-2). After applying Eq. (7.42) to the terminal amino unit and the different amino acids, the resulting $[HA^+]$ values can then be summed to obtain a relation for the molar concentration of positive charges, $[Pos\ Charge]$, in terms of $[P]$. The $[Neg\ Charge]$ value can then be subtracted from the $[Pos\ Charge]$ value to yield the molar concentration of net positive charges, $[Net\ Pos\ Charge]$, as follows:

$$[Net\ Pos\ Charge] = [Pos\ Charge] - [Neg\ Charge] \tag{7.43}$$

Since the molar concentration of net positive charges, $[Net\ Pos\ Charge]$, is expressed in terms of the molar concentration of protein, $[P]$, $[Net\ Pos\ Charge]$ can be divided by $[P]$ to yield the net positive charge per protein. If this net positive charge per protein is positive (or negative), the protein has an overall net positive (or negative) charge.

For lysozyme, cytochrome *c*, and ovalbumin, their net charges at the pH of the buffer (7.2) were estimated to be +7.65, +9.25, and -11.23, respectively, based on their amino acid sequences. With regard to catalase, it is comprised of 4 identical subunits, and therefore, its net charge was estimated as -11.23 by multiplying the net charge of one subunit by 4.

7.4 Results and Discussion

7.4.1 Mapping the Three-Dimensional Phase Diagram of the $C_{10}E_4$-SDS-Buffer System between 19.8°C and 23.1°C

The three-dimensional phase diagram of the $C_{10}E_4$-SDS-buffer system between 19.8°C and 23.1°C is shown in Figure 7-2. For each temperature investigated, a transition from the one-phase region to the two-phase region is attained by crossing the solid line from higher SDS

Table 7-2: Typical pKa's of amino acids and terminal groups.[123]

Amino Acid or Terminal Group	pKa
Terminal Carboxyl	3.1
Aspartic Acid	4.4
Glutamic Acid	4.4
Histidine	6.5
Terminal Amino	8.0
Cysteine	8.5
Tyrosine	10.0
Lysine	10.0
Arginine	12.0

concentrations to lower SDS concentrations. Therefore, for each temperature investigated, the two-phase region is inside the "loop," while the one-phase region is outside the "loop." Each "loop" intersects the 0 wt% SDS plane twice. These two intersections correspond to the concentrations of $C_{10}E_4$ in the two phases in equilibrium with each other in the $C_{10}E_4$-buffer system (without SDS). In other words, the intersection of the three-dimensional phase diagram with the 0 wt% SDS plane will yield the two-dimensional phase diagram of the $C_{10}E_4$-buffer system shown in Figure 4-1. The three-dimensional phase diagram can therefore be viewed as half an ice cream cone, where the two-phase region is inside the cone (where the ice cream would be) and the one-phase region is outside the cone. The tip of this ice cream cone corresponds to 19.0°C, which is the lower critical point of the $C_{10}E_4$-buffer system shown in Figure 4-1. Accordingly, phase separation in the $C_{10}E_4$-SDS-buffer system only occurs above 19.0°C.

As shown in Figure 7-2, higher SDS concentrations can be accessed by increasing the phase separation temperature. Adding SDS increases the phase separation temperature because it introduces electrostatic repulsions between the micelles. To counter these electrostatic repulsions, higher phase separation temperatures are necessary, since increasing the temperature increases the attractive interactions between these predominantly $C_{10}E_4$ micelles, which are required for phase separation to occur (see Chapter 1).

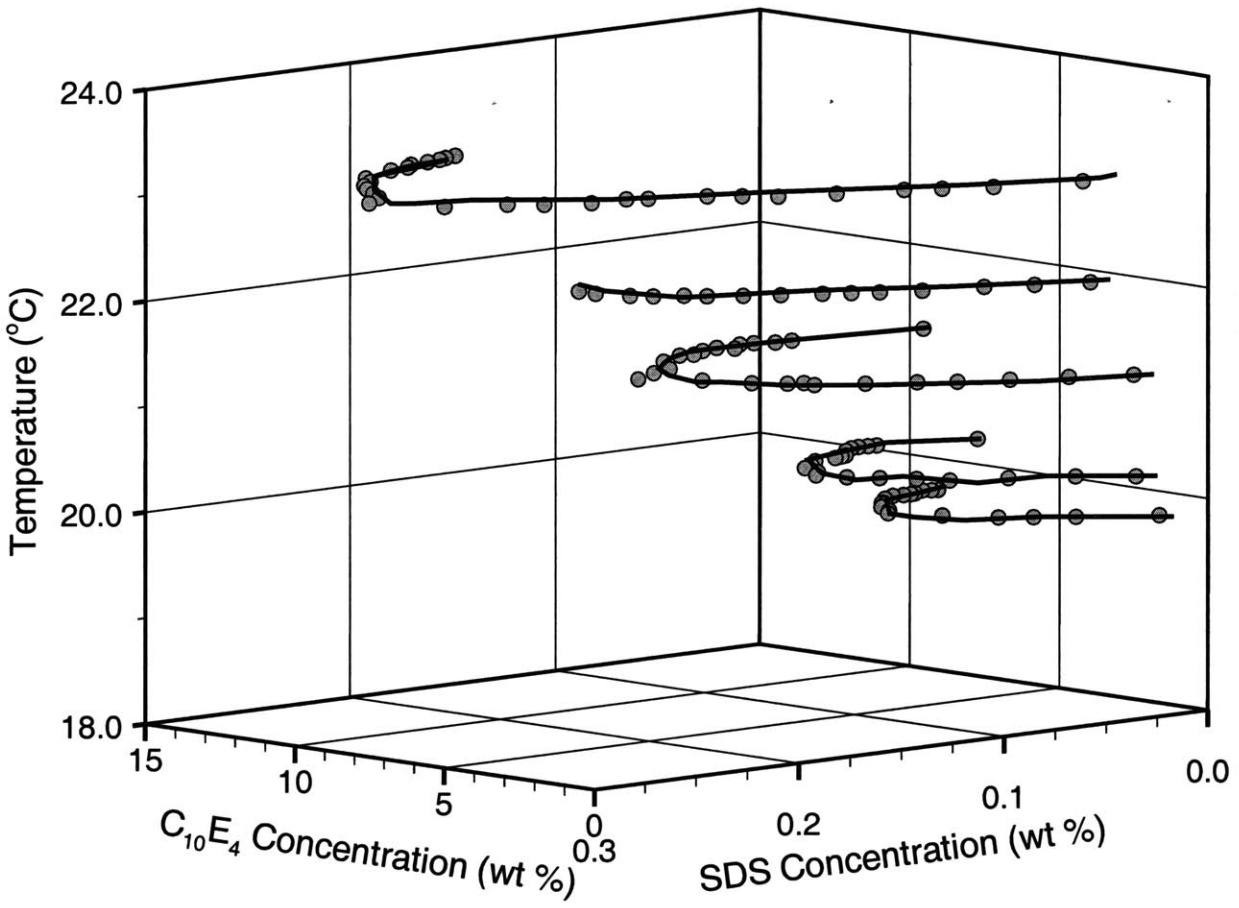

Figure 7-2: The three-dimensional phase diagram of the $C_{10}E_4$-SDS-buffer system between 19.8°C and 23.1°C. The gray circles correspond to the experimentally measured data points. Each solid line was drawn to help visualize the intersection between a constant temperature horizontal plane and the phase diagram. The error bars have not been shown to avoid further complicating the presentation of the phase diagram. For each temperature above 19.0°C (the lower critical point in the $C_{10}E_4$-buffer system shown in Figure 4-1), a transition from the one-phase region to the two-phase region can be attained by decreasing the concentration of SDS.

7.4.2 Mapping the Coexistence Curve of the $C_{10}E_4$-SDS-Buffer System at a Temperature of 25.2°C

As discussed in Section 7.2.3, in order to experimentally observe an effect of the electrostatic interactions in the protein partitioning experiments, it is desirable to form a two-phase system with the top, micelle-rich phase containing a relatively high concentration of SDS. In addition, based on the results of Section 7.4.1, it was concluded that higher SDS concentrations can only be accessed with higher operating temperatures. However, an operating temperature of only 25.2°C was selected for the protein partitioning experiments, since: (i) proteins can become thermally denatured, and (ii) this experimental study served only as a proof-of-principle demonstration that electrostatic interactions could be triggered between the proteins and the micelles by mixing some ionic surfactant with a nonionic surfactant. The coexistence curve of the $C_{10}E_4$-SDS-buffer system at 25.2°C and an operating tie line were therefore required prior to conducting any protein partitioning experiments. The coexistence curve that was mapped out is shown in Figure 7-3.

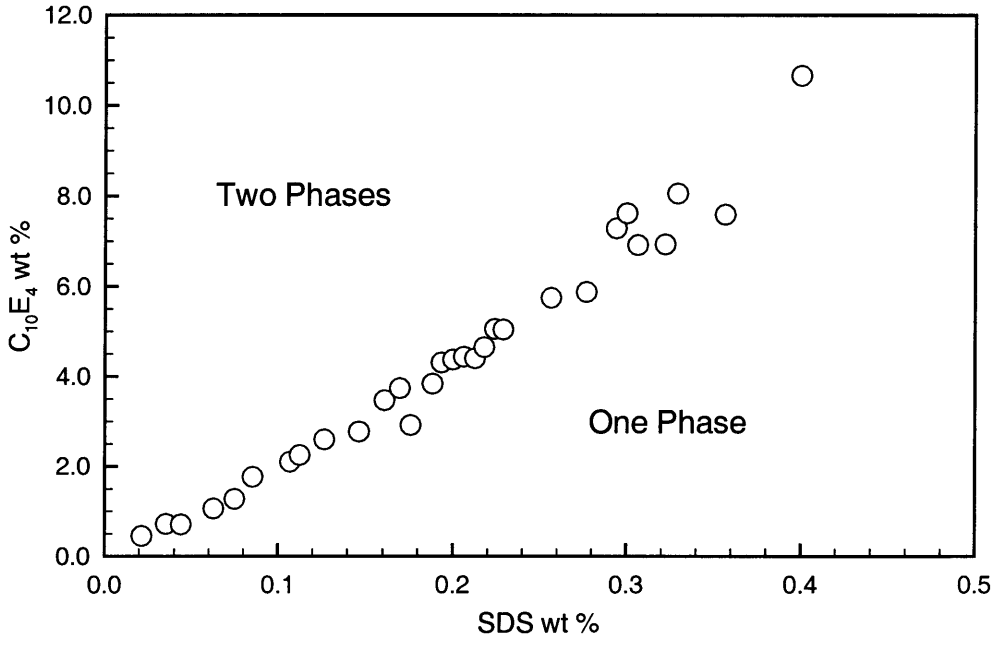

Figure 7-3: The coexistence curve of the $C_{10}E_4$-SDS-buffer system at 25.2°C. The error bars have not been shown to avoid further complicating the presentation of the coexistence curve.

In contrast to the $C_{10}E_4$-buffer system, more experiments are required to locate tie lines for the $C_{10}E_4$-SDS-buffer system. One tie line was located on the $C_{10}E_4$-SDS-buffer phase diagram at 25.2°C by first passing the best-fit quadratic curve through the experimentally

determined points comprising the coexistence curve, and then finding a line on which seven (SDS wt%, $C_{10}E_4$ wt%) points yielded experimentally measured volume ratios that were approximately equal to the predicted volume ratios based on the lever rule result in Eq. (7.3). The best-fit quadratic curve (with an r^2 of 0.98), the seven (SDS wt%, $C_{10}E_4$ wt%) points, and the located tie line are shown in Figure 7-4.

A quadratic fit was chosen in order to capture the physical essence of the coexistence curve with the least fitted parameters. Although a first order (linear) fit would correspond to the least fitted parameters, such a fit would not make physical sense for a ternary phase diagram, because curvature is required in order for a tie line to precisely connect two points on the coexistence curve. A tie line could never connect only two points on a linear curve. Indeed, in that case, it would intersect only at one point or at an infinite number of points, that is, the tie line and the coexistence curve would be collinear. In addition, the ability to locate an operating tie line based on the quadratic fit provided the *a posteriori* justification that the coexistence curve in Figure 7-3 was quadratic and indeed had some curvature.

The tie line that was located intersects the coexistence curve at (0.0029 wt% SDS, 0.087 wt% $C_{10}E_4$) and (0.18 wt% SDS, 3.77 wt% $C_{10}E_4$). Therefore, if a solution is prepared with initial SDS and $C_{10}E_4$ concentrations corresponding to a point on the tie line, the system would phase separate to yield a bottom, micelle-poor phase with 0.0029 wt% SDS and 0.087 wt% $C_{10}E_4$ and a top, micelle-rich phase with 0.18 wt% SDS and 3.77 wt% $C_{10}E_4$. Based on these values, the molar ratio of $C_{10}E_4$ to SDS is 18.1 in the top phase and 25.9 in the bottom phase, indicating that both phases contain much more $C_{10}E_4$ than SDS.

Although the $C_{10}E_4$-SDS-buffer system is actually composed of five components (SDS in addition to the four components in the $C_{10}E_4$-buffer system), the coexistence curve and operating tie line in Figure 7-4 correspond to those for a ternary system. The justification for approximating the $C_{10}E_4$-SDS-buffer system as a pseudo-ternary system is provided in Appendix C.2.

7.4.3 Partitioning Proteins in the $C_{10}E_4$-Buffer and the $C_{10}E_4$-SDS-Buffer Systems

In order to determine the strength of the electrostatic interactions between the proteins and the charged micelles, two net positively-charged proteins and two net negatively-charged proteins were partitioned in the $C_{10}E_4$-buffer and the $C_{10}E_4$-SDS-buffer systems at conditions where the excluded-volume interactions between the proteins and the micelles were maintained constant. As discussed in Section 7.3.2, according to Eq. (1.4), the excluded-

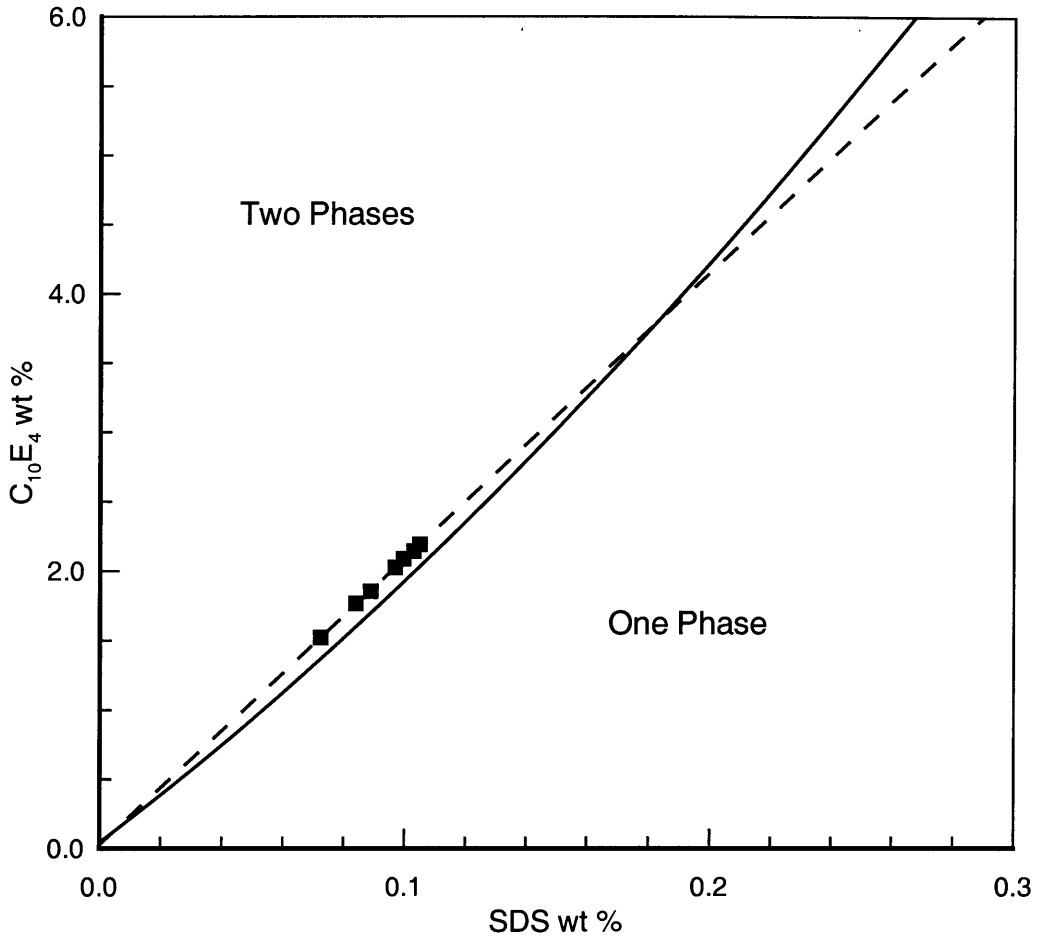

Figure 7-4: The coexistence curve of the $C_{10}E_4$-SDS-buffer system at 25.2°C with the located tie line. The solid line corresponds to the best-fit quadratic curve through the experimentally measured points shown in Figure 7-3. The dashed line corresponds to the tie line that was located by finding seven points (which are shown as black squares) along a line for which the experimentally measured volume ratios were approximately equal to the predicted volume ratios based on the lever rule.

volume interactions between the proteins and the micelles can be maintained constant by holding $(\phi_t - \phi_b)$ constant for fixed R_p and R_0 values. For a given protein, R_p is fixed and independent of the system in which it is partitioned. With regard to R_0, Program PREDICT (a computer program developed by our group to predict fundamental micellar properties for single surfactant systems)[54] predicted the cross-sectional radii of the cylindrical $C_{10}E_4$ micelles (without SDS) to be approximately 21 Å. For the cylindrical mixed ($C_{10}E_4$/SDS) micelles in the two phases connected by the tie line in Figure 7-4, Program MIX2[54,108,114] predicted the cross-sectional radii to also be approximately 21 Å. It is not surprising that the cross-sectional radii are similar because each of the phases connected by the tie line in Figure 7-4 contains about 20 times more $C_{10}E_4$ molecules than SDS molecules. In other words, the mixed ($C_{10}E_4$/SDS) micelles closely resemble the $C_{10}E_4$ micelles (without SDS) due to the overwhelming number of $C_{10}E_4$ molecules. Since R_p and R_0 are constant, the excluded-volume interactions between a particular protein and the micelles can also be maintained constant by finding the temperature in the $C_{10}E_4$-buffer system that yields a tie line with the same $(\phi_t - \phi_b)$ value as the one located in the $C_{10}E_4$-SDS-buffer system in Figure 7-4. This desired temperature in the $C_{10}E_4$-buffer system was found to be 19.3°C as shown in Figure 7-5.

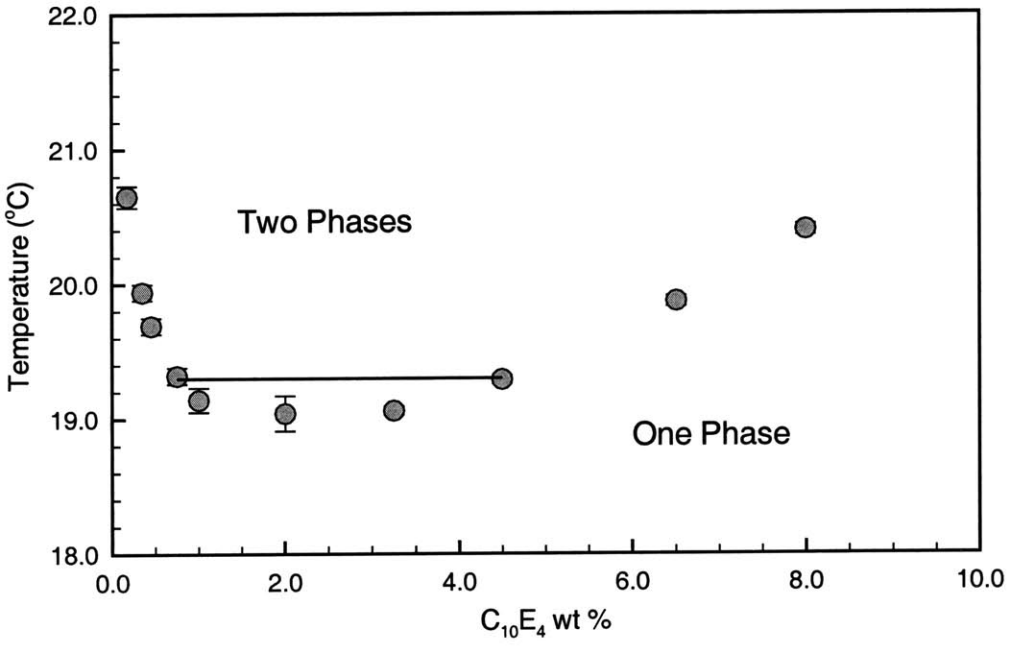

Figure 7-5: The coexistence curve of the $C_{10}E_4$-buffer system with the tie line at 19.3°C. Tie lines in this phase diagram can easily be located, since they correspond to the intersections of constant temperature horizontal lines with the coexistence curve.

At the pH of the buffer used in the experiments (pH=7.2), two net positively-charged proteins (lysozyme and cytochrome *c*) and two net negatively-charged proteins (ovalbumin and catalase) were partitioned along the tie lines shown in Figures 7-4 and 7-5. The results of all the partitioning experiments are shown in Figure 7-6. For each protein, the difference between the partition coefficients measured in the $C_{10}E_4$-buffer and the $C_{10}E_4$-SDS-buffer systems was statistically significant, indicating that electrostatic interactions do indeed have an effect. In particular, for the two net positively-charged proteins (lysozyme and cytochrome *c*), the proteins were electrostatically attracted or "fished" into the top, micelle-rich phase, which contained a greater number of negatively-charged mixed micelles. The two net negatively-charged proteins (ovalbumin and catalase), on the other hand, were electrostatically repelled or "hammered" from the top, micelle-rich phase into the bottom, micelle-poor phase, which contained fewer negatively-charged mixed micelles. The mass balances on all the proteins closed to 100% within the experimental error. Based on these experimental results, the $C_{10}E_4$-SDS-buffer system has shown the capability to modulate both excluded-volume and electrostatic interactions between the proteins and the charged micelles. In addition, it should be noted that the electrostatic interactions between the proteins and the charged micelles can be further increased by the addition of more SDS, since, in this study, the molar ratio of SDS to $C_{10}E_4$ was only about 1 to 20..

7.4.4 Theoretically Predicting Protein Partition Coefficients in the $C_{10}E_4$-SDS-Buffer System

In order to test our theory for predicting protein partition coefficients in two-phase aqueous mixed (nonionic/ionic) micellar systems, the experimental data from Section 7.4.3 were compared to the predictions obtained using Eqs. (1.3), (7.14), and (7.31). In order to implement the theory, the concentrations of SDS in both phases were required, and they were determined from the intersections of the tie line with the coexistence curve in Figure 7-4. With regard to the net charge or valence of each protein, that was estimated as described in Section 7.3.4. The theoretically predicted protein partition coefficients are compared to the experimental ones in Figure 7-7. As shown in Figure 7-7, there is reasonable agreement between the predicted and measured protein partition coefficients, which indicates that the simple theory developed here captures reasonably well the underlying physics. Therefore, it can also be concluded that the effect of the electrostatic potential difference between the two phases, which was neglected to obtain Eq. (7.8), is small for the proteins examined in this system.

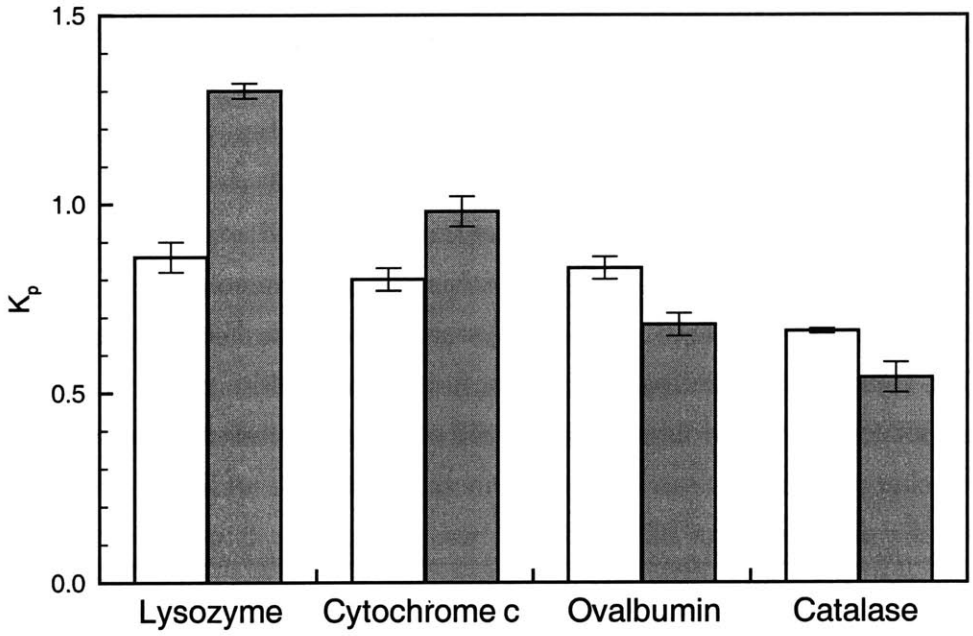

Figure 7-6: The experimentally measured protein partition coefficients in the $C_{10}E_4$-buffe and the $C_{10}E_4$-SDS-buffer systems. The white and gray bars correspond to the protein par tition coefficients measured in the $C_{10}E_4$-buffer system and the $C_{10}E_4$-SDS-buffer system respectively. The two net positively-charged proteins (lysozyme and cytochrome *c*) are at tracted into the top, micelle-rich phase, relative to the case without SDS, as evidenced b their K_p values being smaller than one as well as smaller than those attained without SDS The two net negatively-charged proteins (ovalbumin and catalase) are repelled from the top micelle-rich phase into the bottom, micelle-poor phase, relative to the case without SDS, a evidenced by their K_p values being greater than one as well as greater than those attaine without SDS. The error bars correspond to 95% confidence limits for the measurements.

With the exception of lysozyme, the theory overpredicts the strength of the electrostatic interactions between the proteins and the micelles. For the net positively-charged cytochrome *c*, the theory predicts that more of the cytochrome *c* will be "fished" into the top, micelle-rich phase than is experimentally observed. For ovalbumin and catalase, the theory predicts that more of each net negatively-charged protein will be "hammered" into the bottom, micelle-poor phase than is experimentally observed. The strength of the electrostatic interactions may have been overestimated due to a possible overestimation of the magnitude of the electrostatic potential of each micelle. The magnitude of the electrostatic potential obtained by using the Debye-Hückel approximation may be higher than the one obtained by solving the full Poisson-Boltzmann equation, which happens to be the case for charged flat plates.[124] However, it should be noted that an analytical solution to the Poisson-Boltzmann equation only exists for flat plates,[119] and that either numerical methods or an analytical approximation (such as the Debye-Hückel approximation) are required to implement the full Poisson-Boltzmann equation in the case of infinite cylinders. The strength of the electrostatic interactions may also have been overestimated by modeling each protein as a point ion with a charge equal to its net charge, since this may overestimate the charge which can actually approach the surface of the micelle, where the magnitude of the electrostatic potential of the micelle is the highest. Although modeling each protein as a sphere is possible, numerical methods are required to evaluate the interaction between an infinitely long cylinder and a sphere, and an analytical solution is not available.[121,122]

Although the above-mentioned suggestions may improve the theoretical predictions for cytochrome *c*, ovalbumin, and catalase, they will further increase the discrepancy between theory and experiment for lysozyme. In the case of lysozyme, the theory is already underpredicting the strength of the electrostatic interactions, since more of the net positively-charged lysozyme is actually being "fished" into the top, micelle-rich phase than is theoretically predicted. This underprediction could be explained if some of the amino acids of lysozyme had pKa values that differed significantly from the typical values that were used in the predictions. The observed discrepancy could indeed be accounted for if the actual net charge of lysozyme was only a few positive charges greater than the predicted net charge.

Although the theory (Eq. (7.31)) may be quantitatively improved by implementing some of the above-mentioned modifications, the current analytical expression already does a reasonable job of predicting protein partition coefficients in the $C_{10}E_4$-SDS-buffer system. In addition, since there is nothing in the theory that prevents it from being applied to other two-phase aqueous mixed (nonionic/ionic) micellar systems, future experiments should be

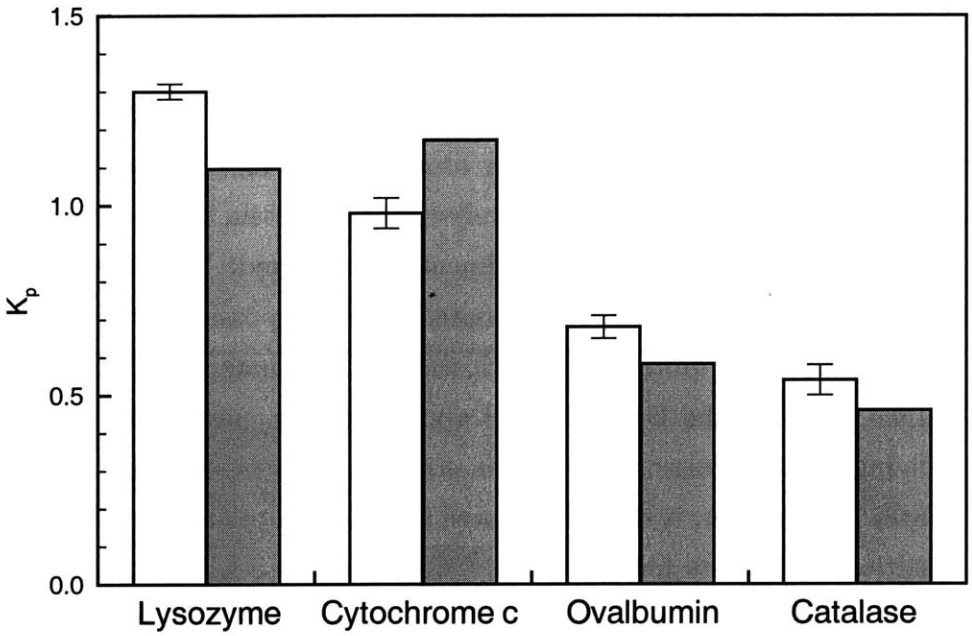

Figure 7-7: Comparison between the experimentally measured (shown by the white bars) and theoretically predicted (shown by the gray bars) protein partition coefficients in the $C_{10}E_4$-SDS-buffer system.

performed in other systems to test the robustness of the theory. The simplified theory, therefore, has the potential of being used to design operating conditions. Specifically, the advantage of having an analytical result is that it can be used to quickly identify the relative importance of certain variables in influencing the protein partition coefficient, as demonstrated in Chapter 8. Through the dependence of κ on ionic strength and z_p on pH, the theory can predict the effect of changing ionic strength and pH on the protein partition coefficient. The theory can also aid in determining the types of surfactant to use, since Eq. (7.31) is a function of R_0, l_{SDS}, σ_t, and σ_b. As discussed and shown in Section 7.3.3 and Appendix H, these quantities are all functions of the type of nonionic surfactant, type of ionic surfactant, the relative concentrations of these two surfactants used in the system, and the ionic strength of the solution. This is very useful, since our group is able to predict mixed micellar properties, such as R_0, l_{SDS}, σ_t, and σ_b, based solely on the molecular structures of the two surfactants, the concentrations of the two surfactants, and the ionic strength of the solution. The concentrations of the two surfactants also enter Eq. (7.31) through ϕ_t and ϕ_b. Accordingly, the ionic strength, pH, type and concentration of nonionic surfactant, and type and concentration of ionic surfactant have the potential of all being simultaneously optimized using Eq. (7.31) in concert with Program MIX2.[54,108,114]

7.5 Conclusions

Both experimental and theoretical studies were conducted in the fundamental investigation presented in this chapter. The experimental study demonstrated proof-of-principle that two-phase aqueous mixed (nonionic/ionic) micellar systems can indeed be used to modulate both electrostatic and excluded-volume interactions between the proteins and the charged micelles. After mapping out the required coexistence curves and justifying their applicability, two net positively-charged proteins (lysozyme and cytochrome *c*) and two net negatively-charged proteins (ovalbumin and catalase) were partitioned in the $C_{10}E_4$-buffer and $C_{10}E_4$-SDS-buffer systems at conditions where the excluded-volume interactions between the proteins and the micelles were maintained constant. Comparison of the partitioning results between the two systems indicated that the electrostatic interactions between the proteins and the charged mixed ($C_{10}E_4$/SDS) micelles did have an effect on protein partitioning.

A theory was also developed to predict protein partition coefficients in two-phase aqueous mixed (nonionic/ionic) micellar systems. The theory incorporated the dominant interactions, namely, the excluded-volume and electrostatic interactions, between the proteins and the charged mixed micelles. With regard to the excluded-volume interactions, they were previously modeled by others in our group,[71,74] and therefore, the main component of the theoretical study presented here was modeling the electrostatic interactions. Each charged micelle was modeled as an infinitely-long cylinder with an associated electrostatic potential obtained by using the Debye-Hückel approximation to the Poisson-Boltzmann equation. Each protein was modeled as a point ion with a charge equal to its net charge, which was predicted based on its amino acid sequence, typical pKa values,[123] and the Henderson-Hasselbalch equation. Program MIX2[54,108,114] was also used to obtain values of the various parameters (R_0, l_{SDS}, $y_{SDS,t}$, and $y_{SDS,b}$) associated with the charged mixed micelles. The theoretical predictions were compared with the experimental data, and the theory was shown to provide reasonable quantitative predictions of protein partition coefficients in the $C_{10}E_4$-SDS-buffer system.

Solving the full Poisson-Boltzmann equation and modeling the electrostatic interactions between a spherical protein and an infinitely-long charged micellar cylinder are expected to improve the quantitative agreement between the predicted and measured protein partition coefficients. Although the theory can be quantitatively improved by implementing the modifications suggested above, the current analytical expression for the protein partition coefficient already does a reasonable job of predicting protein partitioning in the $C_{10}E_4$-SDS-buffer system. In addition, the simplified theory has the potential of being used to quickly design operating conditions, as demonstrated in Chapter 8.

Chapter 8

Theoretical Analyses of Protein Partitioning in Two-Phase Aqueous Mixed Micellar Systems

8.1 Introduction

Using the theory developed in Chapter 7, one can develop design strategies to optimize the protein partition coefficient, K_p, without conducting any experiments. As shown in Chapter 7, this theory was derived from first principles, and has no fitted parameters. Since an analytical expression is available for K_p, the theory can be used to quickly ascertain the relative importance of various experimentally controllable variables that can affect the protein partition coefficient without the need for performing any measurements. In this chapter, three of the variables that can be tuned by the scientist or engineer will be investigated. These variables include: (i) the solution pH, (ii) the ionic strength of the solution, and (iii) the type of ionic surfactant. Possible coupled effects between these three variables can also be investigated using the theory developed in Chapter 7, and a response surface of the protein partition coefficient as a function of these variables can then be generated theoretically to identify the optimum operating conditions.

In this chapter, the theory presented in Chapter 7 to predict protein partition coefficients in two-phase aqueous mixed (nonionic/ionic) micellar systems will also be extended to include: (i) ionic surfactants having charges located beyond the hydrophilic head of the nonionic surfactant, and (ii) zwitterionic surfactants in place of the nonionic surfactant. Although zwitterionic surfactants have both positive and negative charges, they possess no net charge, that is, they can be regarded as being "noncharged", and some of them can also exhibit phase separation in aqueous solutions. In the discussions that follow, we will denote both nonionic and zwitterionic surfactants as "noncharged". Based on the theoretical ex-

pressions derived for K_p for cases (i) and (ii), a theoretical comparison will be made between different two-phase aqueous mixed ("noncharged"/ionic) micellar systems regarding their protein purification capabilities.

The remainder of this chapter is organized as follows. In Section 8.2, the analytical expression for K_p derived in Chapter 7 is used to examine the effects of various experimentally controllable variables on the protein partition coefficient. Section 8.3 describes the use of the theory to conduct a factorial design and to generate a response surface. In Section 8.4, the partitioning theory is extended to include ionic surfactants having charges located beyond the hydrophilic head of the nonionic surfactant. Section 8.4.1 provides the details associated with extending the partitioning theory to include zwitterionic surfactants in place of the nonionic surfactant. Finally, concluding remarks are presented in Section 8.5.

8.2 Analyzing the Relative Effects of Various Experimentally Controllable Variables on the Protein Partition Coefficient

An important benefit of the theory developed in Chapter 7 is the ability to provide useful guidelines to optimize the protein partition coefficient without performing a single experiment. As such, this theory, which does not require any experimentally measured protein partition coefficients as inputs, may be used by industrial researchers to save time-consuming trial-and-error experimentation and associated human and financial resources. Since an analytical expression is available for K_p, the effect of various independent experimentally controllable variables on the protein partition coefficient can be quickly ascertained. This section demonstrates this concept using the expression for the protein partition coefficient derived in Chapter 7, and repeated below for clarity:

$$K_p = K_p^{EV} K_p^{elec} \tag{7.14}$$

where the excluded-volume (EV) contribution to K_p is given by:

$$K_p^{EV} = \exp\left[-\left(\phi_t - \phi_b\right)\left(1 + \frac{R_p}{R_0}\right)^2\right] \tag{1.4}$$

and the electrostatic (elec) contribution to K_p is given by:

$$K_p^{elec} = \exp\left[\frac{-8\pi z_p e K_1(\kappa R_0)}{\kappa^2 \epsilon_w R_0 k_B T K_1(\kappa l_{SDS})}\left(\sigma_t \phi_t - \sigma_b \phi_b\right)\right] \tag{7.31}$$

In Eqs. (1.4) and (7.31), ϕ_t and ϕ_b are the surfactant volume fractions in the top and bottom phases, respectively, R_p is the hydrodynamic radius of the protein, R_0 is the cross-sectional radius of the cylindrical micelle, z_p is the valence of the protein, κ is the inverse Debye-Hückel screening length, ϵ_w is the dielectric constant of water, k_B is the Boltzmann constant, T is the absolute temperature, l_{SDS} is the length of a SDS molecule (a model anionic surfactant), K_1 is the modified Bessel function of the second kind of order 1, and σ_t and σ_b are the surface charge densities (charge/area) of the mixed micelles in the top and bottom phases, respectively. The length of a SDS molecule, l_{SDS}, is given by the following relation:

$$l_{SDS} = l_c + d_{ch} \tag{8.1}$$

where l_c is the length of the hydrocarbon tail, and d_{ch} is the distance from the end of the hydrocarbon tail to the negative charge on the sulfate group.

Lysozyme, which is one of the proteins examined in Chapter 7, was selected as the model protein in the theoretical analysis presented here because its separation from bacteriophage P22 was investigated experimentally in this thesis (see Chapters 6 and 9). In the theoretical analysis that follows, all the variables examined were maintained at their values from Chapter 7, except for the particular variable under investigation whose value was allowed to vary within a given range. This scenario may actually be encountered in practical separation cases when additional constraints on the process prevent the manipulation of all the variables except one. The values of the variables from Chapter 7 used to evaluate Eqs. (1.4), (7.14), and (7.31), as well as the corresponding values of K_p^{EV}, K_p^{elec}, and K_p for lysozyme, are summarized in Table 8-1. Based on the theory, three of the variables that can be manipulated include: (i) the solution pH, (ii) the ionic strength of the solution (IS), and (iii) the distance from the end of the hydrocarbon tail to the charge of the *anionic* surfactant (d_{ch}). Although the theoretical analysis presented here focused on anionic (negatively charged) surfactants, a similar analysis can also be carried out in the case of cationic (positively charged) surfactants.

The influence of the solution pH on the protein partition coefficient was first investigated. In this analysis, the solution pH is assumed to only affect the net charge or valence of the protein, z_p, in Eq. (7.31). The net charge of the protein varies with changes in the pH as described in Section 7.3.4. However, note that, in some cases, the solution pH may also have an effect on the coexistence curve of the two-phase aqueous mixed micellar system, that is, on the ϕ_t and ϕ_b values in Eqs. (1.4) and (7.31). The predicted effect of pH on K_p is shown in Figure 8-1. The pH range of 2 to 12 was selected in this analysis because it

Table 8-1: The values of the variables used to predict the partition coefficient of lysozyme in Chapter 7. The corresponding predicted values of K_p^{EV}, K_p^{elec}, and K_p from Chapter 7 have also been included for completeness. [a]See Eq. (8.2) for the relation between κ and IS. [b]See Section 7.3.4 for the relation between z_p and pH. [c]See Eq. (8.3) for the relation between σ_t or σ_b and the following variables: (i) the micelle composition (the molar ratio of SDS to total surfactant in every micelle) in the top and bottom phases, $y_{SDS,t}$ and $y_{SDS,b}$, (ii) the valence of SDS, z_{SDS}, and (iii) the volumes of the hydrocarbon tails of $C_{10}E_4$ and SDS, $v_{tail,C_{10}E_4}$ and $v_{tail,SDS}$.

Variable	Value
electronic charge (e)	4.8029×10^{-10} esu
ionic strength (IS)	0.04911 M
κ	7.305×10^6 1/cm [a]
pH	7.2
z_p	+7.65 [b]
ϵ_w	78
R_0	21 Å
R_p	19 Å
k_B	1.38066×10^{-16} erg/K
T	298.32 K
k_BT	4.1188×10^{-14} erg
l_c	11.83 Å
d_{ch}	3.7 Å
l_{SDS}	15.53 Å
ϕ_t	0.0377
ϕ_b	0.00087
σ_t	-4211 esu/cm^2 [c]
σ_b	-3660 esu/cm^2 [c]
$y_{SDS,t}$	0.053
$y_{SDS,b}$	0.046
z_{SDS}	-1
$v_{tail,C_{10}E_4}$	2.695×10^{-22} cm^3
$v_{tail,SDS}$	3.233×10^{-22} cm^3
K_p^{EV}	0.875
K_p^{elec}	1.24
K_p	1.09

encompasses the majority of the entire pH range. However, the pH range between 2 and 12 may not be accessible for some proteins that denature at high or low solution pH. As indicated in Figure 8-1, the protein partition coefficient decreases as the pH is increased. The predicted trend is physically intuitive because increasing the pH changes the net charge on lysozyme from a net positive value to a net negative value. At pH values lower than the pI of lysozyme (which has been predicted to be 9.0 based on the equations in Section 7.3.4), the net positively-charged lysozyme is attracted electrostatically into the top, micelle-rich phase that has the greater number of net negatively-charged mixed micelles. On the other hand, at pH values higher than the pI of lysozyme, the net negatively-charged lysozyme is repelled electrostatically into the bottom, micelle-poor phase from the top, micelle-rich phase. At the pH value equal to the theoretically predicted pI of 9.0, the protein partition coefficient is equal to the excluded-volume contribution to the protein partition coefficient, $K_p^{EV} = 0.87$, since the electrostatic contribution to the protein partition coefficient, K_p^{elec}, equals 1 at the pI. The slanted regions in the K_p vs. pH curve (3.5<pH<5.0 and 8.0<pH<12.0) correspond to the pH ranges where lysozyme's amino acids gain or lose charge. Specifically, these pH ranges correspond to the pKa's of the charged amino acids that primarily comprise lysozyme. Specifically, the pKa's of aspartic acid and glutamic acid are both 4.4, while the pKa's of cysteine, tyrosine, lysine, and arginine are 8.5, 10.0, 10.0, and 12.0, respectively.[123] On the other hand, the regions in the K_p vs. pH curve where the slope is almost zero (2.0<pH<3.5 and 5.0<pH<8.0) correspond to the pH ranges where the majority of lysozyme's amino acids do not change charge. Note that it was not within the scope of this thesis to verify experimentally this predicted variation of the partition coefficient of lysozyme with the solution pH. Accordingly, an experimental value for the partition coefficient of lysozyme was only available (from Chapter 7) at one solution pH value as shown in Figure 8-1.

The predicted variation of the protein partition coefficient with the ionic strength of the solution, IS, was examined next. This analysis inherently assumes that the ionic strength is independent of the solution pH, since only independent variables can be manipulated individually while the other variables are held constant. Consequently, the ionic strength must be controlled by adding salts that are different from the buffer salts used to maintain the solution pH. The concentrations of these salts must therefore be higher than the concentrations of the buffer salts. Note that, contrary to the theoretical analysis presented here, the buffer salts controlled the ionic strength in Chapter 7. In this analysis, the ionic strength is assumed to affect solely the inverse Debye-Hückel screening length, κ, in Eq. (7.31) as

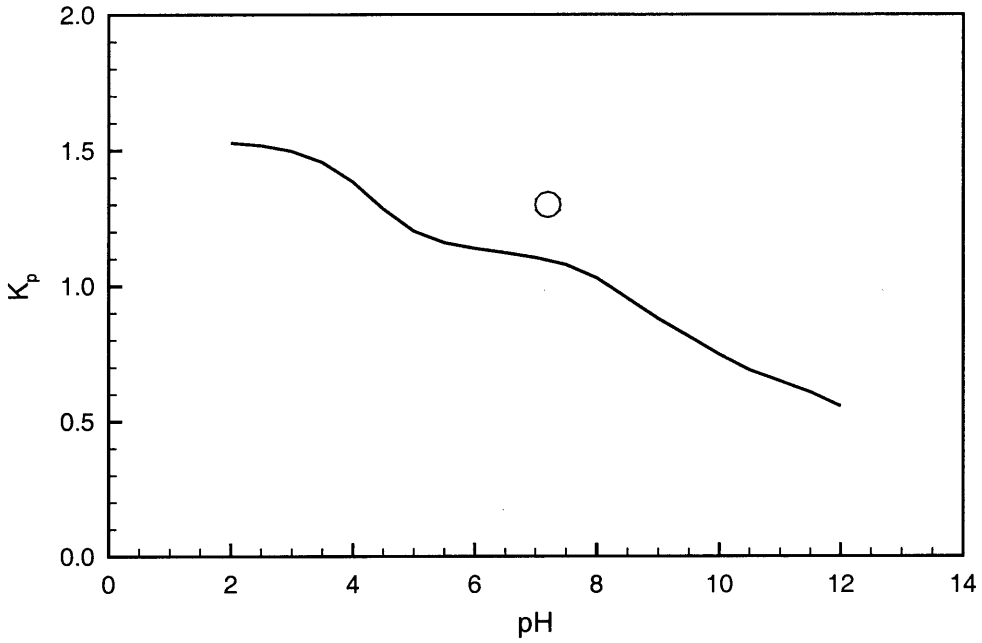

Figure 8-1: The predicted partition coefficient of lysozyme as a function of the solution pH. All other variables were kept constant at their values from Chapter 7. The white circle corresponds to the experimentally measured partition coefficient of lysozyme reported in Chapter 7.

follows:

$$\kappa = \left[\frac{(8\pi e^2)\,(IS)\,(N_{Avo})}{1000\epsilon_w k_B T} \right]^{1/2} \tag{8.2}$$

where e=4.8029×10^{-10} esu is the electronic charge, ϵ_w=78 is the dielectric constant of water, k_B=1.38066×10^{-16} erg/K is the Boltzmann constant, T=298.32K is the absolute temperature used in Chapter 7, N_{Avo}=6.022×10^{23} is Avogadro's number, IS is the ionic strength in molarity units, and κ has the units of 1/cm. Note, however, that the ionic strength of the solution may also have an effect on the coexistence curve of the two-phase aqueous mixed micellar system, that is, on the ϕ_t and ϕ_b values in Eqs. (1.4) and (7.31). The effect of the ionic strength on the predicted protein partition coefficient is shown in Figure 8-2. The lower limit on the ionic strength was chosen to be 0.01 M, since there is generally always some salt present in the solutions. For example, the buffer salts must be present to maintain the solution pH. The upper limit on the ionic strength was selected to be 0.25 M because the electrostatic attractions between the net negatively-charged mixed micelles and the net positively-charged lysozyme were expected to be completely screened by the salt ions at this concentration. Specifically, κ^{-1} (the Debye-Hückel screening length), which is the length scale that characterizes the range of the electrostatic interactions, is only 6.1 Å for an ionic

strength of 0.25 M. Indeed, as indicated by the plateau in Figure 8-2, these electrostatic attractions are already effectively screened at an ionic strength of about 0.10 M. At an ionic strength of 0.10 M, the protein partition coefficient is already approaching the excluded-volume contribution to the protein partition coefficient, $K_p^{EV} = 0.87$, since the electrostatic contribution to the protein partition coefficient, K_p^{elec}, is very close to 1. As in the case of varying the solution pH, an experimental value for the partition coefficient of lysozyme was only available (from Chapter 7) at one ionic strength value as shown in Figure 8-2.

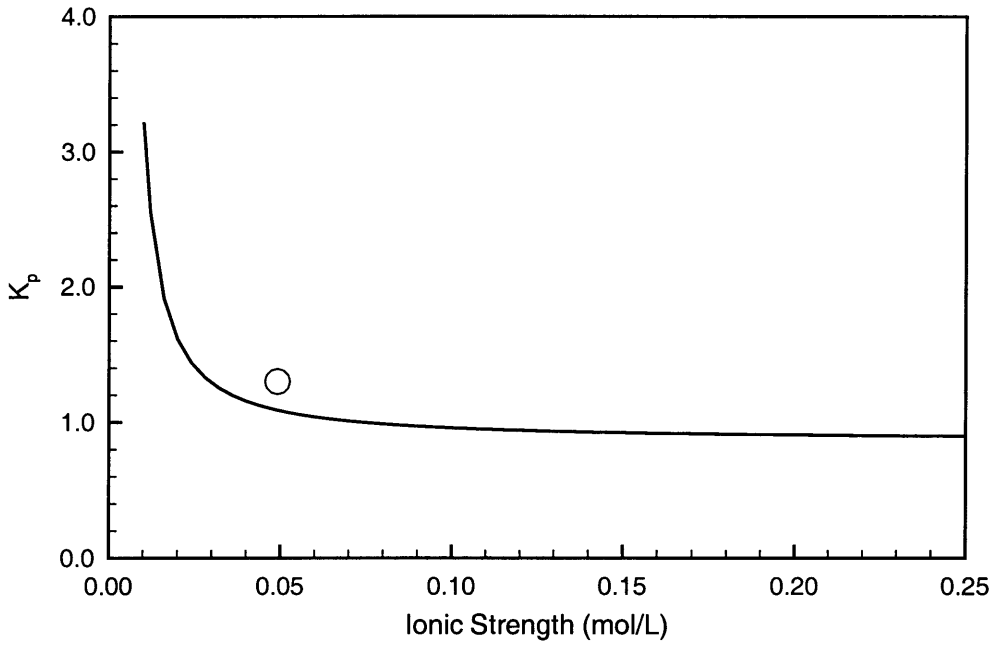

Figure 8-2: The predicted partition coefficient of lysozyme as a function of the ionic strength of the solution. All other variables were maintained constant at their values from Chapter 7. The white circle corresponds to the experimentally measured partition coefficient of lysozyme reported in Chapter 7.

The effect on the predicted protein partition coefficient of varying the distance from the end of a twelve carbon alkyl tail to the negative charge of the anionic surfactant was also investigated. In this example, the length of the hydrocarbon tail, l_c, was maintained constant, while the distance from the end of the hydrocarbon tail to the negative charge, d_{ch}, was increased. Varying d_{ch} gives rise to a change in l_{SDS} as indicated in Eq. (8.1). The minimum and maximum values of d_{ch} were 0 Å ($l_{SDS} = 12$ Å, the length of the hydrocarbon tail in a mixed micelle comprised of primarily $C_{10}E_4$) and 9 Å ($l_{SDS} = 21$ Å, the length of the nonionic $C_{10}E_4$ surfactant), respectively. Although the negative charge of the anionic surfactant can be located beyond the hydrophilic head of the nonionic surfactant, a new theoretical expression for K_p is required in this case (see Section 8.4). Varying d_{ch} changes

K_p via the l_{SDS}, σ_t, and σ_b terms in Eq. (7.31). The surface charge density of every micelle in each phase α, σ_α, is affected by changes in l_{SDS} because σ_α was shown to be a function of l_{SDS} in Appendix H. The key expression is repeated below for clarity:

$$\sigma_\alpha = \frac{y_{SDS,\alpha} z_{SDS}\ e\ l_{c,\alpha}^2}{2 l_{SDS,\alpha} \left[(1 - y_{SDS,\alpha})\, v_{tail,C_{10}E_4} + y_{SDS,\alpha} v_{tail,SDS}\right]} \tag{8.3}$$

where $y_{SDS,\alpha}$ is the micelle composition (molar ratio of anionic surfactant to total surfactant in each micelle) in phase α, z_{SDS} is the valence of SDS (-1), $l_{c,\alpha}$ is the length of the hydrocarbon tail of each surfactant in the mixed micelle (the radius of the cylindrical, hydrophobic core), $l_{SDS,\alpha}$ is the length of the anionic surfactant in phase α, $v_{tail,C_{10}E_4}$ is the volume of the hydrophobic tail of the $C_{10}E_4$ surfactant molecule, and $v_{tail,SDS}$ is the volume of the hydrophobic tail of the SDS surfactant molecule. Note that the subscript n denoting the micelle aggregation number was omitted because, as discussed in Chapter 7 and Appendix H, the values of σ_α, $l_{c,\alpha}$, $l_{SDS,\alpha}$, and $y_{SDS,\alpha}$ are constant for all the micelles in phase α, regardless of their aggregation number. The predicted variation of the protein partition coefficient with d_{ch} is shown in Figure 8-3. As in the case of varying the solution pH and the ionic strength, an experimental value for the partition coefficient of lysozyme was only available (from Chapter 7) at one d_{ch} value as shown in Figure 8-3.

Although the protein partition coefficient was predicted to increase with an increase in d_{ch} (see Figure 8-3), this finding is not so obvious because of the existence of two opposing effects. One effect acts to decrease the protein partition coefficient by weakening the electrostatic attractions between the net negatively-charged mixed micelles and the net positively-charged lysozyme. The electrostatic attractions are weakened because there is a decrease in the surface charge density (charge/area) of the mixed micelles. The surface charge density decreases because an increase in the length of the anionic surfactant increases the surface area of the cylindrical surface of charge. Specifically, the surface area of a cylinder, neglecting end effects, is directly proportional to the radius of the charged cylinder, which is given by the length of the anionic surfactant. Consequently, for a fixed charge, the surface charge density decreases with an increase in the length of the anionic surfactant (see Eq. (8.3)). A decrease in the surface charge density, in turn, is expected to decrease the strength of the electrostatic interactions because it reduces the magnitude of the electrostatic potential generated by the charged micelle. The relation between the surface charge density and the electrostatic potential has been described mathematically in Eq. (7.22) of Chapter 7, and is

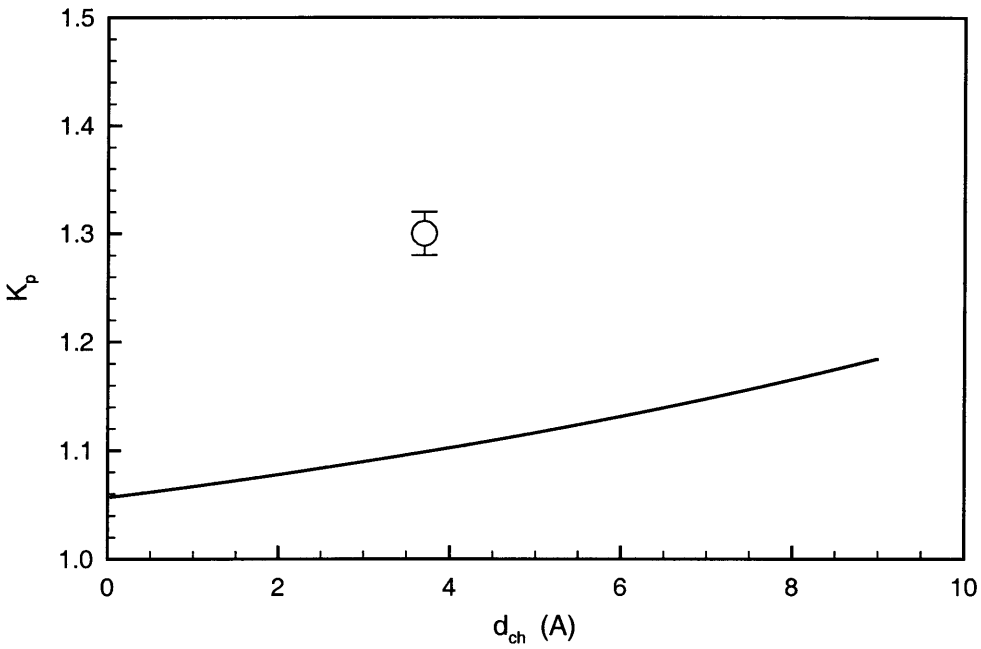

Figure 8-3: The predicted partition coefficient of lysozyme as a function of d_{ch}, the distance from the end of the hydrocarbon tail to the negative charge of the anionic surfactant. All other variables were maintained constant at their values from Chapter 7. The white circle corresponds to the experimentally measured partition coefficient of lysozyme reported in Chapter 7.

repeated below for clarity:

$$\psi_{cyl}(r) = \frac{4\pi\sigma K_0(\kappa r)}{\kappa\epsilon_w K_1(\kappa R_{cyl})} \tag{7.22}$$

where $\psi_{cyl}(r)$ is the electrostatic potential at a radial distance, r (in the cgs system of units), σ is the surface charge density of the cylinder, and R_{cyl} is the radius of the cylinder. Note that the effect of decreasing the surface charge density is also captured in Eq. (7.31), since decreasing σ_t will decrease the protein partition coefficient. Although σ_b in Eq. (7.31) will also be reduced, the $\sigma_b\phi_b$ term is usually negligible since ϕ_b has been found experimentally to be close to zero in typical micelle-poor phases.

On the other hand, there is an opposing effect that acts to increase the protein partition coefficient by increasing the electrostatic attractions between the net negatively-charged mixed micelles and the net positively-charged lysozyme. The electrostatic attractions are increased by bringing the negative charge of the anionic surfactant closer to lysozyme as shown in Figure 8-4. Since the electrostatic potential associated with the charged mixed micelle decays with the radial distance, r (see Eq. (7.22)), increasing the length of the anionic surfactant increases the magnitude of the electrostatic potential that is felt by the protein. This effect is also captured mathematically in Eq. (7.31), since increasing l_{SDS} increases the argument of the exponential in Eq. (7.31) by decreasing $K_1(\kappa l_{SDS})$. Our theory, which captures both competing effects, predicts that increasing the length of the anionic surfactant results in an overall increase in the strength of the electrostatic attractions between the mixed micelles and lysozyme (see Figure 8-3). Consequently, bringing the negative charge of the anionic surfactant closer to the protein is predicted to have a bigger electrostatic effect than decreasing the surface charge density.

Although the protein partition coefficient is also influenced by the surfactant volume fraction in each phase (ϕ_t and ϕ_b) and the micelle composition (the molar ratio of anionic surfactant to total surfactant in each mixed micelle) in each phase ($y_{SDS,t}$ and $y_{SDS,b}$), these variables are not independent of each other. Only one of these variables is independent for a given temperature, since fixing one of the variables automatically fixes the other three by the operating tie line. It should be noted that we have assumed that the micelle composition is approximately equal to the solution composition (the molar ratio of total anionic surfactant to total surfactant in a particular phase), which is a good approximation for the conditions encountered in most partitioning experiments.[108,114] Before predicting the effect of one of these variables on the protein partition coefficient, the relationships between all four variables must be determined by experimentally identifying many operating tie lines. Due to the significant time investment associated with identifying operating tie lines in multi-component

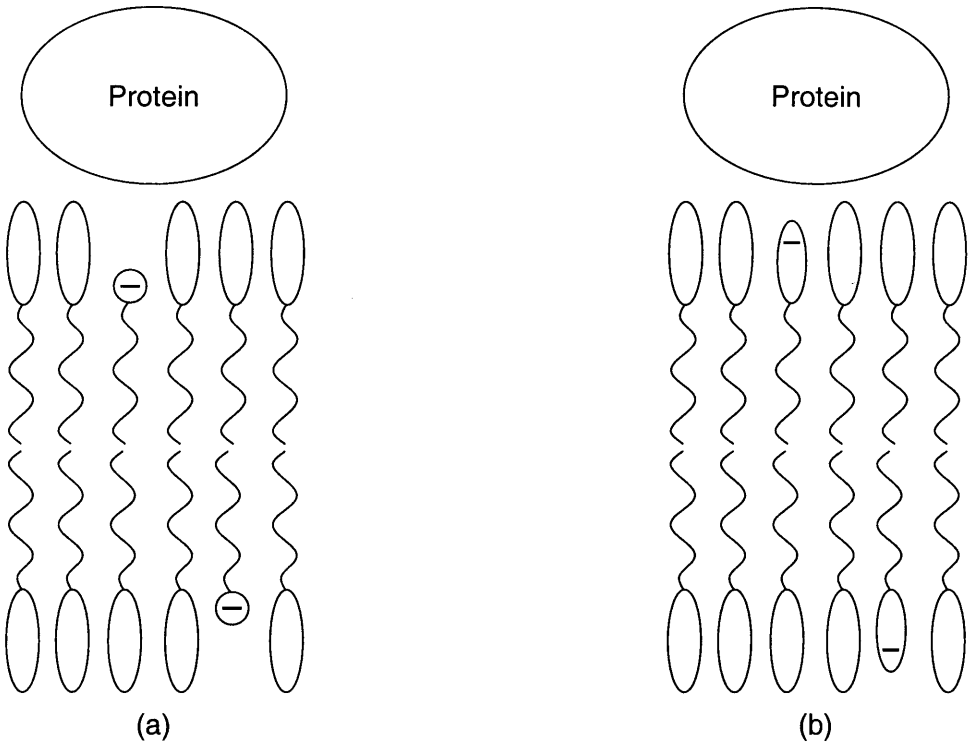

Figure 8-4: Schematic representation of a portion of a cylindrical mixed micelle where a nonionic surfactant is mixed with an anionic surfactant that has: (a) a smaller d_{ch}, and (b) a larger d_{ch}. The length of the hydrocarbon tail was maintained constant. Recall that the nonionic surfactant comprises the majority of each mixed micelle.

phase diagrams, this analysis was not within the scope of this thesis.

8.3 Conducting a Theoretical 2^3 Factorial Design and Generating a Response Surface

In some cases, the scientist or engineer is not restricted to varying only a single variable at a time, and many variables may instead be manipulated simultaneously for the purpose of optimizing the protein partition coefficient. In that case, it is desirable to identify any interactions, or coupled effects, among the various variables, since strongly interacting variables cannot be considered independently when designing operating conditions. In the case of protein partitioning, the variables are said to interact when their individual average, or main, effects on the protein partition coefficient are not simply additive. After identifying the variables that interact strongly with each other, a more thorough investigation of their combined effect on K_p can be conducted.[125] For example, if two variables are found to have a very strong coupled effect, a response surface may be generated for the protein partition

coefficient as a function of these two variables. This response surface can then be used to identify the optimum operating conditions.

In order to determine any interactions among the previously discussed variables of pH, ionic strength (IS), and distance from the end of the hydrocarbon tail to the negative charge of the anionic surfactant (d_{ch}), a theoretical 2^3 factorial design was conducted using the analytical results for the protein partition coefficient given in Eqs. (1.4), (7.14), and (7.31). Since the theory was used to conduct the 2^3 factorial design, not even a single experiment was performed. A 2^3 factorial design corresponds to a total of $2^3 = 8$ experiments (or predictions in our case), where all 8 possible combinations of 3 variables having 2 possible conditions or levels (high or low) are investigated. The high and low conditions for the three variables are listed in Table 8-2.

Table 8-2: Low (-) and high (+) conditions for the three variables examined in the 2^3 factorial design of the protein partition coefficient, K_p. The three variables are: the solution pH (pH), the ionic strength of the solution (IS), and the distance from the end of the hydrocarbon tail to the negative charge of the anionic surfactant (d_{ch}).

Variable	Low (-) Condition	High (+) Condition
pH	2	12
IS	0.01 mol/L	0.25 mol/L
d_{ch}	0 Å	9 Å

The results of the theoretical 2^3 factorial design are shown in Table 8-3. Yates's algorithm was used to analyze the results to estimate any coupled effects among the variables. Individual average, or main, effects of the variables were also estimated with the algorithm.[125] Each individual main effect corresponds to the average change in the protein partition coefficient as a particular variable is increased from its low to high condition for fixed values of the other variables. An example calculation is shown in Table 8-4 for estimating the main effect of pH on the protein partition coefficient. As shown in Table 8-4, the change in the protein partition coefficient as the pH was increased from 2 to 12 was evaluated for fixed values of IS and d_{ch}. Since there are four possible combinations of IS and l_{an}, this change in the protein partition coefficient was evaluated for the four different cases and averaged. When the pH was increased from 2 to 12, the average change in the protein partition coefficient was estimated to be -12.41 (see Table 8-4).

With regard to estimating the interactions between two variables, or the two-factor interactions, an example calculation is shown in Table 8-5. In this example, the two-factor

Table 8-3: Theoretically predicted protein partition coefficients for lysozyme under the conditions that were specified in a 2^3 factorial design. The low (-) and high (+) values for each of the three variables examined (pH, IS, and d_{ch}) are shown in Table 8-2.

pH	***IS***	d_{ch}	K_p
-	-	-	17.98
+	-	-	0.07
-	+	-	0.91
+	+	-	0.85
-	-	+	31.47
+	-	+	0.05
-	+	+	1.01
+	+	+	0.78

Table 8-4: Example calculation of the main effect of pH on K_p. The main effect was evaluated from the average change in K_p when pH was changed from its low (-) condition of 2 to its high (+) condition of 12 for the four possible combinations of IS and d_{ch}. The K_p values used in the calculation were obtained from Table 8-3.

IS	d_{ch}	K_p **(high pH) -** K_p **(low pH)**
-	-	0.07 - 17.98 = -17.91
+	-	0.85 - 0.91 = -0.06
-	+	0.05 - 31.47 = -31.42
+	+	0.78 - 1.01 = -0.23
	Average	-12.41

interaction, or coupled effect, between pH and ionic strength was evaluated. First, the average effect of pH on the protein partition coefficient was estimated for the low condition of IS. Specifically, while holding IS at the value of 0.01 M, the change in the protein partition coefficient as the pH was increased from 2 to 12 was evaluated for each value of d_{ch}, and then averaged. Subsequently, the average effect of pH on the protein partition coefficient was similarly estimated for the high condition of IS. The difference between these two average effects were then taken and divided by two, where the factor of two arises from convention. The estimated coupled effect of pH and IS on the protein partition coefficient was evaluated to be 12.26 (see Table 8-5). It should be noted, that if two variables were not interacting, the average effect of the first variable on the protein partition coefficient would be the same regardless of the value of the second variable. Accordingly, a value of zero would be estimated for such a coupled effect. The estimation of interactions between three variables, or three-factor interactions, was calculated following an approach similar to the one used for the two-factor interactions.

Table 8-5: Example calculation of the effect on K_p of the two-factor interaction between pH and IS. The effect of the two-factor interaction was obtained from one-half of the difference between: (i) the average change in K_p predicted when pH was increased from its low condition to its high condition at low IS, and (ii) the average change in K_p predicted when pH was increased from its low condition to its high condition at high IS, for each value of d_{ch}. The K_p values used in the calculation were obtained from Table 8-3.

Average Effect of pH on K_p at Low IS	
d_{ch}	**K_p (high pH) - K_p (low pH)**
-	0.07 - 17.98 = -17.91
+	0.05 - 31.47 = -31.42
Average	-24.67

Average Effect of pH on K_p at High IS	
d_{ch}	**K_p (high pH) - K_p (low pH)**
-	0.85 - 0.91 = -0.06
+	0.78 - 1.01 = -0.23
Average	-0.15

Estimated Coupled Effect	$\frac{1}{2} \times [-0.15 - (-24.67)] = 12.26$

Table 8-6 summarizes the main and interactive effects of pH, IS, and d_{ch} on the protein partition coefficient. Since the theory was used in this statistical factorial design, the standard error for the estimates of the main and interactive effects was approximated based on the experimental protein partitioning data presented in Chapter 7. The standard error was estimated to be 0.14, and a main or interactive effect is considered to be significant only if its absolute value is larger than the standard error. If the magnitude of the main or interactive effect is less than the standard error, the effect is considered negligible and within the experimental error. As indicated in Table 8-6, all the main and interactive effects were significant in this 2^3 factorial design. However, the main effects of pH and IS, as well as their coupled effect, were the largest. Due to the strong interaction between pH and IS, they must be considered simultaneously, since their individual main effects are not additive. Specifically, the change in the protein partition coefficient when the pH is changed will depend on the value of the ionic strength. This highly coupled effect between pH and IS can be visualized graphically as shown in Figures 8-5 and 8-6.

Table 8-6: Estimates of the individual main effects and the interactive effects between the three variables, pH, IS, and d_{ch}, for the 2^3 factorial design on the protein partition coefficient, K_p. The standard error for the estimates of the main and interactive effects was 0.14.

Variable(s)	**Estimate of Effect on K_p**
Main Effects	
pH	-12.41
IS	-11.51
d_{ch}	3.37
Two-Factor Interactions	
pH $\times$ IS	12.26
pH $\times$ d_{ch}	-3.42
IS $\times$ d_{ch}	-3.36
Three-Factor Interactions	
pH $\times$ IS $\times$ d_{ch}	3.34

In Figure 8-5, d_{ch} is maintained at its low condition. With this value for d_{ch}, the predicted protein partition coefficients at the four different possible combinations of pH and IS were plotted. As indicated in Figure 8-5, the change in the protein partition coefficient as IS is increased from the low to the high condition depends on the pH condition. Specifically, a

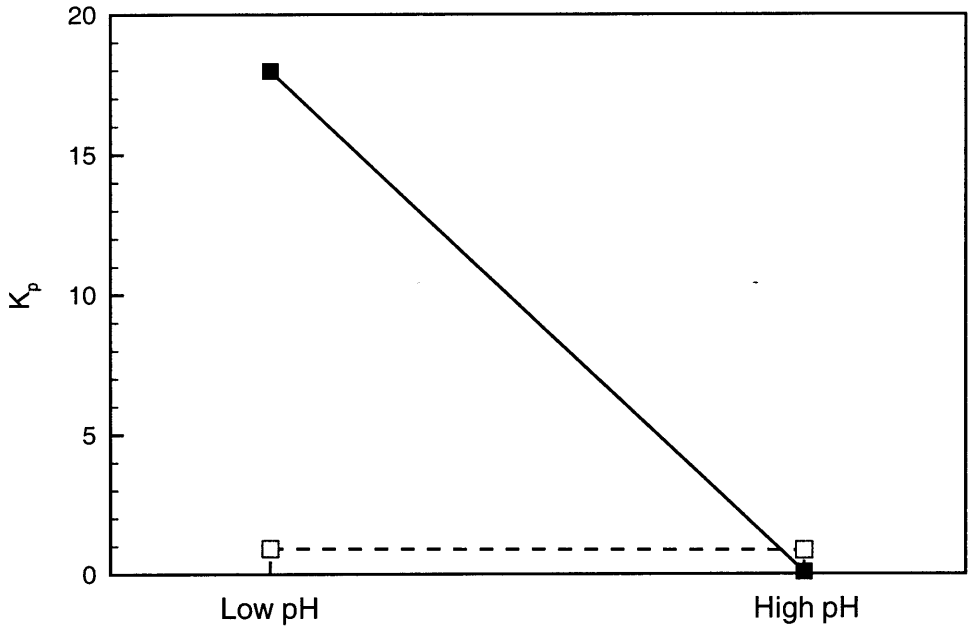

Figure 8-5: The effect on K_p of the two-factor interaction between pH and IS at the low d_{ch} condition. The black and white squares correspond to the protein partition coefficients that were predicted for the four different combinations of pH, IS, and d_{ch}. The black and white squares represent the low and the high IS conditions, respectively.

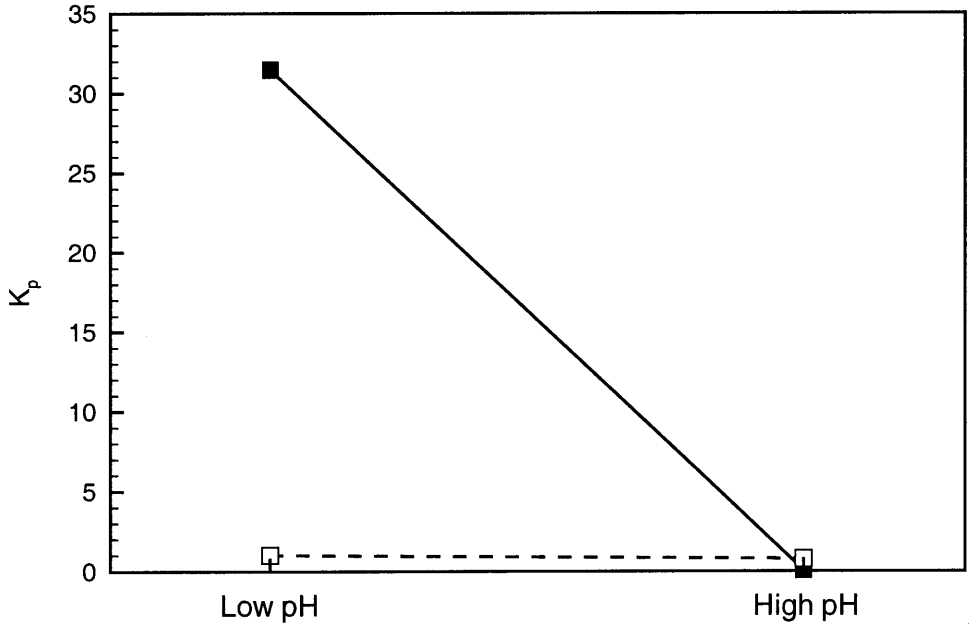

Figure 8-6: The effect on K_p of the two-factor interaction between pH and IS at the high d_{ch} condition. The black and white squares correspond to the protein partition coefficients that were predicted for the four different combinations of pH, IS, and d_{ch}. The black and white squares represent the low and the high IS conditions, respectively.

large *decrease* is predicted in the protein partition coefficient at the low pH condition, while a very small *increase* is predicted at the high pH condition. The predicted reversal can be understood by recalling that an increase in IS decreases the electrostatic interactions between the mixed micelles and lysozyme. Accordingly, at low pH, where lysozyme is net positively-charged, increasing IS prevents lysozyme from being electrostatically attracted into the top, micelle-rich phase, and lysozyme partitions based on excluded-volume interactions alone. On the other hand, at high pH, where lysozyme is net negatively-charged, increasing IS prevents lysozyme from being electrostatically repelled into the bottom, micelle-poor phase. Consequently, the protein partition coefficient slightly increases as IS increases at high pH. Similar trends were predicted at the high d_{ch} condition as shown in Figure 8-6. As indicated in Table 8-6, the three-factor interaction between pH, IS, and d_{ch} was also significant when compared to the standard error. This three-factor interaction can also be visualized by comparing the change in the protein partition coefficient at the low pH condition between Figures 8-5 and 8-6. Specifically, the *increase* in the protein partition coefficient as IS is *decreased* is much larger for the high d_{ch} condition (31.47 - 1.01 = 30.46) than the low d_{ch} condition (17.98 - 0.91 = 17.07). This is a result of the electrostatic interactions being greater when d_{ch} is larger as discussed earlier.

Based on the 2^3 factorial design, the solution pH and the ionic strength are two very important variables to consider when optimizing the protein partition coefficient. A theoretical response surface was therefore generated for the predicted lysozyme partition coefficient as a function of these two variables as shown in Figure 8-7. The value of d_{ch}, on the other hand, was maintained constant at 3.7 Å. As indicated in Figure 8-7, the optimum condition (highest K_p) corresponds to using the lowest possible solution pH and ionic strength. This is physically intuitive, because decreasing the pH will increase the net positive charge of lysozyme, while decreasing the ionic strength will decrease the number of ions that can screen the electrostatic attractions between the net positively-charged lysozyme and the net negatively-charged mixed micelles. Also, note that the response surface captures the trend of *decreasing* K_p, or *increasing* electrostatic repulsions between the net *negatively-charged* lysozyme and the net negatively-charged mixed micelles, as the ionic strength is decreased at high pH values. In addition, at the pH equal to the theoretical pI of 9.0, where lysozyme has no net charge, K_p is a constant at $K_p^{EV} = 0.875$ for all the ionic strength values.

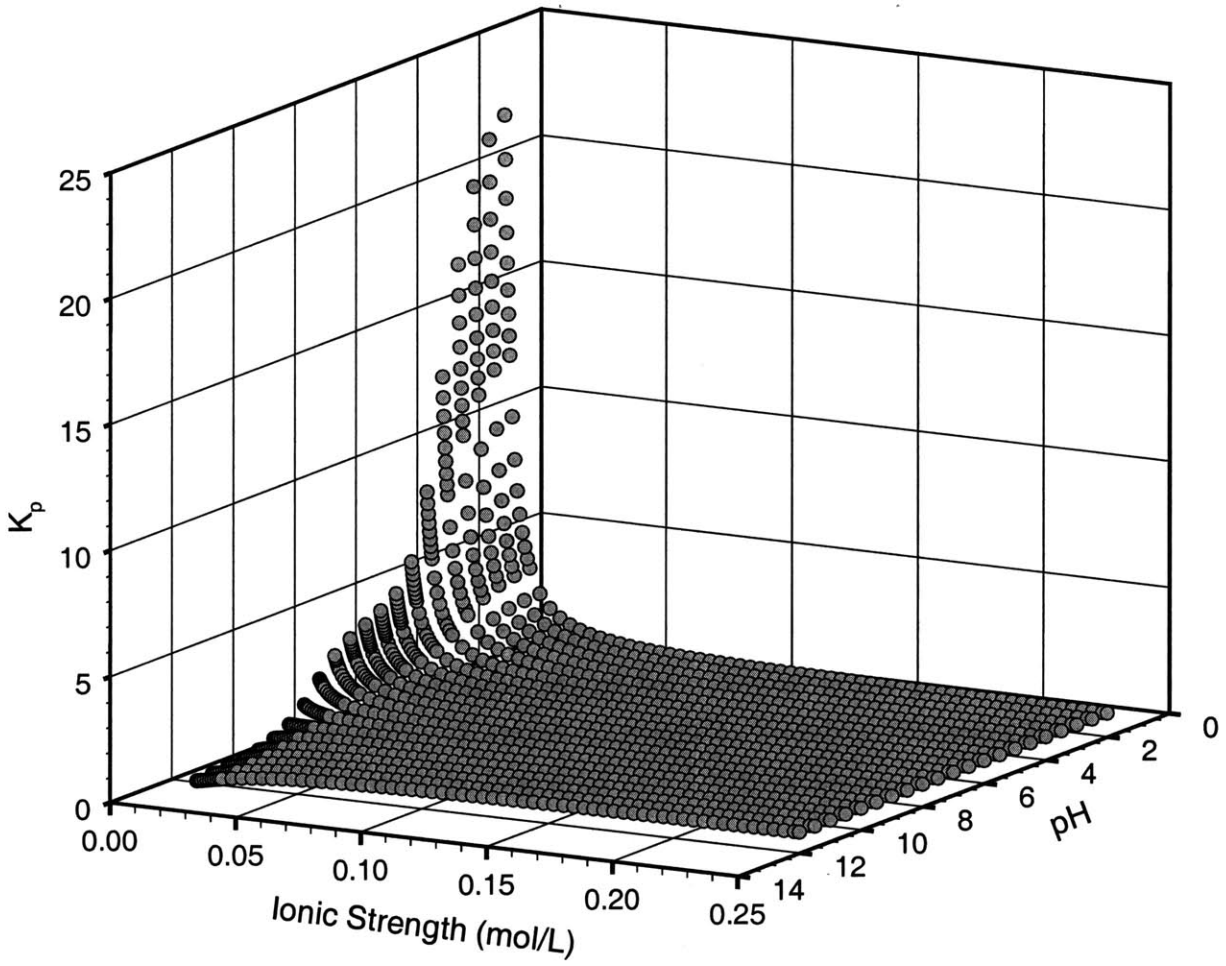

Figure 8-7: The theoretical response surface for the predicted partition coefficient of lysozyme as a function of the solution pH and ionic strength. The gray circles correspond to the partition coefficients that were predicted using the theory developed in Chapter 7.

8.4 Examining the Effect of Using an Anionic Surfactant Having its Negative Charge Located Beyond the Hydrophilic Head of the Nonionic Surfactant

In Section 8.2, increasing d_{ch} was predicted to increase the protein partition coefficient. Accordingly, in this section, the effect of using an anionic surfactant having its negative charge positioned beyond the hydrophilic head of the nonionic surfactant was examined theoretically. The analogous situation is sometimes observed in ion-exchange chromatography when the spacer arm is extended to place the charge further out into the solution. This allows the protein and the charge on the column to come in closer contact with less steric hindrance. A similar scenario can be achieved in two-phase aqueous mixed micellar systems by increasing d_{ch} to larger values. Increasing the length of the hydrocarbon tail, on the other hand, will not place the charge further out into the solution because the tail will remain as part of the hydrophobic core of the micelle. An interesting example of an anionic surfactant that has a fairly large d_{ch} value is sodium dodecyl hexa(ethylene oxide) sulfate (SDE_6S). As shown in Figure 8-8, the difference between the hydrophilic head of SDE_6S and that of SDS results from the presence of six ethylene oxide units between the hydrophobic tail (which is the same for both surfactants) and the sulfate group.

SDE_6S: CH_3–$(CH_2)_{11}$–$(OCH_2CH_2)_6$–OSO_3^- Na^+

SDS: CH_3–$(CH_2)_{11}$–OSO_3^- Na^+

Figure 8-8: The chemical formulas of sodium dodecyl hexa(ethylene oxide) sulfate (SDE_6S) and sodium dodecyl sulfate (SDS).

To analyze the use of an anionic surfactant such as SDE_6S, a new theoretical expression must be derived for the electrostatic contribution to the protein partition coefficient. Specifically, the lower limit of integration in Eq. (7.21) of Chapter 7 would change from R_0 (the length of a $C_{10}E_4$ molecule in each micelle) to l_{SDE_6S} (the length of a SDE_6S molecule in each micelle) because l_{SDE_6S} is greater than R_0. This change is shown below:

$$U_\alpha^{ex,elec} = \sum_{n_\alpha = n^\circ_{cyl,\alpha}}^{\infty} \int_{l_{SDE_6S}}^{\infty} [N_{n_\alpha}] \left[u_{np,\alpha}(r)\right] [C_{p,\alpha} 2\pi r L_{n_\alpha} dr] \tag{8.4}$$

where $U_\alpha^{ex,elec}$ is the electrostatic contribution to the excess internal energy, N_{n_α} is the number of micelles of aggregation number n in phase α, r is the radial distance from the

cylindrical micelle axis of symmetry, $u_{np,\alpha}(r)$ is the interaction potential between a micelle of aggregation number n and a protein in phase α, $C_{p,\alpha}$ is the number density (molecules/mL) of protein in phase α, L_{n_α} is the length of a micelle of aggregation number n in phase α, and $n^{\circ}_{cyl,\alpha}$ is the aggregation number of the smallest cylindrical micelle in phase α. Changing this lower limit of integration increases the strength of the electrostatic interactions because the protein can now approach the sulfate charge in the solution, where the magnitude of the electrostatic potential of the mixed ($C_{10}E_4$/SDE_6S) micelle is the highest. On the other hand, in the $C_{10}E_4$-SDS-buffer system, the sulfate charge is buried between the ethylene oxide units of the $C_{10}E_4$ molecules, since l_{SDS} (the length of a SDS molecule in each micelle) is smaller than R_0. Therefore, a radial distance of $(R_0 - l_{SDS})$ is inaccessible to the protein, and this reduces the electrostatic interactions, since this corresponds to the region where the magnitude of the electrostatic potential of the mixed ($C_{10}E_4$/SDS) micelle is the highest. Using Eq. (8.4) and following the derivation in Chapter 7, the electrostatic contribution to the protein partition coefficient in the $C_{10}E_4$-SDE_6S-buffer system can be shown to be given by the following expression:

$$K^{elec}_{p,SDE_6S} = \exp\left[\frac{-8\pi z_p\ e\ l_{SDE_6S}}{\kappa^2 \epsilon_w R_0^2 k_B T}\left(\sigma_t \phi_t - \sigma_b \phi_b\right)\right] \tag{8.5}$$

In contrast to Eq. (7.31), the modified Bessel functions of the second kind of order 1, K_1, cancel in Eq. (8.5) because the lower limit of integration in Eq. (8.4) is the same as the radius of the surface of charge, l_{SDE_6S}.

In addition to bringing the protein and the sulfate charge closer together, there is also a competing effect associated with increasing the length of the anionic surfactant as discussed in Section 8.2. For a fixed charge, the surface charge density decreases with a change in the anionic surfactant from SDS to SDE_6S, since there is an inverse dependence of the surface charge density on the length of the anionic surfactant. For the $C_{10}E_4$-SDE_6S-buffer system, the derivation of the surface charge density of every micelle in phase α, $\sigma_{SDE_6S,\alpha}$, is the same as the one presented in Appendix H with the exception of replacing "SDS" with "SDE_6S" in the subscripts. Therefore, $\sigma_{SDE_6S,\alpha}$ is given by:

$$\sigma_{SDE_6S,\alpha} = \frac{y_{SDE_6S,\alpha} z_{SDE_6S}\ e\ l^2_{c,\alpha}}{2 l_{SDE_6S,\alpha}\left[\left(1 - y_{SDE_6S,\alpha}\right) v_{tail,C_{10}E_4} + y_{SDE_6S,\alpha} v_{tail,SDE_6S}\right]} \tag{8.6}$$

where z_{SDE_6S} is the valence of a SDE_6S molecule, $l_{c,\alpha}$ is the radius of the hydrophobic core of each cylindrical micelle in phase α, $l_{SDE_6S,\alpha}$ is the length of a SDE_6S molecule in each micelle

in phase α, $v_{tail,C_{10}E_4}$ is the volume of the hydrophobic tail of $C_{10}E_4$ in any micelle, v_{tail,SDE_6S} is the volume of the hydrophobic tail of SDE_6S in any micelle, and $y_{SDE_6S,\alpha}$ is the micelle composition (molar ratio of SDE_6S to the total surfactant in every micelle). Combining Eqs. (8.5) and (8.6) removes the dependence of K^{elec}_{p,SDE_6S} on l_{SDE_6S} as shown below:

$$K^{elec}_{p,SDE_6S} = \exp\left[\frac{-8\pi z_p\, e}{\kappa^2 \epsilon_w R_0^2 k_B T}\left(\sigma^*_{SDE_6S,t}\phi_t - \sigma^*_{SDE_6S,b}\phi_b\right)\right] \tag{8.7}$$

where

$$\sigma^*_{SDE_6S,\alpha} = \frac{y_{SDE_6S,\alpha} z_{SDE_6S}\, e\, l^2_{c,\alpha}}{2\left[\left(1 - y_{SDE_6S,\alpha}\right) v_{tail,C_{10}E_4} + y_{SDE_6S,\alpha} v_{tail,SDE_6S}\right]} \tag{8.8}$$

The theory therefore predicts that the electrostatic attractions between the mixed micelles and lysozyme should remain constant as the negative charge of the anionic surfactant is positioned beyond the hydrophilic head of the nonionic surfactant. This prediction, which can be tested experimentally in the future, results from not allowing the protein and the buffer salt ions to access the region corresponding to the radial distance, (l_{SDE_6S} - R_0), in the theory. In fact, Eqs. (8.7) and (8.8) correspond to the maximum protein partition coefficient predicted by Eqs. (7.31) and (H.4) in Section 8.2. Specifically, when the length of the anionic surfactant, l_{SDS}, is set equal to the length of the nonionic surfactant, R_0, in Eqs. (7.31) and Eq. (H.4), Eqs. (8.7) and (8.8) are obtained with $y_{SDS,\alpha}$, z_{SDS}, and $v_{tail,SDS}$ in place of $y_{SDE_6S,\alpha}$, z_{SDE_6S}, and v_{tail,SDE_6S}. (Note that z_{SDS}=z_{SDE_6S} and $v_{tail,SDS}$= v_{tail,SDE_6S} because both surfactants have a valence of -1 and the same hydrocarbon tail, respectively.) Consequently, from a design perspective, the anionic surfactant should be at least equal in length to the nonionic surfactant.

In addition, since $l_{SDE_6S} > R_0 > l_{SDS}$, the theory predicts that a stronger electrostatic effect will be observed with SDE_6S than with SDS for the same micelle composition in each phase ($y_{SDE_6S,\alpha} = y_{SDS,\alpha}$). To test this prediction, proteins must be partitioned in the two systems at conditions where the total molar concentrations of $C_{10}E_4$ and the anionic surfactant in the top and bottom phases of one system are equal to those in the top and bottom phases of the other system, respectively. This will guarantee that the surfactant volume fractions (ϕ_t and ϕ_b) are the same between the two systems. This will also ensure that the micelle compositions in the top and bottom phases of one system are approximately equal to those in the top and bottom phases of the other system, respectively, since the micelle composition in each phase is approximately equal to the solution composition in each phase. However, identifying the conditions to perform these protein partitioning experiments requires a significant amount of time. In particular, the coexistence curves of both systems

must first be mapped out at several temperatures, and many operating tie lines must be located on each coexistence curve. Two tie lines, one for each system, must then be identified, where the concentrations of $C_{10}E_4$ and the anionic surfactant in the top and bottom phases of one system are the same as those in the other system. Finally, after identifying these two operating tie lines, proteins can be partitioned. Due to the large investment in time, the initial weight percent (wt%) concentrations of $C_{10}E_4$ and the anionic surfactant were instead maintained constant in the experimental study conducted in Chapter 9. The rationale behind this decision was a practical one, since the mass of material required in a unit operation is one of the variables that are considered in industry prior to selecting a system. However, the experiments described above may be conducted in the future to unequivocally demonstrate which anionic surfactant is more effective in generating electrostatic interactions in two-phase aqueous mixed ($C_{10}E_4$/anionic) micellar systems.

8.4.1 Investigating Two-Phase Aqueous Zwitterionic Micellar Systems

Aqueous solutions of some zwitterionic surfactants can also phase separate upon changing the temperature. An interesting example is dioctanoyl phosphatidylcholine, or C_8-lecithin, which has the chemical formula shown in Figure 8-9.

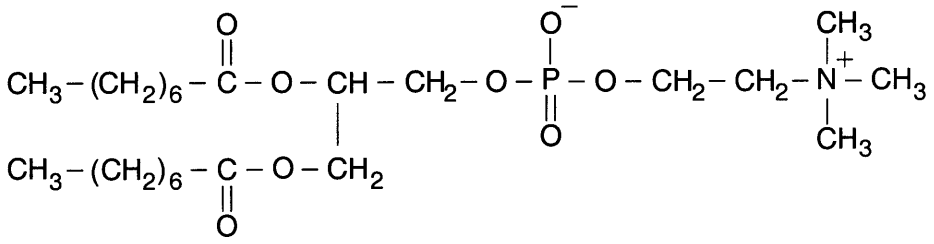

Figure 8-9: The chemical formula of dioctanoyl phosphatidylcholine (C_8-lecithin). The negative charge is on the phosphate group, while the positive charge is on the amino group. Accordingly, the positive charge is located further from the ends of the two hydrophobic tails than the negative charge.

The two-phase aqueous C_8-lecithin micellar system also has the attractive feature of exhibiting an upper critical point (see Figure 8-10). Therefore, unlike the two-phase aqueous $C_{10}E_4$ micellar system, this system phase separates as the temperature is decreased. Consequently, low temperatures are accessible, which is desirable because proteins generally are more stable at about 4°C. The phase separation behavior of aqueous C_8-lecithin solutions can be explained by analyzing the following equation:

$$G = H - TS \tag{8.9}$$

where G, H, and S are the Gibbs free energy, enthalpy, and entropy of the solution, respectively. The enthalpic contribution in Eq. (8.9) provides the driving force for the system to phase separate, while the entropic contribution tries to maintain a single phase solution. As the temperature decreases, the entropic contribution in Eq. (8.9) decreases. Eventually, the temperature becomes low enough that the enthalpic contribution dominates Eq. (8.9), and the system phase separates. It should also be noted that, in comparison to the two-phase aqueous $C_{10}E_4$ micellar system, the locations of the micelle-rich and micelle-poor phases are reversed. Specifically, the top phase is micelle-poor, while the bottom phase is micelle-rich in the two-phase aqueous C_8-lecithin micellar system. However, the micelles in the C_8-lecithin-buffer two-phase system are cylindrical just like those in the $C_{10}E_4$-buffer two-phase system.[43,44]

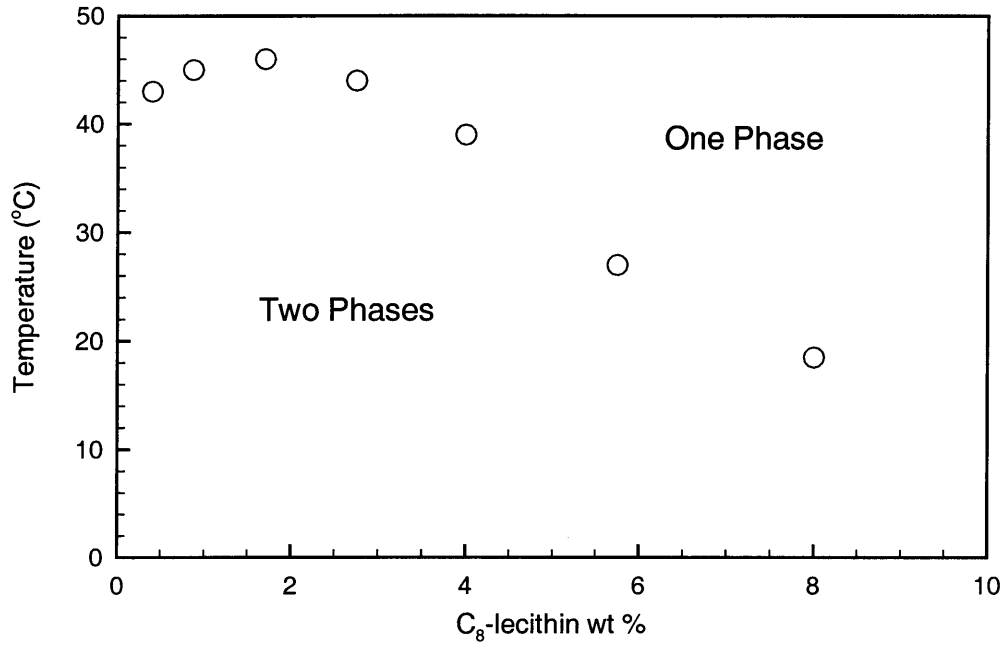

Figure 8-10: Previously measured coexistence curve of the two-phase aqueous C_8-lecithin micellar system.[70] The error bars correspond to 95% confidence limits for the measurements.

The partitioning behavior of water-soluble proteins in the two phase aqueous C_8-lecithin micellar system was also previously rationalized as being primarily driven by steric, excluded-volume interactions between the micelles and the proteins.[70,72] This result was not surprising because, although C_8-lecithin is zwitterionic, it has no net charge. Accordingly, following the work on the two-phase aqueous mixed ($C_{10}E_4$/anionic) micellar systems, it was both logical and interesting to theoretically investigate the partitioning behavior of water-soluble proteins in two-phase aqueous mixed (C_8-lecithin/anionic) micellar systems. In this theoret-

ical development, the anionic surfactant will be chosen to have a negative charge positioned between the positive and negative charges of the C_8-lecithin molecule. An example of such an anionic surfactant is sodium dodecyl ethylene oxide sulfate, SDE_1S, where one ethylene oxide unit is present between the twelve carbon alkyl tail and the charged sulfate group. The mixed micelles in such a system will be modeled as three concentric charged cylinders, corresponding to the positive and negative charges of C_8-lecithin and the negative charge of the anionic surfactant, as shown in Figure 8-11. Since the surfactant molecules are continuously moving in and out of the micelles, the three cylinders will be modeled as having a uniform distribution of charge on their surfaces, which represent time-averaged surface charge densities. As discussed in Chapter 7, an expression for the electrostatic potential in the region where the proteins are present is required to derive an expression for the electrostatic contribution to the protein partition coefficient. As shown in Figure 8-11, this electrostatic potential is denoted as ψ_{IV} for the mixed (C_8-lecithin/anionic) micelle. Note, however, that the derivation presented here can be easily extended to other configurations (for example, where the negative charge of the anionic surfactant is positioned beyond the positive charge of C_8-lecithin). Although detailed derivations for the other configurations will not be presented, the final analytical results will be presented and compared at the end of this section to determine the most favorable configuration for protein partitioning. (In addition, note that modeling the C_8-lecithin micelle in the absence of any ionic surfactant as two concentric charged cylinders yields the same result as treating the micelle as a non-charged entity. Based on Gauss's law, the electrostatic potential outside of the C_8-lecithin micelle is constant because the micelle has no net charge.)

As a first approximation in the derivation of the expression for ψ_{IV}, salt ions will be assumed to be absent from Regions I, II, and III (see Figure 8-11). Accordingly, Laplace's equation applies for the electrostatic potentials in these three regions devoid of ions. Specifically,[126]

$$\nabla^2 \psi_m = 0 \tag{8.10}$$

where ψ_m represents ψ_I, ψ_{II}, or ψ_{III}. With regard to Region IV, there are buffer salt ions present, and therefore, Poisson's equation in dielectric media (in the cgs system of units) applies:[126,127]

$$\nabla^2 \psi_{IV} = -\frac{4\pi\rho}{\epsilon_{IV}} \tag{8.11}$$

where ϵ_{IV} is the dielectric constant of Region IV, and ρ is the charge density due to the ions

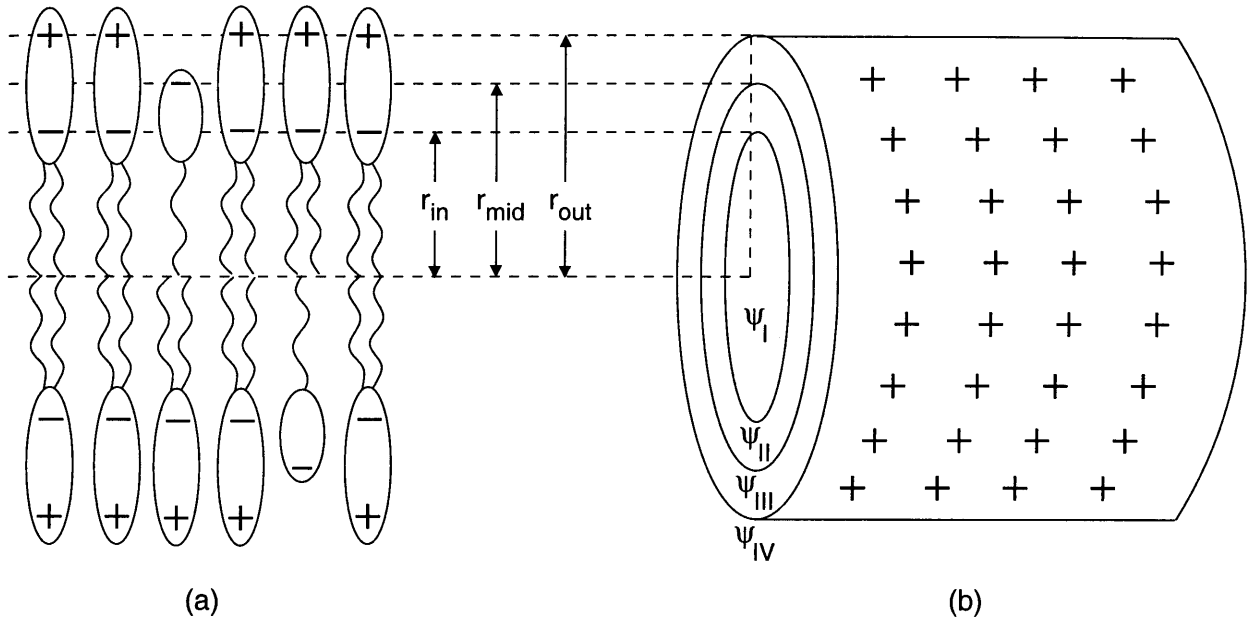

Figure 8-11: In (a), a portion of the cylindrical mixed (C_8-lecithin/anionic) micelle is schematically represented, where the micelle is comprised primarily of the zwitterionic C_8-lecithin surfactant. In (b), the three concentric charged cylinders used to model the mixed micelle are shown. The radii r_{in}, r_{mid}, and r_{out} correspond to the positions of the negative charge of C_8-lecithin, the negative charge of the anionic surfactant (for example, SDE_1S), and the positive charge of C_8-lecithin, respectively. In addition, ψ_I, ψ_{II}, ψ_{III}, and ψ_{IV} denote the electrostatic potentials in Regions I, II, III, and IV, respectively.

that come from the buffer salt. Accordingly, ρ is given by:

$$\rho = \sum_i n_i z_i e \tag{8.12}$$

where i is a buffer salt ion (Na^+ or HPO_4^{-2}), n_i is the number density of ion i positioned at a radial distance r away from the cylindrical micelle axis of symmetry, and z_i is the valence of ion i. Accordingly, ρ is the time-averaged charge density at any radial position, where the buffer salt ions are being modeled as a continuous distribution of charge. This is a reasonable approximation since the buffer salt ions are mobile.[126] Assuming a Boltzmann distribution for the ions yields the following expression for n_i:

$$n_i = C_i \exp\left(\frac{-z_i e \psi_{IV}}{k_B T}\right) \tag{8.13}$$

where C_i denotes the bulk concentration of each ion i. Combining Eqs. (8.11), (8.12), and (8.13) yields the well-known Poisson-Boltzmann equation:[119]

$$\nabla^2 \psi_{IV} = -\frac{4\pi}{\epsilon_{IV}} \sum_i C_i z_i e \exp\left(\frac{-z_i e \psi_{IV}}{k_B T}\right) \tag{8.14}$$

Since the Debye-Hückel approximation to the Poisson-Boltzmann equation was shown to be reasonable in Chapter 7, it will again be used as follows:

$$\exp\left(\frac{-z_i e \psi_{IV}}{k_B T}\right) \approx 1 - \frac{z_i e \psi_{IV}}{k_B T} \tag{8.15}$$

Substituting Eq. (8.15) into Eq. (8.14) yields:

$$\nabla^2 \psi_{IV} = -\frac{4\pi}{\epsilon_{IV}} \left[\sum_i C_i z_i e - \sum_i \frac{z_i^2 e^2 C_i \psi_{IV}}{k_B T}\right] \tag{8.16}$$

Since $\sum_i C_i z_i e = 0$ by electroneutrality, Eq. (8.16) simplifies to:

$$\nabla^2 \psi_{IV} = \kappa^2 \psi_{IV} \tag{8.17}$$

where

$$\kappa \equiv \left[\frac{4\pi e^2}{\epsilon_{IV} k_B T} \sum_i C_i z_i^2\right]^{\frac{1}{2}} \tag{8.18}$$

is the inverse Debye-Hückel screening length.

Equations (8.10) and (8.17) can be simplified by writing an explicit expression for $\nabla^2\psi$. In cylindrical coordinates,

$$\nabla^2\psi = \frac{1}{r}\frac{\partial}{\partial r}\left(r\frac{\partial\psi}{\partial r}\right) + \frac{1}{r^2}\frac{\partial^2\psi}{\partial\theta^2} + \frac{\partial^2\psi}{\partial z^2} \tag{8.19}$$

Since the micelles are infinitely-long cylinders, there is no variation of ψ in the θ and z directions. Therefore, Eq. (8.19) simplifies to:

$$\nabla^2\psi = \frac{1}{r}\frac{d}{dr}\left(r\frac{d\psi}{dr}\right) \tag{8.20}$$

Substituting Eq. (8.20) into Eq. (8.10) yields the following equations for ψ_m in Regions I, II, and III:

$$\frac{1}{r}\frac{d}{dr}\left(r\frac{d\psi_m}{dr}\right) = 0 \tag{8.21}$$

Solving Eq. (8.21) yields:

$$\psi_m = A_m \ln r + B_m \tag{8.22}$$

where A_m and B_m are integration constants. Accordingly, the electrostatic potentials in Regions I, II, and III are given by the following three expressions:

$$\psi_I = A_I + B_I \ln r \tag{8.23}$$

$$\psi_{II} = A_{II} + B_{II} \ln r \tag{8.24}$$

$$\psi_{III} = A_{III} + B_{III} \ln r \tag{8.25}$$

With regard to Region IV, combining Eqs. (8.17) and (8.20) yields:

$$\frac{1}{r}\frac{d}{dr}\left(r\frac{d\psi_{IV}}{dr}\right) = \kappa^2\psi_{IV} \tag{8.26}$$

Defining a new variable x as $x \equiv \kappa r$, Eq. (8.26) can be rewritten as follows:

$$x^2\frac{d^2\psi_{IV}}{dx^2} + x\frac{d\psi_{IV}}{dx} - x^2\psi_{IV} = 0 \tag{8.27}$$

Equation (8.27) is a modified Bessel equation of order 0. The solution to Eq. (8.27) is given by:

$$\psi_{IV} = A_{IV} I_0(x) + B_{IV} K_0(x) \tag{8.28}$$

or

$$\psi_{IV} = A_{IV} I_0 (\kappa r) + B_{IV} K_0 (\kappa r) \tag{8.29}$$

where I_0 and K_0 are the modified Bessel functions of the first and second kind, respectively, of order 0.

Equations (8.23), (8.24), (8.25), and (8.29) have eight unknowns (A_I–A_{IV} and B_I–B_{IV}). To find these, eight boundary conditions are required. One of the boundary conditions is derived by applying Gauss's law in a dielectric media to Region IV when $r \to \infty$. According to Gauss's law, the electrostatic potential is a constant in this electroneutral bulk region. This constant was set equal to zero to yield the first boundary condition given by:

$$\lim_{r \to \infty} \psi_{IV} = 0 \tag{8.30}$$

The electrostatic potential must also be continuous across the boundaries separating the different regions,[126] and this is captured in the following three boundary conditions:

$$\psi_I|_{r=r_{in}^-} = \psi_{II}|_{r=r_{in}^+} \tag{8.31}$$

$$\psi_{II}|_{r=r_{mid}^-} = \psi_{III}|_{r=r_{mid}^+} \tag{8.32}$$

$$\psi_{III}|_{r=r_{out}^-} = \psi_{IV}|_{r=r_{out}^+} \tag{8.33}$$

where r_{in}, r_{mid}, and r_{out} are indicated in Figure 8-11, and correspond to the radii of the inner, middle, and outer charged cylinders.

The four remaining boundary conditions, which are derived in detail in Appendix I, are given by:

$$\frac{d\psi_I}{dr} = 0, \quad for\ 0 < r \leq r_{in} \tag{8.34}$$

$$\epsilon_{II} \left(\frac{d\psi_{II}}{dr} \right)_{r=r_{in}^+} - \epsilon_I \left(\frac{d\psi_I}{dr} \right)_{r=r_{in}^-} = -4\pi\sigma_{in} \tag{8.35}$$

$$\epsilon_{III} \left(\frac{d\psi_{III}}{dr} \right)_{r=r_{mid}^+} - \epsilon_{II} \left(\frac{d\psi_{II}}{dr} \right)_{r=r_{mid}^-} = -4\pi\sigma_{mid} \tag{8.36}$$

$$\epsilon_{IV} \left(\frac{d\psi_{IV}}{dr} \right)_{r=r_{out}^+} - \epsilon_{III} \left(\frac{d\psi_{III}}{dr} \right)_{r=r_{out}^-} = 4\pi\sigma_{in} \frac{r_{in}}{r_{out}} \tag{8.37}$$

where σ_{in} and σ_{mid} are the surface charge densities of the inner and middle charged cylinders, respectively. They are therefore the surface charge densities that correspond to the location of the negative charges of C_8-lecithin and the anionic surfactant, respectively. Applying

the eight boundary conditions to Eqs. (8.23), (8.24), (8.25), and (8.29), yields the following relation for ψ_{IV}:

$$\psi_{IV} = \frac{4\pi\sigma_{mid}r_{mid}}{\epsilon_{IV}\kappa r_{out}K_1(\kappa r_{out})}K_0(\kappa r) \tag{8.38}$$

Equation (8.38) can be substituted into the derivation from Chapter 7 to yield:

$$K_p^{elec} = \exp\left[\frac{-8\pi z_p e r_{mid}}{\kappa^2\epsilon_{IV}r_{out}^2 k_B T}\left(\sigma_{mid,t}\phi_t - \sigma_{mid,b}\phi_b\right)\right] \tag{8.39}$$

where $\sigma_{mid,t}$ and $\sigma_{mid,b}$ are the surface charge densities of the cylinders defined by the position of the negative charge of the anionic surfactant in the micelles in the top and bottom phases, respectively. Equation (8.39) can also be rewritten as follows:

$$K_p^{elec} = \exp\left[\frac{-8\pi z_p e l_{an}}{\kappa^2\epsilon_w R_0^2 k_B T}\left(\sigma_{an,t}\phi_t - \sigma_{an,b}\phi_b\right)\right] \tag{8.40}$$

since the dielectric constant in Region IV (ϵ_{IV}) is that of water (ϵ_w), r_{mid} corresponds to the length of the anionic surfactant (l_{an}), r_{out} is approximately equal to the entire length of C_8-lecithin, which is approximately equal to the length of $C_{10}E_4$ (R_0),[70,72] and the surface charge densities of the middle cylinder in the top and bottom phases ($\sigma_{mid,t}$ and $\sigma_{mid,b}$) are the surface charge densities due to the anionic surfactant in the mixed micelles present in the top and bottom phases ($\sigma_{an,t}$ and $\sigma_{an,b}$). As in the case of Eq. (8.5), the modified Bessel functions of the second kind of order 1, K_1, cancel in the derivation of Eq. (8.40). In fact, Eq. (8.40) is equal to Eq. (8.5), which is the expression derived for the $C_{10}E_4$-SDE_6S-buffer system. The same expression is obtained, even though Eq. (8.40) was derived for $l_{an} < R_0$, because the salt ions were assumed to be absent from Regions I, II, and III of Figure 8-11. Accordingly, the electrostatic potential of the middle charged cylinder due to the anionic surfactant is not screened by the salt ions until Region IV.

In addition, as in the case of the $C_{10}E_4$-SDE_6S-buffer system, the dependence of K_p^{elec} on l_{an} can be removed by considering the expression for the surface charge density of the cylinder corresponding to the anionic surfactant in the mixed micelle in phase α, $\sigma_{an,\alpha}$. The derivation of $\sigma_{an,\alpha}$ is the same as the one presented in Appendix H with the exception of replacing "SDS" with "an", and replacing "$C_{10}E_4$" with "C_8-lecithin", in the subscripts. Therefore, $\sigma_{an,\alpha}$ is given by:

$$\sigma_{an,\alpha} = \frac{y_{an,\alpha}z_{an}\,e\,l_{c,\alpha}^2}{2l_{an,\alpha}\left[(1-y_{an,\alpha})\,v_{tail,C_8\text{-}lecithin} + y_{an,\alpha}v_{tail,an}\right]} \tag{8.41}$$

where z_{an} is the valence of the anionic surfactant, $l_{c,\alpha}$ is the radius of the hydrophobic core of each cylindrical micelle in phase α, $l_{an,\alpha}$ is the length of the anionic surfactant in each micelle in phase α, $v_{tail,C_8\text{-}lecithin}$ is the volume of the hydrophobic tail of C_8-lecithin in any micelle, $v_{tail,an}$ is the volume of the hydrophobic tail of the anionic surfactant in any micelle, and $y_{an,\alpha}$ is the micelle composition (molar ratio of anionic surfactant to total surfactant in every micelle). Combining Eqs. (8.40) and (8.41) yields:

$$K_p^{elec} = \exp\left[\frac{-8\pi z_p\, e}{\kappa^2 \epsilon_w R_0^2 k_B T}\left(\sigma^*_{an,t}\phi_t - \sigma^*_{an,b}\phi_b\right)\right] \tag{8.42}$$

where

$$\sigma^*_{an,\alpha} = \frac{y_{an,\alpha} z_{an}\, e\, l_{c,\alpha}^2}{2\left[(1-y_{an,\alpha})\, v_{tail,C_8\text{-}lecithin} + y_{an,\alpha} v_{tail,an}\right]} \tag{8.43}$$

The theory therefore predicts that the electrostatic attractions between the mixed micelles and lysozyme should remain constant as the negative charge is positioned anywhere *between* the two charges of C_8-lecithin.

In addition, two other configurations were considered theoretically as shown in Figure 8-12. In one configuration, the negative charge of the anionic surfactant (for example, SDS) is positioned before the negative charge of the C_8-lecithin molecule (see Figure 8-12a), while in the other configuration, the negative charge of the anionic surfactant (for example, SDE_6S) is positioned after the positive charge of the C_8-lecithin molecule (see Figure 8-12b). Although the detailed derivations will not be presented here, the exact same expressions as those in Eqs. (8.42) and (8.43) were derived for these two configurations. Since there is no dependence on $l_{an,\alpha}$ in Eqs. (8.42) and (8.43), the theory predicts that, for the same micelle composition, the electrostatic attractions between the mixed micelles and lysozyme should remain constant *wherever* the negative charge of the anionic surfactant is positioned. For the configuration shown schematically in Figure 8-12a, this results from assuming that the salt ions are absent from the entire region corresponding to the cylinder of radius R_0. Accordingly, the electrostatic potential of the inner charged cylinder due to the anionic surfactant is not screened by the salt ions until $r > R_0$. On the other hand, for the configuration shown schematically in Figure 8-12b, the same electrostatic attractions are predicted because the theory does not allow the protein and the buffer salt ions to access the region corresponding to the radial distance, (l_{an} - R_0). In the future, experiments can be performed with the anionic surfactants SDS, SDE_1S, and SDE_6S to test the assumptions of the theory that result in K_p^{elec} being independent of the length of the anionic surfactant for the same micelle composition.

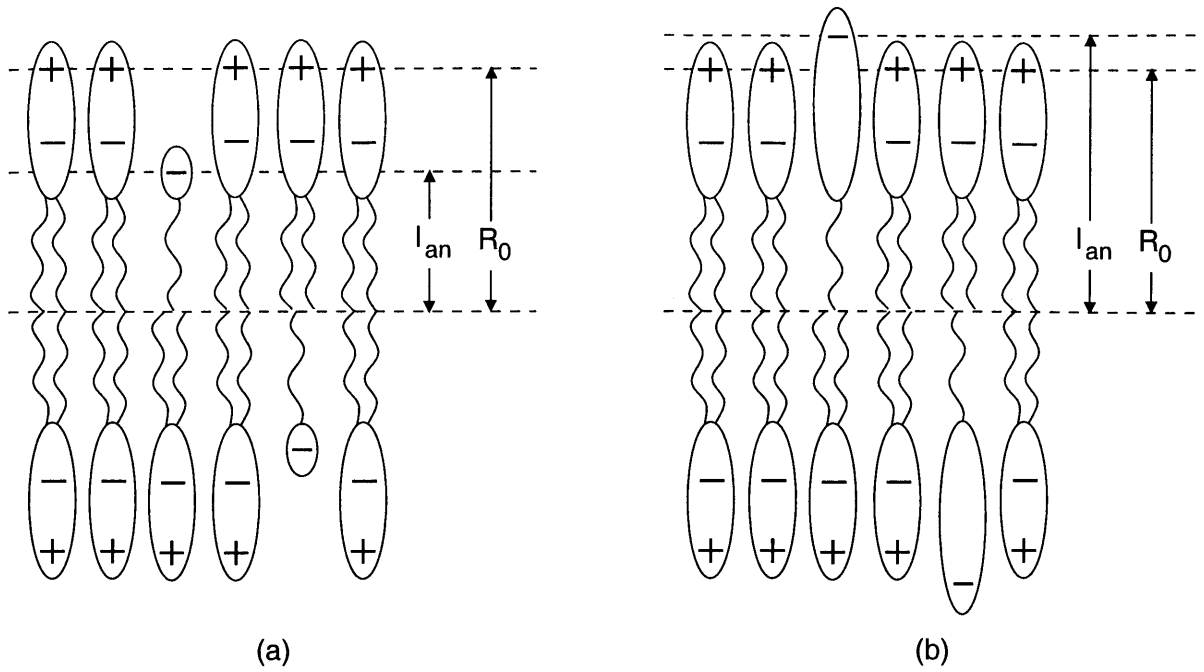

Figure 8-12: In (a), the negative charge of the anionic surfactant (for example, SDS) is positioned before the negative charge of the C_8-lecithin molecule. In (b), the negative charge of the anionic surfactant (for example, SDE_6S) is positioned after the positive charge of the C_8-lecithin molecule. l_{an} and R_0 correspond to the lengths of the anionic and zwitterionic surfactants, respectively.

8.5 Conclusions

The theoretical study presented in this chapter has demonstrated some examples of using the theory developed in Chapter 7 to optimize the protein partition coefficient. Specifically, the effects of three experimentally controllable variables (pH, IS, and d_{ch}) on the protein partition coefficient were first examined using the analytical expression for K_p derived in Chapter 7. The theoretical expression for the protein partition coefficient was also used in a 2^3 factorial design to estimate theoretically the main effects of the individual variables and the interactive effects between these variables. Based on this theoretical design, the solution pH and the ionic strength (IS) were found to have a strong interactive effect. Consequently, a theoretical response surface of the protein partition coefficient as a function of these two variables was generated to identify the optimum conditions. New theoretical expressions were also derived to predict protein partition coefficients in two-phase aqueous mixed ("noncharged"/ionic) micellar systems where: (i) the ionic surfactant has its charge located beyond the hydrophilic head of the nonionic surfactant, and (ii) the "noncharged" surfactant is zwitterionic.

The predictions of this chapter can be tested experimentally in the future. For example, for the same micelle composition of anionic surfactant to "noncharged" surfactant, the theoretical expressions derived in this chapter predict that the same electrostatic effect will be observed in the C_8-lecithin-SDS-buffer system as in the $C_{10}E_4$-SDE_6S-buffer system. In addition, this electrostatic effect is expected to be stronger than that present in the $C_{10}E_4$-SDS-buffer system. Experimentally measuring more protein partition coefficients will be useful because they will test the assumptions underlying the theoretical expressions derived in this chapter. However, as discussed in Section 8.4, many experiments are required to experimentally test these predictions, since lysozyme must be partitioned in the two systems at conditions where the total molar concentrations of the "noncharged" and anionic surfactants in the top and bottom phases of one system are equal to those in the top and bottom phases of the other system, respectively. Although these experiments are not within the scope of this thesis, they may be performed in the future. With respect to this thesis, only the initial weight percent concentrations of the "noncharged" and anionic surfactants were maintained constant in the experimental study described in Chapter 9. The rationale behind this decision was a practical one, since the mass of material required in a unit operation is one of the variables that are considered in industry prior to selecting a system.

Chapter 9

Separating Lysozyme from Bacteriophage P22 in Two-Phase Aqueous Mixed Micellar Systems

9.1 Introduction

Different two-phase aqueous mixed ("noncharged"/ionic) micellar systems were investigated experimentally regarding their ability to separate protein from virus. This investigation was motivated by the results obtained in Chapter 7. In particular, in Chapter 7, it was shown that net positively-charged proteins, such as lysozyme, can be attracted electrostatically into the top, micelle-rich phase, which contained the greater number of the net negatively-charged mixed ($C_{10}E_4$/SDS) micelles. Consequently, it was anticipated that the addition of an anionic surfactant, like SDS, to the two-phase aqueous micellar system may yield a better separation of lysozyme from bacteriophage P22 when compared to the $C_{10}E_4$-buffer system studied in Chapter 6. Specifically, for the same volume ratio, the yield of lysozyme in the top, micelle-rich phase may be increased beyond 75%, which is the yield observed in the $C_{10}E_4$-buffer system. With this in mind, lysozyme was separated from bacteriophage P22 in different two-phase aqueous mixed ("noncharged"/ionic) micellar systems at conditions similar to the ones used in the $C_{10}E_4$-buffer system, and the results of this investigation will be reported in this chapter. This experimental study represents a test for determining if two-phase aqueous mixed ("noncharged"/ionic) micellar systems can improve the separation of protein from virus. Investigating different two-phase aqueous micellar systems is also interesting because it is always useful from a practical viewpoint to have a variety of systems available. Indeed, the scientist or engineer can then choose from the various available systems to select the best one for a particular application based on the specific goals and constraints of the separation problem.

The remainder of this chapter is organized as follows. In Section 9.2, the materials and experimental methods are detailed. Section 9.3 provides a brief review of the parameters that are important in determining the performance of an extraction process. In Section 9.4, the experimental results are presented and discussed. Finally, concluding remarks are presented in Section 9.5.

9.2 Materials and Methods

9.2.1 Materials

The nonionic surfactant *n*-decyl tetra(ethylene oxide) ($C_{10}E_4$) (lot no. 6011) was obtained from Nikko Chemicals (Tokyo, Japan). Sodium dodecyl sulfate (SDS) (lot no. 64H02972) and lysozyme (lot no. 57H7045) were purchased from Sigma (St. Louis, MO). A 26 wt% sodium dodecyl hexa(ethylene oxide) sulfate (SDE_6S) aqueous solution (Exp. 5348-41) was obtained from Witco (Houston,TX). Dioctanoyl phosphatidylcholine (C_8-lecithin) (lot no. 80PC-53) was purchased from Avanti Polar-Lipids (Alabaster,AL). Professor Jonathan King's laboratory provided the bacteriophage P22 host bacterium, *Salmonella typhimurium* strain 7155, and two bacteriophage P22 mutants, (9^-am/5^-am/13^-am) and (5^-am/13^-am). Citric acid (lot no. 0616 KCXK) and magnesium sulfate ($MgSO_4$) (lot no. 6070 A31581) were purchased from Mallinckrodt (Paris, KY). Disodium phosphate (lot no. 896726) was obtained from Fisher Scientific (Fair Lawn, NJ). All these materials were used as received. All solutions were prepared using pH 7.2 McIlvaine's buffer consisting of 16.4 mM disodium phosphate and 1.82 mM citric acid in Milli-Q water. Milli-Q water is the product of passing deionized water through Millipore's (Bedford, MA) Milli-Q system. All glassware used in the experiments were subjected to washing in a 50:50 ethanol:1 M sodium hydroxide bath, washing in a 1 M nitric acid bath, rinsing copiously with Milli-Q water, and drying in an oven for at least one day.

9.2.2 Separating Lysozyme from Bacteriophage P22 in the $C_{10}E_4$-SDS-Buffer and the $C_{10}E_4$-SDE_6S-Buffer Two-Phase Systems

For each separation experiment, five 7.0 mL buffered solutions were prepared in graduated 10 mL test tubes. Four of the solutions contained 6.6×10^7 particles/mL of bacteriophage P22, 0.10 g/L of lysozyme, 2 mM $MgSO_4$ (which was required for the stability of bacteriophage P22), 0.320 wt% of one of the anionic surfactants (SDS or SDE_6S), and 4.13 wt% $C_{10}E_4$, which was the concentration of $C_{10}E_4$ used in Chapter 6. The same concentration of

$C_{10}E_4$ was employed in this experiment, since the purpose of this study was to determine if the anionic surfactant could improve the separation of lysozyme from bacteriophage P22. The concentration of the anionic surfactant, on the other hand, was increased over 3-fold from the concentration used in Chapter 7 with the hope of "fishing" more of the lysozyme into the top phase. The fifth solution served as the control containing the same concentrations of $MgSO_4$ and the two surfactants, but no protein or virus.

The solutions were mixed gently, and equilibrated at 4°C until each solution exhibited a single phase. For the solutions containing SDS, they were placed in the thermo-regulated device described in Section 3.2.4 to initiate phase separation at 34.1°C. As described in Section 7.4.1, a higher operating temperature was required, since a higher concentration of SDS was employed. With regard to the solutions containing SDE_6S, the desired operating temperature was determined experimentally to be 25.1°C. These temperatures were chosen because, for the above initial concentrations of $C_{10}E_4$ and the anionic surfactant, they yielded volume ratios that were close to the one used when lysozyme was separated from bacteriophage P22 in the $C_{10}E_4$-buffer system. In addition, since both temperatures were less than body temperature, thermal denaturation of lysozyme was expected to be negligible. The solutions were maintained at this condition for 17 hours prior to withdrawing the phases with great care using syringe and needle sets. All the partitioning experiments in this thesis were conducted for *at least* 14 hours, since it was shown previously[70] that partition coefficients measured after overnight partitioning were similar to those measured after partitioning over at least three days. The concentration of bacteriophage P22 in each phase was measured with the plaque assay described in Section 2.2.4. The concentration of lysozyme in each phase was determined by utilizing a procedure similar to the one discussed for cytochrome *c* in Section 5.2.4. The only differences were: (i) lysozyme did not need to be reduced with sodium L-ascorbate prior to measuring its absorbance, and (ii) the wavelength for absorption was 280 nm.

9.2.3 Separating Lysozyme from Bacteriophage P22 in the C_8-lecithin-Buffer and the C_8-lecithin-SDS-Buffer Two-Phase Systems

For each separation experiment, four 7.0 mL buffered solutions were prepared in graduated 10 mL test tubes. For the solutions without SDS, three of the solutions contained 8.5×10^7 particles/mL of bacteriophage P22, 0.10 g/L of lysozyme, 2 mM $MgSO_4$, and 4.13 wt% C_8-lecithin. The fourth solution served as the control containing the same concentrations of C_8-lecithin and $MgSO_4$, but no protein or virus. For the solutions containing SDS,

three of the solutions contained 8.8×10^7 particles/mL of bacteriophage P22, 0.10 g/L of lysozyme, 2 mM $MgSO_4$, 4.13 wt% C_8-lecithin, and 0.320 wt % SDS. The fourth solution again served as the control containing the same concentrations of C_8-lecithin, SDS, and $MgSO_4$, but no protein or virus. In order to make comparisons between the different separation experiments, the concentration of C_8-lecithin was chosen to be the same as that of $C_{10}E_4$ at 4.13 wt%, and the same concentration of anionic surfactant was used at 0.320 wt%. It should be noted that a separation experiment was not performed with SDE_6S because the system did not phase separate when 0.320 wt% SDE_6S was added to 4.13 wt% C_8-lecithin.

In contrast to the solutions containing $C_{10}E_4$ micelles, these solutions needed to be heated in order to exhibit a single phase, since the coexistence curve of the C_8-lecithin-buffer system has an upper critical point. It was desirable, however, to avoid higher temperatures whenever possible to prevent the thermal denaturation of the protein molecules. Accordingly, the solutions were gently mixed and directly placed in the thermo-regulated device without having them first become single phase solutions. The partitioning temperatures were 31.5°C and 36.3°C for the solutions with and without SDS, respectively. These temperatures were chosen because they yielded volume ratios of about 1/4 for the above initial concentrations of C_8-lecithin and SDS. The choice of this volume ratio is explained in Section 9.3. After the solutions were allowed to equilibrate in the thermo-regulated device for 10 minutes, they were gently mixed again and placed back into the device to ensure a well-mixed solution. The solutions were then left unperturbed in the thermo-regulated device for 16 hours before their phases were withdrawn with great care using syringe and needle sets. All the partitioning experiments in this thesis were conducted for *at least* 14 hours, since it was shown previously[70] that partition coefficients measured after overnight partitioning were similar to those measured after partitioning over at least three days. The concentration of bacteriophage P22 in each phase was measured with the plaque assay described in Section 2.2.4. The concentration of lysozyme in each phase was determined as described in Section 9.2.2, with the exception that the temperature of the samples in the cuvettes were maintained at 37°C, and not 14 to 15°C, to prevent the onset of phase separation. The lower temperatures of 14 to 15°C could not be used, since the C_8-lecithin micellar systems phase separate with a decrease in the temperature.

9.3 Theory

In this study, lysozyme was separated from bacteriophage P22 in different two-phase aqueous micellar systems. Accordingly, in order to determine the performance of the separa-

tion processes in the $C_{10}E_4$-ionic surfactant-buffer systems, the equations that were discussed in detail in Chapter 6 are required. These equations, which are summarized below, are also applicable to the $C_{10}E_4$-ionic surfactant-buffer systems because the top and bottom phases are micelle-rich and micelle-poor, respectively, as in the $C_{10}E_4$-buffer system. The protein and viral partition coefficients, K_p and K_v, are defined as follows:[75]

$$K_p \equiv \frac{C_{p,t}}{C_{p,b}} \tag{1.3}$$

and

$$K_v \equiv \frac{C_{v,t}}{C_{v,b}} \tag{1.5}$$

where $C_{p,t}$ and $C_{p,b}$ are the concentrations of protein in the top and bottom phases, respectively, and $C_{v,t}$ and $C_{v,b}$ are the concentrations of virus in the top and bottom phases, respectively. The yield of the protein in the top phase ($Y_{p,t,C_{10}E_4}$), the yield of the virus in the bottom phase ($Y_{v,b,C_{10}E_4}$), and the concentration factor of the virus in the bottom phase ($CF_{v,b,C_{10}E_4}$) are given by:

$$Y_{p,t,C_{10}E_4} = \frac{K_p\left(\frac{V_t}{V_b}\right)}{1 + K_p\left(\frac{V_t}{V_b}\right)} \times 100\% \tag{6.4}$$

and

$$Y_{v,b,C_{10}E_4} = \frac{1}{1 + K_v\left(\frac{V_t}{V_b}\right)} \times 100\% \tag{6.5}$$

and

$$CF_{v,b,C_{10}E_4} = \frac{1 + \frac{V_t}{V_b}}{1 + K_v\left(\frac{V_t}{V_b}\right)} \tag{6.7}$$

where V_t/V_b is the volume ratio. As discussed in detail in Section 6.3.4, these equations indicate that a volume ratio that is larger than one is desirable to attain good recovery of the protein in the top phase, while still maintaining good recovery of the virus in the bottom phase. Such a volume ratio would also give rise to a higher concentration factor of the virus in the bottom phase. A volume ratio similar to the one used in Chapter 6 was utilized in this study to enable a comparison between the different separation experiments.

For the zwitterionic C_8-lecithin micellar systems, which include the C_8-lecithin-buffer and the C_8-lecithin-ionic surfactant-buffer systems, new performance equations must be derived. New equations are required because the locations of the micelle-rich and micelle-poor phases are reversed when compared to those in the $C_{10}E_4$ micellar systems, which include the

$C_{10}E_4$-buffer and the $C_{10}E_4$-ionic surfactant-buffer systems. As discussed in Chapter 8, the top phase is micelle-poor, while the bottom phase is micelle-rich in the C_8-lecithin micellar systems. To distinguish the yields and concentration factor evaluated in the C_8-lecithin micellar systems from those evaluated in the $C_{10}E_4$ micellar systems, "C_8" (and not "$C_{10}E_4$") will be included in the subscripts of these parameters.

Separation experiments in the C_8-lecithin micellar systems were performed where the protein was recovered in the *bottom*, micelle-rich phase, while the virus was recovered in the *top*, micelle-poor phase. The yield of the protein in the *bottom* phase, Y_{p,b,C_8}, is given by:

$$Y_{p,b,C_8} = \frac{C_{p,b}V_b}{C_{p,t}V_t + C_{p,b}V_b} \times 100\% \tag{9.1}$$

Similarly, the yield of the virus in the *top* phase, Y_{v,t,C_8}, can be written as follows:

$$Y_{v,t,C_8} = \frac{C_{v,t}V_t}{C_{v,t}V_t + C_{v,b}V_b} \times 100\% \tag{9.2}$$

Combining Eqs. (9.1), (9.2), and the definitions of the protein and viral partition coefficients yield the following equalities:

$$Y_{p,b,C_8} = \frac{1}{1 + K_p\left(\frac{V_t}{V_b}\right)} \times 100\% \tag{9.3}$$

and

$$Y_{v,t,C_8} = \frac{K_v\left(\frac{V_t}{V_b}\right)}{1 + K_v\left(\frac{V_t}{V_b}\right)} \times 100\% \tag{9.4}$$

Since the virus will be recovered in the *top* phase, the concentration factor of the virus in the *top* phase, CF_{v,t,C_8}, is given by:

$$CF_{v,t,C_8} = \frac{C_{v,t}}{C_{v,0}} \tag{9.5}$$

where $C_{v,0}$ is the initial concentration of the virus prior to the extraction. Recalling the equation for the mass balance on the virus,

$$C_{v,0}\left(V_t + V_b\right) = C_{v,t}V_t + C_{v,b}V_b \tag{4.1}$$

and combining Eqs. (9.5), (4.1), and the definition of the viral partition coefficient yields the

following expression for the concentration factor of the virus in the *top* phase:

$$CF_{v,t,C_8} = \frac{K_v\left(1+\frac{V_t}{V_b}\right)}{1+K_v\left(\frac{V_t}{V_b}\right)} \tag{9.6}$$

For the C_8-lecithin micellar systems, an analysis similar to the one presented in Section 6.3.4 can be conducted with the above equations to show that a volume ratio that is *smaller* than one is desirable to attain good recovery of the protein in the *bottom* phase, while still maintaining good recovery of the virus in the *top* phase. Such a volume ratio would also give rise to a higher concentration factor of the virus in the *top* phase. It was expected that a volume ratio that is less than 1 is desirable, since the locations of the micelle-rich and micelle-poor phases in the C_8-lecithin micellar systems are reversed in comparison to those in the $C_{10}E_4$ micellar systems. A volume ratio of about 1/4 was used in the C_8-lecithin micellar systems to be consistent with the separation experiments performed in the $C_{10}E_4$ micellar systems, which used a value of 4 for the ratio of the volume of the micelle-rich phase to the volume of the micelle-poor phase. Note that the entrainment of micelle-poor domains in the macroscopic, micelle-rich phase (see Chapter 5) was expected to be present in the separation experiments because the volume of the micelle-rich phase was larger than that of the micelle-poor phase.

9.4 Results and Discussion

9.4.1 Separating Lysozyme from Bacteriophage P22 in the $C_{10}E_4$-SDS-Buffer and the $C_{10}E_4$-SDE_6S-Buffer Two-Phase Systems

The results of the separation experiments conducted in the $C_{10}E_4$-SDS-buffer and the $C_{10}E_4$-SDE_6S-buffer systems are summarized in Table 9-1. The mass balances on lysozyme and bacteriophage P22 in these experiments closed to 100% within the experimental error. The results of the previous separation experiment in the $C_{10}E_4$-buffer system (Chapter 6) have also been included in Table 9-1 for comparison. The addition of SDS at a concentration of 0.320 wt% increased the partition coefficient of lysozyme from K_p=0.78 to K_p=6.7. Accordingly, the yield of lysozyme in the top phase increased from $Y_{p,t,C_{10}E_4}$=75% in the $C_{10}E_4$-buffer system to $Y_{p,t,C_{10}E_4}$=95% in the $C_{10}E_4$-SDS-buffer system. On the other hand, the addition of SDE_6S to the $C_{10}E_4$-buffer system at a concentration of 0.320 wt% only increased the partition coefficient of lysozyme from K_p=0.78 to K_p=1.12. Based on this value of the protein partition coefficient and a lower volume ratio of 3.1, the yield of the protein

in the top phase was $Y_{p,t,C_{10}E_4}$=77%, which was very close to the value of $Y_{p,t,C_{10}E_4}$=75% attained in the $C_{10}E_4$-buffer system. Even if a volume ratio of 4, instead of 3.1, was used in the $C_{10}E_4$-SDE_6S-buffer system, the yield of the protein in the top phase would have been only $Y_{p,t,C_{10}E_4}$=81%.

Table 9-1: Separating lysozyme from bacteriophage P22 in different $C_{10}E_4$ micellar systems. This table shows the results from the separation experiments conducted in this study along with the results from the separation experiment performed in the $C_{10}E_4$-buffer system (Chapter 6). The errors correspond to 95% confidence limits for the measurements.

	$C_{10}E_4$-SDE_6S-Buffer	**$C_{10}E_4$-SDS-Buffer**	**$C_{10}E_4$-Buffer**
$C_{10}E_4$ wt%	4.13	4.13	4.13
SDE_6S wt%	0.320	0	0
SDS wt%	0	0.320	0
V_t/V_b	3.1	3.5	4.0
K_p	1.12 ± 0.02	6.7 ± 0.6	0.78 ± 0.02
K_v	0.0036 ± 0.0012	0.0056 ± 0.0006	0.0061 ± 0.0013
$Y_{p,t,C_{10}E_4}$	77%	95%	75%
$Y_{v,b,C_{10}E_4}$	98%	98%	97%
$CF_{v,b,C_{10}E_4}$	4.0	4.4	4.8

With regard to the partition coefficients of bacteriophage P22, they were all approximately the same to within error. Specifically, the partition coefficients were K_v=5.6 × 10^{-3}, K_v=3.6 × 10^{-3}, and K_v=6.1 × 10^{-3} in the $C_{10}E_4$-SDS-buffer, the $C_{10}E_4$-SDE_6S-buffer, and the $C_{10}E_4$-buffer systems, respectively. Therefore, the yields of the virus in the bottom phase were also all essentially the same. In particular, the yields were $Y_{v,b,C_{10}E_4}$=98%, $Y_{v,b,C_{10}E_4}$=98%, and $Y_{v,b,C_{10}E_4}$=97% in the $C_{10}E_4$-SDS-buffer, the $C_{10}E_4$-SDE_6S-buffer, and the $C_{10}E_4$-buffer systems, respectively. The electrostatic interactions appear to have no effect on the partitioning behavior of bacteriophage P22, even though the net negative charge of bacteriophage P22 has been estimated to be -4750 at the pH of the buffer using the method described in Section 7.3.4. Strong electrostatic repulsive interactions are still most probably present between the net negatively-charged bacteriophage P22 and the net negatively-charged mixed micelles, since significant electrostatic interactions have already been observed for proteins that have net charges that are orders of magnitude smaller than that of bacteriophage P22. However, entrainment effects, such as those investigated in Chapter 5, are most probably causing the partition coefficients of bacteriophage P22 to appear similar in

the absence and in the presence of an anionic surfactant. For the purpose of separating lysozyme from bacteriophage P22 in the $C_{10}E_4$-anionic surfactant-buffer system, however, attaining similar viral partition coefficients is sufficient, since it indicates the possibility of increasing the yield of lysozyme in the top phase, while maintaining the same yield of virus in the bottom phase. With regard to the concentration factor of the virus in the bottom phase, it was lower in the $C_{10}E_4$-SDS-buffer system ($CF_{v,b,C_{10}E_4}$=4.4) and the $C_{10}E_4$-SDE_6S-buffer system ($CF_{v,b,C_{10}E_4}$=4.0), but this was entirely due to using the smaller volume ratios of 3.5 and 3.1, respectively. This decrease in the concentration factor of the virus in the bottom phase from the value of $CF_{v,b,C_{10}E_4}$=4.8 measured in the $C_{10}E_4$-buffer system is not associated with viral partitioning, because similar viral partition coefficients were obtained in the three systems.

In addition, Table 9-1 shows that the measured partition coefficient of lysozyme is larger in the $C_{10}E_4$-SDS-buffer system than in the $C_{10}E_4$-SDE_6S-buffer system. Therefore, it can be concluded that, for the same initial wt% of anionic surfactant and a similar final volume ratio, SDS gives rise to stronger electrostatic attractions with lysozyme than SDE_6S. This difference between SDS and SDE_6S is also reflected in the different operating temperatures used in the two separation experiments. For similar volume ratios, the addition of 0.320 wt% of SDE_6S only increased the phase separation temperature to 25.1°C, while the same concentration of SDS increased the phase separation temperature to 34.1°C. As discussed in Section 7.4.1, adding an ionic surfactant into the $C_{10}E_4$ micelles increases the phase separation temperature because it introduces electrostatic repulsions between the micelles. To counter these electrostatic repulsions, higher phase separation temperatures are required, since increasing the temperature increases the attractive interactions between these $C_{10}E_4$-rich micelles, which are required for phase separation to occur (see Chapter 1). The smaller increase in the phase separation temperature for the $C_{10}E_4$-SDE_6S-buffer system therefore indicates that, for the same initial wt% of ionic surfactant and a similar final volume ratio, SDE_6S gives rise to weaker electrostatic repulsions between the micelles. However, it cannot be concluded that, in general, the $C_{10}E_4$-SDS-buffer system gives rise to stronger electrostatic attractions with lysozyme compared to the $C_{10}E_4$-SDE_6S-buffer system, which would contradict the theoretical prediction of Chapter 8. In order to reach such a conclusion, lysozyme must be partitioned in the two systems at conditions where the total molar concentrations of $C_{10}E_4$ and the anionic surfactant in the top and bottom phases of one system are equal to those in the top and bottom phases of the other system, respectively. This, however, was not the case in the experiments described above, since it requires identifying

the appropriate tie line in each system, which involves many experiments as discussed in Section 8.4. However, the appropriate experiments may be performed in the future to test the assumptions underlying the theoretical predictions of Chapter 8.

9.4.2 Separating Lysozyme from Bacteriophage P22 in the C_8-lecithin-Buffer and the C_8-lecithin-SDS-Buffer Two-Phase Systems

The results of the separation experiments conducted in the C_8-lecithin-buffer and the C_8-lecithin-SDS-buffer systems are summarized in Table 9-2. The mass balances on both lysozyme and bacteriophage P22 closed to 100% within the experimental error. As expected, the addition of SDS to the C_8-lecithin-buffer system "fished" the net positively-charged lysozyme into the *bottom*, micelle-rich phase, which contained the greater number of net negatively-charged mixed micelles. Specifically, the addition of SDS decreased the partition coefficient of lysozyme from K_p=1.4 to K_p=0.38. Accordingly, the yield of lysozyme in the *bottom* phase increased from Y_{p,b,C_8}=70% in the C_8-lecithin-buffer system to Y_{p,b,C_8}=91% in the C_8-lecithin-SDS-buffer system. With regard to the partition coefficient of bacteriophage P22, similar values were attained, to within experimental error, for the C_8-lecithin-SDS-buffer system (K_v=20) and the C_8-lecithin-buffer system (K_v=11). As discussed in Section 9.4.1, strong electrostatic repulsive interactions are still most probably present between bacteriophage P22 and the net negatively-charged mixed micelles, since electrostatic interactions were even observed for lysozyme. However, entrainment effects, such as those investigated in Chapter 5, are most probably causing the partition coefficients of bacteriophage P22 to appear similar. Accordingly, the yields of the virus in the *top* phase were similar between the C_8-lecithin-buffer system (Y_{v,t,C_8}=76%) and the C_8-lecithin-SDS-buffer system (Y_{v,t,C_8}=82%). The concentration factor of the virus in the *top* phase, however, increased from CF_{v,t,C_8}=3.3 in the C_8-lecithin-buffer system to CF_{v,t,C_8}=4.4 in the C_8-lecithin-SDS-buffer system. This increase in the concentration factor of the virus in the *top* phase was entirely due to using a slightly *smaller* volume ratio of 0.23 instead of 0.30. The increase in the concentration factor is not associated with viral partitioning because similar viral partition coefficients were obtained in the two systems.

As discussed earlier, the locations of the micelle-rich and micelle-poor phases in the C_8-lecithin micellar systems are reversed relative to those in the $C_{10}E_4$ micellar systems. Therefore, in order to make comparisons with the values obtained in the $C_{10}E_4$ micellar systems, inverse values of the volume ratio, protein partition coefficient, and viral partition coefficient have been included in Table 9-2. For similar volume ratios and the same initial

Table 9-2: Separating lysozyme from bacteriophage P22 in different C_8-lecithin micellar systems. The results from this experimental study have been summarized in this table. Since the locations of the micelle-rich and micelle-poor phases are reversed in the C_8-lecithin micellar systems relative to the $C_{10}E_4$ micellar systems, inverse values of the volume ratio, protein partition coefficient, and viral partition coefficient have also been included to allow comparison with the corresponding values obtained in the $C_{10}E_4$ micellar systems. The errors correspond to 95% confidence limits for the measurements.

	C_8-lecithin-SDS-Buffer	**C_8-lecithin-Buffer**
C_8-lecithin wt%	4.13	4.13
SDS wt%	0.320	0
V_t/V_b	0.23	0.30
V_b/V_t	4.3	3.3
K_p	0.38 ± 0.13	1.4 ± 0.2
$1/K_p$	2.7 ± 1.0	0.71 ± 0.13
K_v	20 ± 13	11 ± 5
$1/K_v$	0.05 ± 0.04	0.09 ± 0.04
Y_{p,b,C_8}	91%	70%
Y_{v,t,C_8}	82%	76%
CF_{v,t,C_8}	4.4	3.3

concentrations of SDS and "noncharged" surfactant (C_8-lecithin or $C_{10}E_4$), more of the lysozyme was attracted to the micelle-rich phase in the $C_{10}E_4$-SDS-buffer system than in the C_8-lecithin-SDS-buffer system. Specifically, the addition of SDS to the C_8-lecithin micellar system increased the $1/K_p$ value from 0.71 to 2.7, while the addition of SDS to the $C_{10}E_4$-buffer system increased the K_p value from 0.78 to 6.7. However, as discussed in Section 9.4.1, it cannot be concluded that the $C_{10}E_4$-SDS-buffer system generally gives rise to stronger electrostatic attractions with lysozyme than the C_8-lecithin-SDS-buffer system. In order to make such a statement, many more experiments are required.

The value of the viral partition coefficient, however, can be improved. The $1/K_v$ values from the C_8-lecithin micellar systems were about one order of magnitude larger than the K_v values from the $C_{10}E_4$ micellar systems. Since entrainment was found to be a major factor in Chapter 5, the viscosities of buffered C_8-lecithin micellar solutions were measured with a procedure similar to the one detailed in Section 5.2.5. The results of the measurements are shown in Table 9-3 along with the results of the previous viscosity measurements of buffered $C_{10}E_4$ micellar solutions. Since the viscosities of the buffered C_8-lecithin micellar

solutions are higher than those of the buffered $C_{10}E_4$ micellar solutions, the difference in viral partitioning between the C_8-lecithin and $C_{10}E_4$ micellar systems can be attributed to a difference in the degree of entrainment. As explained in Chapter 5, a more viscous micelle-rich phase is expected to entrain more micelle-poor domains in the micelle-rich phase, thereby causing the measured viral partition coefficient to be less extreme.

Table 9-3: Experimentally measured viscosities of buffered C_8-lecithin and $C_{10}E_4$ solutions. The results of the previous viscosity measurements of buffered $C_{10}E_4$ micellar solutions from Chapter 5 are included in the table for comparison. The errors correspond to 95% confidence limits for the measurements.

Surfactant	Concentration (wt%)	Viscosity (cP)
C_8-lecithin	10	167 ± 2
$C_{10}E_4$	10	18.9 ± 0.1
C_8-lecithin	5	41.8 ± 0.3
$C_{10}E_4$	5	7.71 ± 0.08

Although the degree of entrainment is most probably higher in the C_8-lecithin micellar systems, the C_8-lecithin-ionic surfactant-buffer systems are, nevertheless, potential candidates for separating protein from virus, since the increase in $1/K_p$ from 0.71 to 2.7 is reasonable. Future experiments should therefore include increasing the SDS concentration even further. C_8-lecithin micellar systems are also promising because low operating temperatures, which are desirable for maintaining the thermal stability of proteins, are available because C_8-lecithin micellar systems phase separate with a decrease in temperature. As discussed in Chapter 8, the phase separation behavior of aqueous C_8-lecithin solutions can be explained by analyzing Eq. (8.9), where the enthalpic contribution provides the driving force for the system to phase separate, while the entropic contribution tries to maintain a single phase solution. Although low operating temperatures are already available in the C_8-lecithin-buffer system, even lower temperatures can be achieved with the addition of an ionic surfactant. Adding an ionic surfactant to the C_8-lecithin-buffer system decreases the enthalpic driving force for phase separation by introducing electrostatic repulsions between the micelles. Since the enthalpic driving force (associated with the attractive interactions between the micelles) is reduced, phase separation can only occur by further decreasing the entropic contribution. As discussed in Chapter 8, the entropic contribution is reduced by further decreasing the temperature. Therefore, in contrast to $C_{10}E_4$ micellar systems, adding an ionic surfactant decreases the phase separation temperature in C_8-lecithin micellar systems. This was observed

in the separation experiments conducted in this study, since the addition of 0.320 wt% of SDS to a 4.13 wt% C_8-lecithin aqueous solution decreased the phase separation temperature from 36.3°C to 31.5°C for similar final volume ratios. Accordingly, future experiments should be performed in the C_8-lecithin-ionic surfactant-buffer systems at an operating temperature of about 4°C, which is the temperature at which many downstream processes are conducted.

9.5 Conclusions

The separation of lysozyme from bacteriophage P22 was investigated in different two-phase aqueous mixed ("noncharged"/ionic) micellar systems. The addition of an ionic surfactant improved the separation in all cases. In particular, a very good separation of lysozyme from bacteriophage P22 was attained in the $C_{10}E_4$-SDS-buffer system. Although the yield of the virus in the bottom phase was basically the same as the one measured in the $C_{10}E_4$-buffer system, the addition of SDS at a concentration of 0.320 wt% increased the yield of lysozyme in the top phase from $Y_{p,t,C_{10}E_4} = 75\%$ to $Y_{p,t,C_{10}E_4} = 95\%$. Experiments should therefore be conducted in the future to investigate the potential of attaining even higher yields of lysozyme with the addition of more SDS. In addition, liquid-liquid extractions in series should be investigated for the purpose of viral clearance. Future studies should also include investigating the separation of proteins from other biological materials, such as cell debris and DNA.

PART IV

CONCLUDING REMARKS

Chapter 10

Conclusions and Future Research Directions

In an effort to attain good separation of protein from virus, the overall objective of this thesis was to develop a fundamental understanding of protein and viral partitioning in two-phase aqueous micellar systems. Section 10.1 provides a summary of the thesis. Based on the results of this thesis, future research directions were identified, and they are described in Section 10.2. Lastly, Section 10.3 presents some concluding remarks.

10.1 Thesis Summary

The motivation and background for this thesis were described in Part I. For example, the biochemical and biomedical applications requiring the separation of proteins from viruses were reviewed. They included large-scale applications, such as viral clearance and production of gene delivery viral vectors, as well as small-scale applications, such as preparative biochemistry. An overview of surfactants, micellization, and two-phase aqueous micellar systems was also provided in Part I of this thesis.

This thesis was comprised of two directions, *Directions A* and *B*, that were investigated simultaneously. The objective of *Direction A* (Part II of this thesis) was to understand viral partitioning in the two-phase aqueous $C_{10}E_4$ micellar system, since the partitioning behavior of viruses could not be fully explained by considering solely the excluded-volume interactions that operate between the viruses and the $C_{10}E_4$ micelles. Accordingly, *Direction A* was aimed at determining other possible mechanisms, in addition to the excluded-volume interactions, that influence viral partitioning in the two-phase aqueous $C_{10}E_4$ micellar system. By identifying these mechanisms, they may, if possible, be eliminated in the future to yield the extreme viral partition coefficients predicted by the excluded-volume theory. This, in turn, would enhance the separation of protein from virus.

Since the excluded-volume theory is capable of predicting reasonably well the partition coefficients of water-soluble proteins, our approach to determining other possible mechanisms

was based on challenging the assumptions underlying the excluded-volume theory in order to identify the assumptions that are valid for water-soluble proteins but not for viruses. In other words, the search for other possible mechanisms was similar to the search for the culprits in a murder mystery, where the biggest "clue" was that the "suspect" mechanisms significantly influence viral partitioning, while having little or no impact on protein partitioning. Experimental studies were conducted in Chapters 2 and 3 to investigate possible attractive interactions between the tailspikes of bacteriophage P22 and the $C_{10}E_4$ micelles. These possible attractive interactions were investigated because: (i) the excluded-volume theory assumes that only repulsive, excluded-volume interactions operate between the micelles and the partitioning solute, and (ii) the previously studied water-soluble proteins were not expected to have similar attractive interactions for reasons discussed in Chapter 2. Possible attractive interactions could counter the excluded-volume interactions, and allow more of the viral particles to remain in the top, micelle-rich phase. This, in turn, would result in the measured viral partition coefficients being larger than those predicted based on the excluded-volume theory, which was observed experimentally.

The results of the competitive inhibition study conducted in Chapter 2 demonstrated that the presence of the $C_{10}E_4$ micelles did not interfere with the infection process of bacteriophage P22. Accordingly, it was concluded that negligible or no attractive interactions operate between the tailspikes of bacteriophage P22 and the $C_{10}E_4$ micelles. This conclusion was tested further in Chapter 3 with a "cleaner," follow-up experimental study. Specifically, the capsids of bacteriophage P22 without the tailspikes were synthesized and partitioned. The partitioning behavior of the capsids of bacteriophage P22 was found to be essentially the same as that of the intact bacteriophage P22 particles with tailspikes. Accordingly, based on this result and the result of Chapter 2, it was concluded that any attractive interactions between the tailspikes of bacteriophage P22 and the $C_{10}E_4$ micelles are negligible.

Accordingly, any attractive interactions between the bacteriophage P22 particles and the $C_{10}E_4$ micelles must be associated with the capsids of bacteriophage P22. The capsid of bacteriophage P22 is comprised of approximately 420 proteins. These capsids therefore have a greater tendency to exhibit heterogeneous surface properties when compared to the previously studied water-soluble proteins. Certain groups of capsids may therefore exist which have strong attractive interactions with the $C_{10}E_4$ micelles. A double-stage partitioning study was conducted in Chapter 4 to test this hypothesis. The results of the double-stage partitioning study indicated that, even if heterogeneities do exist among the capsids of bacteriophage P22, they cannot be invoked to rationalize the observed discrepancy between the

theoretically predicted and the experimentally measured partition coefficients of bacteriophage P22. Based on this conclusion and those from Chapters 2 and 3, the only remaining source of attractive interactions between the bacteriophage P22 particles and the $C_{10}E_4$ micelles were electromagnetic interactions between the capsids of bacteriophage P22 and the $C_{10}E_4$ micelles. However, since all three, very different bacteriophages discussed in Chapter 1 were found to partition similarly, it was concluded that these attractive, electromagnetic interactions were most probably not responsible for the observed viral partitioning behavior. Specifically, it is difficult to imagine that the repulsive, excluded-volume and attractive, electromagnetic interactions associated with these three bacteriophages having very different sizes and properties (both exterior and interior) would precisely balance each other to yield similar partition coefficients.

In addition to assuming that only repulsive, excluded-volume interactions operate between the viruses and the $C_{10}E_4$ micelles, the excluded-volume theory also assumes that macroscopic phase separation equilibrium is attained in the two-phase aqueous $C_{10}E_4$ micellar system. Macroscopic phase separation equilibrium refers to the condition in which *all* the micelle-rich and micelle-poor domains, which are formed at the onset of phase separation, are in their corresponding macroscopic phases prior to withdrawing the top and bottom phases. However, this may not be true experimentally, since there could be micelle-poor domains entrained in the macroscopic, top, micelle-rich phase, as well as micelle-rich domains entrained in the macroscopic, bottom, micelle-poor phase. Consequently, the concentration of viral particles measured in each phase could be affected by the presence of these entrained domains. In accordance with the biggest "clue" concept, the concentration of protein in each phase, on the other hand, was expected to be negligibly affected by these entrained domains (see the discussion in Chapter 5). The experimental study presented in Chapter 5 demonstrated that the entrainment of micelle-poor domains in the macroscopic, top, micelle-rich phase is the key factor influencing the partitioning behavior of viruses. In addition, a new theoretical description of partitioning was developed in this chapter that combines the excluded-volume theory with this entrainment effect. To account for the entrainment, one fitted parameter, namely, the volume fraction of entrained micelle-poor domains in the macroscopic, top, micelle-rich phase, was incorporated into the theory. With this fitted parameter and the excluded-volume theory, very good agreement between the measured and predicted viral partition coefficients was attained. Therefore, it can be concluded that the primary mechanisms governing viral partitioning in the two-phase aqueous $C_{10}E_4$ micellar system are only the entrainment of micelle-poor domains in the macroscopic, top, micelle-rich phase and the

excluded-volume interactions between the viruses and the micelles.

While the mechanisms governing viral partitioning were being investigated in the context of *Direction A*, *Direction B* of this thesis was being pursued simultaneously. *Direction B*, which corresponds to Part III of this thesis, centered around the less optimistic point-of-view that the viral partition coefficients would not decrease below the experimentally observed values of 10^{-3} to 10^{-2} in the two-phase aqueous $C_{10}E_4$ micellar system. Even with these viral partition coefficients, the virus is excluded more strongly than the protein into the bottom, micelle-poor phase. Accordingly, it was expected that operating parameters could be manipulated to achieve good separation of protein from virus. In Chapter 6, the volume ratio (the volume of the top phase divided by that of the bottom phase) was increased to 4.0 to attain a protein (lysozyme) yield in the top phase of $Y_{p,t,C_{10}E_4}$=75% and a viral (bacteriophage P22) yield in the bottom phase of $Y_{v,b,C_{10}E_4}$=97%. A higher protein yield in the top phase was desirable, however, since a significant amount of protein was still being lost to the bottom phase. Although the volume ratio could be increased further to increase the yield of the protein in the top phase beyond 75%, this would also increase the contamination of the top phase with the virus. Accordingly, it was instead desirable to introduce another mode of interaction, in addition to that of the excluded-volume type, to attract the protein into the top, micelle-rich phase for the purpose of increasing its yield.

Chapter 7 described the fundamental investigation of protein partitioning in the two-phase aqueous micellar system formed by the addition of the anionic surfactant SDS to the nonionic surfactant $C_{10}E_4$. The experimental study in this chapter demonstrated proof-of-principle that two-phase aqueous mixed (nonionic/ionic) micellar systems can indeed be used to modulate both electrostatic and excluded-volume interactions between the proteins and the micelles. After mapping out the required coexistence curves and justifying their applicability, two net positively-charged proteins (lysozyme and cytochrome *c*) and two net negatively-charged proteins (ovalbumin and catalase) were partitioned in the $C_{10}E_4$-buffer and $C_{10}E_4$-SDS-buffer systems at conditions where the excluded-volume interactions between the proteins and the micelles were maintained constant. Comparison of the partitioning results between the two systems indicated that the electrostatic interactions between the proteins and the mixed ($C_{10}E_4$/SDS) micelles did have an effect on protein partitioning. A theory was also developed to predict protein partition coefficients in two-phase aqueous mixed (nonionic/ionic) micellar systems. The theory incorporated the dominant interactions, namely, the excluded-volume and electrostatic interactions, between the proteins and the mixed micelles. Since the excluded-volume theory had already been developed by others

in our group, the main component of the theoretical study was modeling the electrostatic interactions. Each micelle was modeled as an infinitely-long cylinder with an associated electrostatic potential obtained by using the Debye-Hückel approximation to the Poisson-Boltzmann equation. Each protein was modeled as a point ion with a charge equal to its net charge, which was predicted based on its amino acid sequence, typical pKa values, and the Henderson-Hasselbalch equation. Program MIX2 (a program developed by our group to predict fundamental properties of mixed surfactant systems) was also used to obtain values of various required parameters associated with the mixed micelles. The theoretical predictions were compared with the experimental data, and the theory was shown to provide reasonable quantitative predictions of protein partition coefficients in the $C_{10}E_4$-SDS-buffer system.

An important benefit of the theory developed in Chapter 7 is the ability to provide useful guidelines to optimize the protein partition coefficient without performing a single experiment. Accordingly, Chapter 8 presented some examples of using the theory for this purpose. Specifically, the effects of three experimentally controllable variables (the solution pH, the ionic strength, and the distance from the end of the hydrocarbon tail to the charge of the ionic surfactant) on the protein partition coefficient were first quickly examined using the analytical expression for the protein partition coefficient. The theoretical expression for the protein partition coefficient was also used in a 2^3 factorial design to estimate the main effects of the individual variables and the interactive effects between these variables. Based on this theoretical design, the solution pH and the ionic strength were found to have a strong interactive effect. Consequently, a theoretical response surface of the protein partition coefficient as a function of these two variables was generated to identify the optimum conditions. New theoretical expressions were also derived to predict protein partition coefficients in two-phase aqueous mixed ("noncharged"/ionic) micellar systems where: (i) the ionic surfactant has its charge located beyond the hydrophilic head of the nonionic surfactant, and (ii) the "noncharged" surfactant is zwitterionic instead of nonionic.

Different two-phase aqueous mixed ("noncharged"/ionic) micellar systems were investigated experimentally in Chapter 9 regarding their ability to separate protein from virus. This investigation was motivated by the results obtained in Chapter 7. In particular, in Chapter 7, it was shown that net positively-charged proteins, such as lysozyme, can be attracted electrostatically into the top, micelle-rich phase, which contained the greater number of the net negatively-charged mixed ($C_{10}E_4$/SDS) micelles. The "noncharged" surfactants that were investigated included $C_{10}E_4$ and C_8-lecithin, while the ionic surfactants that were examined included SDS and SDE_6S. The addition of an anionic surfactant improved the separation

of lysozyme from bacteriophage P22 in all cases. In particular, a very good separation of lysozyme from bacteriophage P22 was attained in the $C_{10}E_4$-SDS-buffer system. Although the yield of the virus in the bottom phase was basically the same as the one measured in the $C_{10}E_4$-buffer system, the addition of SDS at a concentration of 0.320 wt% increased the yield of lysozyme in the top phase from $Y_{p,t,C_{10}E_4}$=75% to $Y_{p,t,C_{10}E_4}$=95%.

10.2 Future Research Directions

10.2.1 Experimentally Attaining Even Lower Viral Partition Coefficients

As a result of the experimental and theoretical studies presented in Part II of this thesis, the entrainment of micelle-poor domains in the macroscopic, top, micelle-rich phase was found to be the key factor governing viral partitioning in the two-phase aqueous $C_{10}E_4$ micellar system. Although the degree of entrainment may be reduced further in the future by employing a volume ratio of 0.01 or lower, another method for reducing entrainment is required, since there should be some flexibility in the choice of the volume ratio. Specifically, the volume ratio is an operating parameter that should be selected based on the desired yield of product. Accordingly, an experimental apparatus capable of reducing or removing entrainment, regardless of the volume ratio, is desirable. One possibility is the use of microreactor vessels.[128] Due to the small volumes and length scales involved, entrainment may be reduced in these systems. Such a small-scale operation would also be relevant to the area of diagnostics, which involves analyzing low volumes of blood samples. A thorough literature search in the area of liquid-liquid extraction equipment should also be performed.

10.2.2 Exploiting Electrostatic Interactions between the Mixed Micelles and the Proteins

In Part III of this thesis, the two-phase aqueous mixed ("noncharged"/ionic) micellar system was shown to be able to modulate both electrostatic and excluded-volume interactions between the proteins and the mixed micelles. The introduction of electrostatic interactions also improved the separation of lysozyme (a model protein) from bacteriophage P22 (a model virus). Accordingly, the studies described below may be conducted in the future to extend the work that has begun in this area.

Experimentally Testing the Theoretically Predicted Trends in the Protein Partition Coefficient

In addition to predicting reasonably well the protein partition coefficients measured in the $C_{10}E_4$-SDS-buffer system, the theory was also used to predict trends in the protein partition coefficient when certain experimentally controllable variables were adjusted. Some of these trends should be tested experimentally in the future, since the work presented in Chapter 8 provided some guidelines for improving the protein partition coefficient. For example, the solution pH can be decreased to determine if the protein partition coefficient will increase in a two-phase aqueous mixed ("noncharged"/*anionic*) micellar system. Protein partitioning in a two-phase aqueous mixed ("noncharged"/*cationic*) micellar system should also be examined. The ionic strength of the solution can also be decreased to determine if the strength of the electrostatic interactions does indeed increase. The effect of increasing the distance from the end of the hydrocarbon tail to the negative charge of the anionic surfactant can also be tested by using different anionic SDE_nS surfactants, where n is an integer that varies from 0 to 6.

Adding More Ionic Surfactant to the Two-Phase Aqueous Mixed ("Noncharged"/Ionic) Micellar System

To attain even higher yields of lysozyme in the micelle-rich phase in the future, more SDS should be added to the two-phase aqueous mixed ($C_{10}E_4$/SDS) micellar system and the two-phase aqueous mixed (C_8-lecithin/SDS) micellar system. Other anionic surfactants and net positively-charged proteins should also be investigated. For the two-phase aqueous mixed (C_8-lecithin/ionic) micellar systems, separation experiments should also be conducted at 4°C, since many downstream processes are conducted at this temperature to maintain the thermal stability of proteins.

Performing Liquid-Liquid Extractions in Series

In the separation experiment involving lysozyme and bacteriophage P22 in the two-phase aqueous mixed ($C_{10}E_4$/SDS) micellar system, the measured protein and viral partition coefficients are K_p=6.7 and K_v=6×10^{-3}, respectively. These results indicate that there is potential for using two-phase aqueous mixed ("noncharged"/ionic) micellar systems for viral clearance. As discussed in Chapter 1, the parameter of interest is the $\log_{10}$ of viral clearance (LVC), which is the $\log_{10}$ of the ratio of the total number of viral particles fed into a unit

operation to the number of viral particles remaining with the therapeutic protein product after the unit operation. Since the protein product is recovered in the top phase of the two-phase aqueous mixed ($C_{10}E_4$/SDS) micellar system, the $\log_{10}$ of viral clearance in this system is given by:

$$LVC = log\left(\frac{C_{v,t}V_t + C_{v,b}V_b}{C_{v,t}V_t}\right) \tag{10.1}$$

Combining Eq. (10.1) and the definition of the viral partition coefficient yields:

$$LVC = log\left[\frac{1 + K_v\left(\frac{V_t}{V_b}\right)}{K_v\left(\frac{V_t}{V_b}\right)}\right] \tag{10.2}$$

If liquid-liquid extraction stages are conducted in series, each with a volume ratio of 4.0, three stages are required to attain 4.8 $\log_{10}$ viral clearance (a good LVC value) when the viral partition coefficient in each stage is $K_v = 6 \times 10^{-3}$. In addition, an 89% yield of the protein at the end of the three stages can be attained if the protein partition coefficient in each stage is K_p=6.7. This yield is much better than a yield of 43% that is predicted based on the protein partition coefficient of K_p=0.78, which was measured for lysozyme in the absence of SDS (see Chapter 6). A schematic representation of these possible extractions in series is shown in Figure 10-1. Accordingly, future experiments involving extractions in series should be conducted to test this potential for using these mixed micellar systems. Cheaper surfactant alternatives, such as a crude mixture of C_iE_j surfactants, and other net positively-charged proteins should also be investigated in these extractions.

Purifying a Protein from a Fermentation Broth

Since two-phase aqueous mixed ("noncharged"/ionic) micellar systems have been able to attain a practically desirable protein partition coefficient (K_p=6.7), their ability to quickly purify a protein from a fermentation broth should be investigated in the future. Quick purification and concentration of a desired protein can lead to reduction in capital cost, residence time, and cost associated with product loss. In addition, if an anionic surfactant is used, it may repel the highly negatively-charged DNA into the micelle-poor phase away from the desired protein. However, before conducting any such separation experiment, the partitioning of other biomolecules, including DNA and cells, should be investigated individually in the two-phase aqueous mixed ("noncharged"/ionic) micellar systems to determine the partitioning behavior of each biomolecule in the absence of other components.

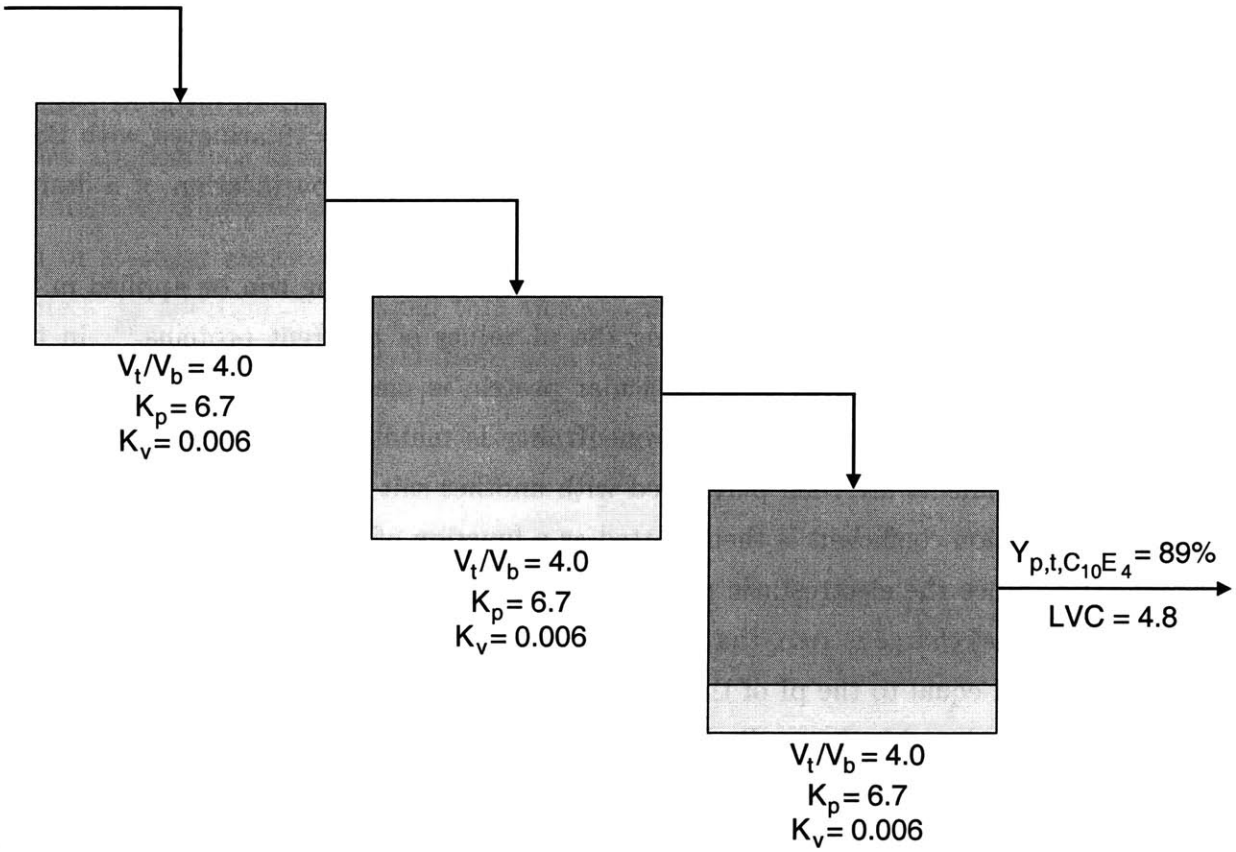

Figure 10-1: Schematic representation of using liquid-liquid extractions in series. For a volume ratio of 4.0 in each liquid-liquid extraction stage, 89% yield of the protein in the final top phase and 4.8 $\log_{10}$ of viral clearance can be achieved if the protein and viral partition coefficients are 6.7 and 6×10^{-3}, respectively, in each stage.

10.2.3 Varying the Solution pH and the Salt Governing Electroneutrality

As shown in the preliminary investigation of Appendix E, the protein partition coefficient can be manipulated by varying the solution pH and the salt governing electroneutrality. Therefore, these changes in the solution conditions may be used in the future to achieve good protein purification. Accordingly, a systematic experimental investigation of pH and salt effects can be performed in the future with different water-soluble proteins, including glucose-6-phosphate dehydrogenase (see Appendix F). For example, the salt ions can be varied based on the Hofmeister series of ions.[75,129–132] For example, some of the salts that may be examined include Na_2SO_4, NaF, NaCl, $NaClO_4$, NaBr, $NaNO_3$, and NaI. If practically desirable protein partition coefficients can be attained, such as K_p=19 achieved with BSA, varying these solution conditions in the future may yield a good purification of a desired protein directly from a fermentation broth.

In addition, an experimental method known as cross-partitioning can be applied in the future as another technique for determining the pI values of different proteins.[75] In this method, the partition coefficient of a particular protein is measured at different solution pH values, while the salt governing electroneutrality is maintained constant. The same partitioning experiments are then performed with another salt governing electroneutrality. The protein partition coefficient is then plotted as a function of the solution pH for the two different salts. Since the electrostatic potential difference has no effect on the partitioning protein when its net charge is zero, that is, at the pI of the protein, the two curves will cross at the solution pH equal to the pI of the protein.

The theory developed in Appendix E has been expressed in terms of interaction parameters, which cannot yet be theoretically estimated. In the future, the theory may be extended, so that the interaction parameters can be predicted based on the properties of the salt ions and the surfactants. Specifically, the ion-dipole, ion-induced dipole, and van der Waals interactions may be quantified based on estimates of the dielectric constants present in the interior of the salt ions and the surfactants.

10.2.4 Partitioning in Two-Phase Aqueous Polymer/Surfactant Systems

Although protein partitioning has been investigated experimentally in two-phase aqueous polymer/surfactant systems,[109,133] theoretical research in this area is still rather new, and may be considered in future investigations. In addition, viral partitioning has not yet been examined experimentally in these systems, and therefore, may also be considered as part of future work. In these systems, an aqueous solution containing polymer (for example,

dextran) and surfactant (for example, $C_{12}E_5$) phase separate when they are mixed together in certain proportions.[133,134] In the case of the two-phase aqueous dextran/$C_{12}E_5$ system, the homogeneous solution phase separates to form a top phase that is rich in $C_{12}E_5$ micelles and a bottom phase that is rich in dextran.[133]

10.3 Concluding Remarks

A fundamental investigation of protein and viral partitioning in two-phase aqueous micellar systems has been presented in this thesis. It is hoped that this understanding can be used to facilitate the implementation of two-phase aqueous micellar systems for the different applications that require the separation of proteins from viruses. Specifically, the entrainment of micelle-poor domains in the macroscopic, micelle-rich phase may be reduced, and/or stronger electrostatic interactions between mixed micelles and proteins may be exploited. In addition, it is hoped that this thesis can provide valuable information for new research conducted in the separations area utilizing two-phase aqueous micellar systems.

APPENDICES

Appendix A

Recipes for the Solutions Used in the Plaque Assay

This appendix lists the ingredients used to prepare the solutions for the plaque assay. In the Department of Biology at MIT, the workers in the media room ("the kitchen") of Building 68 make all these solutions for the researchers in the building.

- Dilution Fluid
  - 0.097 wt% Tryptone
  - 0.68 wt% NaCl
  - 1.9 wt% $MgSO_4$-$7H_2O$
  - 97 wt% Water
- Hard Agar
  - 0.97 wt% Agar
  - 0.97 wt% Tryptone
  - 0.48 wt% Yeast Extract
  - 0.48 wt% NaCl
  - 0.0039 wt% NaOH
  - 97 wt% Water

- Soft Agar
  - 0.78 wt% Luria Broth
  - 0.49 wt% NaCl
  - 0.64 wt% Agar
  - 98 wt% Water
- Luria Broth
  - 0.98 wt% Tryptone
  - 0.49 wt% Yeast Extract
  - 0.49 wt% NaCl
  - 0.016 wt% NaOH
  - 98 wt% water

  It should be noted that Luria broth is also used to grow the host bacterium of bacteriophage P22, *Salmonella typhimurium.*

Appendix B

Estimating the Densities of the Micelle-Poor Phase and the Micelle-Rich Phase

In this appendix, the densities of the micelle-poor phase (ρ_{in}) and of the micelle-rich phase (ρ_{out}) are estimated. Either density (ρ_{in} or ρ_{out}) can be written as follows:

$$\rho_j = \frac{n_{s,j}M_s + n_{w,j}M_w}{n_{s,j}\bar{V}_{s,j} + n_{w,j}\bar{V}_{w,j}} \tag{B.1}$$

where the subscript j denotes either the micelle-rich (in) or the micelle-poor (out) phase, $n_{s,j}$ and $n_{w,j}$ are the number of moles of surfactant and water, respectively, in phase j, M_s and M_w are the molecular weights of the surfactant and water, respectively, and $\bar{V}_{s,j}$ and $\bar{V}_{w,j}$ are the partial molar volumes of surfactant and water, respectively, in phase j. Since the weight fractions of surfactant in the micelle-poor and the micelle-rich phases, $\omega_{s,in}$ and $\omega_{s,out}$, are known from the coexistence curve of the $C_{10}E_4$-buffer system, an expression for $n_{s,j}$ as a function of $\omega_{s,j}$ will now be derived. The weight fraction of surfactant in phase j is given by the following equality:

$$\omega_{s,j} = \frac{n_{s,j}M_s}{n_{w,j}M_w + n_{s,j}M_s} \tag{B.2}$$

Equation (B.2) can be rearranged to yied:

$$n_{s,j} = \frac{n_{w,j}\omega_{s,j}}{1-\omega_{s,j}}\frac{M_w}{M_s} \tag{B.3}$$

Substituting Eq. (B.3) in Eq. (B.2) and rearranging yields:

$$\rho_j = \frac{M_w}{(M_w/M_s)\omega_{s,j}\bar{V}_{s,j} + (1-\omega_{s,j})\bar{V}_{w,j}} \tag{B.4}$$

In some of the bacteriophage P22 partitioning experiments, the weight fractions of the $C_{10}E_4$ surfactant in the micelle-poor phase (in) and the micelle-rich phase (out) were approximately 0.001 and 0.1, respectively. The molecular weights of water and $C_{10}E_4$ surfactant are 18 g/mole and 334.50 g/mole, respectively. The partial molar volumes of each component will be assumed to be equal to the molar volumes of the pure components, that is, $\bar{V}_{w,j} \approx V_w$=18 mL/mole and $\bar{V}_{s,j} \approx V_s$=350 mL/mole. Accordingly, ρ_{in} = 0.99995 g/mL, and ρ_{out} = 0.99539 g/mL.

Appendix C

Pseudo-Binary and Pseudo-Ternary Systems

This appendix provides the justification for treating: (i) the $C_{10}E_4$-buffer system as a pseudo-binary system (see the discussion in Chapters 5 and 7), and (ii) the $C_{10}E_4$-SDS-buffer system as a pseudo-ternary system (see the discussion in Chapter 7).

C.1 The Pseudo-Binary $C_{10}E_4$-Buffer System

As discussed in Section 5.4.4, the $C_{10}E_4$-buffer system is strictly not a binary system, and is instead composed of four components, namely, water, $C_{10}E_4$, disodium phosphate, and citric acid. However, fewer experiments are required to locate tie lines on a pseudo-binary coexistence curve than on a four-component coexistence curve, and therefore, it is experimentally advantageous to use a pseudo-binary coexistence curve whenever it is applicable. To illustrate the issues associated with using a pseudo-binary coexistence curve for a four-component system, a brief discussion of the thermodynamics of multiphase, simple systems will be presented below.

For multi-phase, simple systems, the Gibbs phase rule can be used to determine the number of degrees of freedom, or number of independent intensive variables, L. Specifically,[111]

$$L = n + 2 - \pi \tag{C.1}$$

where n is the number of components and π is the number of phases in the system. For a four component ($n = 4$), two-phase ($\pi = 2$) system (such as the $C_{10}E_4$-buffer system), four ($L = 4$) intensive variables must be specified to determine a point on the coexistence curve or phase boundary. The coexistence curves in Figure 4-1 are still consistent with the Gibbs phase rule because each point on the coexistence curve can be specified with four intensive variables of pressure (1 atm), disodium phosphate concentration (16.4 mM), citric acid concentration (1.82 mM), and temperature. However, the curve must be tested

to determine whether it can be used to identify tie lines. When a horizontal tie line at a particular temperature is drawn on the coexistence curve, the disodium phosphate and citric acid concentrations in both phases are assumed to be equal to each other at values of 16.4 mM and 1.82 mM, respectively, since the entire curve was constructed at these salt concentrations. Although the temperature and pressure of the system can be manipulated, the concentrations of disodium phosphate and citric acid cannot be forced to take on certain values in the top and bottom phases after the system undergoes phase separation. These third and fourth degrees of freedom usually cannot be fixed by the experimentalist, and therefore, they are generally free to vary for any phase-separation process. Accordingly, a four-component coexistence curve is generally required where the concentrations of disodium phosphate and citric acid are allowed to take on multiple values. However, for the special case where both disodium phosphate and citric acid partition evenly between the two coexisting phases (which happens to be true in this system as discussed on the next page), a four-component coexistence curve is not necessary because the third and fourth degrees of freedom can actually be manipulated, as will now be shown. When disodium phosphate (DP) and citric acid (CA) partition evenly,

$$C_{DP,t} = C_{DP,b} \tag{C.2}$$

and

$$C_{CA,t} = C_{CA,b} \tag{C.3}$$

where $C_{DP,t}$ and $C_{DP,b}$ are the concentrations of disodium phosphate in the top and bottom phases, respectively, and $C_{CA,t}$ and $C_{CA,b}$ are the concentrations of citric acid in the top and bottom phases, respectively.

Mass balance equations can also be written for these components as follows:

$$C_{DP,0}(V_t + V_b) = C_{DP,t}V_t + C_{DP,b}V_b \tag{C.4}$$

and

$$C_{CA,0}(V_t + V_b) = C_{CA,t}V_t + C_{CA,b}V_b \tag{C.5}$$

where $C_{DP,0}$ and $C_{CA,0}$ are the initial concentrations of disodium phosphate and citric acid, respectively. Combining Eqs. (C.2) and (C.4) and Eqs. (C.3) and (C.5) yields the following equalities:

$$C_{DP,0} = C_{DP,t} = C_{DP,b} \tag{C.6}$$

and

$$C_{CA,0} = C_{CA,t} = C_{CA,b} \tag{C.7}$$

Accordingly, if disodium phosphate and citric acid partition evenly, the disodium phosphate and citric acid concentrations in the top and bottom phases are equal to their initial concentrations, which can be easily manipulated. If the intial concentrations of disodium phosphate and citric acid are 16.4 mM and 1.82 mM, respectively, the coexistence curves of Figure 4-1 can be used. Therefore, for this special case, the third and fourth degrees of freedom (C_{DP} and C_{CA}) can also be controlled. In other words, a pseudo-binary coexistence curve is sufficient because the experimentalist can ensure that all four degrees of freedom in each phase are consistent with the conditions that are represented in the pseudo-binary coexistence curve.

To test whether or not the pseudo-binary coexistence curve is indeed applicable to the four-component system (that is, to test if disodium phosphate and citric acid partition evenly between the two phases), the lever rule is used along with phase separation experiments. The lever rule is simply another representation of the mass balances for the components. Specifically, the mass balance for any component i can be written as follows:

$$C_{i,0}\,(V_t + V_b) = C_{i,t}V_t + C_{i,b}V_b \tag{C.8}$$

where $C_{i,0}$ is the initial concentration of component i, and $C_{i,t}$ and $C_{i,b}$ are the concentrations of component i in the top and bottom phases, respectively. Solving Eq. (C.8) for the volume ratio yields:

$$\frac{V_t}{V_b} = \frac{C_{i,0} - C_{i,b}}{C_{i,t} - C_{i,0}} \tag{C.9}$$

Equation (C.9) states that the volume ratio can be predicted if the initial concentration of one component is known, and if the concentrations of that component in the two phases after phase separation are known, that is, if the tie line is known. Therefore, in this test, a tie line is first drawn on the pseudo-binary coexistence curve. With this tie line, $C_{C_{10}E_4,t}$ and $C_{C_{10}E_4,b}$ can be determined, and after selecting a particular value for $C_{C_{10}E_4,0}$, a volume ratio can be predicted. Then, the experiment is performed at the particular temperature, pressure, 16.4 mM disodium phosphate concentration, 1.82 mM citric acid concentration, and $C_{C_{10}E_4,0}$. If the predicted and experimental volume ratios are similar, the pseudo-binary coexistence curve is sufficient for determining tie lines, and disodium phosphate and citric acid partition evenly. These tests have been conducted for the pseudo-binary coexistence curve of the $C_{10}E_4$-buffer system, and have been used to prove that the pseudo-binary coexistence curve

is indeed sufficient. It is also physically intuitive that the partition coefficients of these salts are close to 1 because the salt ions are small enough that they do not experience strong excluded-volume interactions with the micelles in either phase. In addition, since the salt ions are not hydrophobic, they also do not experience strong hydrophobic interactions with the micelles that would drive them into the micelle-rich phase.

As an aside, it should be noted that if disodium phosphate and citric acid partition evenly, Eq. (C.9) for these salts simplifies to:

$$\frac{V_t}{V_b} = \frac{0}{0} \tag{C.10}$$

because Eqs. (C.6) and (C.7) apply in this case. Eq. (C.10) is obtained because the mass balance of an evenly partitioning component enforces no constraint on the volume ratio. In other words, an evenly partitioning component will always fulfill its mass balance for any volume ratio. This is therefore another way to explain why a pseudo-binary coexistence curve is sufficient for four-component systems in which two of the components partition evenly.

The addition of a protein to this system also increases the number of degrees of freedom by one. However, in our partitioning experiments, a very low concentration of protein was used to ensure that it had no effect on the coexistence curve, that is, on the phase separation process of the $C_{10}E_4$-buffer system. This was verified experimentally by mapping the coexistence curve of the $C_{10}E_4$-buffer system in the presence of different concentrations of proteins, as was done previously.[70,71,73,78] Therefore, for the range of protein concentrations encountered in our partitioning experiments, the coexistence curve of the $C_{10}E_4$-buffer system remained unperturbed. Similar experiments were also conducted with $MgSO_4$ and bacteriophage P22 that demonstrated that the phase separation process of the $C_{10}E_4$-buffer system was unaffected by the presence of 2 mM $MgSO_4$ and the range of viral concentrations utilized in our partitioning experiments.

C.2 The Pseudo-Ternary $C_{10}E_4$-SDS-Buffer System

In a method similar to the one described above for the $C_{10}E_4$-buffer system, the pseudo-ternary coexistence curve of the $C_{10}E_4$-SDS-buffer system was also shown to be sufficient for the five-component (water, $C_{10}E_4$, SDS, disodium phosphate, and citric acid) system, and for the six-component (with added protein) system.

Appendix D

Derivation of an Expression for the Protein Chemical Potential Using the Number Density as the Unit of Concentration

Various issues associated with changing the concentration units in the expression for the protein chemical potential from mole fractions to number densities, that is, molecules/mL, are detailed in this appendix. The approach taken in this derivation is similar to that of Kirkwood and Oppenheim.[112] The chemical potential of a protein in phase α (top or bottom), $\mu_{p,\alpha}$, is given by:

$$\mu_{p,\alpha} = \mu^{\circ}_{p,\infty} + k_B T \ln X_{p,\alpha} + \mu^{ex}_{p,\alpha} + z_{p,\alpha} e \psi_{\alpha} \tag{D.1}$$

where $\mu^{\circ}_{p,\infty}$ is the infinitely-dilute standard-state chemical potential of the protein, k_B is the Boltzmann constant, T is the absolute temperature, $X_{p,\alpha}$ is the mole fraction of the protein in phase α, $\mu^{ex}_{p,\alpha}$ is the excess chemical potential of the protein in phase α, $z_{p,\alpha}$ is the valence of the protein in phase α, e is the electronic charge, and ψ_{α} is the electrostatic or electrical potential of phase α. The infinitely-dilute standard-state chemical potential of the protein, $\mu^{\circ}_{p,\infty}$, corresponds to a standard state in which there is essentially only one protein molecule in a container filled with solvent molecules. Accordingly, (i) the protein and the solvent are the only two components present, (ii) the protein molecule interacts only with the solvent molecules, (iii) the solvent molecules interact with each other, and (iv) there is no mixing entropy associated with the protein in this standard state. The interactions included in $\mu^{\circ}_{p,\infty}$ are all accounted for at the temperature and pressure of the system. The $k_B T \ln X_{p,\alpha}$ term, as derived from statistical thermodynamics, is the ideal entropy term. The excess chemical potential of the protein in phase α accounts for: (i) the interactions not incorporated in the standard-state chemical potential, such as, protein-micelle interactions, and (ii) any non-

idealities in the entropy. The $z_{p,\alpha}e\psi_\alpha$ term is the electrostatic potential energy of the protein in phase α. It is analogous to the gravitational potential energy, where the charge of the protein ($z_{p,\alpha}e$) is analogous to the mass of an object (m), and the electrostatic potential of phase α (ψ_α) is analogous to the gravitational acceleration (g).

It is important to note that the excess chemical potential of the protein in phase α, $\mu_{p,\alpha}^{ex}$, is the deviation of the actual chemical potential of the protein in phase α, $\mu_{p,\alpha}$, from the generalized ideal chemical potential of the protein in phase α, $\mu_{p,\alpha}^{id}$, which is given by:[111,112]

$$\mu_{p,\alpha}^{id} = \mu_{p,\infty}^{\circ} + k_B T \ln X_{p,\alpha} + z_{p,\alpha}e\psi_\alpha \tag{D.2}$$

Therefore, Eq. (D.1) can also be written as follows:

$$\mu_{p,\alpha} = \mu_{p,\alpha}^{id} + \mu_{p,\alpha}^{ex} \tag{D.3}$$

According to Eq. (D.3), if an expression for $\mu_{p,\alpha}^{ex}$ is derived, it must be added to the expression for $\mu_{p,\alpha}^{id}$ provided in Eq. (D.2) to obtain $\mu_{p,\alpha}$. Although, at first sight, it may appear that Eq. (D.2) is based on the use of mole fraction units, this is, in fact, not the case. Indeed, alternative expressions for $\mu_{p,\alpha}^{id}$ can be derived by making substitutions for the mole fractions in terms of different concentration units. In our case, the number density (molecules/mL) is used as the unit of concentration, and therefore, an equivalent expression for $\mu_{p,\alpha}^{id}$ will now be derived in terms of the number density. An expression for the mole fraction of the protein in phase α, $X_{p,\alpha}$, in terms of the number density of the protein in phase α, $C_{p,\alpha}$, is first required. This relation is given by:

$$X_{p,\alpha} = C_{p,\alpha}\frac{\sum_j N_{j,\alpha}\overline{v}_{j,\alpha}}{N_{tot,\alpha}} = C_{p,\alpha}\sum_j X_{j,\alpha}\overline{v}_{j,\alpha} \tag{D.4}$$

where $N_{j,\alpha}$ is the number of molecules of type j in phase α, $\overline{v}_{j,\alpha}$ is the partial molecular volume of molecules of type j in phase α in mL/molecule, $N_{tot,\alpha}$=$\sum_j N_{j,\alpha}$ is the total number of molecules in phase α, and $X_{j,\alpha}$ is the mole fraction of molecules of type j in phase α. Note that $\sum_j N_{j,\alpha}\overline{v}_{j,\alpha}$ in Eq. (D.4) is the total volume of phase α in mL. Equation (D.4) can be rewritten as follows:

$$X_{p,\alpha} = C_{p,\alpha}X_{p,\alpha}\overline{v}_{p,\alpha} + C_{p,\alpha}\sum_{k\neq p} X_{k,\alpha}\overline{v}_{k,\alpha} \tag{D.5}$$

where $\overline{v}_{p,\alpha}$ is the partial molecular volume of the protein in phase α in mL/molecule, $X_{k,\alpha}$ is the mole fraction of non-protein molecules of type k in phase α, and $\overline{v}_{k,\alpha}$ is the partial

molecular volume of non-protein molecules of type k in phase α in mL/molecule. Note that the index k is used here to denote non-protein molecules, while the index j is used to denote all molecules including proteins. Rearranging Eq. (D.5) yields:

$$X_{p,\alpha} = \frac{C_{p,\alpha}}{1 - C_{p,\alpha}\overline{v}_{p,\alpha}} \sum_{k \neq p} X_{k,\alpha}\overline{v}_{k,\alpha} \tag{D.6}$$

The mole fraction of non-protein molecules in phase α, $X_{k,\alpha}$, can be expressed in terms of the number density of non-protein molecules of type k in phase α, $C_{k,\alpha}$, as follows:

$$X_{k,\alpha} = \frac{N_{k,\alpha}}{\sum_j N_{j,\alpha}} \frac{\left(1/\sum_j N_{j,\alpha}\overline{v}_{j,\alpha}\right)}{\left(1/\sum_j N_{j,\alpha}\overline{v}_{j,\alpha}\right)} = \frac{C_{k,\alpha}}{\sum_j C_{j,\alpha}} \tag{D.7}$$

where $N_{k,\alpha}$ is the number of non-protein molecules of type k in phase α, and $C_{j,\alpha}$ is the number density of molecules of type j in phase α. Substituting Eq. (D.7) in Eq. (D.6) yields:

$$X_{p,\alpha} = \frac{C_{p,\alpha}}{1 - C_{p,\alpha}\overline{v}_{p,\alpha}} \frac{\sum_{k \neq p} C_{k,\alpha}\overline{v}_{k,\alpha}}{\sum_j C_{j,\alpha}} \tag{D.8}$$

Multiplying Eq. (D.8) by 1 in the form of $(C_p^\circ \Omega_w / C_p^\circ \Omega_w)$, and rearranging then yields the following relation:

$$X_{p,\alpha} = \left(\frac{C_{p,\alpha}}{C_p^\circ}\right)\left(C_p^\circ \Omega_w\right)\left[\frac{1}{\Omega_w\left(1 - C_{p,\alpha}\overline{v}_{p,\alpha}\right)} \frac{\sum_{k \neq p} C_{k,\alpha}\overline{v}_{k,\alpha}}{\sum_j C_{j,\alpha}}\right] \tag{D.9}$$

where $C_p^\circ = 1$ protein molecule/mL, and Ω_w is the molecular volume of pure solvent in mL/molecule that is only a function of the temperature and the pressure of the system. An alternative expression for $\mu_{p,\alpha}^{id}$ can now be obtained in terms of the number density by substituting Eq. (D.9) into Eq. (D.2):

$$\begin{aligned} \mu_{p,\alpha}^{id} &= \mu_{p,\infty}^\circ + k_B T \ln\left(C_p^\circ \Omega_w\right) + k_B T \ln\left(\frac{C_{p,\alpha}}{C_p^\circ}\right) \\ &\quad + k_B T \ln\left[\frac{1}{\Omega_w\left(1 - C_{p,\alpha}\overline{v}_{p,\alpha}\right)} \frac{\sum_{k \neq p} C_{k,\alpha}\overline{v}_{k,\alpha}}{\sum_j C_{j,\alpha}}\right] + z_{p,\alpha} e \psi_\alpha \end{aligned} \tag{D.10}$$

A new standard-state chemical potential of the protein, μ_p°, will be defined as follows:

$$\mu_p^\circ \equiv \mu_{p,\infty}^\circ + k_B T \ln\left(C_p^\circ \Omega_w\right) \tag{D.11}$$

where μ_p° is similar to $\mu_{p,\infty}^\circ$ in that it is only a function of the temperature and the pressure

of the system. This standard-state chemical potential of the protein, μ_p°, corresponds to a standard state in which: (i) the protein and the solvent are the only two components present, (ii) the protein molecules interact with the solvent molecules but not with each other, (iii) the solvent molecules interact with each other, *and* (iv) the concentration of the protein is 1 molecule/mL, and therefore, has an ideal entropy corresponding to this concentration. This ideal entropy corresponds to the term $k_B T \ln\left(C_p^\circ \Omega_w\right)$ in Eq. (D.11) as will now be shown. The volume of the solution in the standard state is essentially equal to the volume of the solvent when the concentration of the solute (the protein) is only 1 molecule/mL. Consequently, C_p° can be approximated as follows:

$$C_p^\circ = 1 \; molecule/mL \; of \; solution \approx 1 \; molecule/mL \; of \; solvent \tag{D.12}$$

In addition, since 1 molecule/mL is an extremely dilute concentration for the solute in this standard state, the partial molecular volume of the solvent in the standard state is essentially equal to the pure molecular volume of the solvent. Specifically, the partial molecular volume of the solvent in the standard state in mL/molecule, $\overline{v}_w^\circ$, is given by:

$$\overline{v}_w^\circ = \Omega_w \tag{D.13}$$

Therefore, $C_p^\circ \Omega_w$ is equal to the number of protein molecules divided by the number of solvent molecules in the standard state. Since the total number of molecules is also essentially equal to the number of solvent molecules in this standard state, $C_p^\circ \Omega_w$ is essentially equal to the number of protein molecules divided by the total number of molecules, that is, it is essentially equal to the mole fraction of protein molecules in the standard state. Accordingly, $k_B T \ln\left(C_p^\circ \Omega_w\right)$ in Eq. (D.11) is the ideal entropy of the protein in the standard state, where the concentration of the protein is equal to C_p°=1 molecule/mL.

A different expression for $\mu_{p,\alpha}$ in terms of number densities can now be derived. In particular, combining Eqs. (D.3), (D.10), and (D.11) yields:

$$\begin{aligned} \mu_{p,\alpha} &= \mu_p^\circ + k_B T \ln\left(\frac{C_{p,\alpha}}{C_p^\circ}\right) + k_B T \ln\left[\frac{1}{\Omega_w\left(1 - C_{p,\alpha}\overline{v}_{p,\alpha}\right)} \frac{\sum_{k \neq p} C_{k,\alpha}\overline{v}_{k,\alpha}}{\sum_j C_{j,\alpha}}\right] \\ &\quad + z_{p,\alpha} e \psi_\alpha + \mu_{p,\alpha}^{ex} \end{aligned} \tag{D.14}$$

Since C_p° is 1 protein molecule/mL, Eq. (D.14) then simplifies to:

$$\begin{aligned}\mu_{p,\alpha} &= \mu_p^\circ + k_B T \ln C_{p,\alpha} + k_B T \ln \left[\frac{1}{\Omega_w \left(1 - C_{p,\alpha}\overline{v}_{p,\alpha}\right)} \frac{\sum_{k\neq p} C_{k,\alpha}\overline{v}_{k,\alpha}}{\sum_j C_{j,\alpha}} \right] \\ &\quad + z_{p,\alpha} e\psi_\alpha + \mu_{p,\alpha}^{ex} \end{aligned} \tag{D.15}$$

where $C_{p,\alpha}$ must be expressed in units of the number density (protein molecules/mL of solution). Next, it will be shown that the bracketed term in Eq. (D.15), defined as $\lambda_{p,\alpha}$ below,

$$\lambda_{p,\alpha} \equiv k_B T \ln \left[\frac{1}{\Omega_w \left(1 - C_{p,\alpha}\overline{v}_{p,\alpha}\right)} \frac{\sum_{k\neq p} C_{k,\alpha}\overline{v}_{k,\alpha}}{\sum_j C_{j,\alpha}} \right] \tag{D.16}$$

is essentially zero for the case considered in Chapter 7, which validates neglecting $\lambda_{p,\alpha}$ in Eq. (7.5). Since the partition coefficient is strictly defined in the limit of infinite dilution, each phase is considered to be infinitely dilute in protein (which also reflects what is attained experimentally), and accordingly, the following approximations can be made:

$$\left(1 - C_{p,\alpha}\overline{v}_{p,\alpha}\right) \approx 1 \tag{D.17}$$

and

$$\sum_{k\neq p} C_{k,\alpha}\overline{v}_{k,\alpha} = \frac{\sum_{k\neq p} N_{k,\alpha}\overline{v}_{k,\alpha}}{V_\alpha} \approx \frac{V_\alpha}{V_\alpha} = 1 \tag{D.18}$$

and

$$\sum_j C_{j,\alpha} \approx \sum_{k\neq p} C_{k,\alpha} \tag{D.19}$$

Combining Eqs. (D.16), (D.17), (D.18), and (D.19) yields:

$$\lambda_{p,\alpha} = k_B T \ln \left[\frac{1}{\Omega_w} \frac{1}{\sum_{k\neq p} C_{k,\alpha}} \right] \tag{D.20}$$

Although the buffer salt ions have been lumped along with the water molecules to form a hypersolvent in Chapter 7, they will be treated explicitly in this appendix as a worst case scenario in the proof to show that $\lambda_{p,\alpha}$ is essentially zero. In addition, as part of the worst case scenario, the surfactant monomers have also been considered explicitly in this appendix.

Considering all the components present in the solution, Eq. (D.20) can be rewritten as follows:

$$\lambda_{p,\alpha} = k_B T \ln \left[\frac{1}{\Omega_w} \frac{1}{C_{w,\alpha} + C_{1,\alpha} + \sum_{n_\alpha = n^\circ_{cyl,\alpha}}^{\infty} C_{n_\alpha} + C_{Na,\alpha} + C_{H,\alpha} + C_{HPO_4,\alpha} + C_{Cit,\alpha} + C_{OH,\alpha}} \right] \tag{D.21}$$

where $C_{w,\alpha}$, $C_{1,\alpha}$, $C_{n,\alpha}$, $C_{Na,\alpha}$, $C_{H,\alpha}$, $C_{HPO_4,\alpha}$, $C_{Cit,\alpha}$, and $C_{OH,\alpha}$ are the concentrations of water, free surfactant monomer (not in a micelle), micelles of aggregation number n, Na^+, H^+, HPO_4^{-2}, citrate, and OH^-, all in phase α, respectively, and $n^\circ_{cyl,\alpha}$ is the aggregation number of the smallest cylindrical micelle in phase α. In order to show that $\lambda_{p,\alpha}$ is zero, one needs to show that $\sum_{k \neq p} C_{k,\alpha} \approx C_{w,\alpha}$, since the following approximation is reasonable for dilute solutions where mixing volume effects are negligible:[55,74,113]

$$C_{w,\alpha} \approx 1/\Omega_w \tag{D.22}$$

Indeed, if $\sum_{k \neq p} C_{k,\alpha} \approx C_{w,\alpha} \approx 1/\Omega_w$, then using this result in Eq. (D.20) yields:

$$\lambda_{p,\alpha} = k_B T \ln \left[\frac{1}{\Omega_w} \Omega_w \right] = 0 \tag{D.23}$$

which is the desired result. Therefore, in order to prove that $\lambda_{p,\alpha}$ is indeed zero, estimations for the number density of water, surfactant monomers, micelles, and the ions in the partitioning solutions are required. The value of $C_{w,\alpha}$ was estimated as 3.4×10^{22} molecules/mL based on the molecular weight of water (18 g/mol) and the density of water (1 g/mL). For the ions, their concentrations were estimated in Appendix E, and they are repeated for completeness in Table D-1:

Table D-1: Ion concentrations in phase α.

Ion in Phase α	**Concentration (ions/mL)**
Na^+	2.0×10^{19}
H^+	3.8×10^{13}
HPO_4^{-2}	9.9×10^{18}
Citrate	1.1×10^{18}
OH^-	9.6×10^{13}

All of the surfactant present in the solution will be assumed to be that of $C_{10}E_4$ alone, since the concentration of $C_{10}E_4$ is much higher than that of SDS. Accordingly, the concentra-

tion of the free $C_{10}E_4$ monomers is approximately equal to the critical micelle concentration, which is 0.68 mM at 25°C for $C_{10}E_4$ in water.[95] Therefore, $C_{1,\alpha}$ is approximately equal to 3.7×10^{17} free monomers/mL. For the $C_{10}E_4$ micelles, the worst case scenario will be assumed, where the number density of the $C_{10}E_4$ micelles is the largest. This scenario corresponds to a hypothetical situation where all the micelles are spherical. When the micelles are spheres, they have the lowest possible aggregation number, since more $C_{10}E_4$ monomers are required to form cylinders. Consequently, the concentration of micelles would be at a maximum if all the micelles were spherical. Since the highest concentration of $C_{10}E_4$ encountered in any phase has been 10 wt% or 1.8×10^{20} $C_{10}E_4$ molecules/mL, the concentration of spherical micelles in this hypothetical scenario is given by:

$$C_{hyp} = \frac{1.8 \times 10^{20} - 3.7 \times 10^{17}}{n_{sph,C_{10}E_4}} \tag{D.24}$$

where $n_{sph,C_{10}E_4}$ is the aggregation number of the spherical micelles, and 3.7×10^{17} is the number density of free monomers as discussed above. An estimate for $n_{sph,C_{10}E_4}$ is therefore necessary, and $n_{sph,C_{10}E_4}$ can be evaluated as follows:

$$n_{sph,C_{10}E_4} = \frac{(4/3)\,\pi l^3_{c,sph,C_{10}E_4}}{v_{tail,C_{10}E_4}} \tag{D.25}$$

where $l_{c,sph,C_{10}E_4}$ is the length of the hydrophobic tail in the $C_{10}E_4$ spherical micelle (that is, the radius of the hydrophobic core of the $C_{10}E_4$ spherical micelle), and $v_{tail,C_{10}E_4}$ is the volume of the hydrophobic tail of the $C_{10}E_4$ molecule. A value for $l_{c,sph,C_{10}E_4}$ can be estimated with the maximum length of the hydrocarbon tail of $C_{10}E_4$, $l_{max,C_{10}E_4}$, which can be evaluated using the following relation:[53]

$$l_{max,tail} = 1.54 + 1.265\,(n_c - 1)\,, \text{ in Å} \tag{D.26}$$

where $l_{max,tail}$ is the maximum length of any linear hydrocarbon tail (without double or triple bonds) in Ångstroms, and n_c is the number of carbons in the hydrocarbon tail of interest. Accordingly,

$$l_{c,sph,C_{10}E_4} \approx l_{max,C_{10}E_4,tail} = 12.9 \text{ Å} \tag{D.27}$$

The volume of the hydrophobic tail of $C_{10}E_4$ in units of $Å^3$, on the other hand, can be

evaluated using the following relation:[53]

$$v_{tail} = 27.4 + 26.9\,(n_c - 1)\,, \text{ in Å}^3 \tag{D.28}$$

Therefore, for $C_{10}E_4$, $v_{tail,C_{10}E_4}$ is 270Å^3. Using these values of $l_{c,sph,C_{10}E_4}$ and $v_{tail,C_{10}E_4}$ in Eq. (D.25), $n_{sph,C_{10}E_4}$ is estimated to be 33. Substituting this value of $n_{sph,C_{10}E_4}$ into Eq. (D.24) yields C_{hyp}=5.4 $\times$ 10^{18} spherical micelles/mL. Since the concentrations of all the other components (ions, free $C_{10}E_4$ monomers, and $C_{10}E_4$ micelles) are at least 3 orders of magnitude less than $C_{w,\alpha}$, to an excellent approximation, it follows that:

$$\sum_{k \neq p} C_{k,\alpha} \approx C_{w,\alpha} \tag{D.29}$$

and therefore, that the result in Eq. (D.23) is indeed valid. Consequently, $\lambda_{p,\alpha}$ was neglected in Eq. (7.5) in Chapter 7, since $\mu_{p,\alpha}$ can be written as follows:

$$\mu_{p,\alpha} = \mu_p^\circ + k_B T \ln C_{p,\alpha} + z_{p,\alpha} e\psi_\alpha + \mu_{p,\alpha}^{ex} \tag{D.30}$$

Appendix E

A Preliminary Investigation of the Possible Existence of an Electrostatic Potential Difference Between the Two Coexisting Macroscopic $C_{10}E_4$ Micellar Phases

E.1 Introduction

An electrostatic or electrical potential difference is generally present whenever there is an interface. For example, an electrostatic potential difference between two liquid phases has been observed in two-phase aqueous *polymer* systems.[75] Physically, the existence of an electrostatic potential difference can be understood as follows. When two liquid phases are in equilibrium with each other, the two macroscopic phases and the three-dimensional interfacial region, having a thickness of a few molecular diameters, are all electroneutral. However, the ions in the interfacial region, depending on their interactions with the two macroscopic phases, may orient in a non-uniform manner as shown schematically in Figure E-1a. Accordingly, there can be a net positive charge and a net negative charge on opposite sides of the two-dimensional model for the interface (see Figure E-1b for a schematic representation). An electrostatic potential difference can therefore exist across the interface, and the electrostatic potential energy associated with moving an ion from one macroscopic phase to the other may be significant.

In this appendix, the electrostatic potential difference in the $C_{10}E_4$-buffer two-phase system considered in this thesis will first be shown to be not so important. To demonstrate this, a theory will be developed, and the results of the theory will be compared to past partitioning data. The small or negligible potential difference is shown in Section E.2 to be associated with Na_2HPO_4 governing electroneutrality in each of the macroscopic $C_{10}E_4$

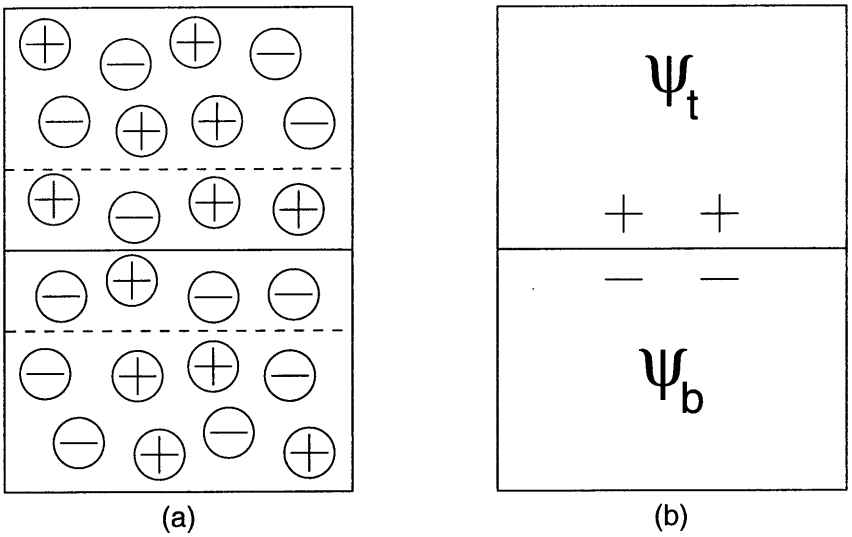

Figure E-1: Schematic representation of: (a) the orientation of positive and negative ions in the two macroscopic phases and the three-dimensional interfacial region, and (b) the net charges that may be present across the two-dimensional model for the liquid-liquid interface. The two dashed lines bound the three-dimensional interfacial region. The solid line represents the two-dimensional model for the interface. ψ_t and ψ_b correspond to the electrostatic or electrical potentials of the top and bottom macroscopic phases, respectively.

micellar phases. Accordingly, if another salt were to govern electroneutrality in each of the macroscopic $C_{10}E_4$ micellar phases, a significant electrostatic potential difference may exist. This possibility was also theoretically and experimentally investigated in this appendix.

The remainder of this appendix is organized as follows. In Section E.2, a theoretical analysis of the effect of an electrostatic potential difference between the two macroscopic $C_{10}E_4$ micellar phases is provided. Based on this analysis, experiments were designed, and Section E.3 describes the materials and experimental methods utilized in this study. In Section E.4, the experimental results are presented and discussed. Finally, concluding remarks are presented in Section E.5.

E.2 Theory

E.2.1 Incorporation of the Electrostatic Potential Difference in the Derivation of the Protein Partition Coefficient

In this section, the electrostatic potential difference between the two macroscopic $C_{10}E_4$ micellar phases will be incorporated into the derivation of the protein partition coefficient. It will then be shown that the electrostatic potential difference for the $C_{10}E_4$-buffer two-

phase system studied in this thesis, where Na_2HPO_4 governs electroneutrality, is not very important. However, a significant electrostatic potential difference can exist between the two macroscopic $C_{10}E_4$ micellar phases when another salt governs electroneutrality. This possibility was also analyzed theoretically in this section.

Since the proteins are allowed to partition over at least 14 hours in all the experiments, the establishment of diffusional equilibrium of the proteins between the two coexisting phases will be assumed. At equilibrium,[111]

$$\mu_{p,t} = \mu_{p,b} \tag{E.1}$$

where $\mu_{p,t}$ and $\mu_{p,b}$ are the chemical (or electrochemical) potentials of the protein in the top and bottom phases, respectively. After some simplification (see details in Appendix D), the chemical potential of the protein in each phase α can be written as follows:[112]

$$\mu_{p,\alpha} = \mu_p^\circ + k_B T \ln C_{p,\alpha} + \mu_{p,\alpha}^{ex} + z_{p,\alpha} e \psi_\alpha \tag{E.2}$$

where α is either top or bottom, μ_p° is the standard-state chemical potential of the protein, k_B is the Boltzmann constant, T is the absolute temperature, $C_{p,\alpha}$ is the number density (molecules/mL) of the protein in phase α, $\mu_{p,\alpha}^{ex}$ is the excess chemical potential of the protein in phase α, $z_{p,\alpha}$ is the valence or net charge of the protein in phase α, e is the electronic charge, and ψ_α is the electrostatic or electrical potential of phase α. The standard-state chemical potential of the protein is only a function of the temperature and the pressure. The excess chemical potential of the protein in phase α accounts for any interactions not accounted for in the standard-state chemical potential, such as, the protein-micelle interactions, and any non-idealities in the entropy. The $z_{p,\alpha} e \psi_\alpha$ term is the electrostatic potential energy of the protein in phase α.

Substituting Eq. (E.2) into Eq. (E.1), recognizing that $z_{p,t} = z_{p,b} = z_p$ since both phases have approximately equal pH values (which was later confirmed experimentally), and rearranging yields:

$$K_p \equiv \frac{C_{p,t}}{C_{p,b}} = \exp\left[\frac{-\left(\mu_{p,t}^{ex} - \mu_{p,b}^{ex}\right) - z_p e\left(\psi_t - \psi_b\right)}{k_B T}\right] \tag{E.3}$$

where K_p is the protein partition coefficient. Accordingly, an expression for the excess chemical potential of the protein in each phase is required, and can be obtained from an expression for the excess Gibbs free energy of each phase by taking the following partial derivative:[111]

$$\mu_{p,\alpha}^{ex} = \left(\frac{\partial G_\alpha^{ex}}{\partial N_{p,\alpha}}\right)_{T,P,N_{k,\alpha \neq p,\alpha}} \tag{E.4}$$

where G_α^{ex} is the excess Gibbs free energy of phase α, $N_{p,\alpha}$ is the number of protein molecules in phase α, $N_{k,\alpha\neq p,\alpha}$ is the number of non-protein molecules of type k in phase α, and T and P are the absolute temperature and the pressure in both phases. The excess Gibbs free energy in phase α will be assumed to result solely from the excluded-volume interactions between the proteins and the micelles, since the partition coefficients of water-soluble proteins have already been predicted reasonably well with this assumption.[70–74,78] Therefore, the excess Gibbs free energy in phase α is given by:

$$G_\alpha^{ex} = G_\alpha^{ex,EV} \tag{E.5}$$

where $G_\alpha^{ex,EV}$ accounts for the excluded-volume interactions between the proteins and the micelles that are not incorporated in the ideal Gibbs free energy. Combining Eqs. (E.3), (E.4), and (E.5) yields:

$$K_p = \exp\left[\frac{-\left(\mu_{p,t}^{ex,EV} - \mu_{p,b}^{ex,EV}\right)}{k_B T}\right] \exp\left[\frac{-z_p e\left(\psi_t - \psi_b\right)}{k_B T}\right] \tag{E.6}$$

where

$$\mu_{p,\alpha}^{ex,EV} = \left(\frac{\partial G_\alpha^{ex,EV}}{\partial N_{p,\alpha}}\right)_{T,P,N_{k,\alpha\neq p,\alpha}} \tag{E.7}$$

Equation (E.6) can further be rewritten as follows:

$$K_p = K_p^{EV} \exp\left[\frac{-z_p e\left(\psi_t - \psi_b\right)}{k_B T}\right] \tag{E.8}$$

where

$$K_p^{EV} = \exp\left[\frac{-\left(\mu_{p,t}^{ex,EV} - \mu_{p,b}^{ex,EV}\right)}{k_B T}\right] \tag{E.9}$$

is the excluded-volume contribution to the protein partition coefficient. With regard to K_p^{EV}, an expression has already been derived by our group for the case of cylindrical micelles, and it is given by:[71,74]

$$K_p^{EV} = \exp\left[-\left(\phi_t - \phi_b\right)\left(1 + \frac{R_p}{R_0}\right)^2\right] \tag{1.4}$$

where ϕ_t and ϕ_b are the surfactant volume fractions in the top and bottom phases, respectively, R_p is the hydrodynamic radius of the protein, and R_0 is the cross-sectional radius of each cylindrical micelle (modeled as a spherocylindrical entity). This theory only in-

corporates steric, excluded-volume interactions that operate between the proteins and the micelles,[71,74] and is able to predict the preferential partitioning of proteins into the micelle-poor phase where they experience fewer excluded-volume interactions with the micelles. Based on Eq. (1.4), for given R_p and R_0 values, the excluded-volume interactions between the proteins and the micelles are determined solely by the difference in the surfactant volume fractions in the two phases, $(\phi_t - \phi_b)$. The surfactant volume fractions in the two phases are obtained from the intersections of the tie lines with the coexistence curves, since the volume fractions can be approximated as being equal to the weight fractions due to the densities of both phases being close to 1 g/mL. Equation (E.8) can further be manipulated to yield the following relation:

$$K_p = K_p^{EV}\left[\exp\left[\frac{-e\left(\psi_t - \psi_b\right)}{k_B T}\right]\right]^{z_p} \tag{E.10}$$

An expression for the electrostatic potential difference will now be derived to further understand its origin. In particular, following an approach similar to the the one used by Albertsson[28] for two-phase aqueous *polymer* systems, the electrostatic potential difference will now be shown to be a function of the excess chemical potentials of two salt ions present in the solution. To begin, the condition of electroneutrality for each macroscopic phase α in the partitioning experiments will be written as follows:

$$z_{Na}C_{Na,\alpha} + z_H C_{H,\alpha} = -\left(z_{HPO_4}C_{HPO_4,\alpha} + z_{Cit}C_{Cit,\alpha} + z_{OH}C_{OH,\alpha} + z_p C_{p,\alpha}\right) \tag{E.11}$$

where z_{Na}, z_H, z_{HPO_4}, z_{Cit}, z_{OH}, and z_p are the valences of Na^+, H^+, HPO_4^{-2}, citrate, OH^-, and a net negatively-charged protein, respectively, and $C_{Na,\alpha}$, $C_{H,\alpha}$, $C_{HPO_4,\alpha}$, $C_{Cit,\alpha}$, $C_{OH,\alpha}$, and $C_{p,\alpha}$ are the number densities (ions/mL or molecules/mL) of Na^+, H^+, HPO_4^{-2}, citrate, OH^-, and a net negatively-charged protein in phase α, respectively. Although a net negatively-charged protein has been assumed in this analysis, it will be shown later that the analysis is independent of the net charge of the protein. $z_{Na}C_{Na,\alpha}$ and $z_{HPO_4}C_{HPO_4,\alpha}$ will now be shown to be the largest terms in Eq. (E.11), and consequently, disodium phosphate (Na_2HPO_4) will be assumed to govern electroneutrality. To prove this, the concentrations of all the ions must be estimated as follows. With the exception of the protein, these ions have partition coefficients that are all very close to unity because they do not experience significant excluded-volume or hydrophobic interactions with the micelles. Qualitatively,

$$K_i \equiv \frac{C_{i,t}}{C_{i,b}} \approx 1 \tag{E.12}$$

where K_i is the partition coefficient of ion i, $C_{i,t}$ and $C_{i,b}$ are the concentrations of ion i in the top and bottom phases, respectively, and i denotes any ion other than the protein. Rearranging Eq. (E.12) yields:

$$C_{i,t} = C_{i,b} \tag{E.13}$$

Substituting Eq. (E.13) into the mass balance of ion i given by:

$$C_{i,0}\left(V_t + V_b\right) = C_{i,t}V_t + C_{i,b}V_b \tag{E.14}$$

yields the following relation:

$$C_{i,0} = C_{i,t} = C_{i,b} \tag{E.15}$$

where $C_{i,0}$ is the initial, overall concentration of ion i, and V_t and V_b are the volumes of the top and bottom phases, respectively. Therefore, the concentration of ion i in each phase can be estimated to be equal to its initial, overall concentration. For Na^+, HPO_4^{-2}, and citrate, their concentrations in each phase can be estimated as being equal to 32.8 mM, 16.4 mM, and 1.82 mM, respectively, based on the buffer salt concentrations. Although Na^+ is also expected to be the major counterion of the net-negatively charged protein, the concentration of Na^+ in the form of the counterion is orders of magnitude smaller than the concentration of Na^+ from the added Na_2HPO_4, since the concentration of protein is only approximately 6.0×10^{15} protein molecules/mL or 0.01 mM (see the discussion below). The concentrations of H^+ and OH^- can be determined from the pH of the solution as follows:

$$[H^+] = 10^{-pH} \tag{E.16}$$

and

$$[OH^-] = 10^{-(14-pH)} \tag{E.17}$$

where $[H^+]$ and $[OH^-]$ are the molar concentrations of H^+ and OH^-, respectively. In the partitioning experiments, the pH is generally maintained at 7.2, and therefore, the concentrations of H^+ and OH^- are 6.3×10^{-5} mM and 1.6×10^{-4} mM, respectively. The value of $z_i C_{i,\alpha}$ for each of these ions is provided in Table E-1. It should be noted that even though the pH is reduced to 3.2 in one of the experiments in this study (see Section E.3.2), the concentration of H^+ is still very low at 0.63 mM or 3.8×10^{17} ions/mL.

With regard to the protein, its partition coefficient is generally between 0.1 and 1. However, based on past protein partitioning experiments, the concentration of protein in each phase can be estimated to be approximately 0.5 g/L. Accordingly, the number density of

Table E-1: Estimates of $z_i C_{i,\alpha}$ for the partitioning solutions.

Ion in Phase α	$z_i C_{i,\alpha}$ (ions/mL)
Na^+	(+1) (2.0×10^{19})
H^+	(+1) (3.8×10^{13})
HPO_4^{-2}	(-2) (9.9×10^{18})
Citrate	(-3) (1.1×10^{18})
OH^-	(-1) (9.6×10^{13})

protein in phase α can be estimated as follows:

$$C_{p,\alpha} \approx \left(\frac{0.5\ g}{L}\right)\left(\frac{L}{1000\ mL}\right)\left(\frac{mole}{50000\ g}\right)\left(\frac{6.022 \times 10^{23}\ molecules}{mole}\right) = 6.0 \times 10^{15} \quad \text{(E.18)}$$

where 50,000 g/mole is a typical molecular weight of a protein. Since a typical valence for a protein is about -10 (see Chapter 7), $z_p C_{p,\alpha}$ is only -6.0×10^{16} protein molecules/mL. Consequently, $z_p C_{p,\alpha}$ is a negligible term in the electroneutrality relation given in Eq. (E.11), and therefore, the analysis that follows is independent of the protein being net positively-charged or net negatively-charged. With these estimates for the valence and concentration of each ion, the total positive charge (that is, the left-hand side of Eq. (E.11)) is slightly smaller in magnitude than the total negative charge (that is, the right-hand side of Eq. (E.11)). Electroneutrality is violated in this case because these estimations are not representative of the *actual* solution conditions, and are instead representative of the worst case scenario. Specifically, estimating $z_{Cit} C_{Cit,\alpha}$ as (-3)(1.1×10^{18} ions/mL) was an overestimation. Citrate is formed from citric acid by the loss of H^+ ions, but the loss of H^+ ions is actually limited by the pH being at a particular value, such as, pH = 7.2. Therefore, all the citric acid molecules cannot be fully ionized, and the valence of -3 used in the estimation is not fully consistent with the need to maintain the pH at 7.2.

Based on these estimations for all the ions, it can be concluded that the $z_{Na} C_{Na,\alpha}$ and $z_{HPO_4} C_{HPO_4,\alpha}$ terms are the largest ones in Eq. (E.11). Therefore, it is a reasonable first approximation to assume that electroneutrality is governed by Na_2HPO_4. The electroneutrality relation in each phase then simplifies to:

$$z_{Na} C_{Na,t} \approx -z_{HPO_4} C_{HPO_4,t} \quad \text{(E.19)}$$

and

$$z_{Na}C_{Na,b} \approx -z_{HPO_4}C_{HPO_4,b} \tag{E.20}$$

where $C_{Na,t}$ and $C_{Na,b}$ are the number densities (ions/mL) of Na^+ in the top and bottom phases, respectively, and $C_{HPO_4,t}$ and $C_{HPO_4,b}$ are the number densities (ions/mL) of HPO_4^{-2} in the top and bottom phases, respectively. Dividing Eq. (E.19) by Eq. (E.20) yields:

$$K_{Na} \equiv \frac{C_{Na,t}}{C_{Na,b}} = \frac{C_{HPO_4,t}}{C_{HPO_4,b}} \equiv K_{HPO_4} \tag{E.21}$$

where K_{Na} and K_{HPO_4} are the partition coefficients of Na^+ and HPO_4^{-2}, respectively.

Expressions for K_{Na} and K_{HPO_4} will now be derived in terms of the excess chemical potentials of Na^+ and HPO_4^{-2}. These expressions for K_{Na} and K_{HPO_4} will then be used to derive an expression for the electrostatic potential difference between the two macroscopic phases in terms of the excess chemical potentials of Na^+ and HPO_4^{-2}. As with the protein, the establishment of diffusional equilibrium of the Na^+ and HPO_4^{-2} ions between the two coexisting phases will first be assumed. Accordingly, at equilibrium,[111]

$$\mu_{Na,t} = \mu_{Na,b} \tag{E.22}$$

and

$$\mu_{HPO_4,t} = \mu_{HPO_4,b} \tag{E.23}$$

where $\mu_{Na,t}$ and $\mu_{Na,b}$ are the chemical potentials of Na^+ in the top and bottom phases, respectively, and $\mu_{HPO_4,t}$ and $\mu_{HPO_4,b}$ are the chemical potentials of HPO_4^{-2} in the top and bottom phases, respectively. The chemical potentials of Na^+ and HPO_4^{-2} in each phase α can be written as follows:[112]

$$\mu_{Na,\alpha} = \mu^{\circ}_{Na} + k_BT \ln C_{Na,\alpha} + \mu^{ex}_{Na,\alpha} + z_{Na}e\psi_{\alpha} \tag{E.24}$$

and

$$\mu_{HPO_4,\alpha} = \mu^{\circ}_{HPO_4} + k_BT \ln C_{HPO_4,\alpha} + \mu^{ex}_{HPO_4,\alpha} + z_{HPO_4}e\psi_{\alpha} \tag{E.25}$$

where μ°_{Na} and $\mu^{\circ}_{HPO_4}$ are the standard-state chemical potentials of Na^+ and HPO_4^{-2}, respectively, and $\mu^{ex}_{Na,\alpha}$ and $\mu^{ex}_{HPO_4,\alpha}$ are the excess chemical potentials of Na^+ and HPO_4^{-2} in each phase α, respectively. The standard-state chemical potential of Na^+ (or HPO_4^{-2}) corresponds to a standard state in which: (i) Na^+ (or HPO_4^{-2}) and the solvent are the only two components present, (ii) the Na^+ (or HPO_4^{-2}) ions interact with the solvent molecules but not with

each other, (iii) the solvent molecules interact with each other, and (iv) the concentration of Na^+ (or HPO_4^{-2}) is 1 ion/mL, and therefore, has an ideal entropy corresponding to this concentration. The interactions, as well as the ideal entropy included in μ°_{Na} (or $\mu^{\circ}_{HPO_4}$), are all accounted for at the temperature and the pressure of the system. A simplification similar to the one used to derive Eq. (E.2) was used to obtain Eqs. (E.24) and (E.25).

Substituting Eq. (E.24) into Eq. (E.22), and rearranging yields:

$$K_{Na} \equiv \frac{C_{Na,t}}{C_{Na,b}} = \exp\left[\frac{-\left(\mu^{ex}_{Na,t} - \mu^{ex}_{Na,b}\right)}{k_B T}\right]\left[\exp\left[\frac{-e\left(\psi_t - \psi_b\right)}{k_B T}\right]\right]^{z_{Na}} \tag{E.26}$$

Similarly, substituting Eq. (E.25) into Eq. (E.23), and rearranging yields:

$$K_{HPO_4} \equiv \frac{C_{HPO_4,t}}{C_{HPO_4,b}} = \exp\left[\frac{-\left(\mu^{ex}_{HPO_4,t} - \mu^{ex}_{HPO_4,b}\right)}{k_B T}\right]\left[\exp\left[\frac{-e\left(\psi_t - \psi_b\right)}{k_B T}\right]\right]^{z_{HPO_4}} \tag{E.27}$$

Combining Eqs. (E.21), (E.26), and (E.27) yields the following relation:

$$\exp\left[\frac{-\left(\mu^{ex}_{Na,t} - \mu^{ex}_{Na,b}\right)}{k_B T}\right]\left[\exp\left[\frac{-e\left(\psi_t - \psi_b\right)}{k_B T}\right]\right]^{z_{Na}} = \exp\left[\frac{-\left(\mu^{ex}_{HPO_4,t} - \mu^{ex}_{HPO_4,b}\right)}{k_B T}\right]\left[\exp\left[\frac{-e\left(\psi_t - \psi_b\right)}{k_B T}\right]\right]^{z_{HPO_4}} \tag{E.28}$$

Rearranging Eq. (E.28) yields:

$$\exp\left[\frac{-e\left(\psi_t - \psi_b\right)}{k_B T}\right] = \left[\frac{\exp\left[\frac{-\left(\mu^{ex}_{HPO_4,t} - \mu^{ex}_{HPO_4,b}\right)}{k_B T}\right]}{\exp\left[\frac{-\left(\mu^{ex}_{Na,t} - \mu^{ex}_{Na,b}\right)}{k_B T}\right]}\right]^{\frac{1}{z_{Na} - z_{HPO_4}}} \tag{E.29}$$

Substituting Eq. (E.29) into Eq. (E.10) then yields:

$$K_p = K_p^{EV}\left[\frac{\exp\left[\frac{-\left(\mu^{ex}_{HPO_4,t} - \mu^{ex}_{HPO_4,b}\right)}{k_B T}\right]}{\exp\left[\frac{-\left(\mu^{ex}_{Na,t} - \mu^{ex}_{Na,b}\right)}{k_B T}\right]}\right]^{\frac{z_p}{z_{Na} - z_{HPO_4}}} \tag{E.30}$$

As indicated by Eq. (E.29), the electrostatic potential difference is only a function of the

excess chemical potentials of the Na^+ and HPO_4^{-2} ions. The excess chemical potentials of the Na^+ and HPO_4^{-2} ions are expected to be independent of the protein, since the protein is only present at very dilute concentrations. On the other hand, the excess chemical potentials of the Na^+ and HPO_4^{-2} ions are expected to be a function of the $C_{10}E_4$ concentrations in the two coexisting phases, since the Na^+ and HPO_4^{-2} ions are expected to interact with the $C_{10}E_4$ micelles. These interactions include ion-dipole, ion-induced dipole, and van der Waals interactions between the ion (Na^+ or HPO_4^{-2}) and the noncharged $C_{10}E_4$ micelle. Therefore, the electrostatic potential difference, if it does exist, should be a function of the $C_{10}E_4$ concentrations in the two phases. Since the concentrations of $C_{10}E_4$ in the two phases are fixed at a particular temperature by the operating tie line, the electrostatic potential difference is expected to be a function of temperature. Accordingly, the electrostatic potential difference (multipled by the constant e) as a function of temperature was fitted using the partitioning data of one protein, and the resulting fitted electrostatic potential difference was then used to predict the partition coefficients of other proteins. To perform the fit of the electrostatic potential difference, Eq. (E.10) was first rearranged to yield:

$$e\left(\psi_t - \psi_b\right) = \frac{-k_B}{z_p}\left(\ln K_p - \ln K_p^{EV}\right) T \tag{E.31}$$

The K_p and T values were obtained from the partitioning data of a single protein. The K_p^{EV} values were predicted with knowledge of the hydrodynamic radius of the protein, the radius of the cylindrical micelle, and the $(\phi_t - \phi_b)$ values obtained from the coexistence curve of the $C_{10}E_4$-buffer system for the different partitioning temperatures. The valence of the protein, z_p, was predicted using the procedure described in Chapter 7. The values of $e(\psi_t - \psi_b)$ that were obtained using Eq. (E.31) were then plotted as a function of the partitioning temperature. Although $(\ln K_p - \ln K_p^{EV})$ is not necessarily a constant, a simple linear relation between $e(\psi_t - \psi_b)$ and T was assumed in this analysis to introduce the least number of parameters.

The partitioning data of ovalbumin presented in Figure 1-7 was first used to obtain the best-fit line for $e(\psi_t - \psi_b)$ as a function of temperature. The best-fit line and the $e(\psi_t - \psi_b)$ points (obtained by using Eq. (E.31)) are shown in Figure E-2. The fitted model (the solid line in Figure E-2) was used to determine if the fitted electrostatic potential difference could improve the excluded-volume predictions for the proteins. Specifically, with the fitted model for the electrostatic potential difference, new partition coefficients were predicted for ovalbumin, cytochrome c, and catalase using Eqs. (1.4) and (E.10). These predictions are shown in Figures E-3, E-4, and E-5 along with the excluded-volume predictions and the

experimental data presented in Chapter 1.

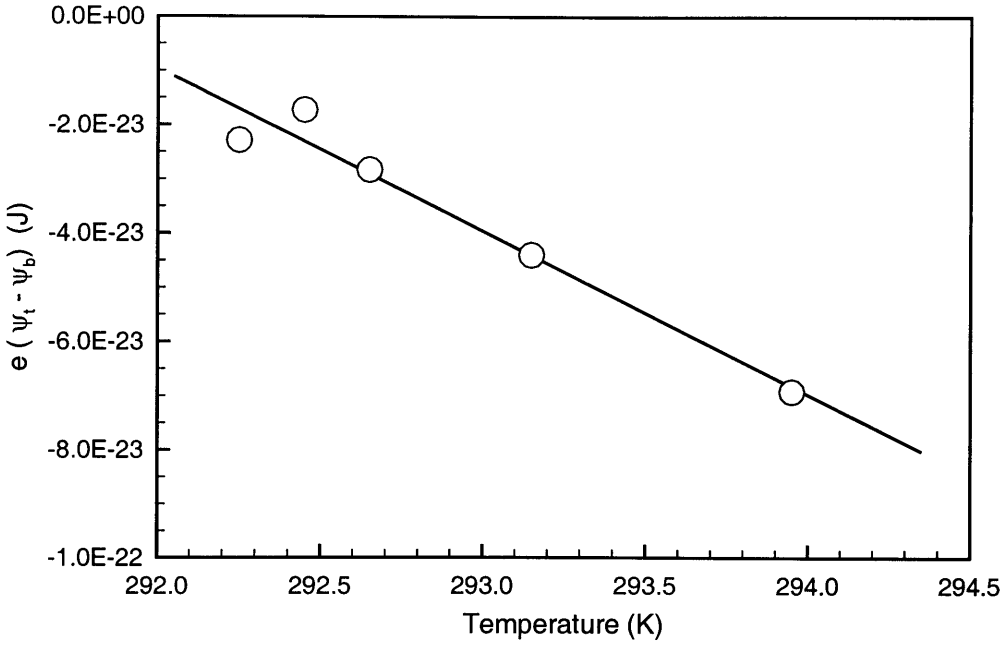

Figure E-2: The variation of $e(\psi_t - \psi_b)$ with temperature when the electrostatic potential difference was fitted to the partitioning data of ovalbumin. The partitioning data of ovalbumin was obtained from Figure 1-7.

As shown in Figures E-3, E-4, and E-5, incorporating the electrostatic potential difference in the theory did not consistently improve the new predictions. Specifically, the predicted partition coefficients of cytochrome *c* became much worse although the predicted partition coefficients of ovalbumin and catalase improved. Accordingly, an electrostatic potential difference between the two macroscopic $C_{10}E_4$ micellar phases can be concluded to be not so important when Na_2HPO_4 governs electroneutrality. This conclusion was also expected *a priori* because of the reasonable agreement that already existed between the experimentally measured protein partition coefficients and the excluded-volume theory that did not incorporate the electrostatic potential difference. Although the results are not presented in this appendix, the electrostatic potential difference was also similarly fit to the cytochrome *c* data presented in Figure 1-6, and used to predict new partition coefficients for ovalbumin, cytochrome *c*, and catalase. Similarly, the electrostatic potential difference was also fit to the catalase data presented in Figure 1-8, and used to predict new partition cofficients for ovalbumin, cytochrome *c*, and catalase. For both cases, the newly predicted partition coefficients also did not consistently improve. Consequently, these additional tests further corroborated the conclusion that the electrostatic potential difference between the coexisting macroscopic

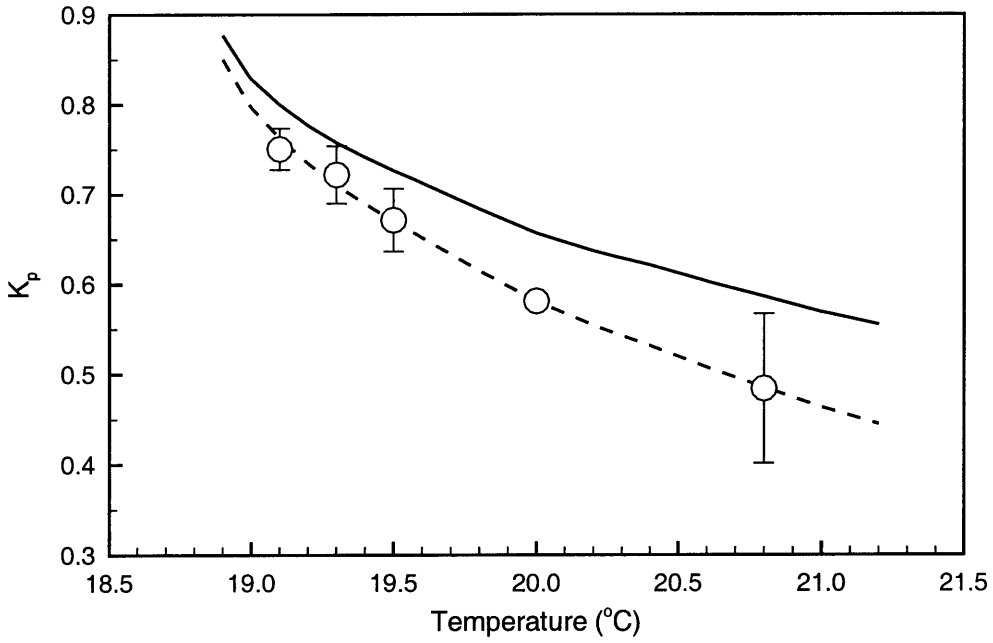

Figure E-3: Comparison between the theoretically predicted and experimentally measured partition coefficients of ovalbumin. The solid line corresponds to the partition coefficients that were predicted based on the excluded-volume theory. The dashed line represents the partition coefficients that were predicted after accounting for both the excluded-volume interactions and the electrostatic potential difference that was fitted to the partitioning data of ovalbumin. The white circle symbols correspond to the partition coefficients of ovalbumin that were obtained from Figure 1-7. The error bars represent 95% confidence limits for the measurements.

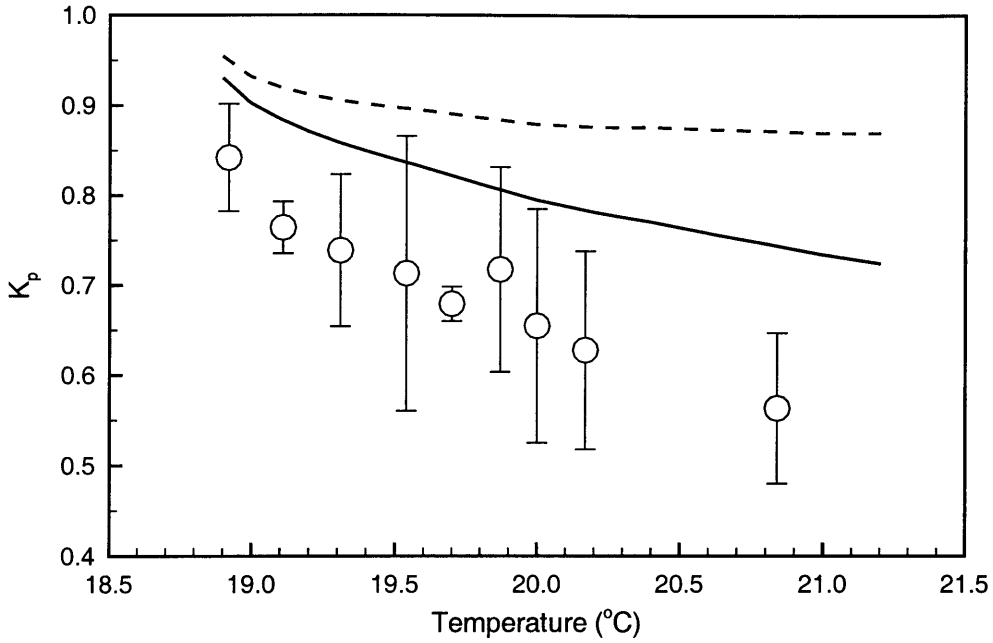

Figure E-4: Comparison between the theoretically predicted and experimentally measured partition coefficients of cytochrome *c*. The solid line corresponds to the partition coefficients that were predicted based on the excluded-volume theory. The dashed line represents the partition coefficients that were predicted after accounting for both the excluded-volume interactions and the electrostatic potential difference that was fitted to the partitioning data of ovalbumin. The white circle symbols correspond to the partition coefficients of cytochrome *c* that were obtained from Figure 1-6. The error bars represent 95% confidence limits for the measurements.

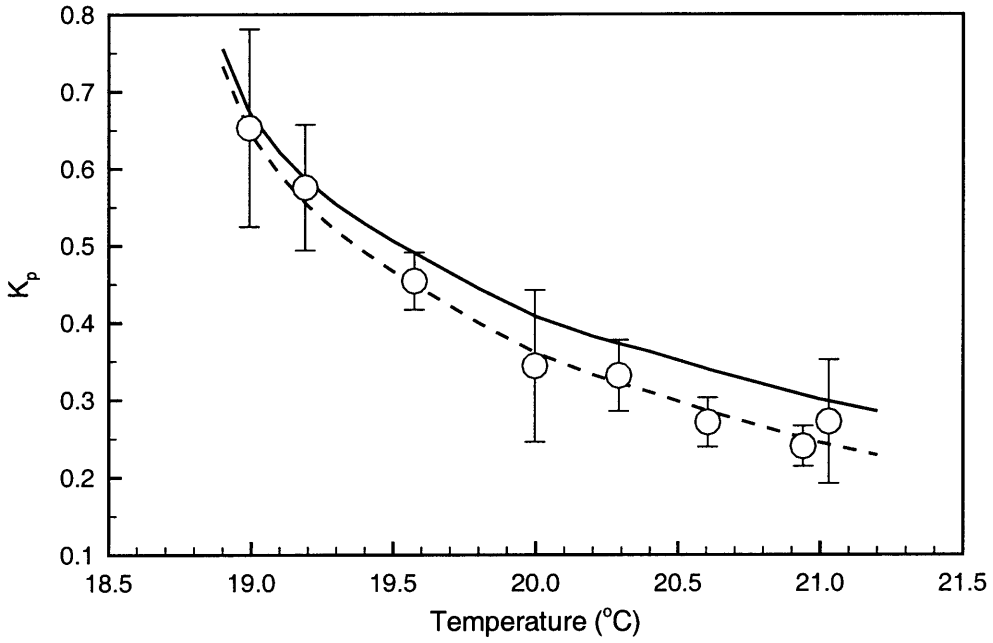

Figure E-5: Comparison between the theoretically predicted and experimentally measured partition coefficients of catalase. The solid line corresponds to the partition coefficients that were predicted based on the excluded-volume theory. The dashed line represents the partition coefficients that were predicted after accounting for both the excluded-volume interactions and the electrostatic potential difference that was fitted to the partitioning data of ovalbumin. The white circle symbols correspond to the partition coefficients of catalase that were obtained from Figure 1-8. The error bars represent 95% confidence limits for the measurements.

$C_{10}E_4$ micellar phases is not very important when Na_2HPO_4 governs electroneutrality. A mutant of bacteriophage P22, which was more negative than the previous ones investigated, was also partitioned in the $C_{10}E_4$-buffer system when Na_2HPO_4 governed electroneutrality. The net charge of this mutant was more negative by approximately 420 because: (i) a glycine to aspartic acid change was made in the coat protein, and (ii) there are approximately 420 coat proteins per bacteriophage P22 particle.[85,87] This amino acid change was also found experimentally to affect the electrophoretic mobility of bacteriophage P22. Using the procedure described in Section 5.2.3, the partition coefficient of this mutant was measured experimentally, and found to be the same as the one measured previously, further demonstrating that the electrostatic potential difference when Na_2HPO_4 governs electroneutrality is not very important.

With the hope of observing a significant electrostatic potential difference between the two macroscopic $C_{10}E_4$ micellar phases, the salt governing electroneutrality was changed from Na_2HPO_4 to NaCl (see Section E.3.2). NaCl was chosen because it is a common salt that is easy to work with in the laboratory. At a 0.5 M concentration of NaCl, the magnitudes of $z_{Na}C_{Na,\alpha}$ and $z_{Cl}C_{Cl,\alpha}$ are large enough that NaCl governs electroneutrality in each phase. The electroneutrality relation in the top and bottom phases can therefore be written as follows:

$$z_{Na}C_{Na,t} \approx -z_{Cl}\, C_{Cl,t} \tag{E.32}$$

and

$$z_{Na}C_{Na,b} \approx -z_{Cl}\, C_{Cl,b} \tag{E.33}$$

where $C_{Cl,t}$ and $C_{Cl,b}$ are the number densities of Cl^- in the top and bottom phases, respectively. Dividing Eq. (E.32) by Eq. (E.33) yields:

$$K_{Na} \equiv \frac{C_{Na,t}}{C_{Na,b}} = \frac{C_{Cl,t}}{C_{Cl,b}} \equiv K_{Cl} \tag{E.34}$$

where K_{Cl} is the partition coefficient of Cl^-. Since Eqs. (E.22) to (E.30) can also be applied to the partitioning experiments where NaCl governs electroneutrality with "Cl" replacing "HPO_4" in the subscripts, Eqs. (E.29) and (E.30) can be rewritten as follows:

$$\exp\left[\frac{-e\,(\psi_t - \psi_b)}{k_BT}\right] = \left[\frac{\exp\left[\frac{-\left(\mu^{ex}_{Cl,t} - \mu^{ex}_{Cl,b}\right)}{k_BT}\right]}{\exp\left[\frac{-\left(\mu^{ex}_{Na,t} - \mu^{ex}_{Na,b}\right)}{k_BT}\right]}\right]^{\frac{1}{z_{Na} - z_{Cl}}} \tag{E.35}$$

and

$$K_p = K_p^{EV}\left[\frac{\exp\left[\frac{-\left(\mu_{Cl,t}^{ex}-\mu_{Cl,b}^{ex}\right)}{k_BT}\right]}{\exp\left[\frac{-\left(\mu_{Na,t}^{ex}-\mu_{Na,b}^{ex}\right)}{k_BT}\right]}\right]^{\frac{z_p}{z_{Na}-z_{Cl}}} \tag{E.36}$$

Since the valence of the protein appears as an exponent in Eq. (E.36), the net charge of the protein was varied to determine if an electrostatic potential difference could exist when NaCl governed electroneutrality. The net charge of the protein was varied by adjusting the solution pH. This experiment could not be conducted when Na_2HPO_4 governed electroneutrality because low solution pH values cannot be easily attained when the solution has a high concentration of Na_2HPO_4. In addition, to vary the solution pH, disodium phosphate and citric acid were again used as the buffer salts in order to be consistent with our past partitioning experiments. Since a solution pH between 2.2 and 8.0 can be achieved by decreasing and increasing the molar ratio of disodium phosphate to citric acid, bovine serum albumin (BSA) was chosen as the model protein because its pI is 4.8,[76] and therefore, its net charge can be changed from positive to negative in the pH range defined by these buffer salts. Specifically, the net charge of BSA can be varied from positive to negative by increasing the solution pH from below 4.8 to above 4.8. Consequently, BSA partitioning experiments were conducted at solution pH values of 3.2 and 6.8 (see Section E.3.2). To solely investigate the effect of changing the net charge of BSA, it was desirable to maintain: (i) the same electrostatic potential difference between the two phases, and (ii) the same excluded-volume interactions between BSA and the micelles during the partitioning experiments (see Eqs. (E.35) and (E.36)). If a significant electrostatic potential difference exists between the two macroscopic $C_{10}E_4$ micellar phases when NaCl governs electroneutrality, different partition coefficients of BSA should be measured as the charge of BSA is varied. As discussed earlier, the same electrostatic potential difference can be maintained between the two partitioning experiments by operating at conditions where the following two equalities are valid:

$$C_{C_{10}E_4,t,3.2} = C_{C_{10}E_4,t,6.8} \tag{E.37}$$

and

$$C_{C_{10}E_4,b,3.2} = C_{C_{10}E_4,b,6.8} \tag{E.38}$$

where $C_{C_{10}E_4,t,3.2}$ and $C_{C_{10}E_4,t,6.8}$ are the concentrations of $C_{10}E_4$ in the top phase for the partitioning experiments conducted at pH values of 3.2 and 6.8, respectively, and $C_{C_{10}E_4,b,3.2}$

and $C_{C_{10}E_4,b,6.8}$ are the concentrations of $C_{10}E_4$ in the bottom phase for the partitioning experiments conducted at pH values of 3.2 and 6.8, respectively. Equations (E.37) and (E.38) also ensure that $(\phi_t - \phi_b)$, and therefore, the excluded-volume condition, is the same between the two partitioning experiments. To accurately identify the conditions at which Eqs. (E.37) and (E.38) are valid, the phase diagrams of the $C_{10}E_4$-buffer systems in the presence of 0.5 M NaCl at solution pH values of 3.2 and 6.8 are required. However, performing the lever rule test described in Appendix C indicated that a pseudo-binary phase diagram was not applicable to these systems. Since much time is required to measure multi-component phase diagrams, an approximation was made to identify the conditions where Eqs. (E.37) and (E.38) were approximately valid. In particular, the concentration of $C_{10}E_4$ in the bottom phase was assumed to be 0 wt% when the concentration of $C_{10}E_4$ in the top phase was 10 wt% or higher, which is close to what has been observed experimentally in the two-phase aqueous $C_{10}E_4$ micellar system. When the concentration of $C_{10}E_4$ in the bottom phase is 0 wt%, the mass balance on $C_{10}E_4$ given by:

$$\omega_{C_{10}E_4,0}(M_t + M_b) = \omega_{C_{10}E_4,t}M_t + \omega_{C_{10}E_4,b}M_b \tag{E.39}$$

simplifies to:

$$\omega_{C_{10}E_4,0}(M_t + M_b) = \omega_{C_{10}E_4,t}M_t \tag{E.40}$$

where $\omega_{C_{10}E_4,0}$ is the initial weight fraction of $C_{10}E_4$, $\omega_{C_{10}E_4,t}$ and $\omega_{C_{10}E_4,b}$ are the weight fractions of $C_{10}E_4$ in the top and bottom phases, respectively, and M_t and M_b are the masses of the top and bottom phases, respectively. Since a volume ratio of 1 has generally been used in the partitioning experiments, the following relation applies:

$$V_t = V_b \tag{E.41}$$

The densities of both phases are also very similar, and therefore, Eq. (E.41) can be rewritten as follows:

$$M_t = M_b \tag{E.42}$$

Substituting Eq. (E.42) into Eq. (E.40), and rearranging yields:

$$2\omega_{C_{10}E_4,0} = \omega_{C_{10}E_4,t} \tag{E.43}$$

According to Eq. (E.43), to obtain a $C_{10}E_4$ concentration of 10 wt% in the top phase (which is required to ensure that the bottom phase concentration of $C_{10}E_4$ is close to 0 wt%), an initial

$C_{10}E_4$ concentration of 5 wt% must be used. Consequently, an initial $C_{10}E_4$ concentration of 5 wt% was used along with a volume ratio of 1 in the partitioning experiments described in Section E.3.2. These initial conditions therefore yielded approximately 10 wt% and 0 wt% $C_{10}E_4$ concentrations in the top and bottom phases, respectively, in the partitioning experiments.

E.2.2 Derivation of Expressions for the Electrostatic Potential Difference in Terms of Interaction Parameters

In Section E.2.1, the electrostatic potential difference was derived in terms of the excess chemical potentials of the Na^+ and HPO_4^{-2} ions in the two phases. In this section, expressions for $\mu^{ex}_{Na,\alpha}$ and $\mu^{ex}_{HPO_4,\alpha}$ will be derived in terms of the interaction parameters between each salt ion and the $C_{10}E_4$ surfactant. The derived relations will then be used to design experiments.

The interactions between each salt ion and the noncharged micelles include ion-dipole, ion-induced dipole, and van der Waals interactions. These interactions will be modeled with an approach similar to that utilized by Blankschtein *et al.* to model the interactions between micelles.[43,44] These interactions will then be used to derive an expression for the excess Gibbs free energy associated with the interactions between the salt ions and the micelles in phase α, $G^{ex,salt}_{\alpha}$, which can then be differentiated to obtain expressions for $\mu^{ex}_{Na,\alpha}$ and $\mu^{ex}_{HPO_4,\alpha}$ as follows:

$$\mu^{ex}_{Na,\alpha} = \left(\frac{\partial G^{ex,salt}_{\alpha}}{\partial N_{Na,\alpha}}\right)_{T,P,N_{j,\alpha\neq Na,\alpha}} \tag{E.44}$$

and

$$\mu^{ex}_{HPO_4,\alpha} = \left(\frac{\partial G^{ex,salt}_{\alpha}}{\partial N_{HPO_4,\alpha}}\right)_{T,P,N_{j,\alpha\neq HPO_4,\alpha}} \tag{E.45}$$

where $N_{Na,\alpha}$ is the number of Na^+ ions in phase α, $N_{j,\alpha\neq Na,\alpha}$ is the number of non-Na^+ ions or molecules of type j in phase α, $N_{HPO_4,\alpha}$ is the number of HPO_4^{-2} ions in phase α, and $N_{j,\alpha\neq HPO_4,\alpha}$ is the number of non-HPO_4^{-2} ions or molecules of type j in phase α. The excess Gibbs free energy associated with the interactions between the salt ions and the micelles in phase α can be written as follows:

$$G^{ex,salt}_{\alpha} = N_{Na,\alpha} \sum_{n_\alpha = n^{\circ}_{cyl,\alpha}}^{\infty} U_{n,Na,\alpha} + N_{HPO_4,\alpha} \sum_{n_\alpha = n^{\circ}_{cyl,\alpha}}^{\infty} U_{n,HPO_4,\alpha} \tag{E.46}$$

where

$$U_{n,Na,\alpha} = u_{Na,C_{10}E_4} \sum_{n_\alpha = n^\circ_{cyl,\alpha}}^{\infty} f_{i,n} C_{n,\alpha} \tag{E.47}$$

and

$$U_{n,HPO_4,\alpha} = u_{HPO_4,C_{10}E_4} \sum_{n_\alpha = n^\circ_{cyl,\alpha}}^{\infty} f_{i,n} C_{n,\alpha} \tag{E.48}$$

where $u_{Na,C_{10}E_4}$ (which is only a function of T and P) measures the interaction potential between one Na^+ ion and one $C_{10}E_4$ molecule, $u_{HPO_4,C_{10}E_4}$ (which is only a function of T and P) measures the interaction potential between one HPO_4^{-2} ion and one $C_{10}E_4$ molecule, $C_{n,\alpha}$ is the concentration of micelles of aggregation number n in phase α, $n^\circ_{cyl,\alpha}$ is the aggregation number of the smallest cylindrical micelle in phase α, and $f_{i,n}$ describes how the average interaction between a salt ion and a micelle depends on the aggregation number of the micelle. The free monomers, that is, those that are not present in the micelles, have been neglected because their concentrations in the two coexisting macroscopic phases are essentially the same. The interactions between the monomers in the micelles and the ions will be modeled as a sum of pairwise interactions in a mean-field approach. Accordingly,

$$f_{i,n} = n \tag{E.49}$$

Equation (E.46) can therefore be rewritten as follows:

$$G_\alpha^{ex,salt} = N_{Na,\alpha} u_{Na,C_{10}E_4} \sum_{n_\alpha = n^\circ_{cyl,\alpha}}^{\infty} n C_{n,\alpha} + N_{HPO_4,\alpha} u_{HPO_4,C_{10}E_4} \sum_{n_\alpha = n^\circ_{cyl,\alpha}}^{\infty} n C_{n,\alpha} \tag{E.50}$$

Since the free monomer concentration is orders of magnitude lower than the total concentration of $C_{10}E_4$ in each phase α, $C_{C_{10}E_4,\alpha}$, the following approximation is valid:

$$\sum_{n_\alpha = n^\circ_{cyl,\alpha}}^{\infty} n C_{n,\alpha} \approx C_{C_{10}E_4,\alpha} \tag{E.51}$$

Therefore, Eq. (E.50) simplifies to:

$$G_\alpha^{ex,salt} = N_{Na,\alpha} u_{Na,C_{10}E_4} C_{C_{10}E_4,\alpha} + N_{HPO_4,\alpha} u_{HPO_4,C_{10}E_4} C_{C_{10}E_4,\alpha} \tag{E.52}$$

The total volume of the solution in phase α will be modeled as follows:

$$V_\alpha = N_{w,\alpha}\Omega_w + N_{p,\alpha}\Omega_p + N_{Na,\alpha}\Omega_{Na} + N_{HPO_4,\alpha}\Omega_{HPO_4} + N_{1,\alpha}\Omega_1 + \sum_{n_\alpha=n^\circ_{cyl,\alpha}}^{\infty} N_{n_\alpha}\Omega_{n_\alpha} \quad \text{(E.53)}$$

where $N_{w,\alpha}$ is the number of water molecules in phase α, Ω_w is the volume of a water molecule, Ω_p is the volume of a protein molecule, Ω_{Na} is the volume of a Na^+ ion, Ω_{HPO_4} is the volume of a HPO_4^{-2} ion, $N_{1,\alpha}$ is the number of free monomers in phase α, Ω_1 is the volume of a free monomer, and Ω_{n_α} is the volume of a cylindrical micelle of aggregation number n in phase α. Ω_i is only a function of temperature and pressure because it is the pure molecular volume of component i. Combining Eqs. (E.44), (E.45), (E.52), and (E.53) yields the following two relations:

$$\mu^{ex}_{Na,\alpha} = u_{Na,C_{10}E_4} C_{C_{10}E_4,\alpha} \quad \text{(E.54)}$$

and

$$\mu^{ex}_{HPO_4,\alpha} = u_{HPO_4,C_{10}E_4} C_{C_{10}E_4,\alpha} \quad \text{(E.55)}$$

Combining Eqs. (E.30), (E.54), and (E.55) yields:

$$K_p = K_p^{EV}\left[\frac{\exp\left[\frac{-u_{HPO_4,C_{10}E_4}\left(C_{C_{10}E_4,t}-C_{C_{10}E_4,b}\right)}{k_BT}\right]}{\exp\left[\frac{-u_{Na,C_{10}E_4}\left(C_{C_{10}E_4,t}-C_{C_{10}E_4,b}\right)}{k_BT}\right]}\right]^{\frac{z_p}{z_{Na}-z_{HPO_4}}} \quad \text{(E.56)}$$

Rearranging Eq. (E.56) yields:

$$K_p = K_p^{EV}\left[\exp\left[\frac{\left(C_{C_{10}E_4,t}-C_{C_{10}E_4,b}\right)\left(u_{Na,C_{10}E_4}-u_{HPO_4,C_{10}E_4}\right)}{k_BT}\right]\right]^{\frac{z_p}{z_{Na}-z_{HPO_4}}} \quad \text{(E.57)}$$

which can be further manipulated to yield the following relation:

$$K_p = K_p^{EV}\left[\exp\left[\frac{\left(u_{Na,C_{10}E_4}-u_{HPO_4,C_{10}E_4}\right)}{k_BT\left(z_{Na}-z_{HPO_4}\right)}\right]\right]^{z_p\left(C_{C_{10}E_4,t}-C_{C_{10}E_4,b}\right)} \quad \text{(E.58)}$$

As discussed in Section E.2.1, the electrostatic potential difference between the two macroscopic $C_{10}E_4$ micellar phases is negligible when Na_2HPO_4 governs electroneutrality. Based on Eq. (E.58), this can be understood as implying that $u_{Na,C_{10}E_4} \approx u_{HPO_4,C_{10}E_4}$. Since the derivation of Eq. (E.58) can be applied to any salt, Eq. (E.58) suggests that a different

partition coefficient can be measured for the same protein under the same excluded-volume conditions just by varying the salt governing electroneutrality. The anion was varied in our experiment (see Section E.3.3) by changing the salt governing electroneutrality from Na_2HPO_4 to $NaClO_4$. As in the case of NaCl discussed in Section E.2.1, a 0.5 M concentration of $NaClO_4$ was utilized in order for $NaClO_4$ to govern electroneutrality in each phase. In this case, Eq. (E.58) can be rewritten as follows:

$$K_p = K_p^{EV}\left[\exp\left[\frac{\left(u_{Na,C_{10}E_4} - u_{ClO_4,C_{10}E_4}\right)}{k_BT\left(z_{Na} - z_{ClO_4}\right)}\right]\right]^{z_p\left(C_{C_{10}E_4,t} - C_{C_{10}E_4,b}\right)} \tag{E.59}$$

$NaClO_4$ was chosen because the interactions of ClO_4^- with $C_{10}E_4$ are expected to be more favorable than those of HPO_4^{-2} with $C_{10}E_4$ and Na^+ with $C_{10}E_4$ based on the Hofmeister series of ions. According to the Hofmeister series, ClO_4^- is less hydrophilic than many other ions because of the low surface charge density, or small charge per surface area. Since the hydrocarbon tail of $C_{10}E_4$ is very hydrophobic, the interactions of ClO_4^- with $C_{10}E_4$ are expected to be less repulsive than those of HPO_4^{-2} with $C_{10}E_4$ and Na^+ with $C_{10}E_4$. In terms of the interaction parameters, this can be written as follows:

$$u_{ClO_4,C_{10}E_4} < u_{Na,C_{10}E_4} \tag{E.60}$$

and

$$u_{ClO_4,C_{10}E_4} < u_{HPO_4,C_{10}E_4} \tag{E.61}$$

In the two partitioning experiments described in Section E.3.3, the pH of the solutions was maintained at 7.2, and the excluded-volume interactions between the protein and the micelles were maintained fairly constant using the approach described in Section E.2.1. The only difference between the two partitioning experiments was the salt governing electroneutrality. Specifically, Na_2HPO_4 governed electroneutrality in one experiment, while $NaClO_4$ governed electroneutrality in the other experiment. Before conducting the experiments, Eq. (E.58) was divided by Eq. (E.59) to predict whether the presence of $NaClO_4$ would increase or decrease the partition coefficient of a particular protein. A protein different from BSA was chosen to demonstrate that the electrostatic potential difference is indeed universal. Lysozyme was selected as the protein because the effect of its charge had already been shown to have a significant effect in Chapter 7. The ratio of Eq. (E.58) to Eq. (E.59) under similar pH and

excluded-volume conditions is given by:

$$\frac{K_{p,NaClO_4}}{K_{p,HPO_4}} = \frac{\left[\exp\left[\frac{\left(u_{Na,C_{10}E_4} - u_{ClO_4,C_{10}E_4}\right)}{k_BT\left(z_{Na} - z_{ClO_4}\right)}\right]\right]^{z_p\left(C_{C_{10}E_4,t} - C_{C_{10}E_4,b}\right)}}{\left[\exp\left[\frac{\left(u_{Na,C_{10}E_4} - u_{HPO_4,C_{10}E_4}\right)}{k_BT\left(z_{Na} - z_{HPO_4}\right)}\right]\right]^{z_p\left(C_{C_{10}E_4,t} - C_{C_{10}E_4,b}\right)}} \tag{E.62}$$

where $K_{p,NaClO_4}$ is the partition coefficient of lysozyme when $NaClO_4$ governs electroneutrality, and K_{p,Na_2HPO_4} is the partition coefficient of lysozyme when Na_2HPO_4 governs electroneutrality. Rearranging Eq. (E.62) yields:

$$\frac{K_{p,NaClO_4}}{K_{p,HPO_4}} = \left[\exp\left[\frac{1}{k_BT}\left(\frac{u_{Na,C_{10}E_4} - u_{ClO_4,C_{10}E_4}}{z_{Na} - z_{ClO_4}} - \frac{u_{Na,C_{10}E_4} - u_{HPO_4,C_{10}E_4}}{z_{Na} - z_{HPO_4}}\right)\right]\right]^{z_p\left(C_{C_{10}E_4,t} - C_{C_{10}E_4,b}\right)} \tag{E.63}$$

Since $z_{Na} = +1$, $z_{ClO_4} = -1$, and $z_{HPO_4} = -2$, Eq. (E.63) simplifies to:

$$\frac{K_{p,NaClO_4}}{K_{p,HPO_4}} = \left[\exp\left[\frac{\left(u_{Na,C_{10}E_4} + 2u_{HPO_4,C_{10}E_4}\right) - 3u_{ClO_4,C_{10}E_4}}{6k_BT}\right]\right]^{z_p\left(C_{C_{10}E_4,t} - C_{C_{10}E_4,b}\right)} \tag{E.64}$$

Based on Eqs. (E.60) and (E.61), the following inequality also applies:

$$\left(u_{Na,C_{10}E_4} + 2u_{HPO_4,C_{10}E_4}\right) - 3u_{ClO_4,C_{10}E_4} > 0 \tag{E.65}$$

Since $C_{C_{10}E_4,t} > C_{C_{10}E_4,b}$ (the top phase is micelle-rich, while the bottom phase is micelle-poor), $z_p > 0$ for lysozyme at pH=7.2 (see Chapter 7), and $k_BT > 0$, Eq. (E.64) can be qualitatively viewed as follows:

$$\frac{K_{p,NaClO_4}}{K_{p,HPO_4}} = \exp\left[a\right] \tag{E.66}$$

where $a > 0$. Accordingly, the ratio of $K_{p,NaClO_4}$ to K_{p,HPO_4} is expected to be greater than 1. The experiment described in Section E.3.3 was performed to test this qualitative prediction.

E.3 Materials and Methods

E.3.1 Materials

The nonionic surfactant *n*-decyl tetra(ethylene oxide) ($C_{10}E_4$) (lot no. 6011) was obtained from Nikko Chemicals (Tokyo, Japan). Lysozyme (lot no. 57H7045) and bovine serum

albumin (BSA) (lot no. 96H0595) were purchased from Sigma (St. Louis, MO). Citric acid (lot no. 0616 KCXK) and sodium chloride (NaCl) (lot no. 7544 KADT) were obtained from Mallinckrodt (Paris, KY). Disodium phosphate (Na_2HPO_4) (lot no. 896726) was purchased from Fisher Scientific (Fair Lawn, NJ). Sodium perchlorate ($NaClO_4$) (catalog no. 91) was obtained from G. Frederick Smith Chemical Company (Columbus, OH). All these materials were used as received. All solutions were prepared using McIlvaine's buffer consisting of disodium phosphate and citric acid in Milli-Q water. The molar ratio of disodium phosphate to citric acid was varied depending on the desired pH of the solution. Milli-Q water is the product of passing deionized water through Millipore's (Bedford, MA) Milli-Q system. All glassware used in the experiments were subjected to washing in a 50:50 ethanol:1 M sodium hydroxide bath, washing in a 1 M nitric acid bath, rinsing copiously with Milli-Q water, and drying in an oven for at least one day.

E.3.2 Partitioning BSA in the $C_{10}E_4$-Buffer Two-Phase System at Different pH Conditions

For the reasons explained in Section E.2.1, two BSA partitioning experiments were conducted, one at a pH of 3.2 and another at a pH of 6.8. For each BSA partitioning experiment, five solutions, each having a total volume of 3.5 mL, were prepared in graduated 10 mL test tubes. Four of the solutions contained 5.00 wt% $C_{10}E_4$, 0.4 g/L of BSA, and 0.50 M NaCl, while the fifth solution served as the control containing the same concentrations of $C_{10}E_4$ and NaCl but no BSA. The reasons for choosing these $C_{10}E_4$ and NaCl concentrations were given in Section E.2.1. BSA was chosen as the model protein because its net charge changes from being positive to being negative when the solution pH is increased from 3.2 to 6.8, and it is also: (i) water-soluble, (ii) available in high purity, and (iii) easy to assay with ultraviolet absorbance measurements.

After the solutions were prepared, they were gently mixed, and equilibrated at 4°C in the refrigerator in order for each solution to exhibit a single phase. The solutions were subsequently placed in the thermo-regulated device, which was described in Section 3.2.4, to initiate phase separation at 16.7°C (for the experiment conducted at pH=3.2) and 16.2°C (for the experiment conducted at pH=6.8). These temperatures were chosen in order to yield a volume ratio of 1 in each partitioning experiment (see Section E.2.1 for an explanation of the choice of this volume ratio). These temperatures were also selected because the difference in surfactant volume fractions between the two phases ($\phi_t - \phi_b$) was approximately 0.1. A value for ($\phi_t - \phi_b$) that was 0.1 or higher was desirable, since it corresponds to the situation where

the $C_{10}E_4$ concentrations in the two phases are very different from each other. Therefore, the Na^+ and Cl^- ions that govern electroneutrality (see Section E.2.1) are expected to experience interactions in the micelle-rich phase that are very different from those in the micelle-poor phase. In other words, the magnitudes of $(\mu^{ex}_{Na,t} - \mu^{ex}_{Na,b})$ and $(\mu^{ex}_{Cl,t} - \mu^{ex}_{Cl,b})$ are expected to increase as $(\phi_t - \phi_b)$ increases. Consequently, according to Eq. (E.35), the effect of the electrostatic potential difference, if it is indeed present, should be more significant for higher $(\phi_t - \phi_b)$ values. The solutions were maintained at the desired partitioning temperature for at least 23 hours prior to withdrawing the phases with great care using syringe and needle sets. All the partitioning experiments in this thesis were conducted for *at least* 14 hours, since it was shown previously[70] that partition coefficients measured after overnight partitioning did not differ from those measured after partitioning over at least three days. The concentrations of BSA in the phases, and subsequently, its partition coefficients, were determined utilizing a procedure similar to the one used for cytochrome *c* in Section 5.2.4. The only differences were: (i) BSA did not need to be reduced with sodium L-ascorbate prior to measuring its absorbance, and (ii) the wavelength for absorption was 280 nm.

E.3.3 Partitioning Lysozyme in the $C_{10}E_4$-Buffer Two-Phase System at pH=7.2 in the Absence and in the Presence of Added $NaClO_4$

For the reasons explained in Section E.2.2, lysozyme partitioning experiments were conducted at pH=7.2 in the absence and in the presence of $NaClO_4$. For each lysozyme partitioning experiment, five buffered solutions, each having a total volume of 3.5 mL, were prepared in graduated 10 mL test tubes. For the partitioning experiments conducted in the absence of $NaClO_4$, four of the solutions contained 5.00 wt% $C_{10}E_4$ and 0.1 g/L of lysozyme, while the fifth solution served as the control containing the same concentration of $C_{10}E_4$ but no lysozyme. For the partitioning experiments conducted in the presence of $NaClO_4$, four of the solutions contained 5.00 wt% $C_{10}E_4$, 0.1 g/L of lysozyme, and 0.50 M $NaClO_4$ (see Section E.2.2 for an explanation of the choice of 0.50 M $NaClO_4$), while the fifth solution served as the control containing the same concentrations of $C_{10}E_4$ and $NaClO_4$ but no lysozyme. The reasons for choosing these $C_{10}E_4$ and $NaClO_4$ concentrations were given in Section E.2.2. Lysozyme was selected as the model protein because its charge had already been shown to have a significant effect on its partitioning in Chapter 7, and it is also: (i) water-soluble, (ii) available in high purity, and (iii) easy to assay with ultraviolet absorbance measurements.

After the solutions were prepared, they were mixed, equilibrated at 4°C in the refrigerator,

and subsequently placed in the thermo-regulated device, which was described in Section 3.2.4, to initiate phase separation at 20.9°C (in the absence of $NaClO_4$) and 34.0°C (in the presence of $NaClO_4$). These temperatures were chosen in order to yield a volume ratio of 1 in each partitioning experiment (see Section E.2.2 for an explanation of the choice of this volume ratio). These temperatures were also selected because the difference in surfactant volume fractions between the two phases ($\phi_t - \phi_b$) was approximately 0.1. A value for ($\phi_t - \phi_b$) that was 0.1 or higher was again desirable, since it corresponds to having two macroscopic phases with $C_{10}E_4$ concentrations that are very different from each other. Accordingly, the Na^+ and HPO_4^{-2} ions, or the Na^+ and ClO_4^- ions, that govern electroneutrality are expected to experience interactions in the micelle-rich phase that are very different from those in the micelle-poor phase. This dependence can be found, for example, in Eq. (E.64) where the exponent is equal to $z_p(C_{C_{10}E_4,t} - C_{C_{10}E_4,b})$. Consequently, the effect of the salts should be greater for higher $(C_{C_{10}E_4,t} - C_{C_{10}E_4,b})$ values, which also correspond to higher $(\phi_t - \phi_b)$ values. The solutions were maintained at the desired operating tempearture for at least 26 hours prior to withdrawing the phases with great care using syringe and needle sets. The concentrations of lysozyme in the phases, and subsequently, its partition coefficients, were determined utilizing a procedure similar to the one used for cytochrome *c* in Section 5.2.4. The only differences were: (i) lysozyme did not need to be reduced with sodium L-ascorbate prior to measuring its absorbance, and (ii) the wavelength for absorption was 280 nm.

E.4 Results and Discussion

E.4.1 Partitioning BSA in the $C_{10}E_4$-Buffer Two-Phase System at Different pH Conditions

The results of the BSA partitioning experiments are shown in Figure E-6. The mass balances on BSA closed to 100% within the experimental error. As indicated in Figure E-6, the partition coefficient of BSA decreased from 19 to 0.32 when the pH of the solution was varied from 3.2 to 6.8. Based on the theoretical analysis of Section E.2.1, this change in the partition coefficient of BSA as its net charge was varied demonstrates the existence of an electrostatic potential difference. It can therefore be concluded that a significant electrostatic potential difference is present in the $C_{10}E_4$-buffer two-phase system when NaCl governs electroneutrality. In addition, measuring a partition coefficient of BSA that was greater than 1 already demonstrated the existence of an electrostatic potential difference, since excluded-volume interactions would always give rise to a partition coefficient that is

less than 1. If only excluded-volume interactions between BSA and the micelles were present, BSA would always partition preferentially into the bottom, micelle-poor phase. It is also interesting that a partition coefficient of 19, which is very desirable from the perspective of protein purification, can be achieved by changing the net charge on BSA even though the $C_{10}E_4$ micelles are noncharged. Accordingly, adjusting the solution pH and varying salts can be used as additional methods for improving the partitioning behavior of proteins.

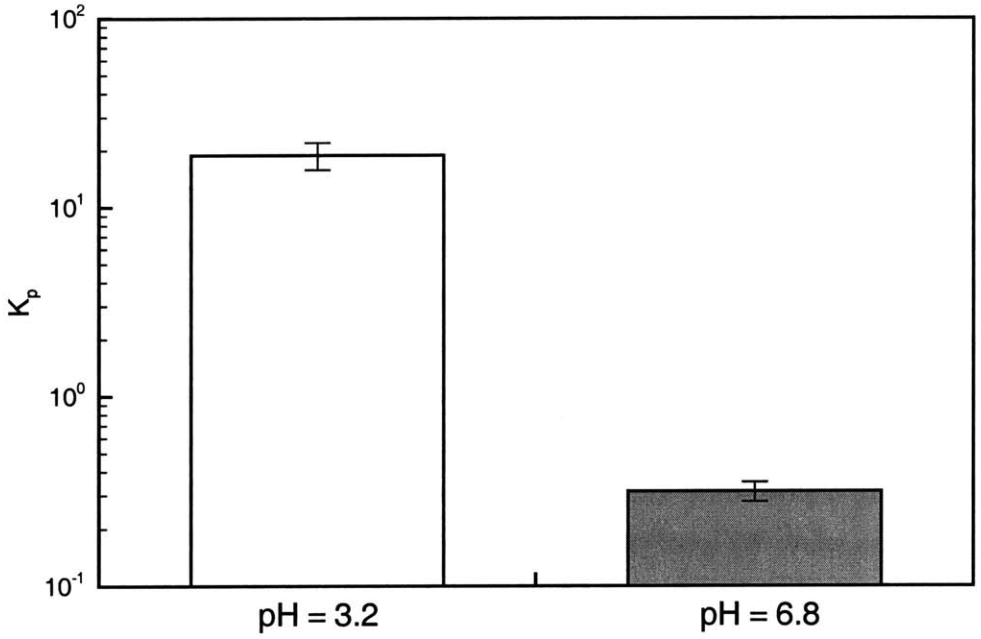

Figure E-6: Experimentally measured partition coefficients of BSA in the presence of 0.50 M NaCl at different pH conditions. The white and gray bars correspond to the partition coefficients of BSA measured at pH=3.2 (below pI) and pH=6.8 (above pI), respectively. The error bars correspond to 95% confidence limits for the measurements.

E.4.2 Partitioning Lysozyme in the $C_{10}E_4$-Buffer Two-Phase System at pH=7.2 in the Absence and in the Presence of Added $NaClO_4$

The results of the lysozyme partitioning experiments are shown in Figure E-7. The mass balances on lysozyme closed to 100% within the experimental error. As indicated in Figure E-7, the partition coefficient of lysozyme increased with the addition of $NaClO_4$. In fact, the ratio of $K_{p,NaClO_4}$ to K_{p,HPO_4} was experimentally determined to be 1.5, which is consistent with the qualitative prediction of Section E.2.2. It can therefore be concluded that a significant electrostatic potential difference exists in the $C_{10}E_4$-buffer two-phase system when $NaClO_4$ governs electroneutrality. In addition, measuring a partition coefficient of 1.03

(in the presence of $NaClO_4$) already demonstrates the existence of an electrostatic potential difference, since excluded-volume interactions would always give rise to a partition coefficient that is less than 1. This experimental study, along with the theoretical analysis presented in Section E.2.2, has shown that the partitioning behavior of proteins can be rationally manipulated by varying the salt governing electroneutrality with some knowledge of the ion-surfactant interaction parameters.

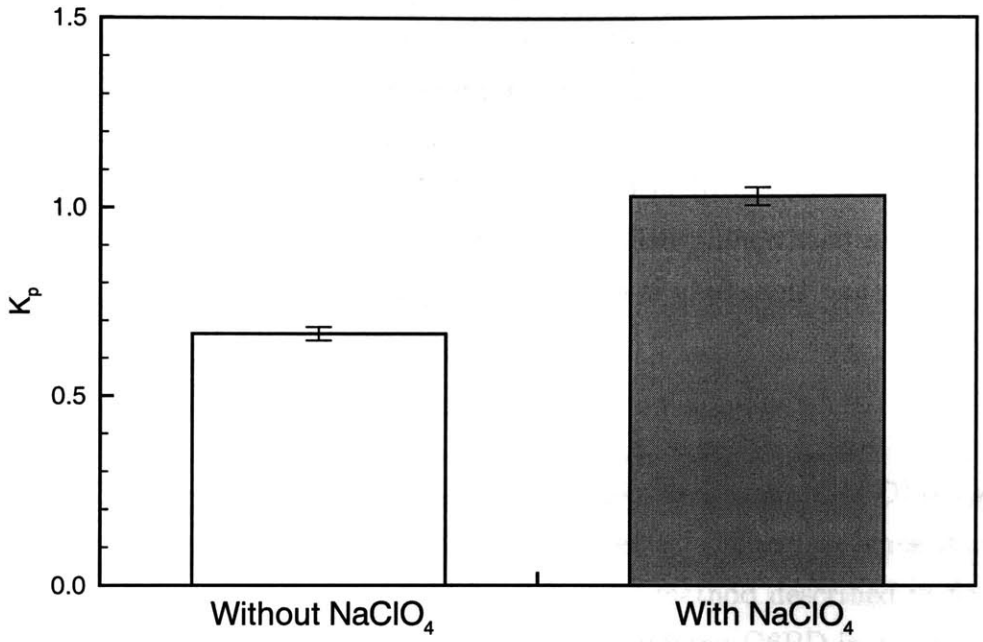

Figure E-7: Experimentally measured partition coefficients of lysozyme at pH=7.2 in the absence and in the presence of 0.50 M $NaClO_4$. The white and gray bars correspond to the partition coefficients of lysozyme measured in the absence and in the presence of 0.50 M $NaClO_4$, respectively. The error bars correspond to 95% confidence limits for the measurements.

E.5 Conclusions

A theory was developed which incorporated the electrostatic potential difference between the two macroscopic $C_{10}E_4$ micellar phases. Utilizing this theory and available protein partitioning data, the electrostatic potential difference in the $C_{10}E_4$-buffer two-phase system considered in this thesis was shown to be not very important. Specifically, this electrostatic potential difference was associated with Na_2HPO_4 governing electroneutrality in each macroscopic phase. The theory also indicated that a significant electrostatic potential difference may be observed if another salt was used to govern electroneutrality. NaCl and $NaClO_4$

were utilized, and they were able to generate a significant electrostatic potential difference between the two macroscopic $C_{10}E_4$ micellar phases. Accordingly, a significant electrostatic potential difference can exist depending on the salt used to govern electroneutrality. Two different proteins were also partitioned to test the generality of the electrostatic potential difference. The results of this study indicate that the electrostatic potential difference can be used in the future to improve the purification of proteins. Consequently, varying salts and pH can be used as new strategies for improving the purification of proteins. Since the effect of the electrostatic potential difference has a strong dependence on the charge of the partitioning protein, future experiments should be conducted with glucose-6-phosphate dehydrogenase (G6PD), which has been predicted to have a net charge of -42.2 at a pH of 7.2 using the method described in Chapter 7. A feasibility study was initially performed to determine if the partitioning behavior of G6PD could be examined in the $C_{10}E_4$-buffer two-phase system, and this study is described in Appendix F.

Appendix F

A Preliminary Investigation of Glucose-6-Phosphate Dehydrogenase Partitioning in the $C_{10}E_4$-Buffer Two-Phase System

F.1 Introduction

As discussed in Appendix E, glucose-6-phosphate dehydrogenase (G6PD) is a good model protein for further investigating the electrostatic potential difference, since its net charge has been estimated to be -42.2 at a pH of 7.2 using the method described in Section 7.3.4. This appendix therefore serves as a starting point for studying G6PD in two-phase aqueous micellar systems. Specifically, in this appendix, the applicability of an enzymatic assay for G6PD in aqueous $C_{10}E_4$ solutions was first investigated. Subsequently, protein partitioning experiments were conducted in the two-phase aqueous $C_{10}E_4$ micellar system.

The remainder of this appendix is organized as follows. In Section F.2, the materials and experimental methods are detailed. Section F.3 provides the theoretical basis for the G6PD assay. In Section F.4, the experimental results are presented and discussed. Finally, concluding remarks are presented in Section F.5.

F.2 Materials and Methods

F.2.1 Materials

The nonionic surfactant *n*-decyl tetra(ethylene oxide) ($C_{10}E_4$) (lot no. 0015) was purchased from Nikko Chemicals (Tokyo, Japan). Glucose-6-phosphate dehydrogenase (G6PD) from *Leuconostoc mesenteroides* (lot no. 18H8628), D-glucose-6-phosphate (G6P) (lot no.

67H7005), and β-nicotinamide adenine dinucleotide phosphate ($NADP^+$) (lot no. 18H7040) were purchased from Sigma (St. Louis, MO). Disodium phosphate (lot no. 896726) and citric acid (lot no. 0616 KCXK) were obtained from Fisher Scientific (Fair Lawn, NJ) and Mallinckrodt (Paris, KY), respectively. All these materials were used as received. All solutions were prepared using pH 7.2 McIlvaine's buffer consisting of 16.4 mM disodium phosphate and 1.82 mM citric acid in Milli-Q water. Milli-Q water is the product of passing deionized water through Millipore's (Bedford, MA) Milli-Q system. All glassware used in the experiments were subjected to washing in a 50:50 ethanol:1 M sodium hydroxide bath, washing in a 1 M nitric acid bath, rinsing copiously with Milli-Q water, and drying in an oven for at least one day.

F.2.2 Assaying G6PD in Aqueous $C_{10}E_4$ Solutions

Although the absorbance of G6PD at 280 nm can be used to measure its concentration in buffered $C_{10}E_4$ solutions (similar to the method described in Section 5.2.4), at least 0.3 g/L of G6PD is required in order for the absorbance to be detectable. Since G6PD is a very expensive enzyme, another assay requiring lower concentrations of G6PD was desirable. Measuring the concentration of G6PD in buffered $C_{10}E_4$ solutions with an enzymatic assay was therefore investigated, because such an assay is capable of measuring extremely low concentrations of the enzyme.

The reaction catalyzed by G6PD is given by:

$$\text{G6P} + \text{NADP}^+ \longrightarrow \text{6-phosphoglucono-}\delta\text{-lactone} + \text{NADPH} + \text{H}^+ \qquad \text{(F.1)}$$

Although a well-established enzymatic assay for G6PD exists, changes were made to the assay to match the conditions of our partitioning experiments. In particular, McIlvaine's pH 7.2 buffer was utilized, and the temperature of the assay was lowered to 15°C to prevent the possible onset of phase separation during the assay. A standard curve of the enzymatic activity of G6PD as a function of G6PD concentration was first measured for G6PD samples taken from buffered solutions without $C_{10}E_4$. This standard curve was measured to determine if the changes in the assay buffer and temperature would affect the accurate measurement of G6PD concentrations. Subsequently, a standard curve of the enzymatic activity of G6PD as a function of G6PD concentration was measured for G6PD samples taken from buffered solutions containing 5.15 wt% of $C_{10}E_4$. This standard curve was measured to determine if the presence of the $C_{10}E_4$ surfactant would interfere with the assay. The concentration of

5.15 wt% was chosen because it is a typical $C_{10}E_4$ concentration encountered in the micelle-rich phase during a partitioning experiment. For each concentration of G6PD, a triplicate of solutions was prepared, and their corresponding activities were measured.

The activity of G6PD was measured by determining the rate of formation of NADPH (see Section F.3 for the theoretical basis of this assay). The rate of formation of NADPH can be monitored because NADPH absorbs ultraviolet light at 340 nm, and the absorbance, or optical density (O.D.), is directly proportional to the concentration of NADPH according to the Beer-Lambert law:[104]

$$A = \epsilon d_p \, [C\text{-}H\,] \tag{F.2}$$

where ϵ is the absorption coefficient of the solution, d_p is the path length of the cuvette, and $[C\text{-}H]$ denotes the molar concentration of NADPH in the solution (see Section F.3 for the reason behind the notation $[C\text{-}H]$). Since ϵ and d_p do not change with time, the change in absorbance (O.D.) with time is directly proportional to the change in the concentration of NADPH with time as shown below:

$$\frac{dA}{dt} = \epsilon d_p \frac{d\,[C\text{-}H\,]}{dt} \tag{F.3}$$

In addition, the change in the concentration of NADPH with time is shown in Section F.3 to be directly proportional to the total concentration of G6PD as follows:

$$\frac{d\,[C\text{-}H\,]}{dt} = \alpha_1 \, [E_T] \tag{F.4}$$

where $[E_T]$ is the total enzyme (G6PD) concentration, and α_1 is a proportionality constant defined in Section F.3. Combining Eqs. (F.3) and (F.4) yields:

$$\frac{1}{\epsilon d_p} \frac{dA}{dt} = \alpha_1 \, [E_T] \tag{F.5}$$

Rearranging Eq. (F.5) gives the following relation:

$$\frac{dA}{dt} = \alpha_1 \epsilon d_p \, [E_T] \tag{F.6}$$

which can also be rewritten as follows:

$$[E_T] = \frac{1}{\alpha_1 \epsilon d_p} \frac{dA}{dt} \tag{F.7}$$

Accordingly, the total concentration of the enzyme can be measured to within a proportionality constant by measuring the change in the absorbance of NADPH with time.

In this assay, 0.13 M $NADP^+$ and 0.50 M G6P solutions were first prepared in the pH 7.2 buffer. 4 μL of 0.13 M $NADP^+$, 20 μL of 0.50 M G6P, and 900 μL of pH 7.2 buffer were then pipetted into each cuvette. The cuvettes containing these solutions were then allowed to thermally equilibrate for 15 minutes at 15°C inside the spectrophotometer. After the cuvettes were thermally equilibrated, 50 μL of each solution containing G6PD were added to each cuvette, giving rise to a 50 μL:974 μL or about a 1:20 dilution of the sample. Each solution in the cuvette was then quickly mixed, and the absorbance (O.D.) at 340 nm was measured as a function of time for 50 seconds. The slope of this curve corresponded to the change in absorbance with time. Control experiments were also performed, where instead of adding 50 μL of a sample containing G6PD, 50 μL of buffer or a 5.15 wt% solution of $C_{10}E_4$ without G6PD were added to each cuvette.

F.2.3 Mapping the Coexistence Curve of the Two-Phase Aqueous $C_{10}E_4$ Micellar System

The coexistence or binodal curve of the two-phase aqueous $C_{10}E_4$ micellar system delineates the two-phase region from the one-phase region in a temperature-$C_{10}E_4$ concentration phase diagram at constant pressure (see the schematic representation in Figure 1-3). Although the coexistence curve of the two-phase aqueous $C_{10}E_4$ micellar system was previously measured at 1 atm in Chapter 4, the coexistence curve was again mapped out at 1 atm because $C_{10}E_4$ from a new lot was used in this experimental study. In other words, the coexistence curve was mapped out to check for any $C_{10}E_4$ lot-to-lot variability. The cloud-point method described in Section 4.2.2 was again employed to measure the coexistence curve of the $C_{10}E_4$-buffer system.

F.2.4 Partitioning G6PD in the $C_{10}E_4$-Buffer Two-Phase System

For every partitioning experiment, five buffered solutions, each with a total volume of 3 mL, were prepared in graduated 10 mL test tubes. Four of the solutions contained $C_{10}E_4$ and 0.07 g/L of G6PD, while the fifth solution served as the control containing the same concentration of $C_{10}E_4$ but no G6PD. Five different partitioning experiments were conducted, and the initial, overall concentrations of $C_{10}E_4$ in the experiments are provided in Table F-1. The solutions were first mixed, and then equilibrated at 4°C in order for each solution to exhibit a single phase. The solutions were subsequently placed in the thermo-regulated de-

vice described in Section 3.2.4 to initiate phase separation at a particular temperature. The different partitioning temperatures are also listed in Table F-1. The partitioning temperatures between 19.2°C and 21.2°C were chosen because they were similar to the operating temperatures that have been used in past partitioning experiments.[70] After selecting the partitioning temperatures, the initial, overall concentrations of $C_{10}E_4$ were chosen for the different experiments to yield volume ratios that were approximately equal to 1. A volume ratio of 1 was chosen to be consistent with the partitioning experiments that were previously conducted.[70]

Table F-1: The conditions of the G6PD partitioning experiments in the two-phase aqueous $C_{10}E_4$ micellar system.

Initial Concentration of $C_{10}E_4$ (wt%)	**Partitioning Temperature (°C)**
2.42	19.2
3.10	19.7
3.87	20.2
4.67	20.7
5.51	21.2

Solutions were maintained at the desired operating temperature for 18 hours before the two coexisting micellar phases were withdrawn with great care using 1 mL syringe and needle sets. All the partitioning experiments in this thesis were conducted for *at least* 14 hours, since it was shown previously[70] that partition coefficients measured after overnight partitioning were similar to those measured after partitioning over at least three days. The partition coefficients of G6PD were evaluated as described in Section F.4.1.

F.3 Theory

This section provides the theoretical basis for the assay described in Section F.2.2. Specifically, it will be shown theoretically that the total concentration of G6PD is directly proportional to the change in the concentration of NADPH with time, which can be measured to within a proportionality constant by monitoring the absorbance of NADPH at 340 nm with time. To begin, the following reaction pathway is proposed:

$$E + S \underset{k_{-1}}{\overset{k_1}{\rightleftharpoons}} ES + C \underset{k_{-2}}{\overset{k_2}{\rightleftharpoons}} ESC \xrightarrow{k_3} E + P + C\text{-}H + H^+ \tag{F.8}$$

where E is the free enzyme (G6PD that is not bound to the substrate or cofactor), S is the substrate (G6P), ES is the enzyme-substrate complex, C is the cofactor ($NADP^+$), ESC is the enzyme-substrate-cofactor complex, P is the product (6-phosphoglucono-δ-lactone), $C\text{-}H$ is the cofactor with a bound hydrogen (NADPH), and k_1, k_{-1}, k_2, k_{-2}, and k_3 are the forward and reverse rate constants for the different steps in the reaction pathway.

Based on the reaction pathway shown in Eq. (F.8), the rate of formation of $C\text{-}H$ (or the change in the concentration of NADPH with time) is given by:

$$\frac{d[C\text{-}H]}{dt} = k_3[ESC] \tag{F.9}$$

where $[ESC]$ is the molar concentration of ESC. The pseudo-steady-state approximation[135] is used under the assumption that the rate of formation of the active intermediate ESC is equal to its rate of disappearance. This yields the following expression for ESC:

$$\frac{d[ESC]}{dt} = 0 = k_2[ES][C] - k_{-2}[ESC] - k_3[ESC] \tag{F.10}$$

Rearranging Eq. (F.10) yields:

$$[ESC] = \frac{k_2}{k_{-2} + k_3}[ES][C] \tag{F.11}$$

The pseudo-steady-state approximation[135] is also applied to the active intermediate ES as follows:

$$\frac{d[ES]}{dt} = 0 = k_1[E][S] + k_{-2}[ESC] - k_{-1}[ES][C] - k_2[ES][C] \tag{F.12}$$

Rearranging Eq. (F.12) gives the following relation:

$$[ES][C] = \frac{k_1[E][S]}{k_{-1} + k_2} + \frac{k_{-2}[ESC]}{k_{-1} + k_2} \tag{F.13}$$

Substituting Eq. (F.13) into Eq. (F.11) yields:

$$[ESC] = \frac{k_2}{k_{-2} + k_3}\left[\frac{k_1[E][S]}{k_{-1} + k_2} + \frac{k_{-2}[ESC]}{k_{-1} + k_2}\right] \tag{F.14}$$

Rearranging Eq. (F.14) yields:

$$[ESC] = k^*[E][S] \tag{F.15}$$

where

$$k^* = \left[\frac{k_1 k_2}{(k_{-2}+k_3)(k_{-1}+k_2)}\right]\left[\frac{1}{1-\frac{k_2 k_{-2}}{(k_{-2}+k_3)(k_{-1}+k_2)}}\right] \tag{F.16}$$

Substituting Eq. (F.15) into Eq. (F.9) gives the following relation:

$$\frac{d[C\text{-}H]}{dt} = k_3 k^* [E][S] \tag{F.17}$$

An expression for $d[C\text{-}H]/dt$ as a function of the *total* enzyme concentration, $[E_T]$, is desired, since this enzymatic assay will be used to determine the *total* enzyme concentration in each phase. Therefore, an expression for $[E]$ in terms of $[E_T]$ is required for substitution into Eq. (F.17). To derive this expression, the mass balance on the enzyme will first be written as follows:

$$[E_T] = [E] + [ESC] + [ES] \tag{F.18}$$

Rearranging Eq. (F.18) yields:

$$[E] = [E_T] - [ESC] - [ES] \tag{F.19}$$

An expression for $[ES]$ to substitute into Eq. (F.19) will now be obtained by rearranging Eq. (F.11) as follows:

$$[ES] = \left(\frac{k_{-2}+k_3}{k_2}\right)\frac{[ESC]}{[C]} \tag{F.20}$$

Substituting Eq. (F.20) into Eq. (F.19) yields:

$$[E] = [E_T] - [ESC] - \left(\frac{k_{-2}+k_3}{k_2}\right)\frac{[ESC]}{[C]} \tag{F.21}$$

Combining Eqs. (F.15) and (F.21) yields:

$$[E] = [E_T] - k^*[E][S] - \left(\frac{k_{-2}+k_3}{k_2}\right)\frac{k^*[E][S]}{[C]} \tag{F.22}$$

Rearranging Eq. (F.22) gives the desired relation between $[E]$ and $[E_T]$:

$$[E] = \frac{[E_T]}{1 + k^*[S] + \frac{k^*(k_{-2}+k_3)}{k_2}\frac{[S]}{[C]}} \tag{F.23}$$

Substituting Eq. (F.23) into Eq. (F.17) yields:

$$\frac{d[C\text{-}H]}{dt} = \frac{k_3 k^* [E_T][S]}{1 + k^*[S] + \frac{k^*(k_{-2}+k_3)}{k_2}\frac{[S]}{[C]}} \tag{F.24}$$

If the concentrations of the substrate (G6P) and the cofactor ($NADP^+$) are in excess relative to the concentration of the enzyme (G6PD), they remain essentially constant over the duration of the assay. In this case, the rate of formation of NADPH is equal to:

$$\frac{d[C\text{-}H]}{dt} = \alpha_1 [E_T] \tag{F.4}$$

which was referred to in Section F.2.2, where α_1 is defined as follows:

$$\alpha_1 \equiv \frac{k_3 k^* [S]}{1 + k^*[S] + \frac{k^*(k_{-2}+k_3)}{k_2}\frac{[S]}{[C]}} \tag{F.25}$$

Although Eq. (F.4) was derived based on the pathway proposed in Eq. (F.8), a linear relationship between $d[C\text{-}H]/dt$ and $[E_T]$ will still be obtained for other proposed pathways as long as the concentrations of the substrate and the cofactor are very high. In other words, the concentrations of G6P (substrate) and $NADP^+$ (cofactor) can always be adjusted to ensure a linear relationship between the rate of change of $[C\text{-}H]$ and the total concentration of G6PD (enzyme).

F.4 Results and Discussion

F.4.1 Assaying G6PD in Aqueous $C_{10}E_4$ Solutions

The results of the enzymatic activity assays are shown in Figure F-1. As indicated in Figure F-1, the rate of change in the absorbance at 340 nm is directly proportional to the concentration of G6PD. Therefore, it can be concluded that the concentration of G6PD can be measured with good accuracy even in the presence of $C_{10}E_4$, the different buffer, and the lower assay temperature. In addition, since the same slopes were obtained for the two standard curves, it can be concluded that $\alpha_1 \epsilon d_p$ in Eq. (F.6) has the same value in the absence and in the presence of $C_{10}E_4$. The path length, d_p, was expected to be the same for the two standard curves because cuvettes of the same path length were used in all the absorbance measurements. Even though the absorption coefficient, ϵ, is a weak function of the environment surrounding NADPH, it is not surprising that it did not vary with the

addition of $C_{10}E_4$, because a 1:20 dilution of each 5.15 wt% $C_{10}E_4$ solution was obtained when it was pipetted into each cuvette. Accordingly, the concentration of $C_{10}E_4$ was only 0.258 wt% in the solutions contained in the cuvette, and therefore, the environment was very similar to that of a buffered solution without $C_{10}E_4$. With regard to the value of α_1, which is defined in Eq. (F.25), it remained at the same value because the same concentrations of G6P (substrate) and $NADP^+$ (cofactor) were used for all the measurements. The reaction rate constants in α_1 also did not vary because the same assay temperature was utilized for all the experiments, and the solution conditions remained very similar between the standard curves. It should also be noted that the concentrations of G6PD reported in Figure F-1 correspond to those present in the solutions preceding the 1:20 dilution. However, the concentrations of G6PD after the dilution could have instead been reported, since a linear relationship between the activity and the G6PD concentration would still have been obtained. Although the results are not shown, all the control experiments without G6PD showed no activity.

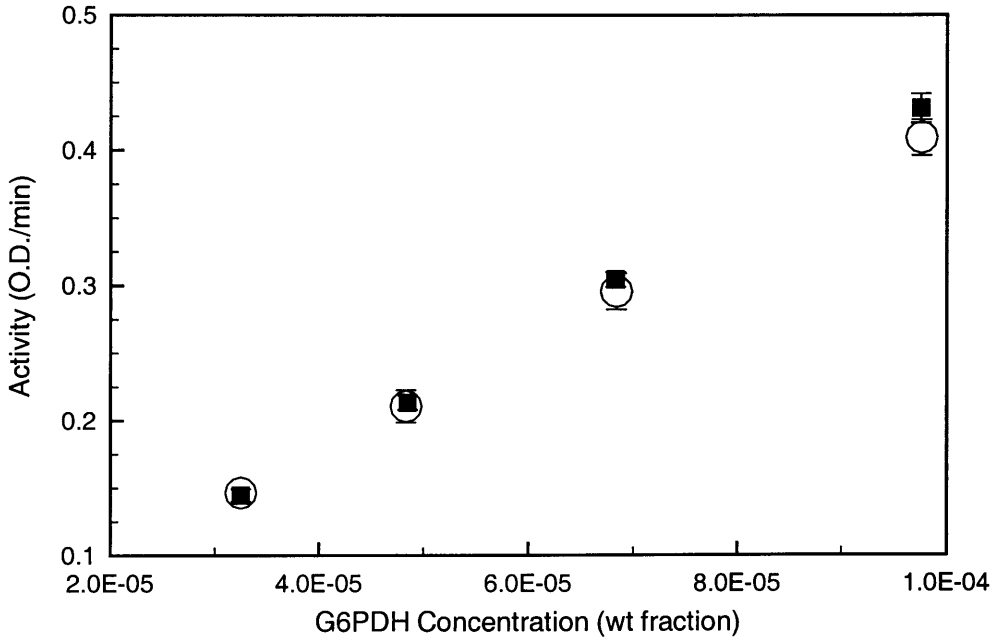

Figure F-1: Enzymatic activity measurements of G6PD solutions in the absence and in the presence of $C_{10}E_4$. The black square and white circle symbols represent the enzymatic activities of G6PD measured in the absence and in the presence of $C_{10}E_4$, respectively. The error bars correspond to 95% confidence limits for the measurements.

Since $\alpha_1 \epsilon d_p$ has been shown to be a constant, the partition coefficient of G6PD can be easily evaluated as follows:

$$K_p \equiv \frac{[E_{T,t}]}{[E_{T,b}]} \tag{F.26}$$

where $[E_{T,t}]$ and $[E_{T,b}]$ are the total molar concentrations of G6PD (enzyme) in the top and bottom phases, respectively. Combining Eqs. (F.7) and (F.26), and recognizing that $\alpha_1 \epsilon d_p$ is a constant, yields:

$$K_p = \frac{\left(\frac{dA}{dt}\right)_t}{\left(\frac{dA}{dt}\right)_b} \tag{F.27}$$

where $(dA/dt)_t$ and $(dA/dt)_b$ are the rates of change of absorbance measured in the top and bottom phases, respectively. In Section F.4.3, the measured values of $(dA/dt)_t$ and $(dA/dt)_b$ are reported, and Eq. (F.27) is used to evaluate the partition coefficients of G6PD.

F.4.2 Mapping the Coexistence Curve of the Two-Phase Aqueous $C_{10}E_4$ Micellar System

The measured coexistence curve of the two-phase aqueous $C_{10}E_4$ micellar system is shown in Figure F-2. For comparison, the previously measured coexistence curves have also been included. Although the $C_{10}E_4$ from the three different lots yield similar coexistence curves, the coexistence curve should be remeasured whenever $C_{10}E_4$ from different lots are used. The coexistence curve of the $C_{10}E_4$ (lot no. 0015)-buffer system was used to obtain the difference in surfactant volume fractions between the two phases $(\phi_t - \phi_b)$ at different temperatures. The $(\phi_t - \phi_b)$ values were required along with the hydrodynamic radius of G6PD in order to make the excluded-volume predictions presented in Section F.4.3. The hydrodynamic radius of G6PD was measured using light scattering to be 80 Å.[136]

F.4.3 Partitioning G6PD in the $C_{10}E_4$-Buffer Two-Phase System

The results of the partitioning experiments, along with the excluded-volume predictions, are shown in Figure F-3. The mass balances on G6PD closed to 100% within the experimental error for all the partitioning experiments. Since reproducible protein partition coefficients could be measured with the enzymatic assay described in this study, the electrostatic potential difference can be investigated in the future using G6PD as a model protein. Although the excluded-volume theory was able to predict the trend of the decreasing partition coefficient with increasing temperature, the deviations between theory and experiment were larger than those observed for the water-soluble proteins discussed in Chapter 1. One possible reason for this discrepancy is the entrainment effect discussed in Chapter 5, since the predicted excluded-volume partition coefficient of G6PD is much lower than that of the other water-soluble proteins due its larger hydrodynamic radius.

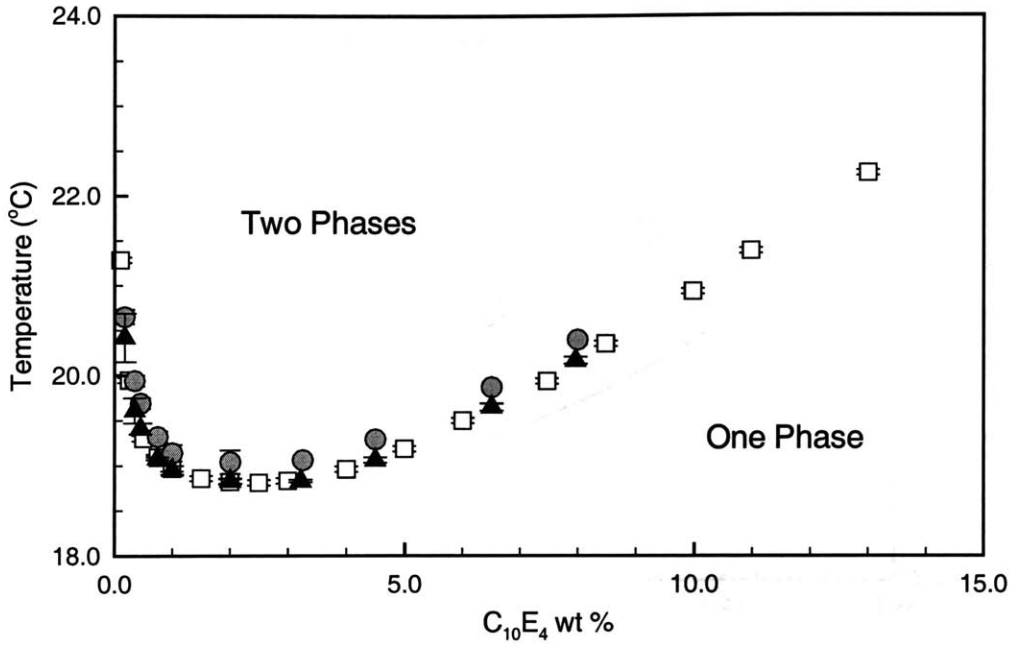

Figure F-2: The coexistence curves of the two-phase aqueous $C_{10}E_4$ micellar system for $C_{10}E_4$ from three different lots. The coexistence curve measured in this study (lot no. 0015) is denoted by the black triangles. The coexistence curve measured in Chapter 4 (lot no. 6011) is denoted by the gray circles. The coexistence curve measured in a previous study[72] (lot no. 1006) is denoted by the white squares. The error bars correspond to 95% confidence limits for the measurements.

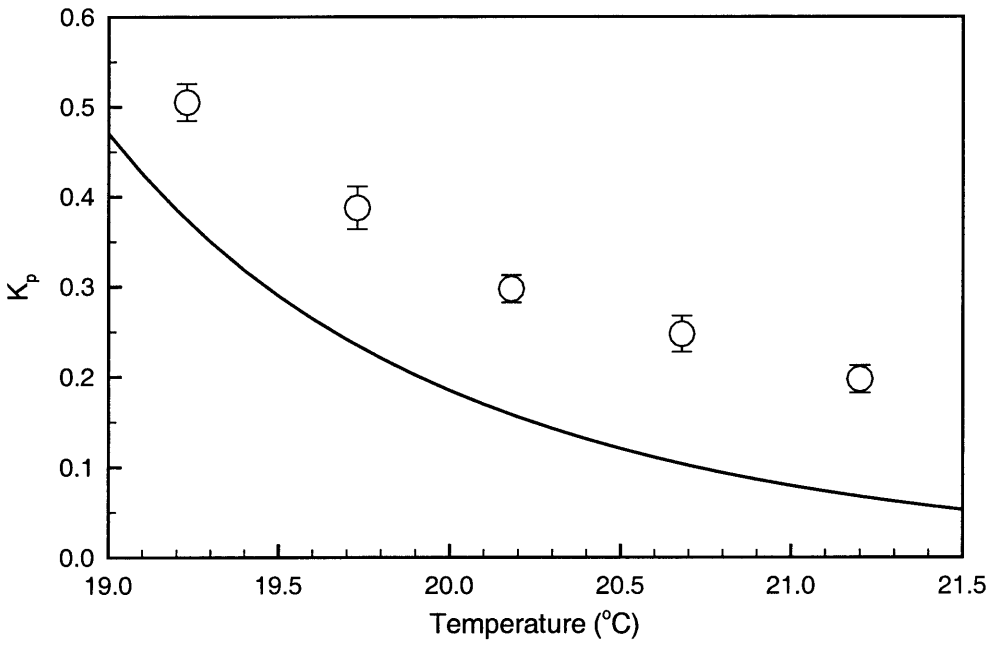

Figure F-3: Comparison between the theoretically predicted and experimentally measured partition coefficients of G6PD. The solid line corresponds to the partition coefficients that were predicted based on the excluded-volume theory. The white circle symbols represent the measured partition coefficients of G6PD. The error bars correspond to 95% confidence limits for the measurements.

F.5 Conclusions

The enzymatic assay described in this study can be used to measure reproducible partition coefficients of G6PD. Therefore, G6PD can be used in the future as a model protein to further investigate the electrostatic potential difference in the two-phase aqueous $C_{10}E_4$ micellar system.

Appendix G

Contributions of V_t^{ex} and V_b^{ex} to $(\mu_{p,t}^{ex} - \mu_{p,b}^{ex})$

The contributions of the excess volumes in the top and bottom phases, V_t^{ex} and V_b^{ex}, to the difference in excess chemical potentials of the protein between the two phases, $(\mu_{p,t}^{ex} - \mu_{p,b}^{ex})$, will now be shown to cancel each other out. The volumes of the $C_{10}E_4$ and SDS monomers free in the solution (not in a micelle) were also incorporated into the expression for the total volume of the solution to show that they can be included without changing the final expression for $(\mu_{p,t}^{ex} - \mu_{p,b}^{ex})$. Specifically, the total volume of the solution in phase α, V_α, can be written as follows:

$$V_\alpha = N_{w,\alpha}\Omega_w + N_{p,\alpha}\Omega_p + N_{1,C_{10}E_4,\alpha}\Omega_{C_{10}E_4} + N_{1,SDS,\alpha}\Omega_{SDS} + \sum_{n_\alpha=n^\circ_{cyl,\alpha}}^{\infty} N_{n_\alpha}\Omega_{n_\alpha} \qquad \text{(G.1)}$$

where $N_{w,\alpha}$ is the number of solvent molecules in phase α, $N_{p,\alpha}$ is the number of protein molecules in phase α, $N_{1,C_{10}E_4,\alpha}$ is the number of $C_{10}E_4$ monomers free in phase α, $N_{1,SDS,\alpha}$ is the number of SDS monomers free in phase α, N_{n_α} is the number of micelles of aggregation number n in phase α, $n^\circ_{cyl,\alpha}$ is the aggregation number of the smallest cylindrical micelle in phase α, Ω_p is the volume of a protein molecule, $\Omega_{C_{10}E_4}$ is the volume of a $C_{10}E_4$ molecule, Ω_{SDS} is the volume of a SDS molecule, and Ω_{n_α} is the volume of a cylindrical micelle of aggregation number n in phase α. Note that Ω_i $(i = w, p, C_{10}E_4, SDS, n_\alpha)$ is only a function of temperature and pressure because it is the pure molecular volume of component i. The index α is required in Ω_{n_α} because Ω_{n_α} is equal to the sum of all the pure molecular volumes of the individual monomers that comprise the micelle, and the molar ratio of ionic to nonionic surfactant can differ depending on whether the micelle is in the top or bottom phase. Note also that the buffer salt ions have been lumped along with the water molecules to form the hypersolvent.

The difference in excess chemical potentials of the protein in the two coexisting phases

is given by the following relation:

$$\mu_{p,t}^{ex} - \mu_{p,b}^{ex} = \left(\frac{\partial G_t^{ex}}{\partial N_{p,t}}\right)_{T,P,N_{k,t\neq p,t}} - \left(\frac{\partial G_b^{ex}}{\partial N_{p,b}}\right)_{T,P,N_{k,b\neq p,b}} \tag{G.2}$$

where $N_{k,t\neq p,t}$ and $N_{k,b\neq p,b}$ are the number of non-protein molecules of type k in the top and bottom phases, respectively. In addition, the excess Gibbs free energy in each phase α can be written as follows:

$$G_\alpha^{ex} = A_\alpha^{ex} + PV_\alpha^{ex} \tag{G.3}$$

where A_α^{ex} is the excess Helmholtz free energy in phase α, P is the pressure, and V_α^{ex} is the excess volume in phase α. Combining Eqs. (G.2) and (G.3) yields:

$$\begin{aligned}\mu_{p,t}^{ex} - \mu_{p,b}^{ex} &= \left[\left(\frac{\partial A_t^{ex}}{\partial N_{p,t}}\right)_{T,P,N_{k,t\neq p,t}} - \left(\frac{\partial A_b^{ex}}{\partial N_{p,b}}\right)_{T,P,N_{k,b\neq p,b}}\right] \\ &\quad + P\left[\left(\frac{\partial V_t^{ex}}{\partial N_{p,t}}\right)_{T,P,N_{k,t\neq p,t}} - \left(\frac{\partial V_b^{ex}}{\partial N_{p,b}}\right)_{T,P,N_{k,b\neq p,b}}\right]\end{aligned} \tag{G.4}$$

The excess volume of phase α is given by the following relation:

$$V_\alpha^{ex} = V_\alpha - V_\alpha^{id} \tag{G.5}$$

where V_α^{id} is the ideal volume of phase α, which is given by:

$$V_\alpha^{id} = \left(\frac{\partial G_\alpha^{id}}{\partial P}\right)_{T,N_{p,\alpha},N_{w,\alpha},N_{n_\alpha},N_{1,C_{10}E_4,b},N_{1,SDS,b}} \tag{G.6}$$

where G_α^{id} is the ideal Gibbs free energy given by:

$$\begin{aligned}G_\alpha^{id} &= N_{w,\alpha}\left(\mu_{w,pure}^\circ + k_BT\ln X_{w,\alpha}\right) + N_{p,\alpha}\left(\mu_{p,\infty}^\circ + k_BT\ln X_{p,\alpha}\right) \\ &\quad + N_{1,C_{10}E_4,\alpha}\left(\mu_{1,C_{10}E_4,\infty}^\circ + k_BT\ln X_{1,C_{10}E_4,\alpha}\right) \\ &\quad + N_{1,SDS,\alpha}\left(\mu_{1,SDS,\infty}^\circ + k_BT\ln X_{1,SDS,\alpha}\right) \\ &\quad + \sum_{n_\alpha=n_{cyl,\alpha}^\circ}^{\infty} N_{n_\alpha}\left(\mu_{n_\alpha,\infty}^\circ + k_BT\ln X_{n_\alpha}\right)\end{aligned} \tag{G.7}$$

where $X_{w,\alpha}$, $X_{p,\alpha}$, $X_{1,C_{10}E_4,\alpha}$, $X_{1,SDS,\alpha}$, and X_{n_α} are the mole fractions of solvent, proteins, free $C_{10}E_4$ monomers, free SDS monomers, and micelles of aggregation number n in phase α,

respectively, $\mu^{\circ}_{w,pure}$ is the pure-component standard-state chemical potential of the solvent, and $\mu^{\circ}_{p,\infty}$, $\mu_{1,C_{10}E_4,\infty}$, $\mu_{1,SDS,\infty}$, and $\mu^{\circ}_{n_\alpha,\infty}$ are the infintely-dilute standard-state chemical potentials of proteins, free $C_{10}E_4$ monomers, free SDS monomers, and micelles of aggregation number n in phase α, respectively. All the standard-state chemical potentials ($\mu^{\circ}_{w,pure}$, $\mu^{\circ}_{p,\infty}$, $\mu^{\circ}_{1,C_{10}E_4,\infty}$, $\mu^{\circ}_{1,SDS,\infty}$, and $\mu^{\circ}_{n_\alpha,\infty}$) are only functions of temperature and pressure. Combining Eqs. (G.1), (G.5), (G.6), and (G.7) yields:

$$\begin{aligned} V^{ex}_{\alpha} &= N_{p,\alpha}\left[\Omega_p - \left(\frac{\partial \mu^{\circ}_{p,\infty}}{\partial P}\right)_T\right] + N_{1,C_{10}E_4,\alpha}\left[\Omega_{C_{10}E_4} - \left(\frac{\partial \mu^{\circ}_{1,C_{10}E_4,\infty}}{\partial P}\right)_T\right] \\ &\quad + N_{1,SDS,\alpha}\left[\Omega_{SDS} - \left(\frac{\partial \mu^{\circ}_{1,SDS,\infty}}{\partial P}\right)_T\right] \\ &\quad + \sum_{n_\alpha = n^{\circ}_{cyl,\alpha}}^{\infty} N_{n_\alpha}\left[\Omega_{n_\alpha} - \left(\frac{\partial \mu^{\circ}_{n_\alpha,\infty}}{\partial P}\right)_T\right] \end{aligned} \tag{G.8}$$

since

$$\Omega_w = \left(\frac{\partial \mu^{\circ}_{w,pure}}{\partial P}\right)_T \tag{G.9}$$

In addition, it should be noted that $\left(\frac{\partial \mu^{\circ}_{p,\infty}}{\partial P}\right)_T$, $\left(\frac{\partial \mu^{\circ}_{1,C_{10}E_4,\infty}}{\partial P}\right)_T$, $\left(\frac{\partial \mu^{\circ}_{1,SDS,\infty}}{\partial P}\right)_T$, and $\left(\frac{\partial \mu^{\circ}_{n_\alpha,\infty}}{\partial P}\right)_T$ are not necessarily equal to the pure molecular volumes Ω_p, $\Omega_{C_{10}E_4}$, Ω_{SDS}, and Ω_{n_α}, respectively. They, instead, correspond to the volumes of the proteins, the free $C_{10}E_4$ monomers, the free SDS monomers, and the micelles of aggregation number n in phase α when the proteins, free $C_{10}E_4$ monomers, free SDS monomers, or micelles are completely surrounded by solvent at infinite dilution. Combining Eqs. (G.4) and (G.8) yields:

$$\mu^{ex}_{p,t} - \mu^{ex}_{p,b} = \left[\left(\frac{\partial A^{ex}_t}{\partial N_{p,t}}\right)_{T,P,N_{w,t},N_{n_t}} - \left(\frac{\partial A^{ex}_b}{\partial N_{p,b}}\right)_{T,P,N_{w,b},N_{n_b}}\right] \tag{G.10}$$

As indicated in Eq. (G.10), the contributions of V^{ex}_t and V^{ex}_b to $(\mu^{ex}_{p,t} - \mu^{ex}_{p,b})$ cancel each other out.

Appendix H

Evaluation of the Surface Charge Density of Every Micelle in Phase α

In this appendix, the surface charge density of a mixed micelle of aggregation number n in phase α, σ_{n_α}, will be shown to be independent of n and only a function of variables that are the same for all the micelles in phase α. Specifically, it will be shown that the surface charge density of every micelle in phase α is a constant, σ_α. The hemispherical endcaps of the micelle will be neglected because the equation for ψ_{cyl} in Eq. (7.22) was derived for infinitely long cylinders without endcaps. Accordingly, the surface charge density of a mixed micelle of aggregation number n in phase α is given by:

$$\sigma_{n_\alpha} = \frac{N_{SDS,n_\alpha} z_{SDS}\, e}{2\pi l_{SDS,n_\alpha} L_{n_\alpha}} \tag{H.1}$$

where N_{SDS,n_α} is the number of SDS molecules in the micelle of aggregation number n in phase α, z_{SDS} is the valence of an SDS molecule (which is -1), e is the electronic charge, l_{SDS,n_α} is the length of an SDS molecule in the micelle of aggregation number n in phase α, and L_{n_α} is the length of the cylindrical micelle of aggregation number of n in phase α. To obtain an expression for L_{n_α} to substitute in Eq. (H.1), the following equation for the volume of the hydrophobic core of the cylindrical micelle is required:

$$\pi l_{c,n_\alpha}^2 L_{n_\alpha} = (N_{C_{10}E_4,n_\alpha} \times v_{tail,C_{10}E_4}) + (N_{SDS,n_\alpha} \times v_{tail,SDS}) \tag{H.2}$$

where l_{c,n_α} is the radius of the hydrophobic core of the cylindrical micelle of aggregation number n in phase α, $N_{C_{10}E_4,n_\alpha}$ is the number of $C_{10}E_4$ molecules in the micelle of aggregation number n in phase α, and $v_{tail,C_{10}E_4}$ and $v_{tail,SDS}$ are the volumes of the hydrophobic tails of

$C_{10}E_4$ and SDS, respectively, and can be evaluated as follows:[53]

$$v_{tail} = 27.4 + 26.9\,(n_c - 1) \tag{H.3}$$

where v_{tail} is the volume of any linear hydrophobic hydrocarbon tail (without double or triple bonds) in any micelle in units of Å^3, and n_c is the number of carbons in the hydrophobic tail of interest. Accordingly, $v_{tail,C_{10}E_4}$ and $v_{tail,SDS}$ are constants. Solving Eq. (H.2) for L_{n_α}, substituting the result in Eq. (H.1), and rearranging yields:

$$\sigma_{n_\alpha} = \frac{y_{SDS,n_\alpha} z_{SDS}\, e\, l_{c,n_\alpha}^2}{2 l_{SDS,n_\alpha} \left[(1 - y_{SDS,n_\alpha})\, v_{tail,C_{10}E_4} + y_{SDS,n_\alpha} v_{tail,SDS}\right]} \tag{H.4}$$

where

$$y_{SDS,n_\alpha} = \frac{N_{SDS,n_\alpha}}{N_{C_{10}E_4,n_\alpha} + N_{SDS,n_\alpha}} \tag{H.5}$$

is known as the composition of the micelle of aggregation number n in phase α. In addition, l_{SDS,n_α} is given by:

$$l_{SDS,n_\alpha} = l_{c,n_\alpha} + d_{ch} \tag{H.6}$$

where d_{ch} is the distance from the end of the hydrophobic tail to the charge on SDS. The value for d_{ch} is obtained from the molecular structure of SDS, and is a constant. With regard to l_{c,n_α} and y_{SDS,n_α}, Program MIX2[54,108,114] minimizes the free energy of micellization with respect to these variables based on the ionic strength of the solution. Accordingly, optimum values for l_{c,n_α} and y_{SDS,n_α} are obtained, which apply to every micelle in phase α regardless of the aggregation number n. Consequently, σ_{n_α} in Eq. (H.4) is a constant for every micelle in phase α, and will be denoted as σ_α.

Appendix I

Derivation of the Boundary Conditions for the Three Concentric Charged Cylinders

This appendix provides the derivation of four of the boundary conditions presented in Chapter 8 for the three concentric charged cylinders. These charged cylinders are shown schematically in Figure 8-11.

The four boundary conditions in the cgs system of units are repeated below for clarity:

$$\frac{d\psi_I}{dr} = 0, \quad for\ 0 < r \leq r_{in} \tag{8.34}$$

$$\epsilon_{II}\left(\frac{d\psi_{II}}{dr}\right)_{r=r_{in}^+} - \epsilon_I\left(\frac{d\psi_I}{dr}\right)_{r=r_{in}^-} = -4\pi\sigma_{in} \tag{8.35}$$

$$\epsilon_{III}\left(\frac{d\psi_{III}}{dr}\right)_{r=r_{mid}^+} - \epsilon_{II}\left(\frac{d\psi_{II}}{dr}\right)_{r=r_{mid}^-} = -4\pi\sigma_{mid} \tag{8.36}$$

$$\epsilon_{IV}\left(\frac{d\psi_{IV}}{dr}\right)_{r=r_{out}^+} - \epsilon_{III}\left(\frac{d\psi_{III}}{dr}\right)_{r=r_{out}^-} = 4\pi\sigma_{in}\frac{r_{in}}{r_{out}} \tag{8.37}$$

The boundary condition corresponding to Eq. (8.34) will first be derived. In Region I ($0 < r \leq r_{in}$), Gauss's law in a media with a dielectric constant, ϵ_I, is given by:[127]

$$\int \epsilon_I \vec{E} \cdot d\vec{S} = (4\pi)(0) = 0 \tag{I.1}$$

where $\vec{E}$ is the electric field, $d\vec{S}$ is the differential surface area with a direction parallel to the outward normal of the surface, and the included charge is zero, since there is no charge within the cylinder with radius between 0 and r_{in}. Due to the cylindrical symmetry, Eq. (I.1) simplifies to:

$$(-\epsilon_I)\left(\frac{d\psi_I}{dr}\right)(2\pi r L) = 0 \tag{I.2}$$

where ψ_I is the electrostatic potential in Region I, and L is the length of the cylindrical micelle. Equation (I.2) therefore simplifies to the desired result:

$$\frac{d\psi_I}{dr} = 0, \quad for\ 0 < r \leq r_{in} \tag{8.34}$$

The boundary condition corresponding to Eq. (8.35) will now be derived. At $r = r_{in}^-$ in Region I, Eq. (I.2) applies with $r = r_{in}^-$ as follows:

$$(-\epsilon_I)\left(\frac{d\psi_I}{dr}\right)_{r=r_{in}^-}(2\pi r_{in}L) = 0 \tag{I.3}$$

Equation (I.3) simplifies to:

$$-\epsilon_I\left(\frac{d\psi_I}{dr}\right)_{r=r_{in}^-} = 0 \tag{I.4}$$

At $r = r_{in}^+$ in Region II, Gauss's law in a media with a dielectric constant, ϵ_{II}, is given by:

$$\int \epsilon_{II}\vec{E}\cdot d\vec{S} = (4\pi)\,(z_{in}e) \tag{I.5}$$

where z_{in} is the valence of the inner cylinder. Since the charge is modeled as being distributed symmetrically on the cylindrical surface, the electric field is also symmetric. Accordingly, the electric field has the same magnitude at all points on the Gaussian surface that is drawn as a cylinder of radius $r = r_{in}^+$ concentric with the charged cylinder.[120] In addition, since the electric field is perpendicular to the surface, Equation (I.5) simplifies to:

$$(-\epsilon_{II})\left(\frac{d\psi_{II}}{dr}\right)_{r=r_{in}^+}(2\pi r_{in}L) = 4\pi z_{in}e \tag{I.6}$$

where ψ_{II} is the electrostatic potential in Region II. Rearranging Eq. (I.6) yields:

$$-\epsilon_{II}\left(\frac{d\psi_{II}}{dr}\right)_{r=r_{in}^+} = 4\pi\sigma_{in} \tag{I.7}$$

where

$$\sigma_{in} = \frac{z_{in}e}{2\pi r_{in}L} \tag{I.8}$$

is the surface charge density of the inner cylinder. Subtracting Eq. (I.7) from Eq. (I.4) yields

the desired result:

$$\epsilon_{II}\left(\frac{d\psi_{II}}{dr}\right)_{r=r_{in}^{+}} - \epsilon_{I}\left(\frac{d\psi_{I}}{dr}\right)_{r=r_{in}^{-}} = -4\pi\sigma_{in} \tag{8.35}$$

Next, let us consider the boundary condition corresponding to Eq. (8.36). At $r = r_{mid}^{-}$ in Region II, Eq. (I.6) applies with $r = r_{mid}^{-}$ as follows:

$$(-\epsilon_{II})\left(\frac{d\psi_{II}}{dr}\right)_{r=r_{mid}^{-}} (2\pi r_{mid}L) = 4\pi z_{in}e \tag{I.9}$$

Rearranging Eq. (I.9) yields:

$$-\epsilon_{II}\left(\frac{d\psi_{II}}{dr}\right)_{r=r_{mid}^{-}} = (4\pi)\left(\frac{z_{in}e}{2\pi r_{mid}L}\right) \tag{I.10}$$

Multiplying Eq. (I.10) by 1 in the form of (r_{in}/r_{in}), and rearranging yields the following relation:

$$-\epsilon_{II}\left(\frac{d\psi_{II}}{dr}\right)_{r=r_{mid}^{-}} = (4\pi\sigma_{in})\left(\frac{r_{in}}{r_{mid}}\right) \tag{I.11}$$

At $r = r_{mid}^{+}$ in Region III, Gauss's law in a media with a dielectric constant, ϵ_{III}, is given by:

$$\int \epsilon_{III}\vec{E}\cdot d\vec{S} = (4\pi)\left[(z_{in} + z_{mid})\, e\right] \tag{I.12}$$

where z_{mid} is the valence of the middle cylinder. Since all the charges are being modeled as being distributed symmetrically on the cylindrical surfaces, the electric field is symmetric at all points on the Gaussian surface drawn as a cylinder of radius $r = r_{mid}^{+}$. Equation (I.12) therefore simplifies to:

$$(-\epsilon_{III})\left(\frac{d\psi_{III}}{dr}\right)_{r=r_{mid}^{+}} (2\pi r_{mid}L) = 4\pi\,(z_{in} + z_{mid})\, e \tag{I.13}$$

where ψ_{III} is the electrostatic potential in Region III. Rearranging Eq. (I.13) yields:

$$-\epsilon_{III}\left(\frac{d\psi_{III}}{dr}\right)_{r=r_{mid}^{+}} = 4\pi\left[\sigma_{in}\left(\frac{r_{in}}{r_{mid}}\right) + \sigma_{mid}\right] \tag{I.14}$$

where

$$\sigma_{mid} = \frac{z_{mid}e}{2\pi r_{mid}L} \tag{I.15}$$

is the surface charge density of the middle cylinder. Subtracting Eq. (I.14) from Eq. (I.11),

and rearranging yields the desired result:

$$\epsilon_{III}\left(\frac{d\psi_{III}}{dr}\right)_{r=r_{mid}^{+}} - \epsilon_{II}\left(\frac{d\psi_{II}}{dr}\right)_{r=r_{mid}^{-}} = -4\pi\sigma_{mid} \tag{8.36}$$

Finally, the boundary condition corresponding to Eq. (8.37) will be derived. At $r = r_{out}^{-}$ in Region III, Eq. (I.13) applies with $r = r_{out}^{-}$ as follows:

$$(-\epsilon_{III})\left(\frac{d\psi_{III}}{dr}\right)_{r=r_{out}^{-}} (2\pi r_{out}L) = 4\pi\left(z_{in} + z_{mid}\right)e \tag{I.16}$$

Rearranging Eq. (I.16) yields:

$$-\epsilon_{III}\left(\frac{d\psi_{III}}{dr}\right)_{r=r_{out}^{-}} = (4\pi)\left(\frac{z_{in}e}{2\pi r_{out}L}\frac{r_{in}}{r_{in}} + \frac{z_{mid}e}{2\pi r_{out}L}\frac{r_{mid}}{r_{mid}}\right) \tag{I.17}$$

Further manipulating Eq. (I.17) gives the following relation:

$$-\epsilon_{III}\left(\frac{d\psi_{III}}{dr}\right)_{r=r_{out}^{-}} = (4\pi)\left(\sigma_{in}\frac{r_{in}}{r_{out}} + \sigma_{mid}\frac{r_{mid}}{r_{out}}\right) \tag{I.18}$$

At $r = r_{out}^{+}$ in Region IV, Gauss's law in a media with a dielectric constant, ϵ_{IV}, is given by:

$$\int \epsilon_{IV}\vec{E}\cdot d\vec{S} = (4\pi)\left[\left(z_{out} + z_{mid} + z_{in}\right)e\right] \tag{I.19}$$

where z_{out} is the valence of the outer cylinder. Equation (I.19) simplifies to:

$$(-\epsilon_{IV})\left(\frac{d\psi_{IV}}{dr}\right)_{r=r_{out}^{+}} (2\pi r_{out}L) = 4\pi z_{mid}e \tag{I.20}$$

where ψ_{IV} is the electrostatic potential in Region IV, and the equality given by:

$$z_{out} = -z_{in} \tag{I.21}$$

was used. Equation (I.21) is valid since the zwitterionic surfactant has equal and opposite charges at r_{in} and r_{out}. Rearranging Eq. (I.20) yields the following relation:

$$-\epsilon_{IV}\left(\frac{d\psi_{IV}}{dr}\right)_{r=r_{out}^{+}} = (4\pi)\left(\frac{z_{mid}e}{2\pi r_{out}L}\right)\left(\frac{r_{mid}}{r_{mid}}\right) \tag{I.22}$$

Simplifying Eq. (I.22) yields:

$$-\epsilon_{IV}\left(\frac{d\psi_{IV}}{dr}\right)_{r=r_{out}^{+}} = 4\pi\sigma_{mid}\frac{r_{mid}}{r_{out}} \tag{I.23}$$

Subtracting Eq. (I.23) from Eq. (I.18) yields the desired result:

$$\epsilon_{IV}\left(\frac{d\psi_{IV}}{dr}\right)_{r=r_{out}^{+}} - \epsilon_{III}\left(\frac{d\psi_{III}}{dr}\right)_{r=r_{out}^{-}} = 4\pi\sigma_{in}\frac{r_{in}}{r_{out}} \tag{8.37}$$

BIBLIOGRAPHY

[1] FDA. Department of Health and Human Services. International Conference on Harmonisation of Technical Requirements for Registration of Pharmaceuticals for Human Use. ICH Harmonised Tripartite Guideline. Viral Safety Evaluation of Biotechnology Products Derived from Cell Lines of Human or Animal Origin. *Federal Register*, Vol. 63, No. 185, September 24, 1998.

[2] P.D. Minor. Ensuring safety and consistency in cell culture production processes: viral screening and inactivation. *TIBTECH*, 12:257–261, 1994.

[3] H. Aranha. Viral clearance strategies for biopharmaceutical safety – Part I: General considerations. *BioPharm*, 14(1):28–35, 2001.

[4] CPMP Biotechnology Working Party. The European Agency for the Evaluation of Medicinal Products. Human Medicines Evaluation Unit. *Note for Guidance on Virus Validation Studies: The Design, Contribution and Interpretation of Studies. Validating the Inactivation and Removal of Viruses.* Revised. CPMP/BWP/268/95.

[5] N. Dumey, D. Larzul, and F. Horaud. Pharmaceuticals and viral safety: A global view. *Pharmaceutical Science and Technology today*, 3(7):220–221, 2000.

[6] FDA. Department of Health and Human Services. Center for Biologics Evaluation and Research. *Points to Consider in the Characterization of Cell Lines Used to Produce Biologicals*, 1993.

[7] J. Myers. Associate Director. Process Biochemistry. Biogen. Cambridge, MA. Personal communication. Spring 1997.

[8] J. Myers. Associate Director. Process Biochemistry. Biogen. Cambridge, MA. Personal communication. Spring 2001.

[9] FDA. US Department of Health and Human Services. Center for Biologics Evaluation and Research. *Points to Consider in the Manufacture and Testing of Monoclonal Antibody Products for Human Use*, February 28, 1997.

[10] A.J. Darling and J.H. Spaltro. Process validation for virus removal: considerations for design of process studies and viral assays. *BioPharm*, 9(9):42–50, 1996.

[11] C.S. Toth. Retention of viral contaminants by 0.04 μm nylon 66 filters. *CHIMICAoggi*, 9:29–30, 1991.

[12] I.F. Tsao, Jr. C. Shipman, and H.Y. Wang. The removal of adventitious viruses and virus-infected cells using a cellular adsorbent: a feasibility study. *BIO/TECHNOLOGY*, 6(11):1330–1333, 1988.

[13] T. Burnouf. Chromatographic removal of viruses from plasma derivatives. In F. Brown, editor, *Developments in Biological Standardization: Virological Safety Aspects of Plasma Derivatives*, volume 81, pages 199–209. Karger, Basel, 1993.

[14] A.J. DiLeo, A.E. Allegrezza, Jr.,, and S.E. Builder. High resolution removal of virus from protein solutions using a membrane of unique structure. *BIO/TECHNOLOGY*, 10:182–188, 1992.

[15] H. Aranha. Viral clearance strategies for biopharmaceutical safety – Part II: Filtration for viral clearance. *BioPharm*, 14(2):32–43, 2001.

[16] Pall Filtron Corporation. OMEGA®VR Virus Reduction Membrane. Element Data Sheet F1. Northborough, MA, 1996.

[17] Millipore. Virus Removal. In *Pharmaceutical Process Filtration Catalogue.* Millipore, Bedford, MA, 1995.

[18] S. Liu, M. Carroll, R. Iverson, C. Valera, J. Vennari, K. Turco, R. Piper, R. Kiss, and H. Lutz. Development and qualification of a novel virus removal filter for cell culture applications. *Biotechnology Progress*, 16(3):425–434, 2000.

[19] S.H. Orkin and A.G. Motulsky. Report and Recommendations of the Panel to Assess the NIH Investment in Research on Gene Therapy. December 7, 1995.

[20] J.M. Le Doux, J.R. Morgan, and M.L. Yarmush. Gene Therapy. In J.D. Bronzino, editor, *The Biomedical Engineering Handbook*, chapter X. CRC Press, Inc., Boca Raton, 1995.

[21] F.M. Boyce and N.L.R. Bucher. Baculovirus-mediated gene transfer into mammalian cells. *Proceedings of the National Academy of Sciences of the USA*, 93:2348–2352, 1996.

[22] C. Hofmann, V. Sandig, G. Jennings, M. Rudolph, P. Schlag, and M. Strauss. Efficient gene transfer into human hepatocytes by baculovirus vectors. *Proceedings of the National Academy of Sciences of the USA*, 92:10099–10103, 1995.

[23] B.G. Huyghe, X. Liu, S. Sutjipto, B.J. Sugarman, M.T. Horn, H.M. Shepard, C.J. Scandella, and P. Shabram. Purification of a type 5 recombinant adenovirus encoding human p53 by column chromatography. *Human Gene Therapy*, 6:1403–1416, 1995.

[24] K. Tamayose, Y. Hirai, and T. Shimada. A new strategy for large-scale preparation of high-titer recombinant adeno-associated virus vectors by using packaging cell lines and sulfonated cellulose column chromatography. *Human Gene Therapy*, 7:507–513, 1996.

[25] P. Fender, R. Ruigrok, E. Gout, S. Buffet, and J. Chroboczek. Adenovirus dodecahedron, a new vector for human gene gene transfer. *Nature Biotechnology*, 15:52–56, 1997.

[26] J. Bischoff, D. Kirn, A. Williams, C. Heise, S. Horn, M. Muna, L. Ng, J. Nye, A. Sampson-Johannes, A. Fattaey, and F. McCormick. An adenovirus mutant that replicates selectively in p53-deficient human tumor cells. *Science*, 274:373–376, 1996.

[27] E. Norrby. The structural and functional diversity of adenovirus capsid components. *Journal of General Virology*, 5:221–236, 1969.

[28] P.-Å. Albertsson. *Partition of Cell Particles and Macromolecules.* Wiley, New York, 2nd edition, 1971.

[29] M. Makino, G. Ishikawa, K. Yamaguchi, Y. Okada, K. Watanabe, Y. Sasaki-Iwaki, S. Manabe, M. Honda, and K. Komuro. Concentration of live retrovirus with a regenerated cellulose hollow fiber, BMM. *Archives of Virology*, 139:87–96, 1994.

[30] P.F. O'Neil and E.S. Balkovic. Virus harvesting and affinity-based liquid chromatography. *BIO/TECHNOLOGY*, 11:173–178, 1993.

[31] K. Maramorosch and H. Koprowski. Preface. In K. Maramorosch and H. Koprowski, editors, *Methods in Virology*, volume 2, pages vii–viii. Academic Press, New York, 1967.

[32] S.A. Weiss. Concentration of baboon endogenous virus in large-scale production by use of hollow-fiber ultrafiltration technology. *Biotechnology and Bioengineering*, 22:19–31, 1980.

[33] R. Markham. The ultracentrifuge. In K. Maramorosch and H. Koprowski, editors, *Methods in Virology*, volume 2, pages 1–39. Academic Press, New York, 1967.

[34] H.M. Mazzone. Equilibrium ultracentrifugation. In K. Maramorosch and H. Koprowski, editors, *Methods in Virology*, volume 2, pages 41–91. Academic Press, New York, 1967.

[35] N.G. Anderson and G.B. Cline. New centrifugal methods for virus isolation. In K. Maramorosch and H. Koprowski, editors, *Methods in Virology*, volume 2, pages 137–178. Academic Press, New York, 1967.

[36] E. Fowler, N. Raab-Traub, and S. Hester. Purification of biologically active epstein-barr virus by affinity chromatography and non-ionic density gradient centrifugation. *Journal of Virological Methods*, 11:59–74, 1985.

[37] D.G. Sharp. Purification and properties of animal viruses. In K.M. Smith and M.A. Lauffer, editors, *Advances in Virus Research*, volume 1, pages 277–313. Academic Press, New York, 1953.

[38] K. Strohmaier. Virus concentration by ultrafiltration. In K. Maramorosch and H. Koprowski, editors, *Methods in Virology*, volume 2, pages 245–274. Academic Press, New York, 1967.

[39] V.P. Perry and M.M. Vincent. Filtration techniques. In K. Maramorosch and H. Koprowski, editors, *Methods in Virology*, volume 2, pages 367–389. Academic Press, New York, 1967.

[40] L. Philipson. Chromatography and membrane separation. In K. Maramorosch and H. Koprowski, editors, *Methods in Virology*, volume 2, pages 179–233. Academic Press, New York, 1967.

[41] M. McGrath, O. Witte, T. Pincus, and I.L. Weissman. Retrovirus purification: Method that conserves envelope glycoprotein and maximizes infectivity. *Journal of Virology*, 25(3):923–927, 1978.

[42] J.N. Israelachvili. *Intermolecular and Surface Forces.* Academic Press, San Diego, 2nd edition, 1992.

[43] D. Blankschtein, G.M. Thurston, and G.B. Benedek. Theory of phase separation in micellar solutions. *Physical Review Letters*, 54(9):955–958, 1985.

[44] D. Blankschtein, G.M. Thurston, and G.B. Benedek. Phenomenological theory of equilibrium thermodynamic properties and phase separation of micellar solutions. *The Journal of Chemical Physics*, 85(12):7268–7288, 1986.

[45] C. Tanford. *The Hydrophobic Effect: Formation of Micelles and Biological Membranes.* Wiley, New York, 2nd edition, 1978.

[46] J.N. Israelachvili. *Intermolecular and Surface Forces: With Applications to Colloidal and Biological Systems.* Academic Press, San Diego, 1985.

[47] Y. Chevalier and T. Zemb. The structure of micelles and microemulsions. *Rep. Prog. Phys.*, 53:279–371, 1990.

[48] K. Meguro, M. Ueno, and K. Esumi. Micelle formation in aqueous media. In M.J. Schick, editor, *Nonionic Surfactants: Physical Chemistry*, pages 109–183. Marcel Dekker, New York, 1987.

[49] J. Sjöblom, P. Stenius, and I. Danielsson. Phase equilibria of nonionic surfactants and the formation of microemulsions. In M.J. Schick, editor, *Nonionic Surfactants: Physical Chemistry*, pages 369–434. Marcel Dekker, New York, 1987.

[50] D.J. Mitchell. Phase behaviour of polyoxyethylene surfactants with water. *J. Chem. Soc., Faraday Trans. 1*, 79:975–1000, 1983.

[51] C.A. Leng. Interacting C_nE_m non-ionic micellar systems. *J. Chem. Soc., Faraday Trans.*, 81(2):145–158, 1985.

[52] J.C. Lang and R.D. Morgan. Nonionic surfactant mixtures. I. Phase equilibria in $C_{10}E_4$-H_20 and closed-loop coexistence. *The Journal of Chemical Physics*, 73(11):5849–5861, 1980.

[53] S. Puvvada and D. Blankschtein. Molecular-thermodynamic approach to predict micellization, phase behavior, and phase separation of micellar solutions. I. Application to nonionic surfactants. *The Journal of Chemical Physics*, 92(6):3710–3724, 1990.

[54] N.J. Zoeller and D. Blankschtein. Development of user-friendly computer programs to predict solution properties of single and mixed surfactant systems. *Industrial & Engineering Chemistry Research*, 34(12):4150–4160, 1995.

[55] N. Zoeller, L. Lue, and D. Blankschtein. Statistical-thermodynamic framework to model nonionic micellar solutions. *Langmuir*, 13(20):5258–5275, 1997.

[56] W.L. Hinze and E. Pramauro. A critical review of surfactant-mediated phase separations (cloud-point extractions): Theory and applications. *Critical Reviews in Analytical Chemistry*, 24(2):133–177, 1993.

[57] T. Saitoh and W.L. Hinze. Concentration of hydrophobic organic compounds and extraction of protein using alkylammoniosulfate zwitterionic surfactant mediated phase separations (cloud point extractions). *Analytical Chemistry*, 63(21):2520–2525, 1991.

[58] C.G. Pinto, J.L.P. Pavon, and B.M. Cordero. Cloud point preconcentration and high-performance liquid chromatographic analysis with electrochemical detection. *Analytical Chemistry*, 64:2334–2338, 1992.

[59] T. Okada. Temperature-induced phase separation of nonionic polyoxyethylated surfactant and application to extraction of metal thiocyanates. *Analytical Chemistry*, 64:2138–2142, 1992.

[60] H. Watanabe and H. Tanaka. A non-ionic surfactant as a new solvent for liquid-liquid extraction of zinc(II) with 1-(2-pyridylazo)-2-naphthol. *Talanta*, 25:585–589, 1978.

[61] H. Hoshino, T. Saitoh, H. Taketomi, and T. Yotsuyanagi. Micellar solubilization equilibria for some analytical reagents in aqueous non-ionic surfactant solutions. *Analytica Chimica Acta*, 147:339–345, 1983.

[62] T.-F. Zhang and L.P. Hager. A single-step large-scale purification of pyruvate oxidase. *Archives of Biochemistry and Biophysics*, 257(2):485–487, 1987.

[63] C. Bordier. Phase separation of integral membrane proteins in Triton X-114 solution. *The Journal of Biological Chemistry*, 256(4):1604–1607, 1981.

[64] R.A. Ramelmeier, G.C. Terstappen, and M.-R. Kula. The partitioning of cholesterol oxidase in Triton X-114-based aqueous two-phase systems. *Bioseparation*, 2:315–324, 1991.

[65] G.C. Terstappen, R.A. Ramelmeier, and M.-R. Kula. Protein partitioning in detergent-based aqueous two-phase systems. *Journal of Biotechnology*, 28:263–275, 1993.

[66] Á. Sánchez-Ferrer, R. Bru, and F. García-Carmona. Phase separation of biomolecules in polyoxyethylene glycol nonionic detergents. *Critical Reviews in Biochemistry and Molecular Biology*, 29(4):275–313, 1994.

[67] D. Werck-Reichhart, I. Benveniste, H. Teutsch, F. Durst, and B. Gabriac. Glycerol allows low-temperature phase separation of membrane proteins solubilized in Triton X-114: Application to the purification of plant cytochromes p-450 and b_5. *Analytical Biochemistry*, 197:125–131, 1991.

[68] N.M. Hooper and A. Bashir. Glycosyl-phosphatidylinositol-anchored membrane proteins can be distinguished from transmembrane polypeptide-anchored proteins by differential solubilization and temperature-induced phase separation in Triton X-114. *Biochem. J.*, 280:745–751, 1991.

[69] K.J. Clemetson, D. Bienz, M.-L. Zahno, and E.F. Luscher. Distribution of platelet glycoproteins and phosphoproteins in hydrophobic and hydrophilic phases in Triton X-114 phase partition. *Biochimica et Biophysica Acta*, 778:463–469, 1984.

[70] C.-L. Liu. *Partitioning of Biomolecules in Two-Phase Aqueous Micellar Systems.* Doctoral Thesis, Massachusetts Institute of Technology, September 1995.

[71] Y.J. Nikas, C.-L. Liu, T. Srivastava, N.L. Abbott, and D. Blankschtein. Protein partitioning in two-phase aqueous nonionic micellar solutions. *Macromolecules*, 25(18):4797–4806, 1992.

[72] C.-L. Liu, Y.J. Nikas, and D. Blankschtein. Partitioning of proteins using two-phase aqueous surfactant systems. *AIChE Journal*, 41(4):991–995, 1995.

[73] C.-L. Liu, Y.J. Nikas, and D. Blankschtein. Novel bioseparations using two-phase aqueous micellar systems. *Biotechnology and Bioengineering*, 52(2):185–192, 1996.

[74] L. Lue and D. Blankschtein. A liquid-state theory approach to modeling solute partitioning in phase-separated solutions. *Industrial & Engineering Chemistry Research*, 35(9):3032–3043, 1996.

[75] P.-Å. Albertsson. *Partition of Cell Particles and Macromolecules.* Wiley, New York, 3rd edition, 1986.

[76] P.L. Dubin and J.M. Principi. Optimization of size-exclusion separation of proteins on a superose column. *Journal of Chromatography*, 479:159–164, 1989.

[77] I.D. Kuntz, Jr. and E. Kauzmann. *Hydration of Proteins and Polypeptides*, volume 28, pages 239–345. Academic Press, New York, 1974.

[78] C. Liu, D.T. Kamei, J.A. King, D.I.C. Wang, and D. Blankschtein. Separation of proteins and viruses using two-phase aqueous micellar systems. *Journal of Chromatography B*, 711:127–138, 1998.

[79] A.S. Tikhonenko. *Ultrastructure of Bacterial Viruses.* Plenum Press, New York, 1970.

[80] P. Serwer. Agarose gel electrophoresis of bacteriophages and related particles. *Journal of Chromatography*, 418:345–357, 1987.

[81] T.F. Anderson. Morphologies of bacteriophage virions. In A.J. Dalton and F. Haguenau, editors, *Ultrastructure of Animal Viruses and Bacteriophages: An Atlas*, pages 347–357. Academic Press, New York, 1973.

[82] V. Israel, H. Rosen, and M. Levine. Binding of bacteriophage P22 tail parts to cells. *Journal of Virology*, 10(6):1152–1158, 1972.

[83] S. Iwashita and S. Kanegasaki. Smooth specific phage adsorption: Endorhamnosidase activity of tail parts of P22. *Biochemical and Biophysical Research Communications*, 55(2):403–409, 1973.

[84] E. Hartwieg, C. Bazinet, and J. King. Dna injection apparatus of phage P22. *Biophysical Journal*, 49:24–26, 1986.

[85] P.A. Thuman-Commike, B. Greene, J. Jakana, B.V.V. Prasad, J. King, P.E. Prevelige, Jr., and W. Chiu. Three-dimensional structure of scaffolding-containing phage P22 procapsids by electron cryo-microscopy. *Journal of Molecular Biology*, 260:85–98, 1996.

[86] B. Fane and J. King. Infection of sites influencing the folding and subunit assembly of the P22 tailspike polypeptide chain using nonsense mutations. *Genetics*, 117:157–171, 1987.

[87] B.V.V. Prasad, P.E. Prevelige, E. Marietta, R.O. Chen, D. Thomas, J. King, and W. Chiu. Three-dimensional transformation of capsids associated with genome packaging in a bacterial virus. *Journal of Molecular Biology*, 231:65–74, 1993.

[88] F.A. Eiserling and L.W. Black. Pathways in T4 morphogenesis. In J.D. Karam, editor, *Molecular Biology of Bacteriophage T4*, pages 209–212. American Society for Microbiology, Washington, D.C., 1994.

[89] S. Iwashita and S. Kanegasaki. Enzymic and molecular properties of base-plate parts of bacteriophage P22. *European Journal of Biochemistry*, 65:87–94, 1976.

[90] U. Eriksson, A.A. Lindberg, H. Jörnvall, and H.V. Bahr-Lindström. Characterization of the enzymatic tail protein of bacteriophage P22. *FEBS Letters*, 72(1):15–18, 1976.

[91] U. Eriksson and A.A. Lindberg. Adsorption of phage P22 to *Salmonella typhimurium*. *The Journal of General Virology*, 34:207–221, 1977.

[92] U. Eriksson, S.B. Svenson, J. Lönngren, and A.A. Lindberg. *Salmonella* phage glycanases: Substrate specificity of the phage P22 *Endo*-rhamnosidase. *The Journal of General Virology*, 43:503–511, 1979.

[93] P.B. Berget and A.R. Poteete. Structure and functions of the bacteriophage P22 tail protein. *Journal of Virology*, 34(1):234–243, 1980.

[94] F. Winston, D. Botstein, and J.H. Miller. Characterization of amber and ochre suppressors in *Salmonella typhimurium*. *Journal of Bacteriology*, 137:433–439, 1979.

[95] M.J. Rosen. *Surfactants and Interfacial Phenomena*. Wiley, New York, 2nd edition, 1989.

[96] W. Earnshaw, S. Casjens, and S.C. Harrison. Assembly of the head of bacteriophage P22: X-ray diffraction from heads, proheads, and related structures. *Journal of Molecular Biology*, 104:387–410, 1976.

[97] H. Lodish, A. Berk, S.L. Zipursky P. Matsudaira, D. Baltimore, and J. Darnell. *Molecular Cell Biology*. W.H. Freeman, New York, 4th edition, 2000.

[98] G. Bertani. Lysogeny. In K.M. Smith and M.A. Lauffer, editors, *Advances in Virus Research*, volume 5, pages 151–193. Academic Press, New York, 1958.

[99] J. King. Professor. Department of Biology. Massachusetts Institute of Technology. Personal communication. Spring 1997.

[100] H. Walter. Retired Professor. Department of Physiology and Biophysics. University of California at Irvine. Laboratory of Chemical Biology. Veterans Administration Medical Center. Long Beach, CA. Personal communication. Fall 1997.

[101] D.E. Brooks. Professor. Departments of Pathology and Chemistry. University of British Columbia. Vancouver, British Columbia. Canada. Personal communication. Fall 1997.

[102] G. Johansson. Professor. Department of Biochemistry. University of Lund. Lund, Sweden. Personal communication. Fall 1997.

[103] P.-Å. Albertsson. *Partition of Cell Particles and Macromolecules.* Wiley, New York, 1st edition, 1960.

[104] D.P. Shoemaker, C.W. Garland, and J.W. Nibler. *Experiments in Physical Chemistry.* McGraw-Hill, New York, 5th edition, 1989.

[105] M.-R. Kula. Professor and Director. Institut für Enzymtechnologie der Heinrich-Heine-Universität Düsseldorf. Forschungszentrum Jülich, Germany. Personal communication. Fall 1997.

[106] K.S. Birdi. Surface tension and interfacial tension of liquids. In K.S. Birdi, editor, *Handbook of Surface and Colloid Chemistry*, pages 71–118. CRC Press, Boca Raton, 1997.

[107] R.E. Treybal. *Mass-Transfer Operations.* McGraw-Hill, New York, 3rd edition, 1980.

[108] A. Shiloach and D. Blankschtein. Measurement and prediction of ionic/nonionic mixed micelle formation and growth. *Langmuir*, 14(25):7166–7182, 1998.

[109] U. Sivars, K. Bergfeldt, L. Piculell, and F. Tjerneld. Protein partitioning in weakly charged polymer-surfactant aqueous two-phase systems. *Journal of Chromatography B*, 680:43–53, 1996.

[110] W.L. McCabe, J.C. Smith, and P. Harriot. *Unit Operations of Chemical Engineering.* McGraw-Hill, New York, 5th edition, 1993.

[111] J.W. Tester and M. Modell. *Thermodynamics and Its Applications.* Prentice-Hall, New Jersey, 3rd edition, 1997.

[112] J.G. Kirkwood and I. Oppenheim. *Chemical Thermodynamics.* McGraw-Hill, New York, 1961.

[113] S. Puvvada and D. Blankschtein. Thermodynamic description of micellization, phase behavior, and phase separation of aqueous solutions of surfactant mixtures. *The Journal of Physical Chemistry*, 96(13):5567–5579, 1992.

[114] A. Shiloach and D. Blankschtein. Predicting micellar solution properties of binary surfactant mixtures. *Langmuir*, 14(7):1618–1636, 1998.

[115] D.A. McQuarrie. *Statistical Mechanics.* Harper & Row, New York, 1976.

[116] L. Blum. Primitive electrolytes in the mean spherical approximation. In H. Eyring and D. Henderson, editors, *Theoretical Chemistry: Advances and Perspectives*, volume 5, pages 1–66. Academic Press, New York, 1980.

[117] G.P. Dube. Electrical energy of two cylindrical charged particles. *Indian Journal of Physics*, 17:189–192, 1944.

[118] R.J. Hunter. *Zeta Potential in Colloid Science: Principles and Applications.* Academic Press, San Diego, 1981.

[119] J.O'M. Bockris and A.K.N. Reddy. *Modern Electrochemistry*, volume 1. Plenum Press, New York, 1970.

[120] D.C. Giancoli. *Physics for Scientists and Engineers: With Modern Physics.* Prentice-Hall, New Jersey, 2nd edition, 1989.

[121] Y. Gu. The electrical double-layer interaction between a spherical particle and a cylinder. *Journal of Colloid and Interface Science*, 231:199–203, 2000.

[122] E.M. Johnson and W.M. Deen. Electrostatic effects on the equilibrium partitioning of spherical colloids in random fibrous media. *Journal of Colloid and Interface Science*, 178:749–756, 1996.

[123] L. Stryer. *Biochemistry.* W.H. Freeman, New York, 3rd edition, 1988.

[124] P.C. Hiemenz and R. Rajagopalan. *Principles of Colloid and Surface Chemistry.* Marcel Dekker, New York, 3rd edition, 1997.

[125] G.E.P. Box, W.G. Hunter, and J.S. Hunter. *Statistics for Experimenters: An Introduction to Design, Data Analysis, and Model Building.* Wiley, New York, 1978.

[126] C. Tanford. *Physical Chemistry of Macromolecules.* Wiley, New York, 1961.

[127] C.A. Coulson. *Electricity.* Oliver and Boyd, Edinburgh, Great Britain, 5th edition, 1958.

[128] K.F. Jensen. Microreaction engineering – is small better? *Chemical Engineering Science*, 56:293–303, 2001.

[129] K.D. Collins and M.W. Washabaugh. The Hofmeister effect and the behaviour of water at interfaces. *Quarterly Review of Biophysics*, 18(4):323–365, 1985.

[130] R. Leberman and A.K. Soper. Effect of high salt concentrations on water structure. *Nature*, 378:364–366, 1995.

[131] V.A. Parsegian. Hopes for hofmeister. *Nature*, 378:335–336, 1995.

[132] A. Ray and G. Némethy. Effects of ionic protein denaturants on micelle formation by nonionic detergents. *Journal of the American Chemical Society*, 93(25):6787–6793, 1971.

[133] U. Sivars and F. Tjerneld. Mechanisms of phase behaviour and protein partitioning in detergent/polymer aqueous two-phase systems for purification of integral membrane proteins. *Biochimica et Biophysica Acta*, 1474:133–146, 2000.

[134] L. Piculell, K. Bergfeldt, and S. Gerdes. Segregation in aqueous mixtures of non-ionic polymers and surfactant micelles. effects of micelle size and surfactant head-group/polymer interactions. *The Journal of Physical Chemistry*, 100(9):3675–3679, 1996.

[135] H.S. Fogler. *Elements of Chemical Reaction Engineering.* Prentice-Hall, New Jersey, 2nd edition, 1992.

[136] A. Pessoa-Jr. Professor. Departamento de Tecnologia Bioquimico-Farmacêutica. Faculdade de Ciências Farmacêuticas. Universidade de São Paulo. São Paulo. Brasil. Personal communication. Fall 2000.